BAW-10192NP

Topical Report
Revision 2
August 2008

- BWNT LOCA -

BWNT Loss-of-Coolant Accident Evaluation Model for Once-Through Steam Generator Plants

Volume I - Large Break

AREVA NP Inc.
P. O. Box 10935
Lynchburg, Virginia 24506

This page is intentionally left blank.

Copyright © 2008

AREVA NP Inc.
All Rights Reserved

This page is intentionally left blank.

AREVA NP Inc.
Lynchburg, Virginia 24506

Topical Report BAW-10192NP
Revision 2
August 2008

- BWNT LOCA -

BWNT Loss-of-Coolant Accident Evaluation Model for Once-Through Steam Generator Plants

Volume I - Large Break

Key Words: Large Break, LOCA, Transient, Water Reactors, Evaluation Model

ABSTRACT

This document presents the generic large and small break models to be used by AREVA NP Inc. (previously known as Babcock & Wilcox, B&W Nuclear Technologies, or BWNT) for evaluating the performance of the emergency core cooling systems (ECCS) following a loss-of-coolant accident (LOCA) for all classes of B&W-designed pressurized water reactors (PWR). The large break model is discussed in Volume I and the small break model in Volume II. Volume III is the licensing addendum, which provides a historical record of related correspondence including responses to NRC questions, NRC Safety and Technical Evaluation Reports, and NRC approval letters. The models have been developed and compared with the required and acceptable features contained in Appendix K of the Code of Federal Regulations, 10CFR50. The evaluation models are shown to conform to Appendix K requirements.

This page is intentionally left blank.

ACKNOWLEDGMENT

AREVA NP Inc. wishes to acknowledge the effort by J. A. Klingenfus, K. S. Pacheco, S. S. Reilly, K. C. Shieh, C. G. Thurston, and G. J. Wissinger in preparation of the material and completion of the analyses contained in this topical report.

This page is intentionally left blank.

Topical Revision Record

Volume I - Large Break

Documentation Revision	Description
0	Original Issue
1	Revision of LBLOCA model Volume I only. Remove REFLOD3B code from LBLOCA code package. Refill/reflood calculations performed by RELAP5 run in a systems configuration, i.e. the entire RCS will be modeled. BEACH routines within RELAP5 will continue to be used, but they will now be dynamically coupled to the entire RCS. No BEACH topical report revisions were made; rather any required changes were incorporated into the RELAP5 revisions given in BAW-10164, Revision 5. (This revision was withdrawn and therefore was not approved)
2	Update NCR-approved source references (e.g. RELAP5, BEACH, M5) Modify Rev. 0 texts to reflect the methods from new source references approved by the NRC (e.g. hot pin methodology, Gadolinia) Expand the discussions on coolable geometry and long-term cooling (e.g. GSI-191) Add references to the RAIs in the main document Typographical corrections (Changed pages from Rev. 1 are not included in Rev. 2)

This page is intentionally left blank.

VOLUME I CONTENTS

VOLUME I CONTENTS (Cont'd)

List of Tables

List of Tables (Cont'd)

List of Figures

List of Figures (Cont'd)

List of Figures (Cont'd)

List of Figures (Cont'd)

List of Figures (Cont'd)

List of Figures (Cont'd)

List of Figures (Cont'd)

List of Figures (Cont'd)

List of Figures (Cont'd)

1. INTRODUCTION

This report describes the features of the emergency core cooling system (ECCS) evaluation model (EM) used by AREVA NP Inc. (previously known as Babcock & Wilcox, B&W Nuclear Technologies, or BWNT) for application to all classes of B&W-designed pressurized water reactors (PWRs). The plant designs for which the evaluation model is applicable are categorized in Table 1-1. There are system design differences for the nuclear steam system (NSS) and the ECCS within each category. These systems, however, are broken into components which are similar in both geometry and thermal hydraulic behavior. This similarity enables these component design features to be individually modeled and coupled using consistent techniques in a generic EM applicable to all plant types. Specific design information for each plant category is considered input to the evaluation model and is generated using the assumptions and techniques described herein. The evaluation model can be used for analysis of fuel designs with either Zircaloy or M5 alloy cladding. For core designs employing the M5 alloy for fuel pin cladding, the material properties, inputs, methods, and correlations, described in BAW-10227P-A (Reference 19) shall supersede, as appropriate, those described for Zircaloy within this report.

The "Acceptance Criteria for Emergency Core Cooling Systems for Light Water Nuclear Power Reactors" (10CFR50.46) was issued by the NRC in January 1974. Appendix K of 10CFR50 defines the required and acceptable features of models to be used to evaluate the performance of the ECC systems. The information presented in this document defines the BWNT evaluation model and shows that the model conforms to Appendix K requirements.

The topical report is presented in three volumes. The first volume presents the large break evaluation model. The second volume presents the small break evaluation model. Volumes I and II contain the following seven sections, which define the respective evaluation models:

1. Definition of model versus input (Section 3).

2. Features of the evaluation model and statements of conformity to Appendix K (Section 4).

3. The calculational technique used to evaluate the maximum local cladding oxidation (Section 5).

4. The calculational technique used to evaluate the maximum hydrogen generation (Section 6).

5. The technique used to evaluate conformance to the coolable geometry criterion (Section 7).

6. The technique used for establishing conformance to the long-term cooling criterion (Section 8).

7. Required documentation necessary to meet 10CFR50.46 (Section 9).

Volume III, the licensing addendum, is included for the purpose of retaining licensing data, responses to NRC questions, position papers, SERs, etc.

Table 1-1. Applicable PWR Plant Categories.

Plant Category	Number FAs	RCS Loop Geometry	Fuel Design	SG Type	ECCS System
1	177	Lowered	15 x 15	OTSG(1)	High Head HPI
2	177	Raised	15 x 15	OTSG(1)	Low Head HPI
3	205	Raised	17 x 17	IEOTSG	High Head HPI

where

OTSG = Once-Through Steam Generator (Recirculating)

IEOTSG = Integral Economizer Once-Through Steam Generator (Non-Recirculating)

HPI = High Pressure Injection

Note (1)- The 177 FA B&W plants have been planning for and replacing the original OTSGs in combination with life extension activities. The replacement steam generator designs use similar straight shell and tube steam generators and are designated as the "Enhanced" OTSG or "Replacement" OTSG designs. These steam generators are functionally equivalent to the original OTSG such that the evaluation model does not need any changes other than what is required in the input geometrical parameters and heat structure properties in the analytical models. When OTSG is described in the text of the evaluation model it refers to the original as well as the replacement designs.

This page is intentionally left blank.

2. COMPLIANCE TO 10CFR50.46

The "Acceptance Criteria for Emergency Core Cooling Systems for Light Water Power Reactors" (10CFR50.46), issued by the Nuclear Regulatory Commission in January 1974, include five criteria that must be met before an emergency core cooling system is acceptable. Conformance to these criteria is established in the following manner:

1. The peak cladding temperature shall not exceed 2200 F.

   The peak cladding temperature is calculated with the evaluation model described herein and shown not to exceed 2200 F.

2. The percentage of local cladding oxidation shall not exceed 17%.

   In the analysis performed to satisfy Criterion 1, the EM calculated total oxide thickness (combining both inside and outside oxide layers) at the location of maximum local oxidation is calculated and shown to be less than 0.17 times the total cladding thickness. A supplemental check of the local oxidation limits with respect to a realistic initial oxidation (or pre-accident oxidation) plus the accident-induced oxidation is also included as described in Section 5.

3. The maximum hydrogen generated during the transient shall not exceed that which would be generated by the oxidation of 1% of the reactor cladding.

   The amount of core wide zirconium oxidation that occurs during a LOCA is conservatively determined using an approach that interpolates and integrates the hot and

average channel local oxidation values over the core power distribution. The final oxidation fractions are reduced by the initial values to calculate the additional oxidation and, therefore, the total hydrogen production during the LOCA. This criterion is satisfied by showing that the increase in core-wide metal-water oxidation is less than one percent.

4. Calculated changes in the core geometry shall be such that the core remains amenable to cooling.

   The changes in geometry that were calculated during the analysis for Criterion 1 are examined to ensure that no gross core blockage or deformation occurs when it is combined with external analyses not explicitly controlled by this Evaluation Model as described in Section 7.

5. The mode of long-term cooling shall be established.

   The analysis of cladding temperature is continued until all temperatures in the core are decreasing, the core level is rising, and no additional challenges to core cooling are foreseen. At this time the path to long-term cooling is established, and the core will continue to cool down without interruption or further incident. Cooling for the long term is established by pumped injection with no interruptions or decreases in coolant flow, thereby maintaining the core temperature at an acceptably low value while removing decay heat. Section 8 gives additional details for showing compliance with this criterion.

Appendix K sets forth certain required and acceptable features of the evaluation model that must be used to show compliance to the five acceptance criteria of 10CFR50.46. Compliance of the BWNT evaluation model to Appendix K is shown in Section 4.

3. DEFINITION OF LBLOCA MODEL VERSUS INPUT

The information presented in this document defines the AREVA ECCS evaluation model for application to all B&W-designed plants. In particular, this document describes the techniques and assumptions used in the evaluation of the consequences of a loss-of-coolant accident. These techniques and assumptions constitute the model. The required features of the ECCS evaluation model are set forth in Appendix K to 10CFR50. The evaluation model for large breaks is given in Chapter 4 along with statements of its conformance to Appendix K. The evaluation model will be changed only if the NRC issues rule changes or if improved analytical techniques become available.

Specific category-related information (such as system design, power level, etc.) is considered input to the model. These numbers are developed using the techniques and assumptions described in the model. This report covers the model only. All other information needed to perform the necessary analyses is considered input. Input may change throughout the design life of a nuclear steam system requiring a reapplication of the evaluation model while not affecting the evaluation model per se.

This page is intentionally left blank.

4. LARGE BREAK EVALUATION MODEL

4.1. Model Applicability

The large break evaluation model described in this section is applicable to all general plant categories presented in Table 1.1 and summarized below as of August 2008. Any item that is applicable only to certain plant categories due to differences in design, such as RCS geometry, containment pressure suppression, ECCS design, or fuel design, will be specifically identified. There are no significant design differences among the components which are contained in the plants within each category.

Category 1 - The group of operating nuclear plants in this category are Arkansas Nuclear Unit 1, Crystal River Unit 3, Oconee Units 1, 2, and 3, and Three Mile Island Unit 1. Inactive plants in this category are Three Mile Island Unit 2 and Rancho Seco. They are characterized by the loop arrangement, in which the OTSGs are at a low elevation relative to the reactor vessel. These plants have eight internal reactor vessel vent valves (RVVVs). A total of 177 Mark-B fuel assemblies with a 15-by-15 pin arrangement are used in these plants.

Category 2 - The design is essentially identical to Category 1 except that the OTSGs are raised in relation to the reactor vessel. The pump suction leg is shorter for these plants due to the raised generator configuration. Only four RVVVs are used in this plant. Davis-Besse Unit 1 is the only operating plant in this category. A total of 177 Mark-B fuel assemblies with a 15-by-15 pin arrangement are also used in this plant. This plant has low-head HPI pumps.

Category 3 - These plants have the raised-loop arrangement of the Category 2 plant, but are larger in physical size and have eight RVVVs. These plants have 205 Mark-C fuel assemblies with a 17-

by-17 pin arrangement and use integral economizer OTSGs. Plants of this type are Bellefonte 1, Bellefonte 2, Mülheim-Kärlich (ABB Germany), and Washington Nuclear Project Number 1. None of the domestic plants of this design are operating as of August 2008.

4.2. Transient Description and Computer Code Interfaces

Large break loss-of-coolant accidents can be treated analytically in three separate phases: blowdown, refill, and reflood. The blowdown phase is characterized by the rapid depressurization of the reactor coolant system to a condition nearly in pressure equilibrium with its immediate surroundings. Core flow is variable and dependent on the nature, size, and location of the break. Departure from nucleate boiling (DNB) is calculated to occur very quickly, and core cooling is by a film boiling process. Since film boiling amounts to only a small fraction of the steady-state cooling, the cladding temperature increases by 600 F to 1200 F. During the last phases of blowdown, cooling is by convection to steam, and the cladding temperature begins to rise again.

Following blowdown, a period of time is required for the ECCS to refill the bottom of the reactor vessel, before final core cooling can be established. During this period, core cooling is marginal, and the cladding experiences a near-adiabatic heatup. This period is designated as the refill phase. When the ECCS water reaches the bottom of the core, the reflood phase begins. Core cooling is by steam generated below the rising core water level. The cladding temperature excursion is generally terminated before a particular elevation is covered by water since the steam-water mixture is sufficient to remove the relatively low decay heat power being generated at this time. The core is eventually covered by a two-phase mixture, and the path to long-term cooling is established through pumped injection to supply makeup.

Large break LOCAs encompass a wide range of break sizes, types, and locations. During a cold leg pump discharge LBLOCA, the break disturbs the core flow such that cladding DNB occurs during the first several seconds after break opening. Breaks with cross-sectional areas in the range of 0.5 to 0.75 ft^2 may demonstrate early cladding DNB depending on the fuel design and plant boundary conditions. Any break size that experiences early DNB up to and including twice the cross-sectional area of the largest reactor coolant pipe are therefore, considered to be in the large break spectrum. Both instantaneous double-ended guillotine and longitudinal split type breaks are considered within the range of large breaks. For the longitudinal splits, breaks up to twice the cross-sectional area of the pipe are considered. Breaks can be located anywhere in the primary system piping.

Figure 4-1 illustrates the interrelation of the computer codes used for large break LOCA analysis for cold leg breaks larger than 2 ft^2. The RELAP5/MOD2-B&W (Ref. 1) code calculates system thermal-hydraulics, core power generation, and the clad temperature response during blowdown. The REFLOD3B (Ref. 2) code determines the length of the refill period and the core flooding rate during reflood. Finally, BEACH (Ref. 3), which is the RELAP5/MOD2-B&W core model with the reflood, fine-mesh rezoning option activated, determines the clad temperature response during the reflood period with input from REFLOD3B.

Cold leg break sizes between the smallest break size that predicts early DNB (the range of approximately 0.5 to 0.75 ft^2) and 2 ft^2 produce thermal-hydraulic behaviors that are transitional in nature, having both large and small break characteristics. The smaller break sizes result in slower transients in which the RVVVs can pass the steam generated in the core region directly to the break. This can occur without totally clearing a steam venting path through the lower plenum. Therefore, no refill period exists for breaks in this range. The smallest breaks may also begin

reflooding the core shortly after core flood tank (CFT) flow begins.

These smaller breaks are not limiting in terms of a peak clad temperature, but they challenge methods that are designed to analyze larger breaks that do produce limiting clad temperatures.

[ ]

with decreasing break size. Additionally, the criteria used to delineate or differentiate the phases of the transient become inconsistent. Two examples are (1) the smallest large breaks, which do not attain end of blowdown before the core has begun or even completed refill, and (2) breaks with prediction of ECCS bypass beyond the time in which the lower plenum has refilled and core reflood should have been initiated. For these reasons the methods used to analyze this range of break sizes necessarily requires a slightly altered form of the nominal LBLOCA EM. These adjustments are described in Section 4.3.7.

Hot leg breaks have many thermal-hydraulic similarities to the transitional breaks. Direct venting of core steam to the break results in no refill period. Core reflooding begins shortly after CFT flow begins. The cold leg LOCA methods are, therefore, not suitable for analyzing these breaks. The techniques used to analyze the hot leg breaks are described in Section 4.3.7.

4.3. Features of Model

This evaluation model description includes guidelines for the use and interfacing of the computer codes used for large break analysis. The following discussion is organized by subject and applies to all codes, as appropriate. The details given in Sections 4.3.1 through 4.3.6 are general features used for break

sizes greater than 2 ft^2. Where specific details apply to only one code, that condition is clearly identified. Section 4.3.7 gives features that are modified or altered specifically for use in analyzing hot leg or transition LBLOCAs.

4.3.1. System Noding

The system noding used for the blowdown analysis (RELAP5/MOD2-B&W) of Category 3 plants is shown in Figures 4-2 through 4-4. Category 1 plants use the loop noding arrangement shown in Figure 4-5. The reactor vessel upper plenum model is slightly revised from that shown in Figure 4-3, reflecting minor plenum cylinder geometrical and hydraulic differences. Category 2 plants use the RCS loop modeling from Figure 4-2 and the reactor vessel model from the Category 1 plants with appropriate hydraulic inputs.

[ ]

There are two types of steam generators found in B&W plants: once-through steam generators and integral economizer once-through steam generators. The primary tube sides are modeled similarly for the two generators. The secondary side models reflect the geometrical differences. Models will include steam generator tube plugging (SGTP) if necessary to model the actual plant configuration. The SGTP fraction should be consistent with, or slightly higher than, the actual plugging fraction in the plant.

The OTSGs have a secondary side downcomer region that extends over the lower sixty percent of the tube region. Main feedwater is injected into the top of the downcomer. Aspiration ports, or holes in the shroud between the tube nest and the upper downcomer, are also located near the top of the downcomer. The aspirator ports allow for the recirculated steam to preheat the main feedwater to near saturation before it flows to the bottom of the tube nest. Saturated and superheated fluid regions are found on the secondary side, with the aspirator ports marking the approximate transition between the two regions. The IEOTSGs have a short downcomer without aspiration ports, and therefore, no recirculating flows. The main feedwater entering the bottom of the secondary side tube nest is subcooled. This flow produces

subcooled, saturated, and superheated fluid regions as the fluid advances up the secondary side.

Five power peaks are analyzed at the midpoints between the spacer grids nearest the 2-, 4-, 6-, 8-, and 10-ft elevations. For the analyses presented herein, an axial peak of [ ] nearest the 6-ft peak was chosen. The power shapes are generated by the LYNXT (Ref. 4) power shape generator with the axial peak specified at the middle elevation between grids.

The control volume representation of the core has been verified previously for Westinghouse 4-loop designs with 17-by-17 fuel assemblies (Ref. 5). This detailed modeling is independent of fuel and plant design. Differences in fuel hydraulic behavior are accounted for in hydraulic inputs and, short of severe design alterations, do not affect the core noding. Plant variations across the categories could affect the vessel noding arrangement but, except for possible flow variations between the bypass and the average core, no alteration in core noding is required.

The noding arrangement presented in this section is applied to all large break blowdown analyses except where modifications are obviously needed to analyze specific accidents or initial system configurations, for example a change in break location. When such changes are made, details will be explained in the specific application.

[

]

[ ]

4.3.2. Sources of Heat

The heat sources used in the analysis are listed in this section. These sources are time-dependent and their representation in the computer codes depends on the phase of the accident being modeled.

4.3.2.1. Initial Power

It is assumed that the reactor has been operating continuously at the analyzed power level (which is at or above the licensed power) plus uncertainties due to power level instrument error. A value of 2 percent of rated power is used for the uncertainty unless the uncertainty is demonstrated to be smaller.

4.3.2.2. Core Peaking Factors

One purpose of the LOCA analysis is to determine the maximum allowable local heating rates for which calculated peak cladding temperatures (and other parameters) will remain below the acceptance criteria of 10CFR50.46. These maximum heating rates are then incorporated into the plant technical specifications as the LOCA limits. To accomplish this, the following procedure is used:

1. A spectrum of break sizes and locations is analyzed to establish the worst break using the mid-plane power shape and estimated peaking factors.

2. Using the worst break established in the first step, the maximum allowable local heating rate is determined for five axial levels within the core. Five calculations are performed with the location of the peak power, axial peaking, changed from approximately 2 feet to 10 feet above the bottom of the core at the midpoint between fuel spacer grid locations. For each axial power profile the peak local heating is iteratively increased in a series of runs until the maximum local heating rate that will not exceed the acceptance criteria has been determined to the accuracy desired.

3. Time-in-life studies are performed for each of the five axial power elevations. These may include consistent fuel parameter inputs from a specific time-in-life or be a composite of bounding parameters used to simulate a range of fuel pin burnup values.

As described in the RAI Response to Question 4 in Volume III page LA-92, a variety of analyses with axial power shapes at different times in life are performed to define a set of linear heat rate limits. These are established for the entire axial length (0 to 12 ft) via extensions of the five intermediate analyzed power shapes (with sensitivity studies or extrapolations to upper and lower elevation spans) for the entire range of licensed fuel burnups. Linear interpolation based on core elevation and burnup may be used for use in determining the effective peaking limits for use in core reload design analyses for elevations and burnups that are not specifically analyzed. Guidance for addressing different radial and axial peaking is provided in the RAI response Question 1 in Volume III page LA-77.

4.3.2.3. Core Stored Energy

The initial temperature distribution in the fuel is determined by an NRC-approved steady-state fuel pin model (at present TACO3 for UO_2 fuel and GDTACO for gadolinia fuel, Ref. 15 and Ref. 17, respectively). The input is consistent with the time in life, or bounds the time-in-life values for the case or range of burnup values that is under investigation in the LOCA study. The initial internal fuel pin pressure, radial fuel power shape, internal pin gas composition, and initial fuel pin oxide thicknesses are derived from the steady-state fuel code as well.

RELAP5/MOD2-B&W runs are initialized using the initial average fuel temperature from the approved steady-state fuel codes. Calculated results and input parameters from the fuel pin code (such as cladding and fuel dimensions, surface roughness, radial power shape within the fuel, gas composition, gas pressure, fuel-clad contact pressure, plenum volumes, etc.) are input. The average fuel temperatures will be adjusted using a pin gap conductance multiplier to match within 20 F, those predicted by the fuel thermal code. The initial fuel stored energy uncertainty for the hot pins, hot assembly, and average channel heat structures will be applied as approved in Revision 4 to BAW-10164P-A (Ref. 1).

4.3.2.4. Fission Heat

During blowdown, fission heat is calculated using the point kinetics model of the RELAP5/MOD2-B&W code (Section 2.3.1 of BAW-10164). The only reactivity effects modeled during blowdown for large break LOCA are the fuel temperature coefficient and the void-moderator coefficient. The effectiveness of the void-moderator coefficient in shutting down the core is so large that modeling other negative reactivities is irrelevant. The values of

the reactivity coefficients are chosen to be conservative to envelope the time in plant life for which the analyses are applicable. For nominal full power analyses, the reactivity coefficients could be consistent with the time in cycle for a specific analysis or they could use a more conservative composite set of parameters. The composite parameters may be selected, because they yield a conservative, or the least negative, reactivity feedback for all times in cycle. Partial power analyses will consider the potential for a positive moderator temperature coefficient to ensure the feedback simulated is conservative. End of cycle analyses with RCS average temperature reductions can include a negative moderator temperature coefficient that is conservative for the time in cycle that the average temperature reduction is permitted. In all cases, the spatial weighting of the reactivity factors is by the flux-squared method.

For the reflood phase, the void-moderator coefficient will become ineffective, so both safety rod insertion and borated water injection are used to maintain the reactor subcritical. No explicit calculation of fission power is made in the LOCA analyses. Rather, the fraction of the fission power to the total power at the end of blowdown is kept constant. Thus, fission power drops during reflood in direct proportion to the decay heat curve. Adequate post-LOCA shutdown margin is confirmed during the core reload process based on the minimum BWST, RCS, and CFT boric acid concentration and available rod worth with the most reactive set of rods stuck out of the core.

4.3.2.5. Decay of Actinides

Heat from the radioactive decay of actinides is included. The calculation conservatively accounts for the energy generated from the radioactive decay of actinides, including neptunium, plutonium, and the isotopes of uranium. (There is additional

information provided in the RAI response to Question 5 in Volume III page LA-94.)

4.3.2.6. Fission Product Decay

The decay heat curve described in the proposed ANS standard, "Decay Energy Release Rates Following Shutdown of Uranium Fueled Thermal Reactors" (approved by subcommittee ANS-5 in October 1971), for infinite operation times a factor of 1.2 is used for evaluating fission product heating. Figure 4-7 shows the total decay heat values (1.2 times the 1971 ANS fission plus actinides) calculated by coefficients input to RELAP5/MOD2-B&W.

4.3.2.7. Heat Distribution

The hot channel represents one fuel assembly, split into a single UO_2 hot pin and the remaining pins, which are peaked to a factor consistent with that of the highest power rod. If the fuel design uses gadolinia fuel, then additional hot pins are modeled in the hot bundle. The gadolinia fuel pins may have lower peaking to account for the material property differences.

A fraction of the neutrons and gamma particles generated in the hot channel leak into the surrounding bundles. In turn, neutrons and gamma particles from the surrounding bundles are absorbed within the hot assembly. Since the hot channel has a higher radial power, the net power deposited within the fuel of the hot channel is less than that generated within the bundle. Therefore, an energy deposition factor is used within the analyses to account for the fraction hot channel power that originates within the fuel pellet of the hot channel. The fraction of the power lost from the hot channel (sometimes referred to as power flattening) is deposited uniformly in the fluid of the average channel.

The power at the peak in the core (PLP) is evaluated by the following formula:

$$PLP = \frac{(1.0 + U) \times kW \times P_f \times F \times P(t)}{\text{total pin feet in core}}, \qquad (4\text{-}1)$$

where

PLP = (peak linear power) linear heating rate, kW/ft,
kW = rated power, kW,
P_f = total peaking factor,
F = appropriate power distribution factor, and
P(t) = normalized transient power,
U = Fractional power level increase to account for uncertainties. It is taken as 0.02 unless the plant has installed equipment that can be used to justify reduced instrument uncertainties.

4.3.2.8. Metal-Water Reaction

The rate of energy release from metal-water reaction is calculated using the Baker-Just equation without steam limiting. In the RELAP/MOD2-B&W and BEACH codes, the implicit formulation of the rate equation is applied to the outside of the cladding and to the inner cladding surface if rupture has occurred. Oxide thinning is considered only in the plastic or ruptured condition in RELAP5/MOD2-B&W and BEACH. For this purpose, the axial dimension of the rupture location is considered to be at least 3 inches. The calculations for metal-water reaction are outlined in Section 2.3.2.4 of BAW-10164 (RELAP5/MOD2-B&W).

The initial oxide thicknesses on the outside and inside cladding surfaces are consistent with or less than the time in life used for the specific analysis. The reference weight gain oxidation curves for Zircaloy-4 exposed to either a water or steam environment are given in Figure 4-8. These data are used to develop the outside oxide layer thickness for analyses with Zircaloy-4 cladding. The data, indicated by the heavier lines in the figure, are based on the curves published by Bettis in WAPD-MRP-107 (Ref. 6). The lines of intermediate weight are an interpolation of the experimental data based on WCAP-3269-56 (Ref. 7). The 680 F oxidation curve was shifted to the left to form a transition point at 110 days, compared with the commonly accepted transition point of 120 days. This shift reflects the results obtained by BWNT on Zircaloy-4 cladding material tested in a reactor system water environment (Ref. 14). A relationship between burnup and effective reactor full power days can be established from the steady-state fuel code. Using this

relationship, the outside oxide layer weight gain can be determined. The conversion factor, 390 mg/(dm^2-mil), is used to determine thickness from weight gain.

Figure 4-9 shows the weight gain oxidation curves for the inside surface of Zircaloy-4 cladding to be used during hot functional testing of the reactor prior to going critical. These curves, based on the data in WAPD-MRP-107, are used to account for the moisture fabricated into the fuel pellets. Once the reactor goes critical, the curve shown in Figure 4-10 is used to represent the inside oxide buildup on Zircaloy-4 cladding resulting from the oxygen generated by the fissioning of UO_2. This curve is based on data reported in BAW-1716 (Ref. 8) and BAW-1874 (Ref. 13). The results of Figure 4-9, added to the data reported in Figure 4-10, give the total inside oxide thickness.

The oxidation increase for M5 cladding is lower than that for Zircaloy-4 as shown in Figure 3-4 of BAW-10227P-A (Ref. 19). The model used for Zircaloy-4 is very conservative lower bound of the data. The M5 outside oxidation thickness data is shown in Figure 3-1 of BAW-10227P-A. The initial oxidation thickness model used for Zircaloy-4 is a conservative lower bound for the M5 material, therefore the outside oxidation model described for Zircaloy-4 is applicable to M5 cladding as well.

4.3.2.9. Primary Metal Heating

Heat transfer from piping, vessel walls, and non-fuel internal structures is taken into account. Appropriate metal slabs are simulated in each control volume of RELAP5/MOD2-B&W. REFLOD3B also models these heat slabs using lumped parameter methods. The

general heat slab model for RELAP5/MOD2-B&W is explained in Section 2.2 of BAW-10164. The primary metal heating model for REFLOD3B is described in Section 2.9 of BAW-10171. A previous sensitivity study on the effect of increasing the primary heat addition (Section 5.7 of topical report BAW-10091) showed minimal effect for this heat source in large break applications.

4.3.2.10. Primary-to-Secondary Heat Transfer

Heat transfer between the primary system and the secondary sides of the steam generators is calculated during all phases of the LOCA. During blowdown, the steam generator tubes are modeled as a boundary across which heat is transferred using the models and heat transfer correlations described in Section 2.2 of BAW-10164 (RELAP/MOD2-B&W). During the reflood phase of the transient the heat is transferred using the model described in Section 2.10 of BAW-10171 (REFLOD3B). A conservatively high steam generator heat transfer coefficient is input in REFLOD3B so that all incoming primary side fluid is vaporized and superheated to the secondary side saturation temperature.

4.3.3. Swelling, Rupture, and Thermal Properties

4.3.3.1. Swelling

Clad thermal expansion, elastic swelling, and plastic deformation are considered in the analysis prior to rupture. The specifics of the models are detailed in the RELAP5/MOD2-B&W and BEACH topical reports (Section 2.3.2 in BAW-10164 and Section 2.2 in BAW-10166). Appendix K requires that clad swelling and rupture calculations be based on applicable data such that the degree of swelling and the incidence of rupture are not underpredicted. In order to establish an industry data base, the NRC has sponsored research

programs on cladding behavior during and after a LOCA. NUREG-0630 (Ref. 9) is based on this research and contains models for clad rupture, strain, and blockage for Zircaloy-4 during and following a LOCA.

The rupture model used for Zircaloy-4 is an implementation of the NUREG-0630 correlations:

1. Rupture temperature is determined by linear interpolation between the NUREG-0630 fast and slow ramp rate rupture temperature versus stress curves, Figure 4-11. The ramp rate for a given location is taken as the instantaneous normalized heating rate for elastic strains. A plastic-weighted, time-averaged heating rate is used after the initiation of plastic deformation at that location.

2. Cladding strain at rupture is also an interpolation between the NUREG-0630 fast and slow ramp rate strain curves, Figure 4-12, based on the plastic-weighted, time-averaged ramp rate after initiation of plastic strain.

3. The coolant flow blockage is an interpolation of the NUREG-0630 curves, Figure 4-13, based on ramp rate.

The rupture model used for M5 cladding is based on the correlations approved in BAW-10227P-A (Figures K-5.9 and K-5.10 Ref. 19). The rupture temperature, cladding strain, and coolant flow blockage for M5 are given in Appendix C of BAW-10227P-A. These fast and slow ramp rate data for M5 cladding are implemented in the same manner as described for Zircaloy-4.

4.3.3.2. Rupture

The effects of rupture are modeled in RELAP5/MOD2-B&W and BEACH. These codes compute transient pin internal pressure and utilize the resultant cladding hoop stress to determine the occurrence of rupture. Once a rupture has occurred, the effects of the cladding strain are imposed on the solution and the problem evaluation continues.

The initial internal pin pressure is either (1) that which occurs at the burnup for which peak cladding temperature is being analyzed, or (2) a pressure that is higher than the highest pressure expected during the time in life of the fuel being evaluated. If the bounding pressure is used, the remaining burnup-dependent fuel parameters are taken at the burnup for which their values, independent of the pin pressure, would produce the highest peak cladding temperature.

The pin pressure calculated at any time is used to determine the cladding hoop stress. The rupture model determines the rupture temperature as a function of the hoop stress using the data from Figure 4-11 for Zircaloy-4 or Figure K-5.11 (0 C/s for Slow Ramp) and Figure K-5.12 (28 C/s for Fast Ramp) of BAW-10227P-A for M5. The calculated cladding temperature is compared continuously to the rupture temperature and, if that temperature is exceeded, then rupture occurs. Once rupture has occurred in a channel, it cannot occur at any other location in that same channel. The details of the models are shown in Section 2.3.2 of BAW-10164 (RELAP5/MOD2-B&W) and Section 2.2 of BAW-10166 (BEACH).

If rupture is predicted to occur ($T_{clad} \geq T_{rupt}$) the internal pressure of the ruptured pin is set equal to the coolant pressure, thereby removing the pressure-induced stress in the cladding. The final cladding deformation and flow blockage for the ruptured pin become functions of the plastic strain at the time of rupture. Using the rupture temperature, the strain at rupture and the flow

blockage for Zircaloy-4 cladding are determined from the data in Figures 4-12 and 4-13, respectively. In a similar manner, the strain at rupture and the flow blockage for M5 cladding are determined from the data in Figures K-5.9 and K-5.10 of BAW-10227P-A (Ref. 19).

[ ]

4.3.3.3. Gap Models

The gap models used to determine the mechanical response of the gap between the fuel and cladding include fuel radial expansion

and clad swelling and rupture. The clad swelling and rupture is based on NUREG-0630 for Zircaloy-4 or the data from BAW-10227P-A for M5. The gap conductance model is based on the GAPCON-THERMAL-2 (Ref. 12) code. The details of these models are documented in Section 2.3.2 of the RELAP5/MOD2-B&W topical report and Section 2.2 of the BEACH topical report.

4.3.3.4. Other Thermal Parameters

The thermal and mechanical properties of the fuel and clad are based on current nuclear industry materials data. The material properties as used in the LOCA analysis models reflect temperature-dependent behavior during the transient. The conductivity of the gas in the fuel pin gap is calculated using kinetic theory which includes the effect of temperature. The details of these calculations are presented in Section 2.3.2 and Appendix E of the RELAP5/MOD2-B&W topical report. The thermal and mechanical properties used in BEACH are the same as those described in RELAP5/MOD2-B&W.

The impact of replacement rods (e.g. stainless steel or low enriched uranium) on the LOCA evaluation will be considered as required by the SER of BAW-2149-A (Ref. 18).

4.3.4. Blowdown Phenomena

4.3.4.1. Discharge Model

The discharge of subcooled fluid through the break is determined using the Extended Henry-Fauske model. Once the fluid in the break control volume saturates, the discharge rate is based on the Moody model using Moody slip. To avoid a step change in the flow between the models, a 0.001 quality criterion (e = 0.001 in the

equation on page 2.1-109 of BAW-10164) is used to transition between the Extended Henry-Fauske and Moody models. The Murdock-Bauman model is used for superheated discharge. The break flow is the minimum of the choked flow and the flow calculated by the momentum equations. Section 2.1.4 of the RELAP5/MOD2-B&W topical report describes the discharge models and the assumptions regarding their use.

A range of discharge coefficients is evaluated in the spectrum analysis. The coefficients are applied to both double-ended and split type breaks. Appendix A Section A.6.1 provides the spectrum of breaks extending from $C_D = 1.0$ to $C_D = 0.4$.

4.3.4.2. End of Bypass

The end of bypass is defined as the point ECCS injection begins to penetrate into the downcomer toward the lower plenum. The end-of-bypass period begins with partial penetration of the ECCS fluid on the side of the downcomer most removed from the high steam velocities that exist near the broken cold leg inlet nozzle. Complete end of bypass occurs when the steam velocities in the upper downcomer are insufficient to entrain any ECCS injection out

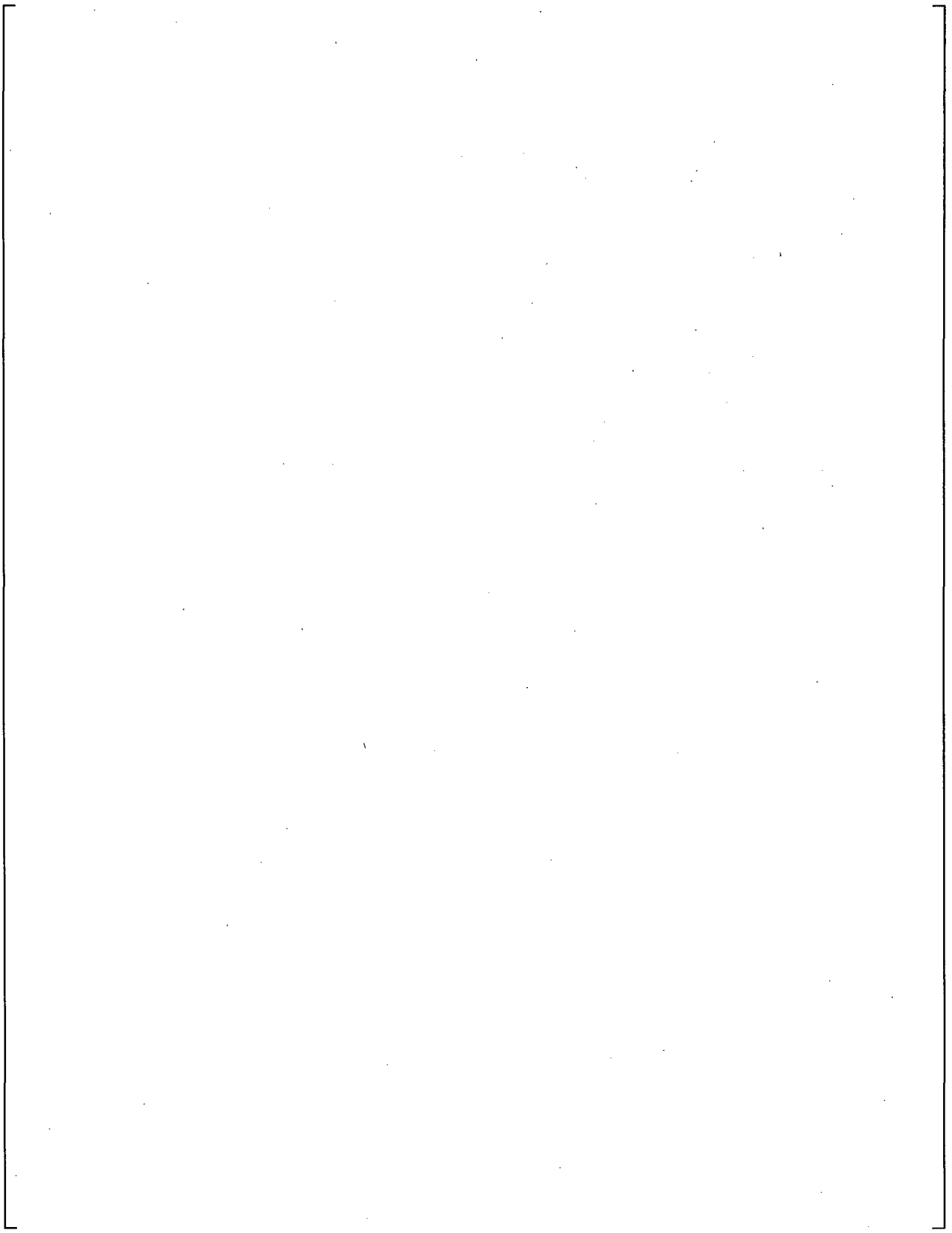

[

]

(Note that the RAI response to Question 4 in Volume III page LA-20 provides additional information on this section.)

4.3.4.3. Momentum Flux

Flow between adjoining control volumes is determined by the phasic momentum equations in RELAP5/MOD2-B&W and by a mixture momentum equation in REFLOD3B. Included in the formulation of the momentum equation are terms that account for (1) time rate of change of momentum, (2) momentum convection, (3) momentum change due to compressibility, (4) momentum flux resulting from area change, (5) pressure loss resulting from wall friction, (6) pressure loss due to area change, and (7) gravitational acceleration. The derivation of the governing fluid flow equations used in RELAP5/MOD2-B&W is given in Section 2.1 of BAW-10164. The derivation and application of the momentum equation used in REFLOD3B is given in Section 2.2.1 and Appendix C of BAW-10171. The momentum equation used in the BEACH code is the same as that of RELAP5/MOD2-B&W.

4.3.4.4. Frictional Pressure Drop

The RELAP5/MOD2-B&W, REFLOD3B, and BEACH computer codes consider friction and form losses. A description of the RELAP5/MOD2-B&W calculation is given in Section 2.1.3 of BAW-10164; REFLOD3B is given in Section 2.0 of BAW-10171; and BEACH is presented in Section 2.1.3 of BAW-10166. The friction and form losses are calculated for the system using best estimate techniques and normalized to available plant or experimental data. The RELAP5/MOD2-B&W code accepts surface roughness and form loss factors as input. Frictional losses are calculated by the code based on the flow conditions and the input surface roughness terms. The frictional terms used in the REFLOD3B code are taken from the initialized RELAP5/MOD2-B&W run by combining terms where a REFLOD3B path encompasses more than one RELAP5/MOD2-B&W path. The BEACH code models separated channels that use the blowdown surface roughness for the frictional loss calculation. The form loss for the grids in BEACH is derived from fuel bundle pressure drop measurements conducted on prototype assemblies. This form loss also corresponds to that used in the RELAP5/MOD2-B&W core model.

4.3.4.5. Pump Model

The RC system centrifugal pump model employed by RELAP5/MOD2-B&W is described in Section 2.1.5.2 of topical report BAW-10164. The model is based on homologous relationships and includes default Westinghouse single- and two-phase performance characteristics. The RELAP5/MOD2-B&W plant specific pump performance tables are given as input for the model to determine dynamic pump conditions during the transient. For each design class analyzed, selection of the pump homologous two-phase difference curve and void-dependent multiplier will be based on reference to an applicable sensitivity study that confirms the conservative application of

the pump model. A constant, locked rotor, flow resistance is used for the REFLOD3B pump simulation to maximize the steam binding effects during the reflood phase.

4.3.4.6. Core Flow

[

]

Filtered RELAP5/MOD2-B&W hot channel core flow is used in the hot channel blowdown heat transfer calculations. This flow is obtained by passing the individual phasic mass fluxes through the equation for a low-pass filter:

$$\frac{dZ}{dT} = -P(Z-W) \qquad (4\text{-}2)$$

where

W = phasic mass flux,
Z = filtered mass flux, and
P = break frequency.

The break frequency is set to remove perturbations with periods less than 0.1 seconds. The filtered phasic mass fluxes are summed to give the total filtered mass flux.

4.3.4.7. Pre-CHF Core Heat Transfer

Pre-CHF (critical heat flux) heat transfer is by convection in single-phase liquid, nucleate boiling, and forced convection vaporization. For the single-phase liquid convection regime, the maximum of the Dittus-Boelter or Rohsenow-Choi correlations is used. Heat transfer for nucleate boiling and forced convection vaporization regimes is by a combination of the Chen, Thom, and Schrock-Grossman correlations. Switching logic and details for the correlations are found in Sections 2.3.3 and 2.3.3.2 of the RELAP5/MOD2-B&W topical report.

4.3.4.8. Core CHF Models

The fuel design determines the appropriate CHF correlation used for DNB safety analyses. The LOCA analyses will use the same CHF correlation that is used for the fuel pin DNB analyses. The core CHF model options available in RELAP5/MOD2-B&W include B&W-2, BWC, BWCMV, BWUMV, and BHTP, all for high flow, high pressure applications. In addition, the RELAP5/MOD2-B&W code has the general form of the BWU and BHTP correlations that will accept user input coefficients. These general options were added to RELAP5/MOD2-B&W in the event future fuel design changes require new inputs. These general forms will not be used without

additional justification for their application. The high pressure CHF correlation is used with the Barnett and modified Barnett correlations to cover the full pressure, high flow range. In the low flow regime, a combination of MacBeth and Griffith correlations is used. For all regimes, a minimum CHF value of 90000 BTU/hr-ft^2 is used. Switching logic and descriptions of the correlations are found in Sections 2.3.3 and 2.3.3.3 of the RELAP5/MOD2-B&W topical report.

4.3.4.9. Core Post-CHF Heat Transfer

The post-CHF heat transfer regimes in the core model include transition boiling, film boiling, and single-phase steam heat transfer. Once CHF has been exceeded, no return to pre-CHF correlations is allowed in RELAP5/MOD2-B&W. The transition boiling correlation of McDonough, Milich, and King is used to connect the regimes of nucleate and film boiling. The maximum of the transition boiling and film boiling correlations is used only as long as the fuel pin cladding temperature remains within 300 F of the saturated fluid temperature. If the transition boiling correlation predicts a heat flux which would exceed that calculated by pre-CHF correlations, then a temporary switch to film boiling is used. Once the 300 F margin has been exceeded, the transition boiling correlation is not reapplied for the remainder of the blowdown phase of the transient. The maximum of the [Condie-Bengston] and Rohsenow-Choi correlations is used in the film boiling regime. The single-phase heat transfer to steam correlation is the sum of a convective term and a radiation term. The convection heat transfer is the maximum of the McEligot or Rohsenow-Choi correlations. The radiation heat transfer is from the Sun correlation. Sections 2.3.3 and 2.3.3.4 of the RELAP5/MOD2-B&W topical report explain the calculations performed for post-CHF heat transfer.

4.3.5. Single Failure

The ECCS system is made up of redundant trains of pumped injection systems providing high and low pressure injection capability. One of these trains will be assumed as nonfunctional, if that assumption is conservative. The operation of an injection system during large break LOCA can cause two effects. First, the availability of more ECCS water can increase the water level in the downcomer faster and create higher initial core flooding rates. Second, higher ECCS injection rates allow more steam condensation in the upper downcomer region and can spill more subcooled water out of the break reducing the containment and the RCS system pressure. The condensation reduces the downcomer elevation head and a reduction in RCS system pressure during reflood creates more steam binding. Together they generally both act to reduce the core reflood rate. Thus, assuming a failure of one train of ECCS can be either conservative or nonconservative depending on the design of the NSSS. If the downcomer can be kept full of water throughout most of the reflood phase by one ECCS train, then the effect of adding a second train is to increase the condensation and spillage of cold water through the break with an attendant reduction of core flooding rate. Conversely, if a single ECCS train cannot maintain the downcomer full, a second ECCS system may increase the reflooding rate. For current ECCS designs, a single ECCS train is expected to maintain a full downcomer. Therefore, the full ECCS injection may be the most limiting condition for analyzing the reflooding phase of the LOCA.

For each design class analyzed, a sensitivity study will be conducted to determine if a single failure of the ECCS system would be conservative. If so, a single diesel and all of the ECCS powered by it will be assumed inoperative. If the failure would be nonconservative, all ECCS systems will be considered operative.

4.3.6. Post-Blowdown Phenomena

4.3.6.1. Containment Pressure

The evaluation of a postulated LOCA assumes a conservative (minimum) containment backpressure during reflood. The selection of the actual pressure for the containment will be done on a plant specific basis using CONTEMPT (Ref. 10) analyses or justifications to previous analyses that conform to this evaluation model.

In general, the evaluation of minimum containment backpressure includes the following assumptions:

1. Maximum cooling from building cooling systems is available at the earliest time consistent with no loss of off-site power. The cooling water for these systems is as cold as possible within the design of the systems.

2. The number of ECCS injection trains used in the containment pressure analysis is consistent with or higher than the number used in the LOCA PCT analysis. Use of all pumped injection trains results in the lowest containment pressure, however, the additional injection may be nonconservative for clad cooling.

3. The containment volume is taken as the design volume plus the uncertainty in volume.

4. The area and mass of the building heat sinks are taken as the maximum values as determined by the building designer.

5. Initial containment conditions are taken as the reasonable conditions that will produce a minimum containment pressure response.

6. All spilled ECCS water is mixed with the containment atmosphere.

7. The containment model utilizes the following conservative condensing heat transfer coefficients for heat transfer to the exposed static heat sinks during the blowdown and post-blowdown phases of the accident:

   a. At the end of blowdown, a maximum condensing heat transfer coefficient four times higher than that calculated using the Aerojet Tagami correlation is assumed

$$h_{max} = F \cdot h_{Tagami} = F \cdot 72.5 \left(\frac{Q}{V \cdot t_p} \right)^{0.62} \qquad (4\text{-}3)$$

where

h_{max} = maximum heat transfer coefficient, (Btu/hr-ft^2-F),

Q = primary coolant energy deposition to containment at end of blowdown, (Btu),

V = net free containment volume, (ft^3),

F = Tagami multiplier = 4.0, and

t_p = time interval to end of blowdown, (sec).

Before the end of blowdown, a linear increase from

$h_{initial}$ = 8 Btu/h-ft^2-F,

to the specified peak value is assumed.

b. During the long-term stagnation phase of the accident, characterized by low turbulence in the containment atmosphere, condensing heat transfer coefficients equal to 1.2 times that obtained from the Uchida data is assumed. The Uchida heat transfer coefficients are shown in Table A-1 of BAW-10095 (CONTEMPT).

c. The heat transfer coefficients during the transition phase between the end of blowdown and the long-term, post-blowdown phase, are smoothed via an exponential decay term. A reasonably conservative decay constant of 0.0255 or the NRC recommended value of 0.025 can be used.

4.3.6.2. Reflood Rate Calculations

The evaluation of the LOCA during the refill and reflood phases is done using the REFLOD3B code. The REFLOD3B topical report (BAW-10171) includes a description of the model and the calculational assumptions.

The fuel pin model used in REFLOD3B is described in Section 2.6 of the topical report. All sensible heat (stored energy plus decay heat) in the fuel is placed at the radius corresponding to the average fuel temperature. A constant fuel conductivity and gap conductance are used in the model. The variables used will be chosen conservatively to maximize heat removal from the fuel.

[

]

[ ]

by CONTEMPT. This process, used only in the REFLOD3B code, leads to higher heat transfer coefficients than those obtained from variable flooding rates and will maximize heat removal from the core. (There is additional information provided in the RAI response to Question 5 in Volume III page LA-25.)

Calculations of liquid entrainment during reflood are based on the BWNT carryout rate fraction correlation, CRF3, which was derived from the PWR FLECHT data. The heat released by the uncovered portion of the core is used to vaporize entrained water and increase the exit quality at the top of the core. This procedure is not directly related to the CRF3 correlation and does not alter the calculated carryout. The development of this correlation is described in Section F-2 of the REFLOD3B topical report.

The reflood rate generally increases for a short time period when the core flood tank empties. The flooding rate response is a result of an increase in the downcomer pressure after the loss of steam condensation on the core flood tank injection. The rapid increase in the core inlet flow would momentarily augment the BEACH cooling. The spike will be artificially removed to conservatively avoid any additional cooling associated with this spike, particularly should the timing coincide with the time of peak cladding temperature. If the peak has already occurred, then removal of the spike is not necessary.

4.3.6.3. Core Flood Tank Cover Gas

The effect of the gas discharged after the core flood tank water is discharged is a slight increase in downcomer pressure and a momentary increase in the flooding rate. Hence, the effect of the core flood tank cover gas will be neglected.

The effect of dissolved gases in the injected core flood tank water on the downcomer density is also negligible. Of the gas initially dissolved in the core flood tank water, the amount above the solubility limit of water at the downcomer condition will separate from the solution upon injection, remain in the upper region of the downcomer, and be passed out of the downcomer through the break. The gas remaining in solution has no effect on the downcomer so long as it remains in solution. Should this gas separate from the solution in the lower region of the downcomer it will have a small, negligible impact on the fluid density. Solubility curves can be used to yield

$$V_s = K(T) P_g \qquad (4\text{-}4)$$

where

P_g = partial pressure of nitrogen,

V_s = dissolved gas volume in water at standard pressure and temperature per unit mass of water, and

$K(T)$ = rate constant depending on temperature T.

Assuming an ideal gas law, the volume ratio between two different states is given by

$$\frac{V_2}{V_1} = \frac{P_1 T_2}{P_2 T_1} \qquad (4\text{-}5)$$

Thus, the volume of the dissolved gas in the downcomer at the downcomer conditions is

$$V_g = \frac{K(T)\,P_s\,T_g}{T_s}, \qquad (4\text{-}6)$$

where

P_s = 14.7 at standard pressure, psia,

T_s = 530 at standard temperature, R, and

T_g = downcomer temperature, R.

Thus, the reduced downcomer density (if this gas comes out of solution) is

$$\rho = \left[\frac{62.4}{1+\frac{K(T)\,(14.7)\,T_g}{530}}\right], \text{ lbm/ft}^3 . \qquad (4\text{-}7)$$

Assuming that the nitrogen gas is in thermal equilibrium with the downcomer water, $T_g = T_{H2O}$, in the range T_{H2O} = 70 to 280 F, K(T) is approximately constant and equal to 0.001. Using a value of T_g = 280 F results in the maximum density decrease, which is given by

$$\frac{\Delta\rho}{\rho} = \frac{K(T)\,(14.7)\,(280+460)}{530} = 0.0205. \qquad (4\text{-}8)$$

This is a negligible decrease in downcomer density. Thus, the effect of dissolved gases in the core flood tank water need not be considered in REFLOD3B calculations.

4.3.6.4. Steam Venting and Steam-Water Interaction

For all B&W-designed plant analyses, credit is taken during the reflood period for steam flow through any cold legs in which the pump suction piping is not blocked by a liquid loop seal at the end of blowdown. Steam flow through the reactor vessel vent valves and open cold legs is permitted. As part of the REFLOD3B input, flow resistance factors (K-factors) for friction and form losses in the loop at steady-state flow are provided. For transient flow, the friction resistance factor is adjusted by the ratio of the friction factor for the transient flow to that of the steady-state flow. The friction resistance factors are modified by Martinelli-Nelson two-phase multipliers, which are functions of upstream quality and pressure and are given in Appendix B of BAW-10171. These values are curve fitted using a third degree polynomial surface fit to determine values between stored entries. The form resistance factor remains constant throughout the transient. (There is additional information provided in the RAI response to Question 6 in Volume III page LA-26.)

[ ]

The leak flow calculation during reflood is discussed in Section 2.8 of the REFLOD3B topical report. A variable containment backpressure is input into REFLOD3B. The values input will be

4.3.6.5. Heat Transfer

During the refill period (the time between the end of blowdown and the beginning of reflood), the core is considered to undergo a

nearly adiabatic heatup. This period is modeled in BEACH by specifying a zero flow core inlet boundary condition with a time-dependent upper plenum pressure control volume. These boundary conditions minimize the heat transfer and approximate a near-adiabatic heatup in the thermal analysis. The ECC water transport time delay, which accounts for the water injected at the top of the downcomer to fall to the lower plenum, is calculated and used to increase the adiabatic heatup period.

Using the flooding rates from REFLOD3B and the fuel pin conditions from the end of blowdown from RELAP5/MOD2-B&W, the BEACH code calculates the fuel pin heatup during the reflood period. The BEACH code is the RELAP5/MOD2-B&W code with the fine mesh rezoning model and the "NEWQUEN" heat transfer option activated. The noding arrangement for the BEACH analysis is shown in Figure 4-14. The code is described in topical report BAW-10166. The topical report includes benchmark comparisons to FLECHT-SEASET, CCTF, SCTF, G-2 and REBEKA-6 tests.

(There is additional information provided in the RAI response to Question 26 from Volume III page LA-57.)

4.3.7. Revised EM for Transition and Hot Leg LOCAs

The small or transition cold leg LBLOCAs and hot leg LBLOCAs are not limiting from a peak cladding temperature perspective due to three factors: (1) high positive core flows, (2) more ECC fluid reaching the lower plenum, and (3) no adiabatic heatup period. Core flows generally remain in the positive direction for the transition breaks because the smaller break sizes do not reverse the core flow upon initiation. The slower transient reduces the core flashing and boiling contribution such that all of the core steam can be vented through the RVVVs for cold leg break simulations. Hot leg breaks accelerate positive flows through the

core because of the break location. In either break classification, the positive flows act to postpone DNB and improve fuel pin heat transfer during blowdown. The positive core flows also ensure that a larger fraction of ECC fluid reaches the lower plenum and core. Therefore, the lower plenum is refilled by the time the end of blowdown is reached. Without a refill period, no adiabatic heatup occurs. The cumulative result is that the cladding temperatures are quite low compared to the limiting, large cold leg breaks.

The methods used to demonstrate compliance with 10CFR50.46 for transitional cold leg LBLOCAs or any hot leg LBLOCA differ from

[ ]

steam venting path is available to the core exit, the lower plenum need not be voided to provide additional venting. The liquid remaining in the lower plenum allows reflood to begin at the end of blowdown. Absence of a refill phase leaves only the blowdown and reflood phases of the transient. RELAP5/MOD2-B&W can calculate both of these phases without the REFLOD3B system calculation. Several changes to the input model, described in Sections 4.3.1 through 4.3.6 and in Tables 9-1 and 9-2, are also needed to allow the analysis of these classes of breaks. The slight alterations from the general models are described in the following two subsections for the transitional cold leg LOCAs and the hot leg LOCAs, respectively.

(There is additional information provided in the RAI response to Question 2 from Volume III page LA-90.)

4.3.7.1. Transition Cold Leg LOCA Methods

RELAP5/MOD2-B&W is used exclusively to perform the entire transient for cold leg break sizes that experience early DNB (generally 0.5 to 0.75 ft^2) up to 2 ft^2. Various modeling techniques are changed to simulate the entire transient without the REFLOD3B code. They include the following list of items.

[

]

4.3.7.2. Hot Leg LOCA Methods

RELAP5/MOD2-B&W is used exclusively to perform the entire transient. Various modeling techniques are changed to simulate the entire transient without the REFLOD3B code. They include the following list of items.

[

]

4.4. Compliance of Model

This section shows that the features of the large break evaluation model described in Section 4.3 conform to the required features of the evaluation model set forth in Appendix K. To accomplish this, the organization of this section parallels that of Appendix K, and references are made to the appropriate parts of Section 4.3.

I. Required and Acceptable Features

A. Heat Sources During LOCA

As required, the initial power considers the rated or conservatively high power that is further increased to account for such uncertainties due to power level instrumentation error (Section 4.3.2.1). A value of 1.02 is used for the uncertainty factor unless the plant can justify a lower uncertainty. The method by which a series of power shapes will be analyzed effectively encompasses the requirements of this paragraph (Section 4.3.2.2).

A.1. Initial Stored Energy of Fuel

The initial fuel temperatures are consistent with an approved steady-state evaluation code (Section 4.3.2.3) and include appropriate uncertainties as discussed in Section 4.3.2.3. The gap model and other variables of concern are determined as a function of burnup and temperature (Sections 4.3.3.3 and 4.3.3.4).

(There is additional information provided in the RAI response to Question 8 from Volume III page LA-29.)

A.2. Fission Heat

Section 4.3.2.4 of the model directly incorporates all of the requirements of this section of Appendix K.

A.3. Decay of Actinides

The level of actinide heating is higher than that proposed by the ANS standard (Section 4.3.2.5).

(There is additional information provided in the RAI response to Question 5 from Volume III page LA-94.)

A.4. Fission Product Decay

The ANS curve is multiplied by 1.2 (Section 4.3.2.6).

A.5. Metal-Water Reaction Rate

Section 4.3.2.8 of the model directly incorporates all of the requirements of this section of Appendix K.

A.6. Reactor Internals Heat Transfer

Section 4.3.2.9 of the model directly incorporates all of the requirements of this section of Appendix K.

A.7. Pressurized Water Reactor Primary-to-Secondary Heat Transfer

Section 4.3.2.10 of the model directly incorporates all of the requirements of this section of Appendix K.

B. Swelling, Cladding Rupture, and Fuel Rod Thermal Parameters

Sections 4.3.3.1 through 4.3.3.4 of the model directly incorporate all of the requirements of this section of Appendix K.

C. Blowdown Phenomena

C.1. Break Characteristics and Flow

C.1.a. Spectrum of Breaks

A spectrum of breaks will be analyzed (Sections 4.2, 4.3.2.2 and 4.3.4.1).

C.1.b. Discharge Model

The discharge model conforms to the conditions of this paragraph (Section 4.3.4.1). The required series of discharge coefficients will be applied to double-ended and split ruptures (Section 4.3.4.1). The possible worst-case smaller break is allowed for by analyzing a series of breaks.

C.1.c. End of Blowdown

End of blowdown is defined as the time when the reactor vessel upper plenum pressure is less than or equal to the containment pressure.

C.1.d. Noding Near Break and ECCS Injection Points

The areas have been investigated for spatial convergence (Section 4.3.1).

C.2. Frictional Pressure Drops

Section 4.3.4.4 of the model directly incorporates all of the requirements of this section of Appendix K.

C.3. Momentum Equation

All terms of the momentum equation are included in the RELAP5/MOD2-B&W and REFLOD3B codes (Section 4.3.4.3).

C.4. Critical Heat Flux

The correlations employed are acceptable as set forth in Section 4.3.4.8. A conservative approach is used with respect to the condition of return to nucleate boiling following calculation of CHF (Section 4.3.4.9).

C.5. Post-CHF Heat Transfer Coefficient

The correlations and method of application used for post-CHF heat transfer are acceptable (Section 4.3.4.9).

C.6. Pump Modeling

The pump model conforms to the requirements of this paragraph in that it is dynamic, obtained from experimental data, and contains allowance for two-phase degradation (Section 4.3.4.5).

C.7. Core Flow Distribution During Blowdown

The hot region is taken as one fuel assembly for hydrodynamic modeling (Section 4.3.1). Crossflow and possible bundle blockage are considered (Section 4.3.4.6). The hot region flow is smoothed by an appropriate filter for use in the heat transfer correlations (Section 4.3.4.6).

D. Post-Blowdown Phenomena -- Heat Removal by ECCS

D.1. Single Failure Criterion

The selected treatment of this criterion will maximize the calculated cladding temperature based on appropriate sensitivity studies (Section 4.3.5).

D.2. Containment Pressure

A conservative containment pressure will be used to underpredict the pressure response (Section 4.3.6.1).

D.3. Calculation of Reflood Rate for PWRs

Reflood rates are calculated by a dynamic code (REFLOD3B) that fully accounts for the transient properties of the system and the fluid. The pump rotor is modeled in its most resistive condition, where credit is taken for flow through it (Section 4.3.6.4). The carryover rate fraction has been developed from the FLECHT-SEASET experiments (Section 4.3.6.2). The effects of core cover gas have been considered.

This section applies directly to the REFLOD3B code. Therefore, it is not directly applicable to the hot leg and transition LOCAs, which are calculated exclusively with RELAP5/MOD2-B&W and BEACH. BEACH has been benchmarked against FLECHT-SEASET experiments. A comparison to the REFLOD3B results is also included in Section A.6.4 to confirm the validity of BEACH for these special applications. The pump rotors were allowed to spin freely as discussed in Section 4.3.7.

(There is additional information provided in the RAI response to Question 9 from Volume III page LA-29.)

D.4. Steam Interaction with ECC Water in PWRs

Steam interaction has been considered by increasing the resistance to flow for ECC water entering the reactor vessel (Section 4.3.6.4).

This section applies directly to the REFLOD3B code. Therefore, it is not directly applicable to the hot leg and transition LOCAs, which are calculated exclusively with RELAP5/MOD2-B&W and BEACH. For these special applications, the CFT line resistance has been increased by a factor of ten, which reduces the ECC water entering the reactor vessel.

(There is additional information provided in the RAI response to Question 9 from Volume III page LA-29.)

D.5. Refill and Reflood Heat Transfer for PWRs

During refill the heatup is assumed to be nearly adiabatic (Section 4.3.6.5.). The correlations used for hot channel reflood heat transfer have been compared with the FLECHT-SEASET data (see Appendix G and H of BAW-10166P-A).

This page is intentionally left blank.

FIGURE 4-1. LARGE BREAK ANALYSIS CODE INTERFACE.

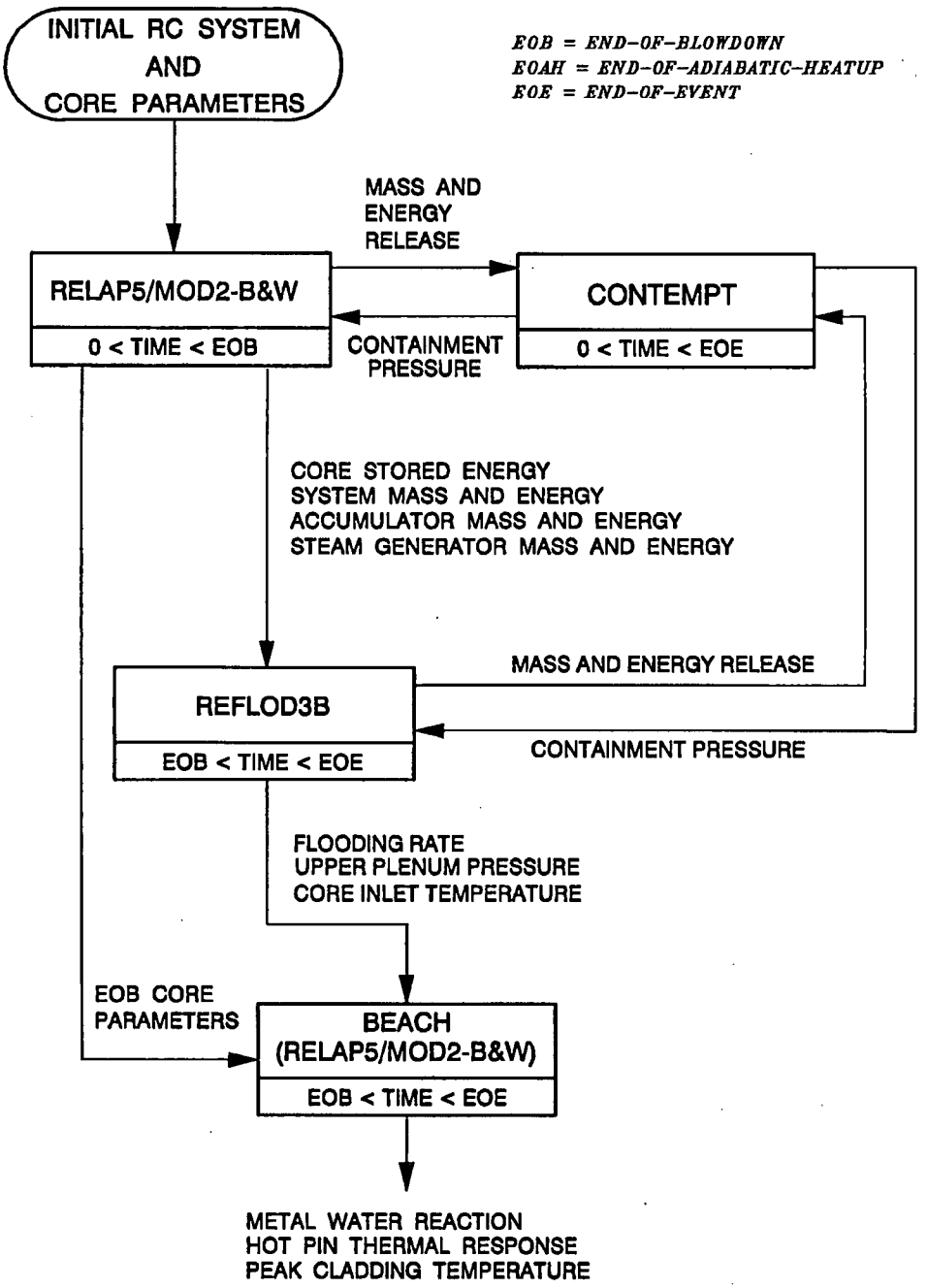

FIGURE 4-2. LBLOCA LOOP NODING ARRANGEMENT (205 RL PLANT).

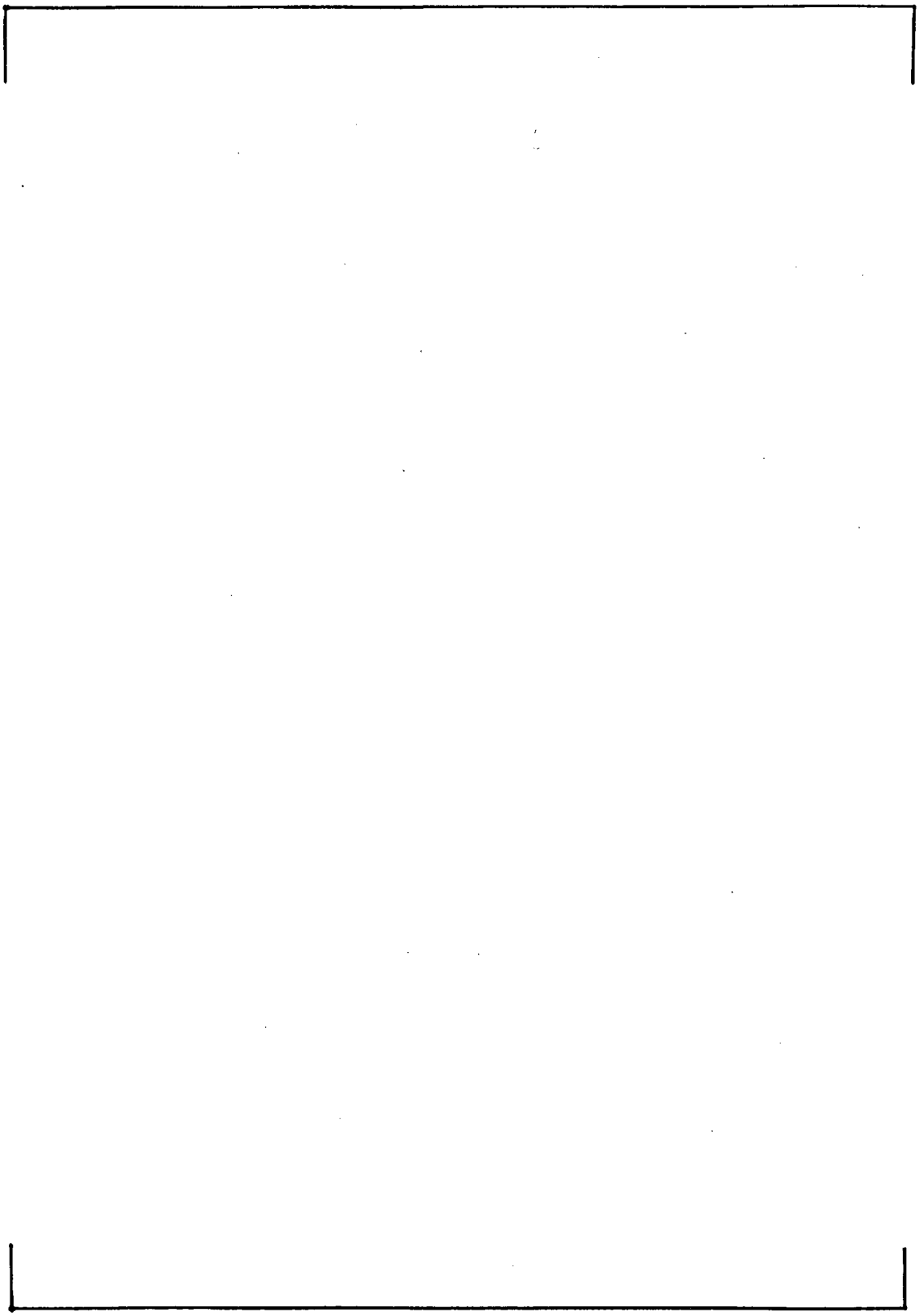

FIGURE 4-3. LBLOCA REACTOR VESSEL NODING ARRANGEMENT (205 RL PLANT).

FIGURE 4-4. LBLOCA CLPD BREAK NODING ARRANGEMENT.

FIGURE 4-5. LBLOCA LOOP NODING ARRANGEMENT (177 LL PLANT).

FIGURE 4-6. REFLOD3B NODING ARRANGEMENT (205 RL PLANT).

FIGURE 4-7. DECAY HEAT CURVE.

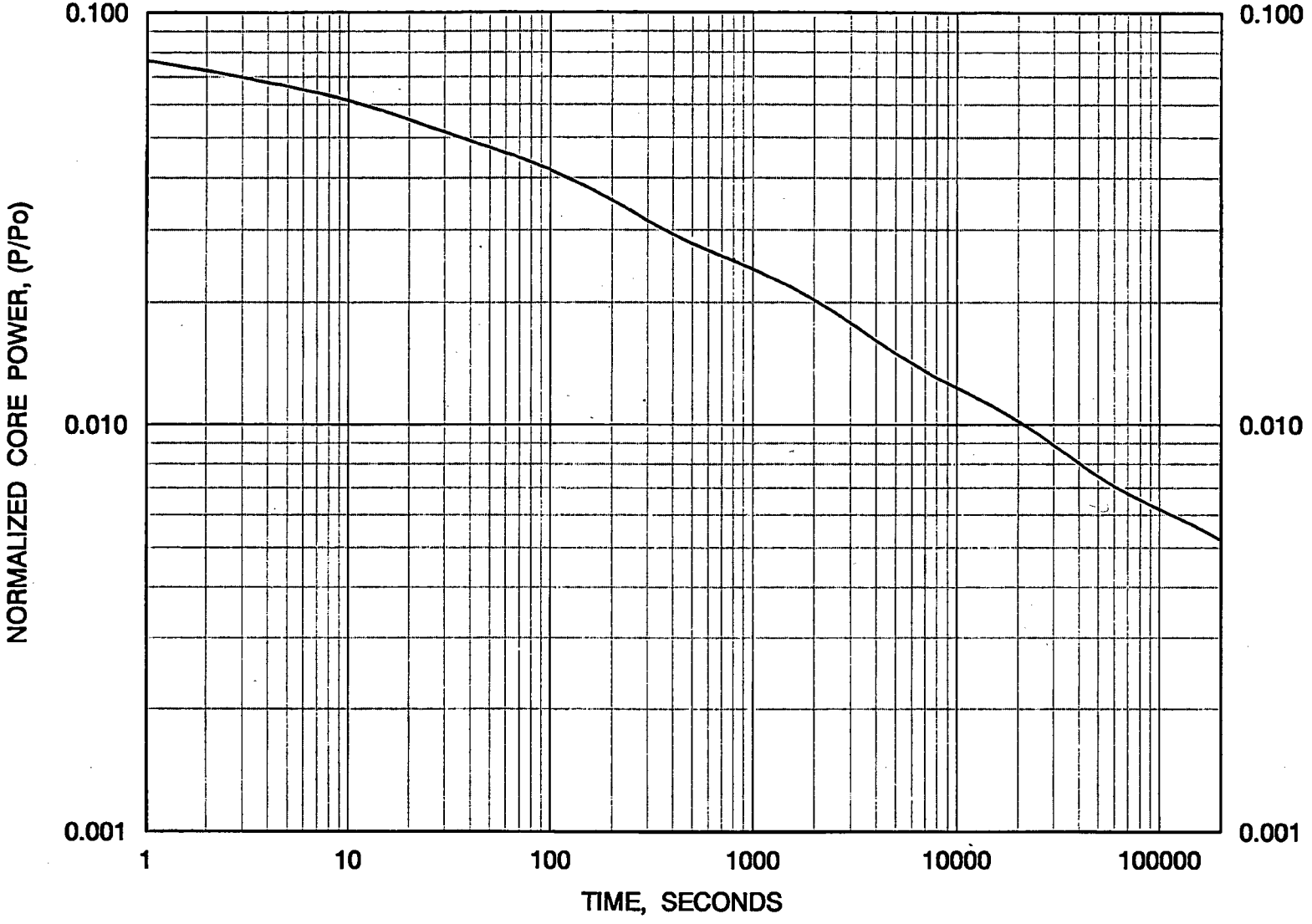

FIGURE 4-8. OUTSIDE WEIGHT GAIN OXIDATION CURVES FOR ZIRCALOY - 4 and M5.

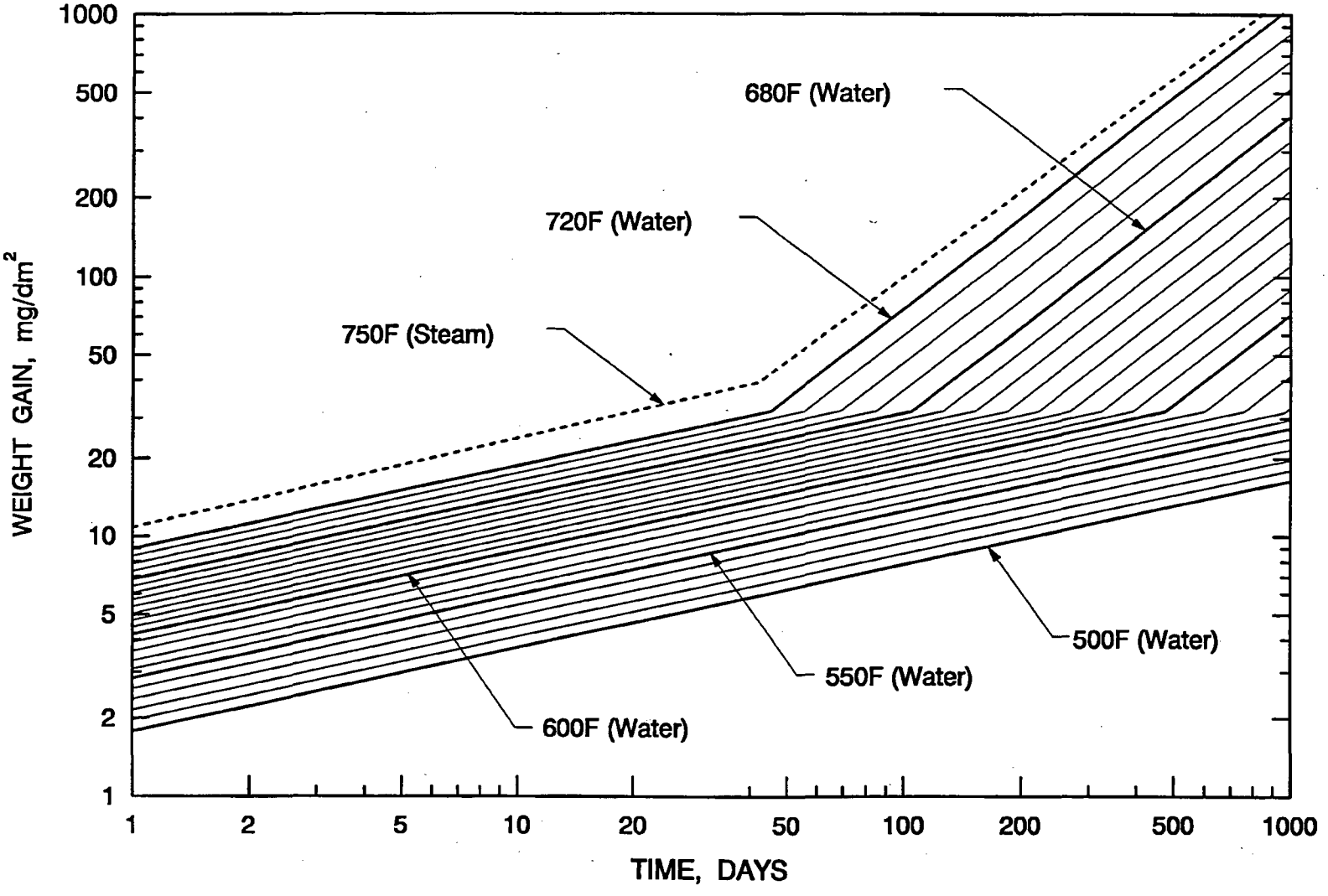

FIGURE 4-9. INSIDE OXIDATION WEIGHT GAIN FOR ZIRCALOY - 4 AND M5 IN WATER AND STEAM.

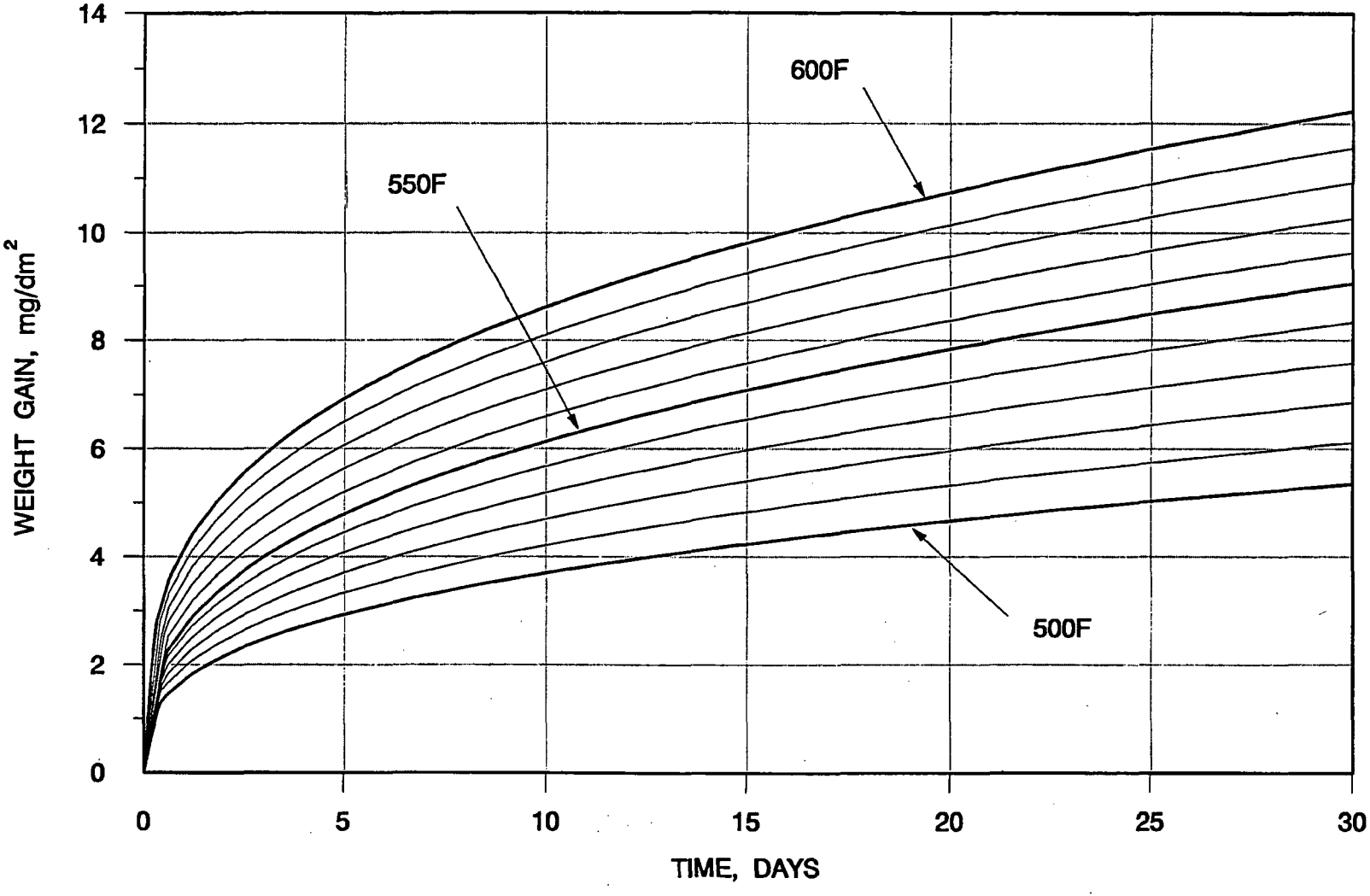

FIGURE 4-10. INSIDE OXIDATION WEIGHT GAIN FOR ZIRCALOY-4 AND M5 RESULTING FROM FISSION

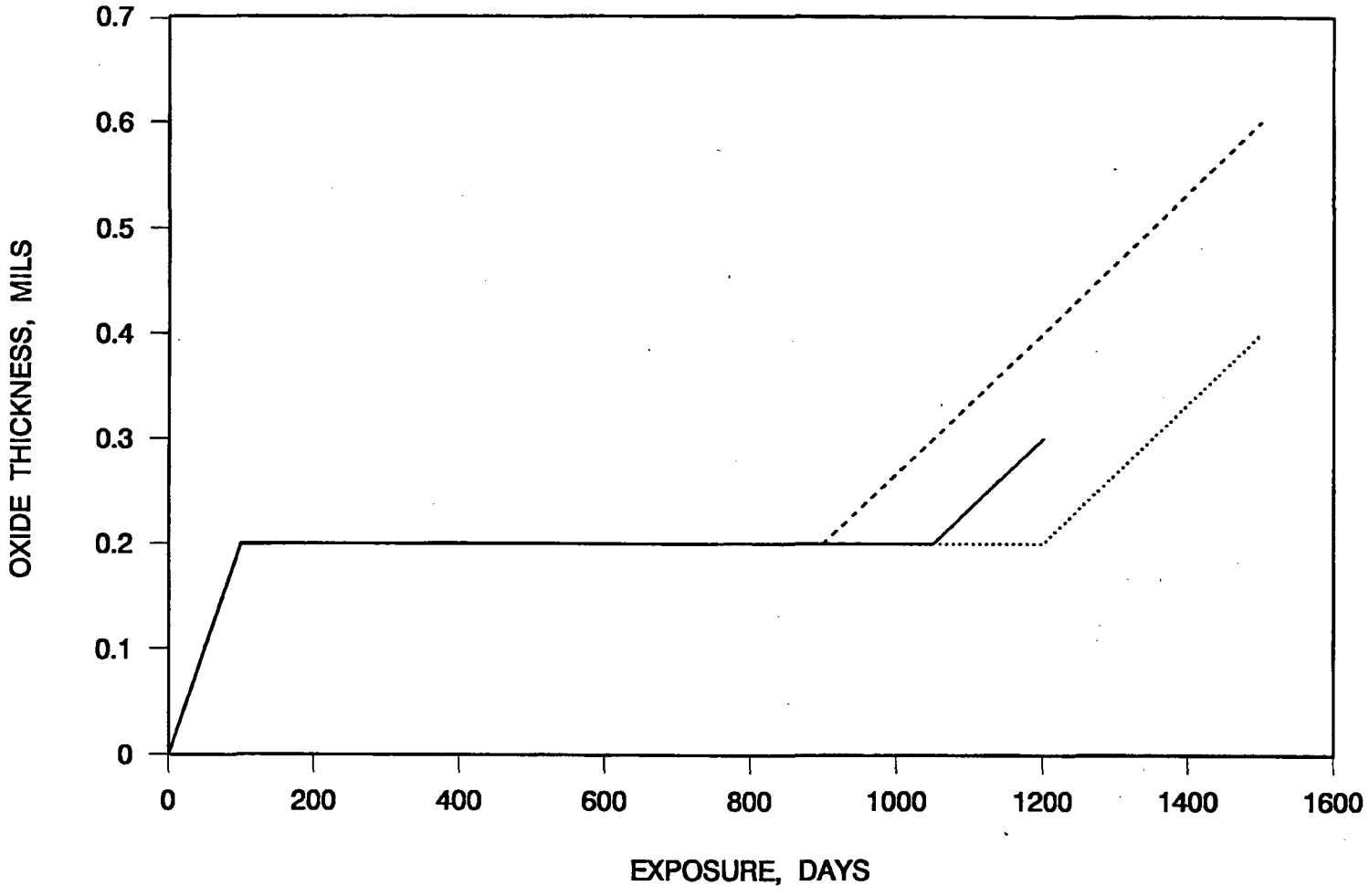

FIGURE 4-11. CLADDING RUPTURE TEMPERATURE AS A FUNCTION OF ENGINEERING HOOP STRESS AND HEATING RAMP RATE.

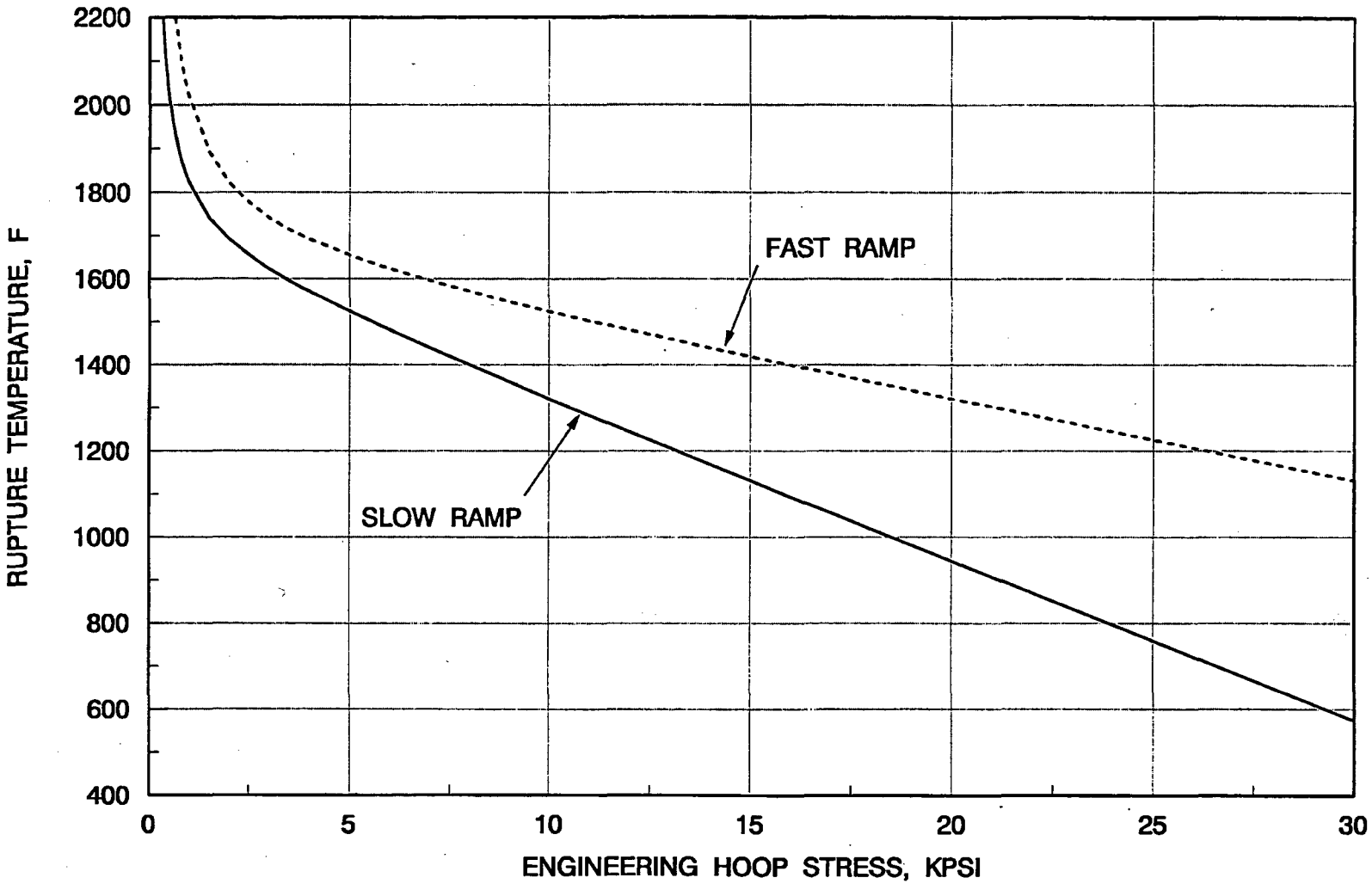

FIGURE 4-12. CIRCUMFERENTIAL BURST STRAIN AS A FUNCTION OF RUPTURE TEMPERATURE.

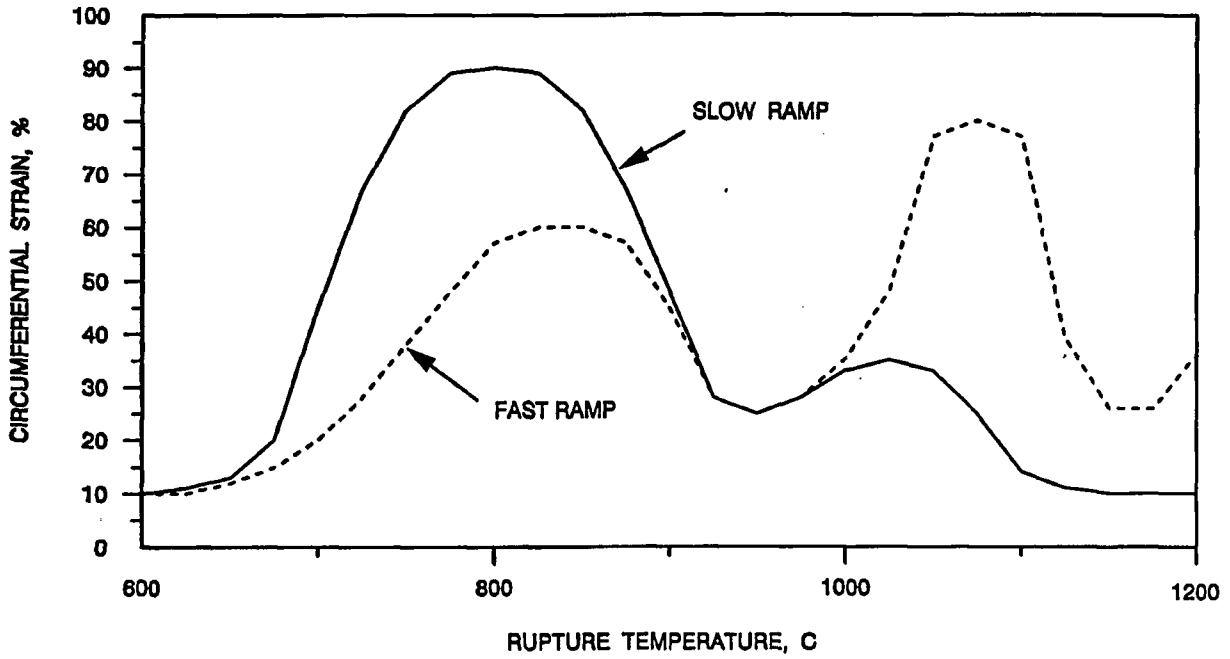

FIGURE 4-13. CHANNEL FLOW AREA REDUCTION AS A FUNCTION OF RUPTURE TEMPERATURE.

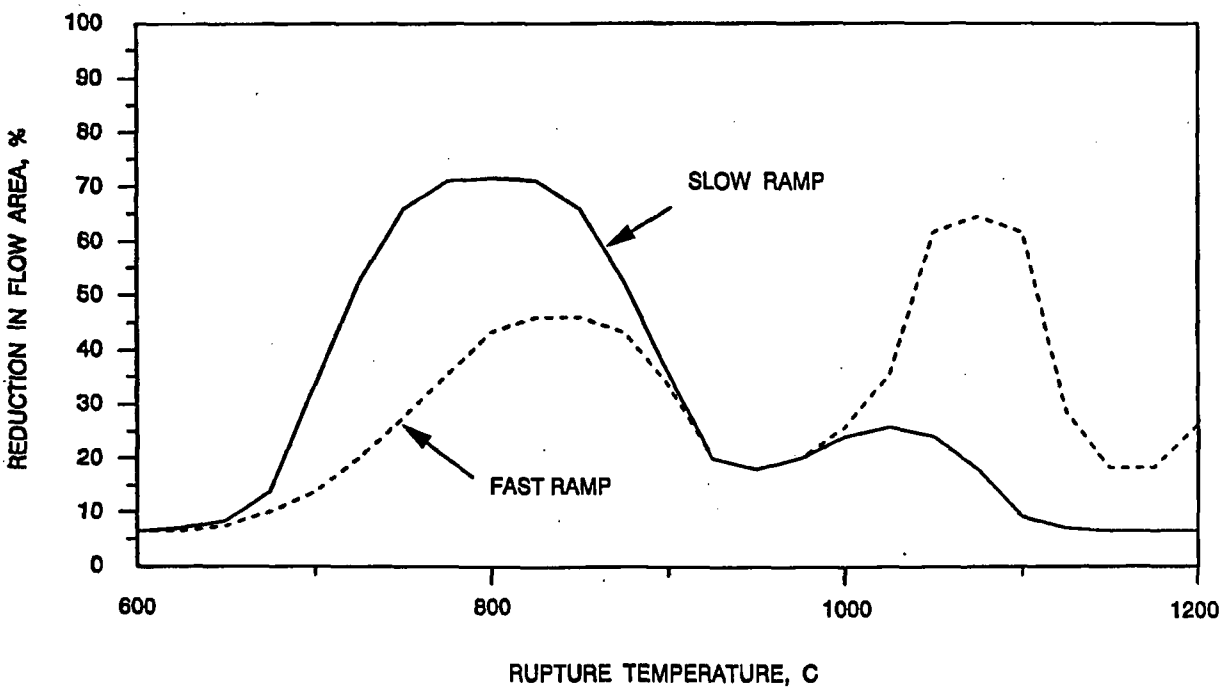

Figure 4-14. BEACH NODING ARRANGEMENT.

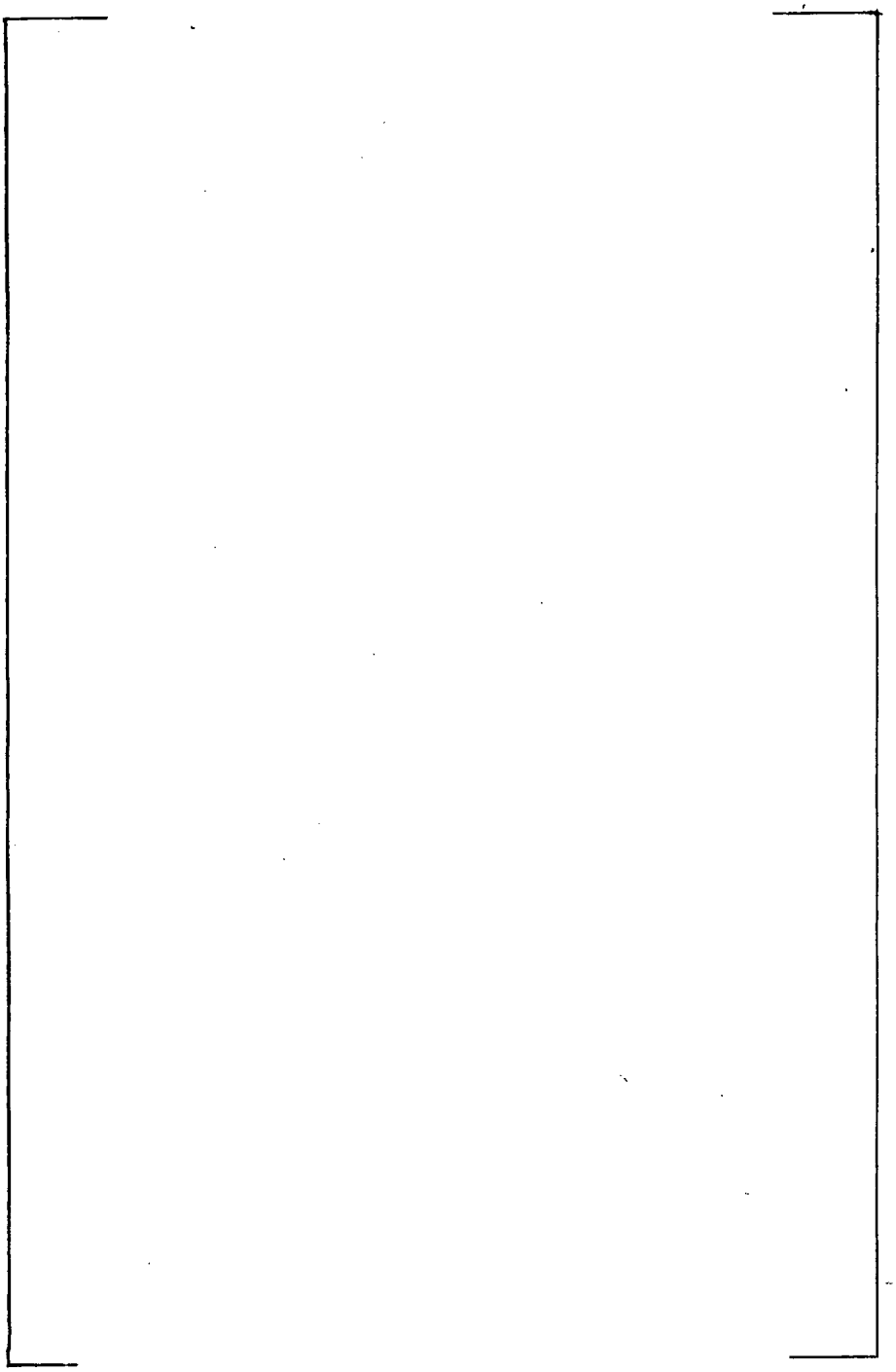

This page is intentionally left blank.

5. LOCAL CLADDING OXIDATION

Criterion 2 of 10CFR50.46 requires that the maximum local degree of cladding oxidation not exceed 17 percent. Compliance to this criterion is obtained by evaluating the results of the calculation for peak cladding temperature. In the calculation, local cladding oxidation is computed as long as the cladding temperature remains above 1000 F and the BEACH average channel analysis shows that the average core quench front is below the top of the core heated region. The amount of oxide thickness at each location is computed on a mass basis. In addition, a check of the local oxidation limits with respect to a realistic initial oxidation (or pre-accident oxidation) is performed to ensure that the 17 percent criterion would not be exceeded with a realistic initial oxidation. This supplemental check can be performed in one of two ways, using either a composite approach or separate analysis. The composite approach is the simplest form, but it will produce the minimum margin to the oxidation limit. It adds the transient oxidation increase predicted by the peak cladding temperature analyses with the minimum initial oxide layer to the initial realistic oxidation value. If this composite method is too restrictive, a separate oxidation verification case can be performed by using the realistic oxide thickness as input to a new analysis to show that the reduction in the transient oxide increase will keep the total oxidation less than the 17 percent criterion.

This page is intentionally left blank.

6. MAXIMUM HYDROGEN GENERATION

Criterion 3 of 10CFR50.46 states that the maximum amount of hydrogen generated from cladding oxidation during a LOCA shall be limited to one percent of the entire cladding in the heated core region. The demonstration of compliance to this criterion is accomplished by calculating the amount of core-wide hydrogen generation, via oxidation increases, for each of the power shapes used in the LOCA limits study.

The determination of whole-core oxidation increase for each analysis is provided by one of two methods. The first method simply compares the hot channel average oxidation increase against the 10CFR50.46 criteria. If the hot channel average oxidation increase is less than or equal to one percent, then the whole-core hydrogen generation increase will be reported as less than one percent, and no additional calculations will be performed. The hot channel average hydrogen generation rate using this method is determined by

$$\overline{O}_x\Big|_{hc} = \sum_{chan}\left(Z_{seg} \cdot O_x(Z)_{hc}\right) \Big/ \sum_{chan}\left(Z_{seg}\right) . \qquad (6\text{-}1)$$

Should the hot channel average hydrogen generation exceed one percent, then a detailed calculation will be used. This method uses the hot and average channel oxidation increases with a typical core power map to calculate the whole-core average oxidation increase. This calculation involves a detailed summation of the weighted axial contributions interpolated from the hot and average channel local oxidations at each axial elevation.

The detailed method determines the metal-water reaction at each core axial position as shown graphically in Figure 6-1. The hot

and average channel local oxidation increases are used to determine the oxidation increase for assemblies in which the radial power factor lies between them. The assemblies with radial power factors below the average channel value use the average channel oxidation increases. The whole-core oxidation increase at each elevation is multiplied by the normalized axial length for the segment to give a normalized volume weight. The sum of this volume weight results in a conservative whole-core hydrogen generation value for the transient.

The axial oxidation increase for assemblies in which the radial power factor falls between the hot and average bundles is calculated by a linear interpolation on local power level.

$$O_x(x,y,z) = O_x(Z)_{hc} - \left[O_x(Z)_{hc} - O_x(Z)_{ac}\right] \frac{P_l(Z)_{hc} - P_l(x,y,z)}{P_l(Z)_{hc} - P_l(Z)_{ac}} \qquad (6\text{-}2)$$

For radial power factors less than the average bundle the axial oxidation is set to that of the average channel.

$$O_x(x,y,z) = O_x(Z)_{ac} \qquad (6\text{-}3)$$

The channel average oxidation for any bundle is computed by

$$\bar{O}_x\big|_{(x,y,z)} = \sum_{chan}\left[Z_{seg} \cdot O_x(x,y,z)\right] \Big/ \sum_{chan}\left(Z_{seg}\right). \qquad (6\text{-}4)$$

The variables used in the equations in this section are identified by

$O_x(x,y,z)$ = the increase in oxidation at location (x,y,z) in the core,

$O_x(z)_{hc}$ = the increase in oxidation which occurred at elevation z in the hot channel,

$O_x(z)_{ac}$ = the increase in oxidation which occurred at elevation z in the average channel,

$P_l(x,y,z)$ = the local power at location (x,y,z) in the core,

$P_l(z)_{hc}$ = the local power at elevation z in the hot channel, and

$P_l(z)_{ac}$ = the local power at elevation z in the average channel.

An integration of these channels over the entire core results in the core-wide oxidation increase or the amount of hydrogen generation. The core-wide integration requires an assembly power distribution. The distribution, shown in Figure 6-2, has been selected for its conservatism in placing a disproportionately high fraction of the core near the hot channel value.

Conservatism in the calculation comes from three sources: (1) the amount of oxidation in the base run is computed using the Baker-Just correlation, which is recognized to be about fifty percent conservative; (2) the core power distribution is a reasonable and representative distribution that has been pushed to the peak powers allowed by plant technical specifications; and (3) the use of a power ratio to determine the degree of oxidation for lower power zones is conservative. Since the oxidation rate increases exponentially with temperature, a decrease in power can be expected to produce a greater than proportional decrease in oxidation. Use of the average channel oxidation as a minimum adds additional margin of conservatism.

To demonstrate the expected range of results of the technique it was applied to the most severe large break LOCA transient (Section A.11). The hot channel average oxidation increase was calculated to be 0.84 percent (Table A-25). The amount of core-wide metal-water reaction that is predicted for this case is 0.36 percent. In this case, the values produced by both techniques comply with the one percent criterion of 10CFR50.46. Of course, during an actual application, only one technique is needed to demonstrate compliance to 10CFR50.46.

This page is intentionally left blank.

Figure 6-1. AXIALLY - DEPENDENT LOCAL OXIDATION USED FOR WHOLE - CORE EVALUATION.

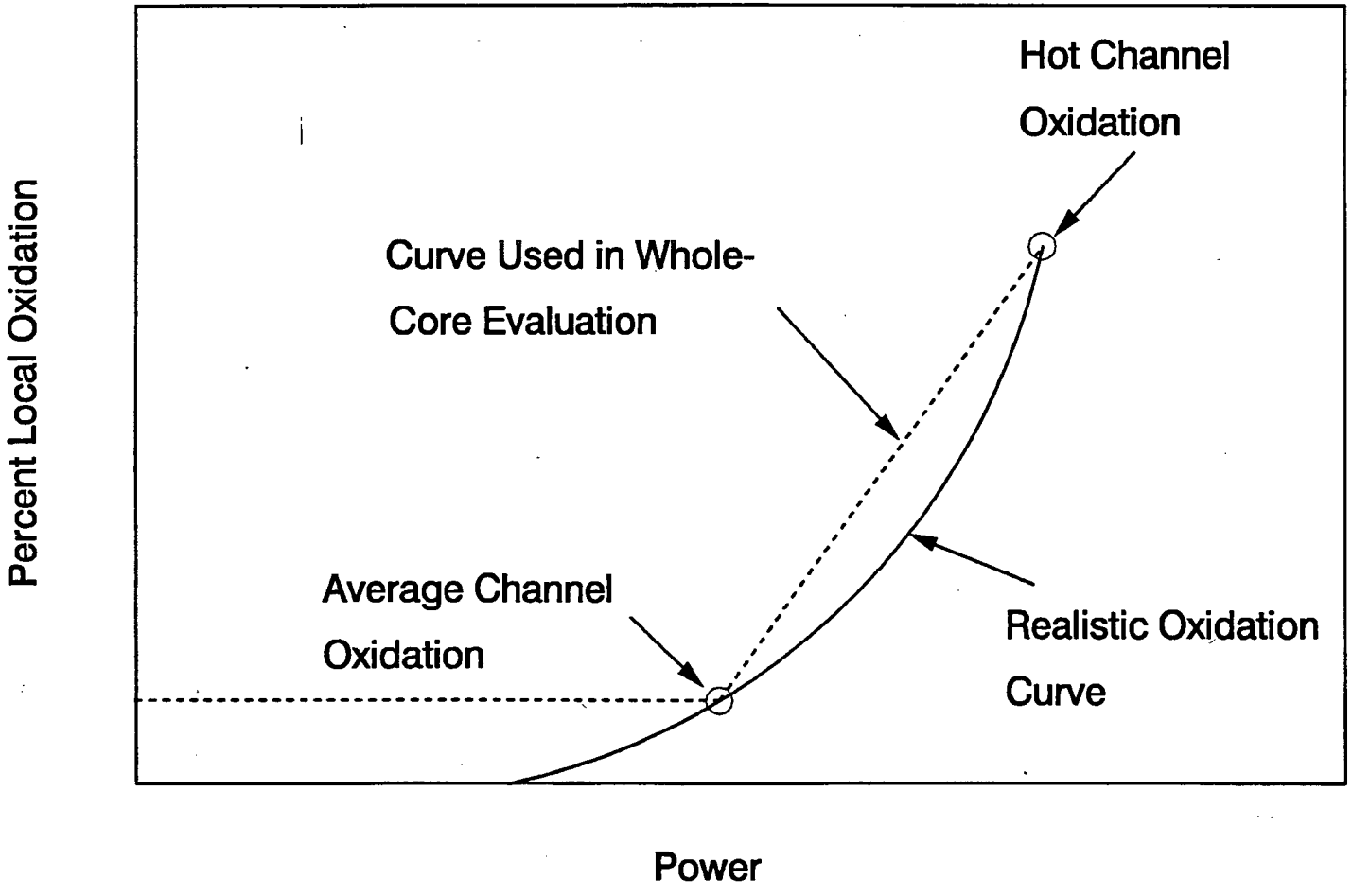

Figure 6-2. Core Radial Power Fraction for Whole - Core Hydrogen Generation Calculations.

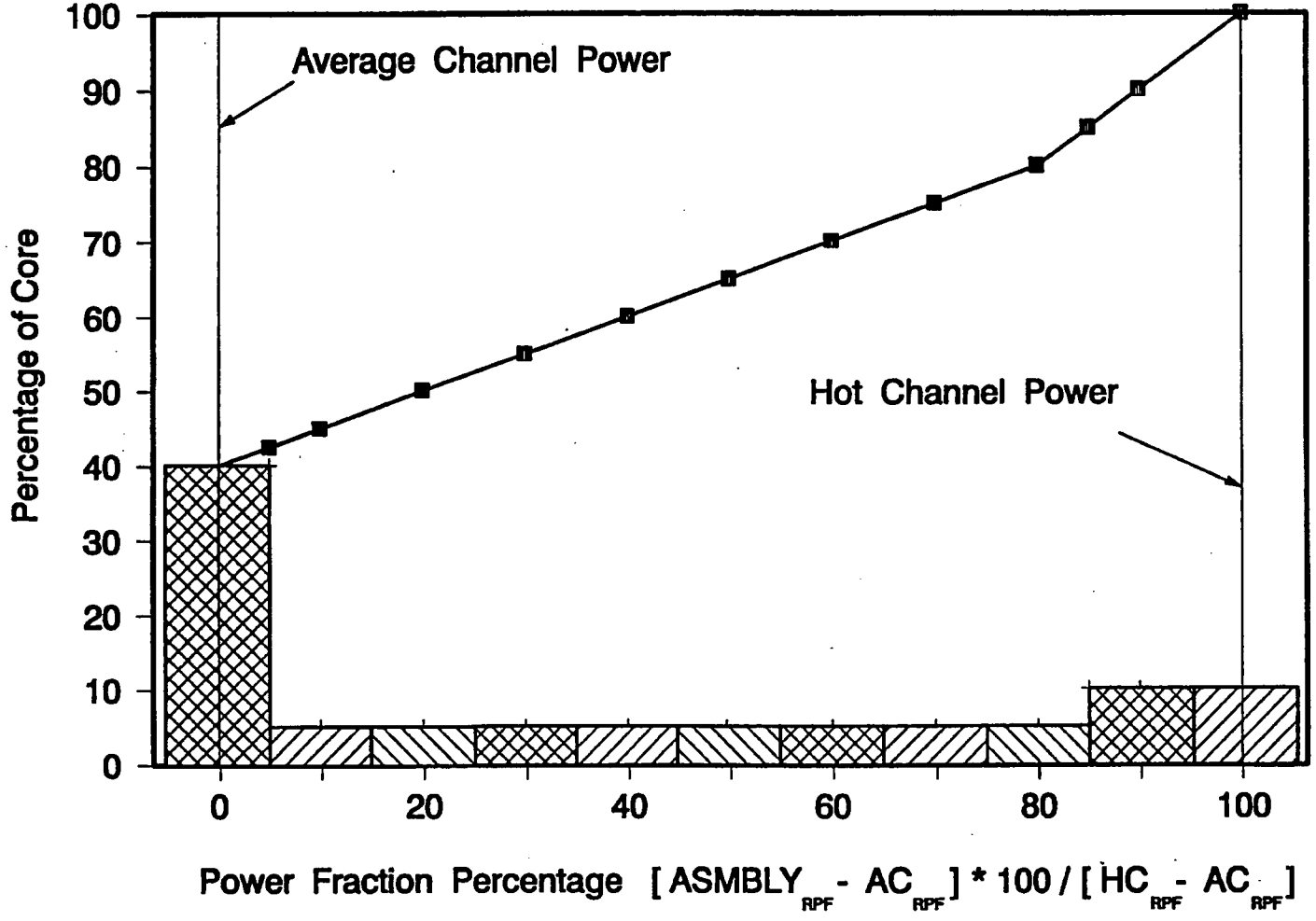

7. COOLABLE GEOMETRY

Criterion 4 of 10CFR50.46 states, "Calculated changes in core geometry shall be such that the core remains amenable to cooling." The analysis for predicting the peak cladding temperature, local oxidation, and whole core hydrogen generation involves specific analysis of the hottest fuel pin in the core. Compliance with this criterion involves a variety of considerations and analyses not explicitly controlled by this Evaluation Model but referenced by fuel reload analyses to demonstrate compliance to this 10 CFR 50.46 criterion. These calculations include consideration of the condition of the fuel rods, the fuel assemblies, and other components in the core just prior to the LOCA transient plus any changes in geometry calculated as a result of the mechanical loads from the limiting structural LOCA event plus an independent seismic event. It also includes consideration of the transient thermal effects on these components or the control rods that are inserted in the core from the 10 CFR 50.46 LOCA break consequences.

The mechanical loads from the seismic plus the limiting structural LOCA are statistically combined and compared to the elastic limits for the fuel bundles used in core at normal full power conditions. When the loading is less than the elastic limit, the nominal fuel bundle flow areas are used in the 10 CFR 50.46 LOCA analyses. If the loading exceeds the elastic limits, the deformation or distortion of the impacted fuel bundles will be applied to the channel geometry used in the prediction of the first three 50.46 criteria.

Any initial structural deformation predicted is used to predict any local flow blockage that will be combined with any changes in the core geometry that occur due to the fuel pin swelling and rupture consequences from the analyzed 50.46 LOCA. Compliance with this core cooling criteria is demonstrated when there is no

gross core flow blockage that prevents adequate fuel pin heat removal or disfiguration of the control rod guide tubes that restricts control rod insertion beyond that which is credited in the LOCA analyses. For compliance purposes, gross core blockage is defined as greater than 90 percent blockage for any bundle. If necessary, it is acceptable to apply power limitations to peripheral or low power bundles if they have significant initial mechanical distortions or gross flow blockage greater than 90 percent. In these situations, the reduction in power can be used to compensate for more severe time-dependent reductions in the flow area and transient coolant flow necessary to demonstrate compliance to this criterion.

The peak fuel pin thermal analysis includes the effect of clad swelling and flow blockage based on NUREG-0630 for Zircaloy-4 cladding or Appendix K of BAW-10227P-A for M5 cladding. Combination of any initial flow blockage with the transient swelling and rupture flow blockage is added together and compared to the 90 percent limit. When the hot bundle blockage is less than or equal to 90 percent and the peak cladding temperature remains below 2200 F, then a coolable core geometry can be maintained for the peak power bundle. The combination of core geometry, coolant flow, and local power for all other bundles in the core is also considered. The conclusions drawn for the coolable core geometry of the hot bundle is generally applicable to all other bundles because the transient cladding temperatures remain below that of the fuel pin analyzed in the peak cladding temperature calculation and there is less power to be removed. Therefore, the all fuel pins and assemblies remain in a geometry "amenable to cooling."

8. LONG-TERM COOLING

Criterion 5 of 10CFR50.46 states, "A low core temperature must be maintained following the calculated successful initial operation of the ECCS and that decay heat must be removed for an extended period of time." As with the coolable core geometry criterion, this criterion involves a variety of considerations and analyzes not explicitly controlled by this Evaluation Model but referenced by fuel reload analyses to demonstrate compliance to this 10CFR50.46 criterion. This section describes some of the considerations and assumptions used to meet this condition.

8.1. Establishment of Long-Term Cooling

The analysis of a LOCA that establishes the first three criteria of 50.46 is continued until the cladding temperature at all locations in the core is decreasing, the fluid level in the core is rising, and no additional challenges to core cooling are foreseen. At this time, the path to long-term cooling is established. The fluid within the core will continue to rise, and the cladding at all elevations will quench without further temperature excursions. Once quenched, the core is maintained within a few degrees of the coolant temperature through a continuous flow of water maintained by the ECCS.

Plant operators follow the emergency operating procedures that have been established to support successful short-term and long-term core cooling. They have been reviewed by the NRC for the smooth transition to long-term cooling during which water is recirculated from the reactor building sump through a heat exchanger to the reactor vessel. The procedures direct them to have adequate to abundant core cooling flows from the operating ECCS pump(s) to at least two flow paths. Having redundancy in the ECCS injection locations ensures that there is adequate to

abundant core cooling reaching the core regardless of where the LOCA was in relation to the ECCS injection location. The pumped ECCS that is injected into paths that do not encounter the LOCA site is available for core cooling.

For hot leg breaks, the establishment of sump recirculation is one of the last major required operator actions for initiating long-term stable cooling. For cold leg breaks, however, coolant supplied to the vessel may not flow to the core. In the most severe case, the core continues to boil for an extended period, and only water sufficient to make up for the boiloff is actually passed to the core. Boiling, without throughput of water, will concentrate boric acid. To prevent the crystallization of boric acid within the core, a liquid throughput flow is assured by RVVV recirculation, hot leg nozzle gap leakage, and operator action. The final computation of the ECCS evaluation model is to demonstrate that this action is timely, assuring the effective establishment of long-term cooling.

During the long-term core cooling phase the operators observe the ECCS pump operation, initiate needed repairs when possible, and verify there is adequate NPSH for the pumps considering the available instrumentation and any symptoms that may arise. Loss of sump inventory, potential plugging of flow paths from debris (GSI-191), or any other symptoms must be effectively managed so long as core cooling is needed. The time duration is highly variable with break location or size as the operators could establish decay heat removal for some scenarios within a few hours or days, while others could take a month or more. Under extreme conditions, ECCS injection may be needed for periods lasting a year or more. Given the possible variations in the required pumped injection period, a reasonable pump mission time may be established as the licensing basis for each plant. If none is established, then a 30 day mission time is considered reasonable.

Given the variability of the event duration it is impossible to consider all equipment availably scenarios. Restoration of equipment is generally not credited in analyses, however, the plant operators will be initiating actions that will fix or replace damaged or lost equipment and refill the BWST and EFW tanks as necessary. If the duration of the event is weeks, months, or years there are many options that may be pursued.

8.2. Boric Acid Concentration

Since all ECC systems inject borated water, salts could build up, precipitate, and block core channels during long-term cooling. To prevent this, operator action is taken to establish a flow of water through the core regardless of the type or location of the break. Concentration calculation that accounts for boiling at the decay heat rate with minimal or no core throughput (water passed through the core) is performed from the initiation of the event to the time of operator action. The concentration calculated must be shown to be below the saturation limit of boric acid for the core conditions. The rate of concentration at the time of operator action is shown to be less than the loss of boric acid caused by the throughput flow. This assures that the concentration will thereafter decrease.

This page is intentionally left blank.

9. REQUIRED DOCUMENTATION

This section verifies compliance with the documentation requirements (Part II) of the Appendix to 10CFR50 and is arranged according to the section division of Part II.

II. Required Documentation

1.a. The computer codes that form the basis for the ECCS evaluation model for breaks larger than 2 ft^2 are described in an approved revision of the following BWNT topical reports:

RELAP5/MOD2-B&W	BAW-10164 (Ref. 1)
REFLOD3B	BAW-10171 (Ref. 2)
BEACH	BAW-10166 (Ref. 3)
CONTEMPT	BAW-10095 (Ref. 10)

These topical reports include the derivations of the equations used in the codes, starting with fundamental physical laws and including all approximations. Any assumptions made in the derivation of the solution technique used by the code and the value of all code specified parameters are disclosed in these reports. The reports also describe the general application of the codes to applicable problems including potential code interfaces and input parameter selection.

The computer code options used in the evaluation model for breaks larger than 2 ft^2 are summarized in Table 9-1. At several locations throughout all of the computer codes, correlations have been programmed to include user input multipliers. These constants shall all have a value of one unless specifically stated to the contrary. Programmed constants that are part of the correlations or part of the

BWNT implementation of the correlations will have the value as published in the individual code topical reports.

1.b. Any changes in the ECCS evaluation model that result in a deviation of more than 50 F in the calculated cladding temperature transient will be documented by appropriate amendments to the evaluation model description.

1.c. BWNT computer codes, including their source coding, are controlled through a systematic process that has been audited and approved by the NRC. Each code is tracked by a unique name, version number, and revision level. Authorization to change an approved version of a code involves a multiple review and approval process. The source listing of the current or past approved versions of the ECCS codes can be made available to the NRC, at the BWNT offices in Lynchburg, Virginia, upon their request.

Inputs used during an evaluation can be categorized as follows:

Generic: User-supplied values or constants whose values are controlled by the evaluation model. The materials properties are a good example of this type of input.

Prescribed: Input for which a determining procedure is specified in the evaluation model without the specification of a value. The use of hot fluid volumes within the RELAP5/MOD2-B&W model is a good example of this type of input.

Plant: Input which is taken from documentation for the individual plant or plants to be covered

by the evaluation. Plant geometry inputs are examples of this type of input.

Case: Input which will vary depending on the accident being evaluated. Break area is a good example of this type of input.

The BWNT evaluation model controls these different types of inputs in various ways. Generic and prescribed inputs are controlled in the same fashion as code options and are documented in context within the evaluation model report. A summary of the generic and prescribed inputs is given in Table 9-2.

Plant input is controlled by BWNT internal calculational procedures and not by the evaluation model. These procedures are written to adhere to ANSI quality assurance standards. For the most part these procedures require that the inputs come from controlled design documentation, that they be referenceable, that use be documented, and that an independent review be conducted to assure that this has been done. The documents attesting to this for any given evaluation are controlled documents, maintained at the BWNT offices in Lynchburg, Virginia, and are available for audit upon request.

Case input is similar to assumptions. It is not controlled by either the evaluation model or BWNT procedures other than that it must be documented along with the plant input in controlled stored records of the calculation. Case input is also available for audit upon request.

2. Convergence of solution techniques is demonstrated in Appendix A of this topical report. System modeling and noding are described in Section 4.3.1 of this report. Time step selection is presented in Appendix A of this report.

3. Appropriate sensitivity studies using the EM methodology described in this report are presented in Appendix A of this topical report. Additional sensitivity studies, which must be performed for each specific plant category, will be documented as part of the specific analysis presented for that category.

4. Predictions and experimental data are being compared continually to the evaluation model and portions of it. Code topical reports contain comparison to applicable experimental data as appropriate.

5. The BWNT topical reports listed in Section 9.II.1.a which, along with this report, describe the ECCS evaluation model, provide the technical basis for the adequacy of the computational methods as well as compliance with 10CFR50 Appendix K. The evaluation model description provides sufficient flexibility that it is applicable to all the plant categories presented in Table 1-1.

Table 9-1. Additional Evaluation Model Guidelines

Code Options Used in Evaluation Model.

OPTION	SELECTION
RELAP5/MOD2-B&W	
Flow Film Boiling Lock-In	No lock-in until $T_w-T_s \geq 300$ F
Fine Mesh Rupture Option	Used
Critical Flow Model	Subcooled - Ext. Henry-Fauske Two-phase - Moody Superheat - Murdock-Bauman
[	]
Friction	Calculated by RELAP5/MOD2-B&W
[	]
Heat Transfer Model	Core model is used for the core heat structures & the System model is used elsewhere
[	]
High Pressure, High Flow CHF Correlation	BHTP for Mark-B-HTP fuel BWC for other Mark-B fuel BWCMV for Mark-B11 and Mark-C fuel
Metal-Water Reaction Model	Baker-Just, 1000 F threshold temperature
Clad Rupture Temperature	A plastic weighted, time averaged ramp rate is used
Rupture Form Loss Resistance	Automatic code calculation
[	]

Table 9-1. Additional Evaluation Model Guidelines
Code Options Used in Evaluation Model. (Cont'd)

OPTION	SELECTION
REFLOD3B	
CRF/Core Heat Transfer	CRF3 option
[	]

Table 9-1. Additional Evaluation Model Guidelines

Code Options Used in Evaluation Model. (Cont'd)

OPTION	SELECTION
BEACH	
Friction	Calculated with input fuel pin surface roughness
Reflood	"NEWQUEN" Reflood option selected
Fine Mesh Rupture Option	Selected
Nonconcentric Fuel Pellet	Use Nonconcentric option with TACO3 or GDTACO
Metal-Water Reaction Model	Baker-Just, 1000 F threshold temperature
Clad Rupture Temperature	A plastic weighted, time averaged ramp rate is used
Clad Rupture Effect Parametersoption	Internal code calculation
Rupture Form Loss Resistance	Automatic code calculation
[	]

Table 9-2. Additional Evaluation Model Guidelines

Generic and Prescribed Inputs for the Evaluation Model.

INPUT	SELECTION
RELAP5/MOD2-B&W	
Fluid Volumes	Hot - from design drawings
Attached Piping Volumes	Only the core flood line and pressurizer surge line volumes are included. The sum of other attached piping volume lies within the accuracy of the system volume calculation
Initial Reactor Coolant System Flows	The system flow rates are those used in the at power minimum DNB analyses. The hot and cold leg temperatures are set by nominal control system response to that RCS flow
Two-Phase Pump Degradation	Conservative selection of two-phase difference curve (RELAP5 versus SEMISCALE) and void-dependent multiplier M1 or M3-Modified curves based on sensitivity studies.
Initial Inventories for Reactor Coolant System, Secondary System, and ECCS Systems Pressure	Set by nominal operation design levels, except for CFT. The CFT inventory and pressure is set based on sensitivity studies that consider minimum to maximum ranges. The volume of attached piping, except for the CFT line and pressurizer surgeline is not included in the LOCA model
Primary Metal	Structures are lumped together by material properties, thicknesses, and location. Grouping is user controlled
Over Power Factor	Uncertainties (2% unless determined to be otherwise) due to power level instrumentation error applied to both average and hot assembly powers

Table 9-2. Additional Evaluation Model Guidelines

Generic and Prescribed Inputs for the Evaluation Model.

(Cont'd)

INPUT	SELECTION
RELAP5/MOD2-B&W	
[	]
Decay Heat	120% ANS 1971 based on core power plus uncertainty. Actinide power accounts for the energy generated from the radioactive decay of actinides including: neptunium, plutonium, and the isotopes of uranium.
Initial Fuel Temperatures	Adjusted to agree within ± 20 F to an NRC approved steady-state fuel performance code (such as TACO3 or GDTACO).
Rupture Data	NUREG-0630 ramp rate dependant data for Zircaloy-4 cladding. Data from Appendix K of BAW-10227P-A for M5 cladding.
Time Step Control Option	Option 3, mass error checking, consistent hydrodynamic and heat structure solution time advancement

Table 9-2. Additional Evaluation Model Guidelines

Generic and Prescribed Inputs for the Evaluation Model.

(Cont'd)

INPUT	SELECTION
RELAP5/MOD2-B&W	
ECCS Fluid Temperatures	Settings vary from nominal year average temperatures per system to boundingly high values
ECCS Time Delays	Includes provision for signal, diesel startup, pump startup, and line filling for all evaluations
Containment Pressure	Set from FSAR, bounding analysis, or calculated by CONTEMPT
Steam Generator Tube Plugging	SGTP is set at or above the plant tube plugging level for the PCT analyses

Table 9-2. Additional Evaluation Model Guidelines

Generic and Prescribed Inputs for the Evaluation Model.

(Cont'd)

INPUT	SELECTION
REFLOD3B	
Unrecoverable Loss Factors	Input separately from friction loss factors
Loss Factors Source	RELAP5/MOD2-B&W steady-state
ECCS Time Delays	Includes provision for signal, diesel startup, pump startup, and line filling for all evaluations
Containment Pressure	Set from FSAR, bounding analysis, or calculated by CONTEMPT
Decay Heat	120% ANS 1971 based on core power plus uncertainty. Actinide power accounts for the core average energy generated from the radioactive decay of actinides including: neptunium, plutonium, and the isotopes of uranium.
RC Pump Resistance	Appropriate for locked rotor condition
ECCS Fluid Temperatures	Settings vary from nominal year average temperatures per system to boundingly high values
Primary Metal	Primary metals are included with structures lumped together by material properties, thicknesses, and location. Upper head metal is modeled in the RCS hot legs. Grouping selections are user controlled

Table 9-2. Additional Evaluation Model Guidelines

Generic and Prescribed Inputs for the Evaluation Model.

(Cont'd)

INPUT	SELECTION
REFLOD3B	
[	]
System Initialization	Core and upper head regions are saturated steam, hot legs and steam generators are superheated steam for the loops models
ECC Water Transport Time Delay	Input as zero. The transport delay is calculated and added separately to the adiabatic heatup period
[	]

Table 9-2. Additional Evaluation Model Guidelines

Generic and Prescribed Inputs for the Evaluation Model.

(Cont'd)

INPUT	SELECTION
BEACH	
Form Loss Factors	From assembly tests
[ ]	
Rupture data	NUREG-0630 ramp rate dependant data for Zircaloy-4 cladding. Data from Appendix K of BAW-10227P-A for M5 cladding.
Number of Fine Mesh Points for Axial Conduction	8

This page is intentionally left blank.

10. REFERENCES

1. J. A. Klingenfus, et al., "RELAP5/MOD2-B&W -- An Advanced Computer Program for Light Water Reactor LOCA and Non-LOCA Transient Analysis," BAW-10164P-A, Revision 6, AREVA NP, Lynchburg, Virginia, June 2007.

2. C. K. Nithianandan, "REFLOD3B -- Model for Multinode Core Reflooding Analysis," BAW-10171P-A, Revision 3, AREVA NP, Lynchburg, Virginia, December 1995.

3. N. H. Shah, et al., "BEACH -- A Computer Program for Reflood Heat Transfer During LOCA," BAW-10166P-A, Revision 5, AREVA NP, Lynchburg, Virginia, November 2003.

4. J. H. Jones, et. al., "LYNXT - Core Transient Thermal-Hydraulic Program," BAW-10156-A, Revision 1, AREVA NP, Lynchburg, Virginia, August 1993.

5. BAW-10168P, "RSG LOCA - BWNT Loss-of-Coolant Accident Evaluation Model for Recirculating Steam Generator Plants," Revision 4, AREVA NP, Lynchburg, Virginia, July 2000.

6. Pressurized Water Reactor (PWR) Project -- Technical Progress Report, Oct. 24, 1963 - Jan. 23, 1964, WAPD-MRP-107, Westinghouse (1964), p 88.

7. E. N. Aqua, "Corrosion and Hydriding of Zircaloy Under Heat Transfer Conditions," WCAP-3269-56, Westinghouse, August 1967.

8. C. G. Dideon and G. M. Bain, "Fuel Performance Under Extended Burnup Operation B&W 15x15 Design," BAW-1716, AREVA NP, Lynchburg, Virginia.

9. D. A. Powers and R. O. Meyer, "Cladding Swelling Models for LOCA Analysis," NUREG-0630, April 1980.

10. Y. H. Hsii, "CONTEMPT - Computer Program for Predicting Containment Pressure-Temperature Response to LOCA," - B&W-Revised Version of Phillips Petroleum Co. Program (L. C. Richardson, et. al., June 1967), BAW-10095A, Revision 1, AREVA NP, Lynchburg, Virginia, April 1978.

11. B. M. Dunn, et al, "B&W's ECCS Evaluation Model Report with Specific Application to 177 FA Plants with Lowered Loop Arrangement," BAW-10091, AREVA NP, Lynchburg, Virginia, August 1974.

12. C. E. Beyer, et al, "GAPCON-THERMAL-2: A Computer Program for Calculating the Thermal Behavior of an Oxide Fuel Rod," BNWL-1898, November 1975.

13. L. W. Newman, "The Hot Cell Examination of Oconee 1 Fuel Rods After Five Cycles of Irradiation," BAW-1874, AREVA NP, Lynchburg, Virginia.

14. B. M. Dunn, et. al., "B&W's ECCS Evaluation Model," BAW-10104P-A, Revision 5, AREVA NP, Lynchburg, Virginia, November 1986.

15. D. A. Wesley and K. J. Firth, "TACO3 - Fuel Pin Thermal Analysis Code," BAW-10162P-A, AREVA NP, Lynchburg, Virginia, October 1989.

16. "Reactor Safety Issues Resolved by the 2D/3D Program," NUREG/IA-0127, July 1993.

17. D. A. Wesley, et al, "GDTACO - Urania Gadolinia Fuel Pin Thermal Analysis Code," BAW-10184P-A, Revision 0, B&W Fuel Company, Lynchburg, Virginia, February 1995.

18. J.M. Alvis and J. M. Cuta, "Evaluation of Replacement Rods in BWFC Fuel Assemblies", BAW-2149-A, AREVA NP, September 1993.

19. D. B. Mitchell and B. M. Dunn, "Evaluation of Advanced Cladding and Structural Material (M5) in PWR Reactor Fuel," BAW-10227P-A, Revision 1, AREVA NP, Lynchburg, Virginia, June 2003.

This page is intentionally left blank.

APPENDIX A
DEMONSTRATION and SENSITIVITY STUDIES

The material in Appendix A is from demonstration and sensitivity studies performed and documented to support the methodology and NRC review and approval of Revision 0 of this EM. Only acknowledged error corrections have been incorporated into Revision 2 along with pointers to other material that changes, amends, or provides additional information deemed important to define the methodology.

This page is intentionally left blank.

A.1. Introduction

Numerous sensitivity studies were performed with the evaluation model to demonstrate its acceptability to analyze LOCA, to provide a basis for the selection of input parameters, and to satisfy the requirements of Appendix K. These studies were performed and evaluated based on EM results from both individual components and global analyses. For example, various stand-alone sensitivity studies were performed on the blowdown phase with RELAP5/MOD2-B&W (Ref. A-1), and on the reflood phase with REFLOD3B (Ref. A-2) or BEACH (Ref. A-3). Although the analyses were only performed for a specific phase, the conditions encountered that could significantly impact other elements of the overall EM response were considered in the conclusions obtained. When the overall impact of the changes could not be clearly quantified, the analysis was extended to cover the entire transient and not just the phase in question. The analyses, which were performed to demonstrate compliance and convergence, and the conclusions reached from the results are the subject of this appendix.

The first step involved choosing a base or reference case for these studies. An instantaneous, double-ended guillotine break in the cold leg piping between the reactor vessel inlet nozzle and the pump discharge nozzle was chosen. Each side of the break used the full pipe area with a discharge coefficient, C_D, of 1.0. The break geometry and location were chosen based on the most severe LOCA reported in previous licensing calculations for a B&W raised-loop plant (Ref. A-4). Although different licensing codes and models may not predict the same worst break conditions, it is a reasonable starting point from which to begin sensitivity studies.

The base case used the raised-loop, 205-fuel assembly plant with Mark-BW 17x17 fuel assemblies and an initial power level of 3800 MW. A 6.285-ft axial power shape with a [ ] peak was selected for use. The hot channel contained one assembly with a peak linear

heat rate initialized at 16.5 kW/ft. A loss of offsite power was assumed at break initiation.

All EM input models for the raised-loop plant were developed based on the requirements identified in Section 4. The individual elements of the EM were first evaluated with RELAP5/MOD2-B&W during the blowdown phase via eight separate studies. Two system reflood phase studies were performed with REFLOD3B, and two reflood heat transfer studies were completed with BEACH. Minor changes were integrated into the models or methods as the studies progressed. The changes are clearly identified and applied to all analyses performed and discussed after integration. Following completion of the individual studies, six full EM studies were performed. These studies consisted of the core peaking factor, break spectrum, time-in-life, three-pump operation at 75 percent full power, core LOCA limit, and minimum versus maximum pumped ECCS demonstration analyses. The results and individual conclusions are discussed in each subsection. The global results are reiterated in the most severe break and summary and conclusion sections.

A.2. RELAP5/MOD2-B&W Blowdown Studies

Various separate blowdown cases were analyzed using RELAP5/MOD2-B&W. This section presents the following eight blowdown studies: time step, pressurizer location, break noding arrangement, core crossflow resistance, core spatial noding detail, two-phase pump degradation, reactor coolant pumps (RCPs) powered, and ECCS bypass. For these studies, comparisons were made of five variables: primary system pressure, RV- and pump-side break mass flow rates, core hot channel flow rate, and core cladding temperatures (the latter two at the peak power location). End-of-blowdown (EOB) conditions, EOB time, peak clad temperature, liquid volume remaining in the reactor vessel and intact cold legs, integrated core flood tank (or accumulator) injection, and total integrated leak mass and energy removal are also summarized in tables.

A.2.1. RELAP5/MOD2-B&W Time Step Study

The first study performed was the time step study. In RELAP5/MOD2-B&W, the user specifies a time step that may be modified by the RELAP5 time step control due to convergence or Courant limitations. The base case generally used the maximum time step as specified by the user. To verify that the code convergence criteria were adequate, two cases were executed: one with a time step that was well below that which the base case used, and another that used essentially the same time step as the base case with slight variations early in the transient. Comparison results from the base, reduced, and early increased time step cases are presented in Figures A-1 through A-5 and in Table A-1. The variable time steps, shown in Table A-2, produced essentially identical results as shown in the system pressure, leak mass flow rates, hot channel clad temperature, and hot channel mass flow rates.

Figure A-6 plots the base case Courant limit with the code advancement time step sizes for all three cases. During the first two seconds the Courant limit is clearly off-scale. The time steps are restricted by user input during this interval to allow the rapid gradients resulting from the break initiation to subside. Between two and eight seconds the Courant limit declines and reduces the requested time step. Oscillations in the Courant limit lead to some additional reductions of the time step near the end of blowdown.

These cases demonstrate and support the conclusion that the specified base case time steps with the code internal time step control is appropriate and adequate for the EM applications. Results of the base case demonstrated convergence even when compared against the results produced with a significant time step reduction below the code-limited value used in the base case analyses. Therefore, no restrictions on the time step size are required except during the first two seconds of the blowdown, when the Courant limit is high. An upper limit will be set to assure reasonable control for the EM analyses of reduced break sizes.

Specifically, the EM time steps will be controlled in the first two seconds of LBLOCAs to 0.0025 seconds or less. The remainder of the LBLOCA is adequately controlled by the RELAP5/MOD2-B&W Courant and internal time step limitations activated with the "03" time step control option. A maximum time step for the blowdown will be set at 0.025 seconds. This time set is increased specifically for the transition LBLOCA analyses. Generally, the largest break sizes produce the limiting LBLOCA events. These faster transients will be Courant limited, with time steps expected in the 0.01 to 0.005 second range. No restriction of the time step size is required after two seconds because the code time step algorithms adequately control the time step and provide converged solutions for LBLOCA blowdown analyses.

Additional information on this topic is provided in the answer to LBLOCA Round 1 RAI 11 on page LA-31 of Volume III.

A.2.2. RELAP5/MOD2-B&W Pressurizer Location Study

The base case includes the pressurizer within the intact loop. For this study, the pressurizer surge line connection was removed from Control Volume 105 (Figure 4-5) and switched to Control Volume 205 in the broken loop. Comparison results are presented in Figures A-7 through A-11 and in Table A-3. The new pressurizer location produced timing phase shifts and a slightly later end-of-blowdown time. The EOB peak clad temperature was lower, and there was more liquid remaining in the vessel due to the change in pressurizer location. Although differences between the two cases were minimal, the base case produced more conservative results. Therefore, the pressurizer will remain connected to the intact loop for all future analyses.

A.2.3. RELAP5/MOD2-B&W Break Noding Study

This study evaluated the impact of increased spatial noding detail adjacent to both sides of the cold leg pump discharge break. Previous experimental results as well as tests conducted using RELAP5/MOD2-B&W provide insights to the appropriate modeling of

[ ]

[

]

Comparisons of the results are shown in Figures A-13 through A-17 and in Table A-4. The clad temperatures and mass flow rates at the peak power location in the hot channel show some disagreement in results between four to twelve seconds; however, the EOB conditions are very similar. The mass flow rates out the break are similar. The results demonstrate that convergence has been

[

]

A.2.4. RELAP5/MOD2-B&W Core Crossflow Study

Appendix K requires that core crossflow be considered for cases with parallel core channels. The LBLOCA causes large axial pressure gradients across the core that generally dominates the core axial flows. When the core axial flow is dominant, crossflow has little impact on the fuel pin heat removal. However, when the axial flow approaches zero, the impact of the crossflow becomes more important. Two periods of near-zero axial flow occur during the transient. The first period occurs within the first second because of the initial core flow reversal caused by the break opening and subsequent recovery. The later period of near-zero flow occurs at approximately eight seconds, when increased lower plenum voiding clears the liquid loop seal, thus opening the lower plenum path for core steam venting to the break. The choice of the crossflow resistance can affect hot channel axial flows and peak cladding temperatures because of the radial crossflow variations at these times. Therefore, a study was performed, in

which the constant crossflow K-factor was varied, to determine the effect on results.

[ ]

crossflow sensitivity study are shown in Figures A-18 through A-23 and in Table A-5. The EOB conditions are similar among the cases. As expected, the minor variations are seen before one second and near eight seconds. These are the two periods of near-zero axial flow.

The first period of near-zero axial flow occurred within the first second. The biggest difference between the cases was noted in time at which the cladding departure from nucleate boiling (DNB) occurred. Once DNB occurred, the surface heat transfer coefficient decreased by several orders of magnitude, causing the cladding temperature to increase rapidly. At this time, the crossflow was directed out of the hot channel (Figure A-23). The direction of crossflow was governed by higher hot channel flashing and boiling contributions. As the crossflow resistance was increased, the rate of steam accumulation in the hot channel increased. Additional steam within the hot channel volumes increased the quality and reduced the calculated critical heat flux. High crossflow resistances hastened DNB through hot channel steam accumulation within the first several tenths of a second. After the hot channel was nearly completely voided, the hot channel steam production significantly decreased. At that time the average channel steam production was increasing. Therefore, the crossflow direction was reversed. Fluid from this lower power region flowed back into the hot channel. Increasing the crossflow resistance resulted in less flow from the average to the hot channel, which also tended to reduce the hot channel heat removal.

High core crossflow resistances therefore resulted in earlier DNB.

The typical LBLOCA DNB timing was investigated based on test facility benchmarks. The benchmark of Semiscale MOD1 Experiment S-04-6 (Ref. A-1) showed that one of the most significant conservatisms in the EM heat transfer package is the early prediction of DNB. In Test S-04-6, hot pin DNB occurred at three seconds, while the BWNT evaluation model predicted DNB to occur at 0.1 seconds. Significant conservatism in terms of DNB timing was also shown in the BWNT evaluation model benchmark to LOFT Test L2-5. Since significant conservatism has been shown in the EM critical heat flux (CHF) correlations during the LOCA transient, applying additional conservatism via use of an unusually high crossflow resistance is considered excessive and unnecessary. The early DNB from high crossflow resistance leads to higher cladding temperatures that are retained throughout the blowdown transient, as shown in Figure A-19.

During the period of near-zero axial flow at eight seconds, larger differences were again observed in the hot channel cladding temperature at the peak power location. The cladding temperature at that time increased with the crossflow resistance. Once the axial flow again dominated the core flow, the cladding temperatures converged, resulting in the end-of-blowdown conditions being quite similar among the cases. The variations at eight seconds were primarily localized effects from minor changes in the surface heat transfer. The magnitudes of the variations were reduced as the high negative core flows increased the core cooling.

The CHF timing of the highest crossflow resistance case was shown to be overly conservative. The conditions at EOB were shown to be similar among the remaining cases, even given the differences noted near the eight-second time period. The study showed that

the results are converged and that the geometry-based resistance of 72 is reasonable for the two-channel EM applications.

Additional information on this topic is provided in the answer to LBLOCA Round 1 RAI 14 on page LA-33 of Volume III.

A.2.5. RELAP5/MOD2-B&W Core Noding Study

The two-channel core noding arrangement was altered through the addition of a third channel to determine the impact on the fuel pin temperatures. This model arrangement, shown in Figure A-24, consisted of a hot channel with one fuel assembly, a middle channel with eight fuel assemblies surrounding the hot assembly, and the average channel containing the remaining fuel assemblies. The hot channel was connected to the middle channel, which was also connected to the average channel, through crossflow junctions from each axial control volume. The hot channel radial peaking factor (RPF) was held constant for each of the analyses. The middle channel radial peaking was varied between the hot and average channel values to determine the impact on the hot channel response. Four analyses were performed with the middle channel RPFs set equal to:

1. The average channel RPF,
2. Eighty percent of the hot channel RPF,
3. Ninety percent of the hot channel RPF, and
4. The hot channel RPF.

The average channel RPF was adjusted as necessary to preserve the total core power.

The three-channel model is essentially an altered form of crossflow resistance study. Placement of a higher power channel between the hot and average channels was expected to change the

initial crossflow out of the hot channel because of the variations in the middle channel boiling and flashing contributions. As with the core crossflow study, the significant variations are expected during the times when the core axial flows are near zero.

Figures A-25 through A-29 and Table A-6 compare the results of the core noding study with those of the base two-channel model. The hot channel cladding temperature responses for the three higher power middle channel cases show significantly earlier DNB than the base two-channel case or the three-channel case with two average channel RPFs. Similar results were obtained in the crossflow sensitivity study for the highest crossflow resistance. The hot channel voiding increased more rapidly until DNB occurred. A similar increase in the cladding temperatures was observed near eight seconds. The end-of-blowdown conditions among the variable power analyses are, however, quite similar. One other notable difference was the end-of-blowdown time. This shift was related to downcomer condensation variations on the subcooled core flood tank injection. This variation is addressed in the ECCS bypass study contained in Section A.2.8.

The core noding study showed that the radial modeling, like the crossflow resistances, governed the DNB timing and cladding temperature responses. With a reduction of the equivalent three-channel crossflow resistances, similar DNB behavior would be attained by the two- and three-channel models. The difference in DNB timing, however, had little to no effect on the end-of-blowdown conditions in the various core noding analyses. It was thus concluded that the two-channel model adequately predicted the blowdown transient and that the additional detail of the three-channel model is unnecessary.

Additional information on this topic is provided in the answer to LBLOCA Round 1 RAI 14 on page LA-33 of Volume III.

A.2.6. RELAP5/MOD2-B&W Pump Degradation Study

Behavior of the reactor coolant pump for guillotine breaks may alter the blowdown transient characteristics by changing the distribution of the system flow between the vessel and pump sides of the break. To evaluate the sensitivity to the pump two-phase degradation model, a study on pump degradation was performed.

Figure A-30 presents the degradation curves used in this Study. The base case used the semiscale pump degradation curve presented in NUREG/CR-4312, Vol. 1, to obtain realistic degradation characteristics. The most highly degraded pump characteristics were achieved by using the M1 curve. The minimum degradation was achieved through use of the M3 modified curve. The M1 and M3 modified curves were derived in previous Babcock & Wilcox work as bounding curves (Ref. A-4). Both models were incorporated into the base deck and executed in separate calculations.

Comparisons of results are presented in Figures A-31 through A-35 and in Table A-7. The M1 curve shifted slightly more flow through the reactor vessel side of the break. A higher vessel leak flow led to slightly lower hot channel flows between 4 and 10 seconds and correspondingly higher cladding temperatures due to lower heat transfer coefficients. The opposite effect was noted for the M3 modified curve transient with correspondingly lower cladding temperatures. The end-of-blowdown conditions were similar for all three cases, with the M1 curve producing the most severe results. The channel-average local oxidation in the hot channel produced by the M1 curve is a further indication that this case produces the most conservative results. It will be integrated into the base model for the remaining EM LBLOCA analyses.

A.2.7. RELAP5/MOD2-B&W RC Pump Power Study

It is possible that the operating status of the reactor coolant pumps could alter the core flow forcing functions during the blowdown phase. In order to determine the most conservative pump configuration with respect to core heat removal, the base case was executed using the M1 pump degradation curve with the pumps unpowered and also with the pumps powered.

Comparisons of results are presented in Figures A-36 through A-40 and in Table A-8. It is apparent from the cladding temperature comparison plot that the pumps-powered case produces significantly better core cooling during blowdown. The powered pump in the broken loop provides increased resistance, which reduces the pump-side break flow. The pumps in the intact legs provide an increased flow through those legs, which increases the positive core flow. Higher core flows increase the fuel pin heat removal. Slightly higher reactor vessel side break flows were realized with these boundary conditions.

The RCS response with the pumps powered is clearly less severe from a core cooling perspective than the configuration with the pumps unpowered. Therefore, the base case should retain the loss-of-offsite power assumption as the most limiting basis for LBLOCA analyses.

An inconsistency was discovered in the frictional torque input used for each of the four reactor coolant pump components. Pump Component 165 (Figure 4-2) used a best-estimate cubic fit of the homologous speed ratio to determine the pump frictional torque. The other three pump components used a constant frictional torque that was appropriately generated for pump coastdown applications. The mixed set of input values was detected, and switched to the cubic fit prior to performing the pumps-powered case. The impact of a mixed set of inputs was determined to be minimal for the

applications in which the pumps were not powered, therefore, the results and conclusions obtained in the studies with the mixed input remain valid.

The ECCS bypass study gives the impact of the variation between the consistent and mixed-modeling approaches. Figures A-42 through A-46 give a direct comparison for the first twelve seconds, prior to core flood tank flow. The ECCS injection case used the mixed set of inputs, while the ECCS bypass model case used the consistent cubic fit coefficients. Minor shifts in the break flow rates were noted during the first three seconds. The hot channel mass flow rate and the cladding temperature response shows small differences that did not change the overall result of the calculations. For consistency, the cubic fit to the pump frictional torque will be integrated into the input model for all future applications. Since the results of prior studies were not affected, the reported results obtained with the mixed input set were retained.

A.2.8. RELAP5/MOD2-B&W ECCS Bypass Study

The ECCS injection was modeled mechanistically in RELAP5/MOD2-B&W for all sensitivity studies reported before this study. That is, the ECCS injection was injected into the downcomer and mechanistically processed out of the break by RELAP5/MOD2-B&W. Near the end of blowdown in most studies, most parameters were observed to closely follow the oscillations associated with the condensation on the core flood tank fluid injected into the downcomer. The results of the mechanistic calculation were not atypical or unphysical. They were simply a result of the downcomer ECCS steam condensation potential versus flow out of the CLPD break. As the RCS pressure approaches containment pressure, the break forcing function on the RCS response declines. During the same period, the ECCS condensation potential is growing from increasing CFT flow. The ensuing battle for the resident steam

results in the oscillations observed during the CFT injection period. The ECCS liquid flowed intermittently from the downcomer to the break resulting in additional oscillations. During some cases, such as the core crossflow and core noding studies, the combination of the condensation and break volumetric discharge oscillations resulted in EOB time shifts. The oscillations do not assist or adversely impact the core cooling aspects. They do however, complicate case-to-case comparisons. For this reason an alternate EM ECCS bypass method was investigated for use during the CFT injection period.

[

]

Comparison of the non-mechanistic and the mechanistic ECCS bypass analyses are shown in Figures A-42 through A-46 and in Table A-9. The non-mechanistic ECCS bypass model demonstrated smoother behavior which should improve the convergence of the end-of-blowdown prediction for all cases.

The end of blowdown was extended with the bypass calculations. The cladding heatup rate during the last five seconds of blowdown approaches the adiabatic heatup rate. Therefore, reported end-of-blowdown temperatures are higher for the ECCS bypass analysis. However, the blowdown extended heatup is offset by a reduction of the refill or adiabatic heatup period calculated with an appropriate ECC gravity delay time for both cases. The ECC liquid injected after end of bypass is reintroduced along with the liquid remaining in the reactor vessel and CLPD regions as resident liquid in the REFLOD3B lower plenum at the end of blowdown.

In the mechanistic bypass analysis, the resident liquid was equivalent to one second of CFT injection. The non-mechanistic bypass analysis predicted partial end of bypass at 18.6 seconds and total end of bypass at 19.3 seconds. The ECC injection integrated after the end of bypass and the resident reactor vessel liquid resulted in an equivalent 2.6 seconds of CFT injection. The end-of-blowdown difference is 21.05 less 19.46 or 1.59 seconds, which is also the difference in the equivalent ECC liquid placed in the lower plenum. Therefore, since the cladding temperatures are nearly equal at 19.5 seconds and the end of adiabatic heatup time is nearly identical, the overall PCT variation between these two analyses is negligible.

Since no difference in PCT was realized with either modeling approach, the technique that produced the best convergence of end-of-blowdown times was adopted for use in the EM. The non-mechanistic ECC liquid bypass approach with the UPTF end-of-bypass definition was therefore taken as the basis for all future analyses.

Additional information on this topic is provided in the answer to LBLOCA Round 1 RAI 4 on page LA-20 of Volume III.

A.2.9. Revised RELAP5/MOD2-B&W Base Blowdown Model

Based on the results of the RELAP5/MOD2-B&W sensitivity studies, the recommended EM LBLOCA blowdown base model described in Section 4 was altered via the introduction of the M1 two-phase pump degradation curve, the best-estimate cubic fit of the pump homologous speed ratio, and the non-mechanistic ECCS bypass model. The M1 curve was integrated into the base input model for the pump power and the ECCS bypass analyses. Inclusion of the M1 curve, cubic pump homologous speed ratio, and the ECCS bypass model into the base model does not invalidate any of the previous sensitivity studies. These models were used in all subsequent sensitivity studies involving REFLOD3B and BEACH, spectrum, core peaking factor, 3-pump, time-in-life, LOCA limit, and ECC injection studies.

A.3. REFLOD3B Sensitivity Studies

Two REFLOD3B sensitivity studies were performed with the RELAP5/MOD2-B&W end-of-blowdown input conditions for the final revised base case (2A/G break in the CLPD with a C_D of 1.0, ECCS bypass, M1 degradation curve, and cubic-fit to the pump frictional torques). These studies were performed to ensure that the base REFLOD3B model meets the requirements of Appendix K. The first sensitivity study performed was a loop nodalization variation. The second study examined the influence of the primary reactor coolant pump flow resistance on the reflooding rate for a locked versus a free-spinning rotor condition.

In REFLOD3B base model, the reactor vessel is represented by the four regions as shown in Figure 4-6. This noding scheme considers thermal-hydraulic behavior occurring in the reactor vessel during the reflooding transient and is adequate to predict the core flooding rate as demonstrated in the benchmark of FLECHT-SEASET experiment 33338 (Appendix I, BAW-10171P). The primary system piping is represented by two loops, similar to the blowdown model. The broken loop has individual cold legs modeled whereas the intact loop cold legs are combined. Any cold leg pump suction pipe that is clear, (i.e. contains no liquid loop-seal) is used to vent the core steam to containment. For plants with eight RVVVs, the four open cold legs allow venting of approximately forty percent of core steam generation. The remaining steam flows through the RVVVs. Flow resistance through the primary coolant pump was based on the locked-rotor assumption. A 0.25 psi pressure drop was imposed on cold leg pipe junctions to account for losses due to steam-water interaction. The CRF3 carryout rate correlation was used to determine core exit flow.

Additional information on this topic is provided in the answer to LBLOCA Round 2 RAI 3 on page LA-91 of Volume III.

A.3.1. REFLOD3B Loop Noding Study

Since a large fraction of the flow passes through the loops, the variation on core inlet flooding rate will be studied with comparisons of the base REFLOD3B model results against a detailed loop representation. The number of loop volumes was doubled for this study as shown in Figure A-47.

A convergent solution from this study is judged on important parameters such as core inlet flooding rate, core and downcomer water levels, and carryout rate fraction. Comparison plots for these parameters are presented in Figures A-48 through A-51. These plots confirm that there is little difference between the base case and the increased noding case. Therefore, it is concluded that the base model is sufficiently detailed and converged for all EM analyses.

A.3.2. REFLOD3B RCP Locked Versus Free-Spinning Rotor Study

Section I.D.3 of Appendix K to 10CFR50 includes the requirement to consider the effect of primary coolant pump resistance on the maximum cladding temperature. For this study the pump impeller was considered to be free-spinning as opposed to locked as in the base reflooding analysis. To quantify the impact on the core reflooding rate with a free-spinning rotor, the pump resistance for REFLOD3B was calculated as an input form loss coefficient, K_{Fj}, based on Equation 2-2 in BAW-10171. The pump homologous data in the RELAP5/MOD2-B&W blowdown model was used to derive the loss coefficient for the locked and free spinning impeller conditions. The pump pressure drop is given by

$$\Delta P = \rho \cdot H/144 = \rho \cdot H_R \left(Q/Q_R\right)^2 \cdot \left(h/v^2\right)/144, \qquad \text{(A-1)}$$

where

P = Pressure (psi),
ρ = Density (lbm/ft^3),
H = Head (ft),
H_R = Rated head (ft),
h = Normalized head,
Q = Volumetric flow (ft^3),
Q_R = Rated volumetric flow (ft^3), and
v = Normalized volumetric flow.

In REFLOD3B, the pump pressure drop is calculated by

$$\Delta P = K_{Fj} \cdot w^2 \Big/ \left(288 \cdot \rho \cdot g_c \cdot A^2 \right), \qquad \text{(A-2)}$$

where

w = Mass flow rate (lbm/sec),
g_c = Gravitational constant = 32.2 ($lbm\text{-}ft/lbf\text{-}sec^2$),
A = Flow area (ft^2), and
K_{Fj} = Loss coefficient.

Combining these two equations, the loss coefficients for the both impeller conditions were determined.

The loss coefficients used for the locked impeller and the free-spinning impeller, based on a flow area of 5.657 ft^2, are 13.85 and 2.05, respectively. Figures A-52 through A-55 give the comparisons of the locked versus the free-spinning rotor REFLOD3B analyses. The free-spinning rotor case has substantially lower loop flow resistance than that of the locked rotor case. Therefore, higher loop venting of the steam flows was calculated. The higher flows reduced the upper plenum steam binding and gave rise to a higher flooding rate. The comparison of core flooding

rates for the two impeller conditions presented in Figure A-52 confirms that the locked rotor assumption used in the base model is conservative and appropriate for use in the EM analyses.

A.4. BEACH Sensitivity Studies

Two BEACH sensitivity studies were performed using the RELAP5/MOD2-B&W blowdown input conditions for the final revised base case (2A/G break in the CLPD with a C_D of 1.0, ECCS bypass, M1 degradation curve, and cubic-fit to the pump frictional torques) and the reflood boundary conditions specified by the base REFLOD3B model. The blowdown case was restarted with all blowdown loop components deleted except for those shown in Figure A-56. The BEACH reflood fine-mesh rezoning and heat transfer model was activated at end of blowdown. The transient was continued well beyond the time of the peak clad temperature prediction. This analysis was designated as the BEACH base case.

Two sensitivity studies were performed with variations of the base model input. The input changes included variation of the maximum user requested time step sizes and increased fine-mesh rezoning studies that increased the maximum axial fuel segmentation. For these studies, various fuel pin temperatures and hot channel heat transfer coefficients at the ruptured and unruptured locations were compared to demonstrate convergence of results.

A.4.1. BEACH Time Step Study

The purpose of this study is to demonstrate convergence of the ruptured and unruptured peak cladding temperatures as the user-requested time step is altered. The code time step control option "03" is used for these cases. This option activates the code internal time step control algorithms, which further reduce the time step if certain stability or convergence criteria are violated.

BEACH calculates the fuel pin response during the refill and reflood phases of the LOCA. These periods impose two distinctly different requirements on the maximum calculational time step

size. During the refill phase, no inlet flow is supplied and a constant upper plenum pressure boundary condition is specified. The no-flow fluid boundary condition results in a near-adiabatic heatup of the fuel rods. Only natural circulation steam flow occurs in the channel, therefore this phase has a high Courant limit. The transient boundary conditions are activated at the REFLOD3B bottom-of-core-recovery (BOCR) time (the time at which the liquid level in the core lower plenum reaches the bottom of the unheated portion of the fuel assembly). Core inlet flow results in rapid steam production from the clad quenching process. The quenching produces high steam velocities that persist throughout the remainder of the reflooding phase. The severity of the initial few seconds of the reflood transient significantly restricts the time step size by both Courant and water property convergence limits. As the quench front advancement slows, the time step sizes become less restrictive.

Table A-10 gives the time step sizes chosen for use in this study. The base time step was chosen based on the allowable size used for benchmark cases and previous LOCA analyses performed on recirculating steam generator plants (Ref. A-8). The reduced time step cut the base time step by more than one-half, and then increased in increments back to the base time step by 45 seconds. The increased time step study doubled the base values in the early part of reflood and then matched the base after 25 seconds. The requested time steps used are illustrated in Figure A-57. A comparison of the actual calculational time steps with a superposition of the base case Courant limit is given in Figure A-58. The results of this study are shown in Figures A-59 through A-64 and summarized in Table A-11.

The variations of the total peak clad temperature predictions were within 20 F for each of the cases. Segment 11 ruptured in each case. The peak unruptured segment location changed from Segment 10 to Segment 13 in the increased time step case. This shift was

attributed to quench front variations that caused slight differences in liquid carryout before 25 seconds.

In these cases the peak clad temperature occurred in the ruptured segment within the first 5.0 seconds of reflood. Early during the reflood transient, the code results are more oscillatory due to the variable inlet reflooding rates and initial quenching with subcooled liquid inlet flows. The results indicated that this early behavior with the high cladding heat fluxes is better resolved with the 0.001 second time step. After this time interval, the final reduced time step was increased to 0.0025 seconds for 5 seconds, and then to 0.005 seconds for the remainder of the analysis. Adequate convergence is demonstrated in the calculated responses for this time step study. Control of the user-selected time steps therefore follows the set of inputs described as the Decreased Time Step case. These will be adhered to for future analyses unless unforseen code convergence problems dictate a change. Whenever a change is required, the requested time step change will be reported in the application with the results of the EM analysis.

Additional information on this topic is provided in the answer to LBLOCA Round 1 RAI 16 on page LA-37 of Volume III.

A.4.2. BEACH Axial Fuel Segmentation Study

The purpose of this study is to examine the sensitivity of the ruptured and unruptured peak clad temperatures to a change in the maximum number of axial rezoning segments used. The fine-mesh rezoning feature in BEACH allows the user to specify the maximum number of two-dimensional micro-mesh intervals permitted per each macroscopic fuel heat structure segment. The final base case results from the time step study was used as the base case for this analysis. The base case used eight fine-mesh rezoning increments. This study consisted of increasing the number of

fine-mesh increments to 16, followed by an increase to 32. An increase in the number of mesh increments improves the resolution of axial wall temperatures and more discretely defines the quench front position.

The results, shown in Figures A-65 through A-72 and Table A-12, indicate good convergence and confirm that the base case contains a sufficient number of fine-mesh rezoning increments. The peak unruptured location again shifted in this study from Segment 11 in the base case to Segment 13 for the increased mesh interval cases. Segments 10 and 13 are quite similar in power and peak cladding temperature; therefore, switching of the peak unruptured segments is not unexpected.

The results obtained in the study are very similar for all three cases, demonstrating adequate convergence of the base model. Therefore, eight fine-mesh increments will be retained as the method to be used in the EM, although more increments are equally acceptable.

A.5. Axial Versus Radial Core Peaking Factor Study

LOCA analyses are performed to provide the maximum power limits at which the core can be adequately cooled (within 10CFR50.46 limits), given the postulated worst break size and location. The core power peaking is analyzed with a reasonable axial power shape that is peaked to the highest allowable linear heat rate that meets the LOCA acceptance criteria. Five axial power shapes are peaked at the midpoint between fuel spacer grids between the two- and ten-foot confines of the core region. These five power shapes are used in Appendix K-based analyses to cover the vast range of possible core axial and radial power shapes. The methods used to perform these analyses are described in more detail in Section A.9.

The allowable LOCA linear heat rate is produced from a reasonable combination of radial and axial peaking factors in the hot

[ ]

This sensitivity study was not performed to define the most conservative power shape for the LOCA analyses. The purpose was to determine whether significant variations in peak cladding temperature or whole-core hydrogen generation would result from different combinations of the radial and axial peaking factors.

[ ]

[

]

curves, all of which peak at the 6.285-ft location (midpoint between fuel spacer grids).

These power shapes were selected because they represent reasonable variations in the radial and axial components. Changes in the core channel heat transfer behavior are expected during both the blowdown and reflood periods due to the shifts in the core power shapes. To better understand the implications of this radial-versus-axial study, the LBLOCA transient, with the nominal [ ] axial peaking factor, was reviewed to predict potential changes in results. The nominal [ ] axial case was used to define the expected changes in results for these two cases.

The reduced axial peak increased the hot channel radial peak. An increase in the radial component is expected to degrade blowdown heat transfer in two ways. First, the integrated hot channel power increases either the initial fluid temperature in the channel or the void fraction for those elevations where saturated conditions are present. Both changes in the fluid conditions should cause lower initial CHF predictions that shorten the time to clad DNB. Second, the integrated power in the channel is expected to produce in more severe fluid conditions used for core heat transfer during late blowdown. The increased power causes earlier dryout and higher steam superheat when reverse core flows are predicted. Both of these conditions should result in less heat removal from the peak power location when compared against the nominal case. Since the end-of-blowdown pin temperatures may be elevated from those of the nominal case, a higher ruptured-segment PCT is expected.

Conversely, a reduction in the radial peaking factor is expected to improve the blowdown heat transfer because of the decrease in the integrated hot channel power. End-of-blowdown temperatures should be lower, but, during the early portion of reflood, the heat removal may be degraded. This degradation is due to reduced stored fuel pin energy and lower decay heat contributions at the bottom of the core. These contributions result in less steam production, and therefore, less liquid carryout. Liquid carryout decreases the steam superheat in the upper regions of the core and improves fuel pin heat removal. Reduction of the carryout is therefore detrimental to early reflood heat transfer, particularly in the upper portions of the core.

During the later portion of reflood, the trend is opposite. The reduced integrated power in the hot channel allows the pool liquid level to advance faster and quench the core sooner. Because the peak cladding temperatures are obtained during the early portion of reflood, the reduced radial peaking is expected to potentially increase the peak cladding temperatures. The ruptured segment is expected to be cooler at the end of blowdown. Therefore, the peak ruptured-segment temperature will most likely be lower than the base case. An unruptured-segment temperature is expected to be limiting for the increased axial case.

The results of the two cases performed for this study are illustrated in Figures A-74 through A-82 and are tabulated in Table A-13. The base [ ] axial case was included for comparison purposes. The [ ] axial peak increased the total hot channel power and compounded the increased power with a corresponding increase in the initial stored energy in the hot assembly. Figure A-79 shows that the highest temperature location (ruptured segment) did not remove these two energy contributions as well as the base case did, particularly during the later portion of the blowdown. Thus, the location of the ruptured-segment shifted down by one segment, and the peak temperature increased by 42 F to 2025 F. The

unruptured-segment location also switched, although its peak temperature was within 1 F of the base case.

The [ ] axial case showed only slight reductions in blowdown fuel pin temperatures in the vicinity of peak power location. The location of rupture was identical to that in the base, but the peak temperature was lower by 35 F. The reduced liquid carryout for this case produced less cooling at Segment 13 and the PCT increased by 39 F to an overall peak of 2022 F. The average-channel hydrogen generation percentage confirms the significance of the initial reflood carryout and its effect on the average channel clad temperatures near the axial power peak location.

These two sensitivity study cases produced the expected variation in results obtained of the base [ ] axial peak case. The highest variation in PCTs was 42 F among these three cases. Both blowdown and reflood heat transfer processes produced differences that were anticipated and observed in results. All three cases met the 10CFR50.46 acceptance criteria at the peak LHR of 16.5 kW/ft. The differences for these altered power peaking components indicate that representative LOCA limits are produced with the base method, which specifies a constant axial peak of [ ] and adjusts the radial peaking factor to give the maximum allowable linear heat rate limit. Typical core maneuvering analyses obtain radial and axial peaking factors similar to those used in the base method. Therefore, this technique is reasonable for EM applications.

Additional information on this topic is provided in the answer to LBLOCA Round 2 RAI 1 on page LA-77 of Volume III.

A.6. Spectrum Studies

A spectrum of break sizes, configurations, and locations were analyzed to determine which would produce the highest peak cladding temperature (PCT). The required spectrum of CLPD break sizes was analyzed for this EM. A variety of break locations was also investigated to confirm that the cold leg pump discharge breaks were most limiting for the generic applications. In addition, smaller transition CLPD breaks were examined to cover the full range of all postulated LBLOCA break sizes. Listed below are the breaks analyzed using the LBLOCA EM.

(1) Four double-ended guillotine breaks in the pump discharge piping with discharge coefficients of 1.0, 0.8, 0.6, and 0.4 were analyzed.

(2) One double-area (twice the cross-sectional area of pipe) split break in the pump discharge with a discharge coefficient of 1.0 was performed.

(3) One double-ended guillotine break in the pump suction piping was performed using a discharge coefficient of 1.0.

(4) Two 2-ft^2 split breaks in the pump discharge were analyzed, both with discharge coefficients of 1.0.

(5) 1.5-, 1-, and 0.75-ft^2 split breaks in the pump discharge were completed with discharge coefficients of 1.0.

(6) One double-ended guillotine break in the hot leg was performed using a discharge coefficient of 1.0.

The general conditions and assumptions used in the spectrum study are identical to the input model from the revised blowdown base case, a double-ended guillotine break at the pump discharge.

A.6.1. CLPD Guillotine Breaks

Results of the CLPD guillotine breaks are presented in Figures A-83 through A-94 with additional results summarized in Table A-14. The hot rod PCT declined with decreasing break size. Three factors are primarily responsible for this reduction in the PCT. As the break size decreased, the core upflow increased during the early phase of the blowdown, the core flooding rates increased because of lower blowdown pin temperatures, and the refill time decreased due to earlier end-of-bypass predictions.

The maximum predicted clad temperature was 1983 F, which was predicted for the full-area CLPD guillotine break with a discharge coefficient of 1.0. This temperature was less than the 2200 F limit in the acceptance criteria of 10CFR50.46.

A.6.2. CLPD Split Break

Results of the CLPD double-area split break are presented in Figures A-96 through A-104 and summarized in Table A-15. The double-area split break in the pump discharge pipe produced greater flows from the reactor vessel side of the leak. Higher core downflows, which provided better cooling, were observed during the later blowdown phase. As a result, the core temperature at the EOB was substantially lower than that of the base case.

A.6.3. CLPS Break

For the pump suction break, the four-volume break arrangement detail used in the pump discharge break was applied to the cold leg piping between the steam generator and the pump. This configuration, shown in Figure A-95, was used for the full area, double-ended, guillotine break with a discharge coefficient of 1.0

in the pump suction piping. The results of the CLPS guillotine break are presented in Figures A-96 through A-104 with additional results summarized in Table A-15. The hot rod cladding ruptured near the EOB. This was caused by relatively stagnant conditions in the core since the break flow rates from the RV side were reduced because of the pump resistance between the RV and the break. However, a significant amount of ECC water was retained in the RV during the blowdown. This shortened the adiabatic heatup period, thereby resulting in a PCT lower than that of the base case.

A.6.4. CLPD Transition Breaks

A set of LBLOCAs at the lower end of the spectrum were analyzed to verify that the larger, double-ended breaks were more limiting and to demonstrate the transition methodology developed in Section 4.3.7.1. A 2-ft^2 analysis was performed using both the large break methodology and the transition methodology to provide a comparison of the methods. Additionally, 1.5-, 1-, and 0.75-ft^2 split breaks were analyzed using the transition methodology. Results of the CLPD 2-ft^2 breaks are presented in Figures A-105 through A-110 with additional results summarized in Table A-16. Results of the CLPD 1.5-, 1-, and 0.75-ft^2 breaks are presented in Figures A-111 through A-118 with additional results summarized in Table A-16.

Additional information on this topic is provided in the answer to LBLOCA Round 1 RAI 7 on page LA-26 of Volume III.

A.6.4.1. CLPD 2-ft^2 Split

The 2-ft^2 CLPD split break was analyzed with both the base LOCA and transition LOCA analysis methods. The purpose was to benchmark the transition LOCA method for use with smaller LBLOCAs.

The base LOCA method includes conservatisms and assumptions that were tailored to the largest CLPD breaks. Certain aspects of these methods (noted in Section 4.3.7) make them inappropriate for transition break sizes. Therefore the transition method was developed to analyze these non-limiting, postulated break sizes.

The comparison of the results between these two cases is shown in Figures A-105 through A-110. Between 15 and 30 seconds the impact of the nonhomogenous core junction modeling in the transition method was noted in the hot channel mass flow rate. Phase separation in the transition method allowed additional liquid to remain in the core during this time period. As a result, the cladding temperature was cooler. After all liquid was depleted from the core region, the near-adiabatic heatup was noted in both cases. BOCR occurred simultaneously for both the RELAP5/MOD2-B&W mechanistic ECC bypass and the RELAP5/MOD2-B&W/REFLOD3B simulation. The core refill rate was slower initially for the transition method as residual lower plenum voiding was condensed. However, by eighty seconds, the refill matched and then exceeded the large LBLOCA rate. The crossflow from the combined channel simulation and the upper plenum drainback through the core baffle and average core allowed the transition method case to reflood the core more rapidly. Since the peak cladding temperatures had already occurred, the increase in the core fill rate was of little benefit.

Accounting for the slight differences in methods, the results of the 2.0-ft^2 analyses match well. This confirms that the upper limit of the transition breaks occurs near this break size. Initial DNB occurred throughout most of the core. The lower plenum cleared, and the core flow reversed. The upflow of steam in the downcomer provided the possibility of ECC liquid bypass. This bypass was properly simulated by the transition LOCA method. The consistent prediction of the lower plenum refill ensured that the peak cladding temperatures were similar. Since the PCTs were near 1600 F, no cladding rupture was predicted.

This benchmark confirms the adequacy of the transition LOCA method for predicting the cladding temperature response for these smaller break sizes. The convergence of results further confirms that this break size is a reasonable point for the two methods to converge. The classical LBLOCA method will therefore be used for break sizes greater than two square feet, while the transition LOCA method will be used for smaller LBLOCAs.

A.6.4.2. CLPD 1.5-ft^2 Split

The 1.5-ft^2 break was analyzed with the transition LOCA methods. The results show similarities to those obtained using the large break methodology. The break size was large enough that the RVVV was not able to handle all of the flow to the break. The lower plenum cleared of liquid allowing an additional path for steam venting. An end-of-blowdown time was calculated at 46 seconds and a lower plenum refill time with a near adiabatic heatup was observed in the 58 to 65 second time frame. BOCR occurred at 65 seconds followed by an orderly core quench. The PCT was 1424 F, therefore no clad rupture occurred.

A.6.4.3. CLPD 1-ft^2 Split

The one square foot break size was the largest which did not clear the reactor vessel lower plenum or predict a classical end of blowdown. The RVVVs were able to pass the core steam production to the break. The steam upflow in the downcomer was reduced because the lower plenum did not totally clear of liquid. Therefore, the ECCS bypass potential was reduced and the core refill was initiated before the core totally dried out. The peak cladding temperature was less than 1100 F, and occurred at nine seconds after break opening from the initial cladding DNB.

A.6.4.4. CLPD 0.75-ft^2 Split

In the 0.75-ft^2 case, the break flow was not the dominant forcing function observed in each of the other break sizes. The results show that the RVVVs were able to pass all of the core steam production to the break. This analysis demonstrated typical SBLOCA behavior, with the minimum hot channel collapsed liquid above two feet. Use of the LBLOCA critical heat flux correlation was the reason that cladding heatup was calculated for this break size. Because of the low cladding temperatures, early core quenching was predicted during the reflood phase.

A.6.5. Hot Leg Break

The double-ended guillotine break in the hot leg used a four-volume break configuration similar to that used for the CLPD and CLPS break modeling. The hot leg modeling for this break location is shown in Figure A-119. The hot leg LOCA was simulated with a double-ended, full-area guillotine break with a discharge coefficient of 1.0. The methods developed in Section 4.3.7.2 were used to analyze this break size and location.

Results of the hot leg break are presented in Figures A-120 through A-124, with additional results summarized in Table A-15. The location of the break ensured that the core flows were significantly positive throughout blowdown. As a result, the heat transfer observed in the core was higher than that seen in the cold leg breaks. Further, the high, positive core flows did not allow the lower plenum to empty, leading to a significantly shortened adiabatic heatup period (1 to 2 seconds). The increased heat transfer also kept the hot channel pin from rupturing. During reflood, the clad temperatures demonstrated a well-behaved quench behavior, with the entire hot channel quenched at the end of the transient.

A.7. Time-in-Life Studies

The LOCA limit analysis is completed by performing a set of analyses using the worst break size and the worst single failure of a safety system to demonstrate compliance with 10CFR50.46 limits. The analyses use the most limiting core power and peaking throughout all elevations in the core and all times in life of the fuel assemblies. The allowable LOCA limits are provided to the fuel cycle designers to be used in combination with all other imposed limits on the fuel pin design to determine the permissible operational states of the plant. The full set of LOCA limit analyses is made up of at least five axial core power peaks that determine the maximum local linear heat rate limits anywhere within the confines of the core. Compliance to the 10CFR50.46 limits must be assured at any core elevation from the initial fuel loading until its maximum burnup.

An NRC-approved steady-state fuel code is used to provide conservative fuel pin initial conditions for LOCA analyses. The fuel inputs may be specific to each LOCA analysis, or be bounding for a set of cases.

The two parameters most significant to LOCA peak cladding temperature are the initial LHR and the fuel stored energy. The most limiting stored energy is found at beginning-of-life (BOL) conditions both for the hot pin and average pin. BOL has the highest initial fuel temperature for the hot pin, although the end-of-life (EOL) temperature is increasing and approaching the BOL value. The fuel temperature decreases early in life because the fuel pellet swells and reduces the gap dimension. The helium-filled gap has the highest thermal conductivity at BOL, however, the gap is the largest. As the fuel is burned, fission gases are produced. Some cause fuel swelling, and some are released into the gap. The fission gases change the gap gas composition and reduce the thermal conductivity of the gap gas. The gap size decrease improves the total gap conductance and initially

overrides the reduced gap gas thermal conductivity. Eventually, the fuel swelling and clad creep allow the gap to become closed. The contact improves the overall conductivity as the contact pressure increases, producing the lowest fuel temperatures. As the fuel continues to increase in burnup, the gap gas composition changes, and the gap conductivity is reduced. A gradual heatup results. Eventually the gas pressure grows until the cladding begins to creep and expand away from the fuel pellet reducing the contact conductance. The burnup gradually reduces the fuel density and fuel thermal conductivity as well. The result is an increase in fuel stored energy.

Elevated pin pressures at high fuel pin burnups could cause clad rupture earlier in blowdown. Once the initial pin pressure reaches the steady-state system pressure, the likelihood of mid-blowdown rupture increases. Mid-blowdown ruptures divert flow from the ruptured location and retain the fuel stored energy by significantly increasing the gap size. Metal-water reaction inside the clad increases the local power generation and further increases the energy that must be removed during the reflood phase. Higher burnup does increase the initial cladding oxide thickness. Since the reaction rate is inversely proportional to the oxide thickness, the energy addition rate is lessened due to reduced metal-water reaction. At the BOL condition, the oxide layers are thin. The increased metal-water reaction rates in combination with the highest stored energy generally makes BOL limiting, at least until mid-blowdown rupture is encountered.

In order to determine the burnup condition that results in the highest PCT during the fuel cycle, and to establish the relationship between burnup and PCT, a sensitivity study was performed at various hot channel burnup conditions. A set of 6.285-ft axial peaks of 16.5 kW/ft were analyzed at 1 (BOL), 10,000, 40,000, and 50,000 MWD/MTU fuel rod burnups. The initial hot pin conditions for the burnup sensitivity study are presented in Table A-17.

Based on the results of the sensitivity studies with the blowdown model, a 2A, double-ended guillotine break with C_D = 1.0 at the pump discharge was selected as the base case to examine the impact of burnup on PCT. RELAP5/MOD2-B&W blowdown calculations were made for all cases listed in Table A-18. The blowdown portion of the 10,000 MWD/MTU case was analyzed twice. The first case applied BOL conditions to the average channel, while the second case applied the 10,000 MWD/MTU conditions. From the blowdown portion of the analysis, it was determined that the most conservative method was to run the average core at BOL conditions. The hot channel blowdown results were similar for both cases. The average channel BOL conditions resulted in higher stored energy that was retained throughout the blowdown. The increased average-channel stored energy at the end of blowdown retarded the reflooding rate because of the increased steam binding. Therefore, the average channel will be maintained at BOL conditions while the hot channel burnup is advanced through the time in life of the fuel to provide the LOCA limit over the warranted fuel performance range.

Table A-18 provides an overall summary of the extended burnup analysis results compared with the base BOL case results. The blowdown upper plenum pressures, reactor vessel-side leak flow rates, pump-side leak flow rates, hot channel mass flow rates at the ruptured location, and hot channel mass flow rates at the peak unruptured clad temperature location are compared in Figures A-125 through A-129. Figure A-130 compares the inlet flooding rate calculated by REFLOD3B. These plots show that the blowdown behavior outside of the fuel pin and the reflooding parameters are relatively insensitive to the burnup conditions.

The clad temperatures, clad heat transfer coefficients, and gap conductance are compared in Figures A-131 through A-136 for the peak unruptured and peak ruptured locations. It is apparent from these figures that the extended burnup conditions significantly

affect the fuel pin results. The primary cause of the differences is the total gap conductance.

The total gap conductance for the fuel pin is described by

$$K_{gap} = h_{gap} \cdot \tau_{g\,cold}\ , \qquad \text{(A-3)}$$

where h_{gap} is the total gap heat transfer coefficient, defined as

$$h_{gap} = h_{gap\,gas} + h_{rad} + h_{fcc}\ . \qquad \text{(A-4)}$$

The portion of the HTC attributable to the gas composition in the gap, $h_{gap\ gas}$, is strongly a function of the gas conductivity, K_{gas}, and the EM pin gap multipliers, M_g. The radiation HTC in the gap, h_{rad}, is a function of the gap temperature to the third power. The fuel-clad contact HTC is represented by h_{fcc}.

The gap gas composition at extended burnups is altered such that K_{gas} is significantly reduced due to the increased presence of Xenon. The EM pin gap multipliers near the peak power location follow a trend similar to the peak initial stored energy, which partially compensates for the decrease in K_{gas} for the EOL type analyses. The fuel-clad contact term, h_{fcc}, decreases as the internal pin pressure increases and the contact pressure decreases. As a result, the total gap conductance is significantly reduced producing an insulative effect on the fuel pin.

An increased difference is obtained between the clad and fuel temperatures for extended burnups versus BOL conditions. The core flows and heat transfer coefficients are essentially unchanged, however, allowing for increased cooling of the clad, increased rate of quench front advancement, a decreased carryout rate fraction, and a higher equilibrium collapsed level in the core.

The initial pin pressure had very little effect on the transient. Pin pressure primarily effects clad rupture, particularly mid-blowdown rupture. For all of the cases examined, rupture occurred near the end of blowdown or during the reflood transient, when the stored energy had been substantially reduced from its initial value.

The conclusions drawn from this study indicate that similar LOCA limits from BOL to approximately 45,000 MWD/MTU burnup can be expected. After 45,000 MWD/MTU burnup, the linear heat rate must be dropped to reduce both the pin pressure and stored energy in the fuel. Plant classification-specific analyses will be performed to verify the LOCA limits with advancing burnup for both UO_2 and urania-gadolinia fuel. The plant-specific applications should use BOL conditions in the average channel to conservatively bound the range of burnup conditions that will be included in the average channel simulation.

This page is intentionally left blank.

A.8. Three Operating RC Pumps at 75 Percent Full Power Study

A LBLOCA analysis was performed with initial conditions based on three operational pumps, with a core power set to 75 percent full power. This study was performed to provide a basis for selection of the most-limiting input parameters and to determine if the four-pump LOCA limits can apply to the three-pump condition. The base case peak linear heat rate of 16.5 kW/ft was used in these three-pump analyses. The base case radial peak was increased from 1.626 to 2.168 to preserve the peak linear heat rate.

Three blowdown calculations were made with the locked rotor located in (1) the broken leg pump (Pump 2A), (2) the intact leg pump of the broken loop (Pump 2B), or (3) one of the intact loop pumps (Pump 1A). A comparison of blowdown results is presented in Figures A-137 through A-141 and in Table A-19. The three-pump case EOB times were all 1.9 to 3.2 seconds longer than the four-pump base case. The case with the locked rotor in the broken leg produced the most severe cladding temperatures at the end of blowdown. This EOB temperature was 15 F below the base case value. It is expected that this case will have lower clad temperatures during reflood due to lower core decay heat and less stored fuel pin energy.

To confirm that the base case remains limiting, the REFLOD3B and BEACH calculations were performed for the worst three-pump operation case. The results are presented in Figures A-142 through A-146 and summarized in Table A-20. They show that the PCT of 1886 F was predicted in an unruptured segment. This peak is 97 F lower than the peak predicted by the base EM case. The higher flooding rates reduced the peak significantly. Therefore, the LOCA limits established for four-pump operation at full power are bounding for three-pump operation at 75 percent power.

This page is intentionally left blank.

A.9. LOCA Limit Demonstration Cases

This EM establishes the methods used in performing LOCA limit analyses for the three classifications of B&W-designed plants. The LOCA limits will be performed at five elevations between the two- and ten-foot elevations within the core with the peaks simulated at the midpoint between the fuel spacer grids. In order to quantify this EM for this purpose, two additional demonstration analyses were performed with peaks near the two- and ten-foot elevations. These cases, in combination with base six-foot analysis, cover the range of elevations to be analyzed in future LOCA limit calculations.

[ ]

studies, the midspan elevations were located at 2.865, 4.575, 6.285, 7.995, and 9.705 feet. Figure A-147 gives the applicable LOCA limit axial power shapes generated by the LYNXT shape generator for this fuel design. The hot channel radial peaking factor was adjusted to give the total normalized peaking factor, F_q, for each elevation. The total peaking factor times the core average power gives the maximum linear heat rate used in the LOCA analysis.

The two LOCA limit demonstration cases were performed with beginning-of-life fuel pin conditions using the instantaneous double-ended CLPD guillotine break with a discharge coefficient of 1.0. The target peak cladding temperatures for these analyses was in the range of 1950 to 2050 F. The peak linear heat rate was adjusted until this criterion was met.

A.9.1. 2.865-ft LOCA Limit Case

This case used a hot channel peak linear heat rate of 16.5 kW/ft at the 2.865-ft elevation in Segment 6 (Figure A-56). The blowdown phase for this case lasted approximately 21 seconds. The RV pressure, leak flows, and core flows are shown on Figures A-148 through A-150 for the blowdown phase. The maximum cladding temperature during blowdown was calculated to be 1867.0 F in Segment 7, at the 3.435-ft elevation. The cladding in the peak power Segment 6 ruptured approximately one second before end of blowdown.

The calculated refill period lasted 6.56 seconds. This near-adiabatic core heatup period was abruptly terminated by BOCR at 27.69 seconds. The rapid initial reflooding rates, shown in Figure A-151, initiated the core quenching process. The steam production resulted in high liquid droplet entrainment that improved cladding heat removal above the quench front. Continued advancement of the quench front provided an almost continuous source for liquid droplet entrainment.

The ruptured-segment cladding temperature peaked at 1986.7 F at 30.0 seconds. The improved surface cooling from the ruptured zone heat transfer effects and approaching quench front quickly dropped the temperatures in the ruptured segment. The peak unruptured segment temperature of 1959.5 F occurred above the peak power location in Segment 7, at nearly the same time as the ruptured segment peak. The temperatures in the upper core segments declined steadily after 70 seconds. By 200.0 seconds, all segment clad temperatures were below 1500 F. The average channel quench front reached the top of the core at 219.8 seconds. The transient responses of the ruptured and peak unruptured cladding temperatures are shown in Figure A-152. The filtered heat transfer coefficients at these locations are shown on Figure A-153. Table A-21 summarizes the key parameters and sequence of events in comparison with the six- and ten-foot cases.

The results of this demonstration case were well within the requirements of 10CFR50.46 and also within the targeted peak cladding temperature range. The skewed bottom-elevation power shape resulted in a peak cladding temperature that was ruptured-segment limited at the location of the axial power peak. The unruptured peak segment temperature occurred one segment above the peak power location. Both of these conditions are typical for the inlet-skewed peak. Rupture near the bottom of the core has the shortest length in which to superheat the steam, and the steam velocities are relatively low. Thus, the ruptured-zone cooling effects from liquid droplet vaporization are reduced, resulting in less cooling immediately above the ruptured location. The advancing quench front quickly reduced the cladding temperatures near the peak power location resulting in the shortest predicted PCT time for both segments. The allowable linear heat rate limit of 16.5 kW/ft is identical to the value established by the six-foot base case.

A.9.2. 6.285-ft LOCA Limit Case

This case was assembled from portions of the sensitivity studies. The blowdown results were taken from the ECCS bypass analysis. The REFLOD3B analysis boundary conditions were as in the base case for the loop noding study. The BEACH results were taken from the final base case time step study. These results were integrated and are discussed in this section for continuity.

The hot channel peak linear heat rate was 16.5 kW/ft at the 6.285-ft elevation in Segment 12. The blowdown phase for this case lasted approximately 21 seconds. The RV pressure, cladding temperature, leak flows, and core flows are labeled as the ECCS Bypass Case on Figures A-42 through A-46 for the blowdown phase. The pressure, leak flows, and two core flows are also given in Figures A-154 through A-156 for consistency with the LOCA limit

discussions. The maximum cladding temperature during blowdown was calculated to be 1831.0 F in Segment 14, at the 7.425-ft elevation. No cladding rupture occurred during blowdown.

The calculated refill period lasted 7.62 seconds, during which the cladding in Segment 11 of the hot channel ruptured. This near-adiabatic core heatup period was abruptly terminated by BOCR at 27.67 seconds. The rapid initial reflooding rates, labeled as the base case on Figure A-48 and also shown in Figure A-157, initiated the core quenching process. The steam production resulted in high liquid droplet entrainment that improved cladding heat removal above the quench front. Advancement of the quench front provided a continuous source for liquid droplet entrainment. The ruptured-segment cladding temperature peaked at 1983.4 F at 30.5 seconds in Segment 11 (5.715 ft). The added cooling from the ruptured zone heat transfer effects and approaching quench front quickly dropped the temperatures in the ruptured segment. The peak unruptured segment temperature of 1958.8 F occurred in Segment 10 (5.145 ft) at approximately 63 seconds. This unruptured peak temperature was approached by Segment 13 (6.855 ft) with a value of 1947.5 F at approximately 52.5 seconds. The transient responses of the ruptured and peak unruptured cladding temperatures are shown in Figure A-57 and A-58, respectively for the final base case. They are also given in Figure A-158. The filtered heat transfer coefficients at theses locations are shown on Figures A-61 and A-62, and repeated in Figure A-159 for the same case.

The temperatures in the upper core segments declined steadily after 80 seconds. By 200.0 seconds, all hot channel segments clad temperatures were below 1500 F. The average channel quench front reached the top of the core at 232.2 seconds. Table A-21 summarizes the key parameters and transient evolution in comparison with the two and ten foot cases.

The results of this full LOCA analysis were well within the requirements of 10CFR50.46 and also within the targeted peak

cladding temperature range for this demonstration case. The midplane power peak resulted in a peak cladding temperature that was ruptured-segment limited. Both the ruptured and peak unruptured segments were located below the axial power peak. The rupture location was shifted below the peak power location because of reduced blowdown cooling during the negative flow period. The peak unruptured node temperature shifted to one level below the rupture because of the rupture zone cooling effects. The rupture effects provided better cooling at the peak power location, Segment 12. Segment 13 was one segment removed, and the rupture effects were accordingly diminished. The peak cladding temperature in Segment 13 approximated the peak found in Segment 10. Slight flooding rate or other boundary condition changes could cause a shift in the peak temperature location between these two segments.

The power shape used for this case increased the distance between the quench front and the peak power location over that of the 2.865 foot case. This distance allowed more steam superheating length, however, the steam velocities increased as additional liquid droplet vaporization took place between the quench front and the higher core locations. Better surface cooling was therefore realized from these high velocities. As a result the peak cladding temperature was pushed to a lower core elevation. The time of the peak was during the long-term reflooding rate interval in which the inlet flooding rate is lower. Therefore, the time of PCT was increased for the unruptured segment. The allowable LOCA limit for this case was consistent with the value established at the two-foot elevation.

A.9.3. 9.705-ft LOCA Limit Case

This case used a hot channel peak linear heat rate of 16.0 kW/ft at the 9.705-ft elevation in Segment 18. The blowdown phase for this case lasted approximately 21 seconds. The RV pressure, leak flows, and core flows are shown on Figures A-160 through A-162 for the blowdown phase. The maximum cladding temperature during blowdown was calculated to be 1834.13 F in Segment 18, at the 9.705-ft elevation. No cladding rupture occurred during blowdown.

The calculated refill period lasted 7.33 seconds, during which the cladding in Segment 18 of the hot channel ruptured. This near-adiabatic core heatup period was ended by BOCR at 27.59 seconds. The rapid initial reflooding rates, shown in Figure A-163, began core quenching. Steam production resulted in high liquid droplet entrainment that improved cladding heat removal above the quench front. Advancement of the quench front provided a continued source for entrained droplets. The ruptured segment cladding temperature dropped by several hundred degrees below its peak temperature of 1906.3 F due to the added surface cooling from the ruptured zone heat transfer effects. The overall PCT of 2020.7 F occurred in Segment 16 at 71.14 seconds. The transient responses of the ruptured and peak unruptured cladding temperatures are shown in Figure A-164. The filtered heat transfer coefficients at theses locations are shown on Figure A-165.

After about 80 seconds, the peak temperatures at other upper core segments began to decline steadily. By 200.0 seconds, the Segment 16 clad temperature was approximately 1500 F. Table A-21 summarizes the key parameters and transient evolution in comparison with the two- and six-foot cases.

The results of this full LOCA analysis were well within the requirements of 10CFR50.46 and within the targeted peak cladding temperature range. The skewed upper-elevation power shape

produced a peak cladding temperature that was unruptured-segment limited, and the peak was located below the axial power peak. Both of these conditions are typical for an exit-skewed peak. Rupture occurs relatively even farther from the quench front, so steam superheat is higher. Conversely, more droplet vaporization occurs over the length of the dispersed flow, and steam velocities are high. The unruptured peak is found below--upstream of--the axial peak because the steam velocities are higher above the peak and the power drops off more steeply. Because the peak power is in the upper portion of the core, the turnaround time for the peak temperature is later. The peak temperature occurs during the lower long-term reflooding rate, which reduces the flows and cladding surface heat transfer. This reduces the allowable linear heat rate limit to 0.5 kW/ft below the values established at the two- and six-foot elevations.

This page is intentionally left blank.

A.10. Minimum Versus Maximum ECCS Injection Study

The basic assumption used in the REFLOD3B analyses presented thus far was the combination of minimum pumped ECC injection and an existing containment pressure calculated with maximum pumped ECC injection would produced the most conservative boundary conditions for hot channel cladding temperature analyses. This assumption was tested via two analyses in which both minimum and maximum pumped ECC injection were imposed on final base case reflood calculations. The blowdown analysis is not affected, since the ECCS actuation time--including delay--occurs after the blowdown phase.

The first step was to complete a CONTEMPT (Ref. A-7) containment pressure analysis with the mass and energy releases from the base blowdown and REFLOD3B analyses with the flow from a single ECC train. The CONTEMPT containment pressure was provided to the REFLOD3B analysis as a new boundary condition from which an iteration was performed. The mass and energy release from REFLOD3B was compared with the original input to CONTEMPT for convergence. Convergence was obtained after one iteration. A similar technique was used for maximum pumped ECC injection (2 trains).

The CONTEMPT containment pressures are shown in Figure A-166 for the original base case and the two new calculations. The mass and energy releases used in the new CONTEMPT analyses are given for both cases in Table A-22 for blowdown and in Table A-23 for reflood. The base case pressure was slightly different during blowdown because those mass and energy releases were taken from an older CRAFT2 analysis (Ref. A-4). The end-of-blowdown containment pressure variation was so small that the RELAP5/MOD2-B&W blowdown was not rerun. The RCS depressurization is so rapid that the end-of-blowdown time, and conditions at that time, will not be appreciably different between the two cases.

Higher ECCS injection has two adverse effects on core flooding rate: Steam-water interaction and condensation in the intact cold leg pipes reduce steam flow into the downcomer, thereby resulting in a lower upper downcomer pressure. Increased ECCS injection reduces containment backpressure causing additional steam binding. The first case evaluated the effects of increased ECC injection on core flooding rate, with the pumped injection increased to its maximum capacity of two LPI pumps and two HPI pumps with a minimum containment pressure. The second case evaluated the minimum ECC injection with the maximum containment pressure. The REFLOD3B

[ ]

condensation in the broken leg will increase steam venting. Comparison plots are shown in Figures A-167 through A-170. Figure A-167 shows a decrease in flooding rate due to increased steam condensation after the accumulators are empty. The downcomer level remained full in the maximum ECC case, however, the condensation penalty offset the higher elevation head.

The REFLOD3B boundary conditions from the two converged analyses were provided to BEACH to perform the hot pin cladding temperature analysis. The results of the two cases are shown in Figures A-171 through A-176 and highlighted in Table A-24. The ruptured segment peak cladding temperatures decreased slightly from the base case. The reduction is attributed to higher carryout due to lower containment pressure at the time of the peak. Higher carryout with the ruptured zone droplet breakup improved the cladding surface heat transfer. The unruptured segment peak was higher and shifted later in time for the maximum injection case because of the reduced flooding rate. The minimum injection unruptured segment peak was slightly higher than the base case because of slower quench front advancement. Lower containment pressure increased the carryout, causing the quench front to lag behind

that observed in the base case. The carryout was not as effective cooling Segment 10 without the ruptured zone effects.

The maximum ECC injection produced the highest peak cladding temperature in this study, but, the minimum ECC injection case is only 35 F cooler. Because of the closeness of these results, this study should be performed for each plant classification for specific LOCA applications studies. Changes in the ECC delay time may cause differences related to filling the downcomer before the core flood tanks empty. In such a case, maximum pumped ECC may improve the flooding rate.

The worst case evaluated in this EM changed because of this study. Nonetheless, the overall effect on the PCT was small because the cladding temperature turnaround occurred during the early phase of the reflooding transient. Thus, the minimum ECCS injection used in the base model for sensitivity studies was acceptable in providing representative cladding temperatures for each of the previous studies.

This page is intentionally left blank.

A.11. Most Severe Break Case

This section summarizes the base RELAP5/MOD2-B&W blowdown, REFLOD3B refill and reflood, and BEACH refill and reflood assumptions and boundary conditions that produced the most limiting peak cladding temperature case. This case was a full double-area, guillotine break in the cold leg pump discharge piping at the elevation of the reactor vessel inlet nozzle. A discharge coefficient of 1.0 was used to maximize the break flow. A loss of offsite power was assumed at the time of break opening, so the reactor coolant pumps and main feedwater pumps were not powered. Pump head degradation using the M1 two-phase multiplier minimized the positive core flow caused by the reactor coolant pumps. The non-mechanistic ECCS bypass method was used during blowdown to discard the ECCS liquid injection prior to prediction of the end of bypass. The maximum time delay of 40 seconds was assumed to start the diesels and initiate two full ECCS trains. For the refill and reflood system analysis, the reactor coolant pump rotors were assumed to be in a fixed position. The maximum ECC fluid temperature was assumed to minimize the steam condensation potential and core inlet subcooling. The maximum ECC flow reduced the containment pressure and adversely affected the reflooding rate and steam binding. Therefore, the peak cladding temperature and highest whole-core hydrogen generation were calculated for this case. The results of this case are given again in Figures A-177 through A-184, and summarized in Table A-25.

This page is intentionally left blank.

A.12. Summary and Conclusions

Numerous RELAP5/MOD2-B&W, REFLOD3B, and BEACH sensitivity studies were performed. The studies were done to demonstrate model convergence and to determine the relative sensitivity of the large break LOCA evaluation model to variations in key input parameters and assumptions. The results either confirmed the base model, or defined changes needed to produce limiting results. Complete LOCA applications that exercised the full complement of codes were also performed. These studies included core peaking factor, break location, break spectrum, time-in-life, three-pump operation, LOCA limits demonstration, and minimum versus maximum pumped ECC injection analyses.

The consistency and continuity of this EM for all LOCA analyses is demonstrated in Figure A-185, which is a plot of peak cladding temperature versus break size for the CLPD break spectrum and several special break analyses. The results of both the large and small break LOCA analyses were obtained using the minimum ECCS injection rate. The peak cladding temperature results were not generated from the worst LBLOCA assumptions and may not necessarily represent the most-limiting SBLOCA results. The cases documented in Section A.6 of Volume I provide the LBLOCA values and Section A.6 of Volume II provide the SBLOCA values contained in this figure. They are given as an indication of the severity of the cladding temperature excursions for different break locations and sizes.

The evaluation model conforms and complies with all of the Appendix K features and criteria. The studies and demonstration cases included in this appendix confirm the convergence and adequacy of the methods described in Volume I of this report. Therefore, this EM is acceptable for use in performing 10CFR50.46 LBLOCA applications for all three classes of B&W-designed plants identified on Table 1-1.

This page is intentionally left blank.

A.13. Appendix A References

Note: These references reflect the revision levels of topical reports used in the sensitivity studies reported in this appendix. The most current revisions of the topicals marked with an "*" are discussed in Section 9 and listed in the Section 10 reference list.

A-1. *J. A. Klingenfus, et al., "RELAP5/MOD2-B&W -- An Advanced Computer Program for Light Water Reactor LOCA and Non-LOCA Transient Analysis," BAW-10164, Revision 3, B&W Nuclear Technologies, Lynchburg, Virginia, October 1992.

A-2. *C. K. Nithianandan, "REFLOD3B -- Model for Multinode Core Reflooding Analysis," BAW-10171, Revision 3, B&W Nuclear Technologies, Lynchburg, Virginia, September 1989.

A-3. *N. H. Shah, "BEACH -- A Computer Program for Reflood Heat Transfer During LOCA," BAW-10166, Revision 4, B&W Nuclear Technologies, Lynchburg, Virginia, October 1992.

A-4. R. J. Lowe, et al., "ECCS Evaluation of B&W's 205FA NSS," BAW-10102, Revision 2, Babcock & Wilcox, Lynchburg, Virginia, December 1975.

A-5. Schyltz, R. R., Sandervag, O., and Hanson, R. G., "Marviken Power Station Critical Flow Data: A Summary of Results and Code Assessment Applications," Nuclear Safety, Vol. 25, No. 6, November-December, 1984.

A-6. NUREG/CR-5194, EGG-2531, "RELAP5/MOD2 Models and Correlations," August 1988.

A-7. Y. H. Hsii, "CONTEMPT - Computer Program for Predicting Containment Pressure-Temperature Response to LOCA," - B&W-Revised Version of Phillips Petroleum Co. Program (L. C. Richardson, et al., June 1967), BAW-10095A Revision 1, Babcock & Wilcox, Lynchburg, Virginia, April 1978.

A-8. *BAW-10168P, "RSG LOCA - BWNT Loss-of-Coolant Accident Evaluation Model for Recirculating Steam Generator Plants," Revision 2, B&W Nuclear Technologies, Lynchburg, Virginia, October 1992.

A-9. J. H. Jones, et al.,"LYNXT - Core Transient Thermal-Hydraulic Program," BAW-10156-A, Revision 1, B&W Fuel Company, Lynchburg, Virginia, August 1993.

A-10. *D. A. Wesley and K. J. Firth, "TACO3 - Fuel Pin Thermal Analysis Code," BAW-10162, Babcock & Wilcox, Lynchburg, Virginia.

Table A-1. RELAP5/MOD2 Parameter Comparison for the Base and Reduced Time Step Cases.

Parameter	Base Case	Decreased Time Step	Increased Time Step
End-of-blowdown (EOB), s	19.460	19.700	19.450
Peak clad temperature at EOB, F	1613.5	1616.6	1602.5
Amount of water in the reactor vessel and cold leg piping at EOB, ft^3	169.703	149.137	166.668
Integrated accumulator injection at EOB, ft^3	621.965	648.274	620.914
Integrated mass out the break at EOB, lbm	578160.	580912.	578333.
Integrated energy out the break at EOB, mBTU	356.317	357.354	356.383

mBTU denotes 10^6 BTU

Table A-2. RELAP5/MOD2 User Requested Time Step Sizes.

Interval	Base Case	Decreased Time Step	Increased Time Step
0.0 - 0.0001 s	0.00001	0.00001	0.00001
0.0001 - 0.5 s	0.0025	0.002	0.0025
0.5 - 2.0 s	0.0025	0.002	0.005
2.0 - 20.0 s	0.010	0.002	0.010
20.0 - 30.0 s	0.005	0.002	0.005

Table A-3. RELAP5/MOD2 Parameter Comparison for the Base and Pressurizer in the Broken Loop Cases.

Parameter	Base Case	Pressurizer Location
End-of-blowdown (EOB), s	19.460	20.110
Peak clad temperature at EOB, F	1613.5	1619.3
Amount of water in the reactor vessel and cold leg piping at EOB, ft^3	169.703	272.122
Integrated accumulator injection at EOB, ft^3	621.965	701.218
Integrated mass out the break at EOB, lbm	578160.	577875.
Integrated energy out the break at EOB, mBTU	356.317	355.746

Table A-4. RELAP5/MOD2 Parameter Comparison for the Base and Break Noding Cases.

Parameter	Base Case	Four Node
End-of-blowdown (EOB), s	19.460	19.750
Peak clad temperature at EOB, F	1613.5	1612.5
Amount of water in the reactor vessel and cold leg piping at EOB, ft^3	169.703	168.703
Integrated accumulator injection at EOB, ft^3	621.965	620.617
Integrated mass out the break at EOB, lbm	578160.	578527.
Integrated energy out the break at EOB, mBTU	356.317	356.026

Table A-5. RELAP5/MOD2 Parameter Comparison for the Base and Core Crossflow Cases.

Parameter	Base Case	[ ]	[ ]	[ ]	[ ]
End-of-blowdown (EOB), s	19.460	19.990	19.520	19.530	20.160
Peak clad temp at EOB, F	1613.5	1600.9	1605.3	1613.3	1643.2
Amount of RV water in cold leg piping at EOB, ft^3	169.703	203.810	172.116	172.631	216.943
Integrated accumulator injection at EOB, ft^3	621.965	677.786	628.297	629.149	694.349
Integrated mass out the break at EOB, lbm	578160.	579214.	578383.	578386.	579500.
Integrated energy out the break at EOB, mBTU	356.317	356.617	356.369	356.397	356.765

Table A-6. RELAP5/MOD2 Parameter Comparison for the Base and Core Noding Cases.

Parameter	Base Case	MC= AC Power	MC=80% of HC Power	MC=90% of HC Power	MC= HC Power
End-of-blowdown (EOB),s	19.460	20.415	19.450	20.230	19.480
Peak clad temp at EOB, F	1613.5	1644.6	1631.1	1648.6	1626.5
Amount of RV water in cold leg piping at EOB, ft^3	169.703	232.793	169.588	224.890	170.497
Integrated accumulator injection at EOB, ft^3	621.965	721.914	621.519	702.852	624.342
Integrated mass out the break at EOB, lbm	578160.	580061.	578137.	579618.	578302.
Integrated energy out the break at EOB, mBTU	356.317	356.869	356.267	356.721	356.382

Table A-7. RELAP5/MOD2 Parameter Comparison for the Base and Pump Degradation Cases.

Parameter	Base Case	M1 Curve	M3 Modified Curve
End-of-blowdown (EOB),s	19.460	19.810	19.560
Peak clad temperature at EOB, F	1613.5	1615.0	1624.8
Amount of water in the reactor vessel and cold leg piping at EOB, ft^3	169.703	183.360	164.542
Integrated accumulator injection at EOB, ft^3	621.965	655.469	641.758
Integrated mass out the break at EOB, lbm	578160.	579231.	579570.
Integrated energy out the break at EOB, mBTU	356.317	356.386	357.083
Hot Channel average oxidation increase, %	0.12	0.14	0.11

Table A-8. RELAP5/MOD2 Parameter Comparison for the Base and Pump Power Study Cases.

Parameter	Base Case	M1 Degr. Pumps Off	M1 Degr. Pumps On
End-of-blowdown (EOB),s	19.460	19.810	20.920
Peak clad temperature at EOB, F	1613.5	1615.0	1603.2
Amount of water in the reactor vessel and cold leg piping at EOB, ft^3	169.703	183.360	158.834
Integrated accumulator injection at EOB, ft^3	621.965	655.469	738.937
Integrated mass out the break at EOB, lbm	578160.	579231.	585920.
Integrated energy out the break at EOB, mBTU	356.317	356.386	358.735

Table A-9. RELAP5/MOD2 Parameter Comparison for the Base and ECCS Bypass Study Cases.

Parameter	Base Case	ECCS Bypass & M1 Degradation
End-of-blowdown (EOB),s	19.460	21.045
Peak clad temperature at EOB, F	1613.5	1653.7
Amount of water in the reactor vessel and cold leg piping at EOB, ft^3	169.703	270.810
Integrated accumulator injection at EOB, ft^3	621.965	792.447
Integrated mass out the break at EOB, lbm	578160.	549268.
Integrated energy out the break at EOB, mBTU	356.317	351.150

Table A-10. BEACH User Requested Time Step Sizes.

Interval	Base Case	Increased Time Step	Decreased Time Step
EOB - 22.0 s	0.05	0.05	0.05
22.0 - 27.0 s	0.05	0.05	0.05
27.0 - 35.0 s	0.0025	0.005	0.001
25.0 - 40.0 s	0.005	0.005	0.001
40.0 - 45.0 s	0.005	0.005	0.0025
45.0 - 80.0 s	0.005	0.005	0.005
80.0 - 300.0 s	0.005	0.005	0.005

Table A-11. BEACH Parameter Comparison for the Base and Reduced Time Step Cases.

Parameter	Base Case	Increased Time Step	Decreased Time Step
RV Lower Plenum Filled, s	27.667	27.670	27.666
LPI Flow Begins, s	40.060	40.060	40.060
CFTs Empty,s	45.330	45.330	45.330
Clad Rupture Time, s	21.195	21.195	21.195
Unruptured Segment:	10	10	10
PCT, F	1968.5	~1977.0	~1958.8
Time, s	~65.0	~65.0	~63.0
Unruptured Segment:	13	13	13
PCT, F	~1956.0	2000.3	1947.5
Time, s	~65.0	46.375	~63.0
Ruptured Segment:	11	11	11
PCT, F	1980.8	1968.7	1983.4
Time, s	30.448	~30.0	30.473
Average Oxidation Increase, %			
Hot Channel	0.73	0.80	0.70
Average Channel	0.066	0.066	0.066

Table A-12. BEACH Parameter Comparison for the Base and Fine-Mesh Rezoning Cases.

Parameter	Base Case	16-Mesh	32-Mesh
RV Lower Plenum Filled, s	27.666	27.666	27.666
LPI Flow Begins, s	40.060	40.060	40.060
CFTs Empty,s	45.330	45.330	45.330
Clad Rupture Time, s	21.195	21.195	21.195
Unruptured Segment:	10	10	10
PCT, F	1958.8	~1939.0	~1951.0
Time, s	~63.0	~53.5	~46.5
Unruptured Segment:	13	13	13
PCT, F	1947.5	1951.3	1976.7
Time, s	~63.0	~46.0	46.030
Ruptured Segment:	11	11	11
PCT, F	1983.4	1983.3	1972.8
Time, s	30.473	30.302	~30.2
Average Oxidation Increase, %			
Hot Channel	0.70	0.70	0.71
Average Channel	0.066	0.066	0.068

Table A-13. Parameter Comparison for the Axial Versus Radial Core Peaking Factor Study.

Parameter	[ ]	[ ]	[ ]
CFT Flow Begins, s	12.8	12.8	12.8
End-of-Bypass, s	18.59	18.57	18.13
End-of-Blowdown (EOB),s	21.045	21.030	21.050
Liquid Mass in RV Lower Plenum at EOB, lbm	15799.8	15823.8	15723.2
Integrated Accumulator Injection at EOB, lbm	48956.7	48965.6	48844.3
Integrated Mass Removed at EOB, lbm			
Break	549268.	549162.	549128.
ECCS Bypass	47796.8	47803.0	47717.9
Integrated Energy out the Break at EOB, BTU	3.5151×10^8	3.5176×10^8	3.5131×10^8
RV Lower Plenum Filled, s	27.666	27.577	27.597
LPI Flow Begins, s	40.060	40.060	40.060
CFTs Empty,s	45.330	45.294	45.314
Clad Rupture Time, s	21.195	20.100	21.350
Unruptured Segment:	10	13	13
PCT, F	1958.8	1959.0	2022.1
Time, s	~63.0	~47.5	47.385
Ruptured Segment:	11	10	11
PCT, F	1983.4	2025.4	1948.1
Time, s	30.473	30.871	~30.0
Average Oxidation Increase, %			
Hot Channel	0.70	0.71	0.73
Average Channel	0.066	0.046	0.090
Whole-Core Hydrogen Generation, %	0.30	0.29	0.33
Average Channel Quench Time, s	232.2	226.3	237.89

Table A-14. Parameter Comparison for the CLPD Guillotine Break Discharge Coefficient Cases.

Parameter	C_D = 1.0	C_D = 0.8	C_D = 0.6	C_D = 0.4
CFT Flow Begins, s	12.8	13.8	16.0	20.8
End-of-Bypass, s	18.590	19.790	22.115	27.450
End-of-Blowdown (EOB),s	21.045	22.855	26.055	32.710
Liquid Mass in RV Lower Plenum at EOB, lbm	15799.8	18748.0	23502.3	31283.0
Integrated Accumulator Injection at EOB, lbm	48956.7	52339.5	57097.4	63277.5
Integrated Mass Removed at EOB, lbm				
Break	549268.	548770.	549047.	548300.
ECCS Bypass	47796.8	51758.6	56520.9	63277.5
Integrated Energy out the Break at EOB, BTU	3.5151×10^8	3.5187×10^8	3.6131×10^8	3.6473×10^8
RV Lower Plenum Filled, s	27.666	28.919	31.378	36.727
LPI Flow Begins, s	40.060	40.060	40.060	40.065
CFTs Empty,s	45.330	46.900	49.51	55.56
Clad Rupture Time, s	21.195	23.205	26.605	38.912
Unruptured Segment:	10	10	13	13
PCT, F	1958.8	1911.0	1882.0	1696.3
Time, s	~63.0	~49.5	53.140	59.820
Ruptured Segment:	11	11	11	12
PCT, F	1983.4	1959.2	1782.2	1654.3
Time, s	30.473	31.802	~32.4	~40.0
Average Oxidation Increase, %				
Hot Channel	0.70	0.53	0.39	0.16
Average Channel	0.066	0.052	0.038	0.0012
Whole-Core Hydrogen Generation, %	0.30	0.23	0.17	0.06
Average Channel Quench Time, s	232.2	208.4	190.1	140.6

Table A-15. Parameter Comparison for the CLPD Split, CLPS Guillotine, and Hot Leg Guillotine Break Cases.

Parameter	Base Case	CLPD Split	CLPS	Hot Leg
CFT Flow Begins, s	12.8	13.2	11.8	10.0
End-of-Bypass, s	18.59	19.92	15.64	8.68
End-of-Blowdown (EOB),s	21.045	22.010	20.210	15.435
Liquid Mass in RV Lower Plenum at EOB, lbm	15799.8	11349.5	34681.3	NA
Integrated Accumulator Injection at EOB, lbm	48956.7	50675.3	48955.4	~23416.3
Integrated Mass Removed at EOB, lbm				
Break	549268.	549788.	564195.	~532366.
ECCS Bypass	47796.8	49346.2	NA	NA
Integrated Energy out the Break at EOB, BTU	3.5151×10^8	3.6056×10^8	3.5334×10^8	$\sim 3.5777 \times 10^8$
RV Lower Plenum Filled, s	27.666	29.430	23.445	NA
LPI Flow Begins, s	40.060	40.063	40.045	42.000
CFTs Empty,s	45.330	46.249	45.024	40.000
Clad Rupture Time, s	21.195	25.810	18.225	None
Unruptured Segment:	10	12	12	12
PCT, F	1958.8	1873.6	1913.7	1619.7
Time, s	~63.0	49.860	45.650	30.480
Ruptured Segment:	11	13	13	NA
PCT, F	1983.4	1858.5	1904.2	NA
Time, s	30.473	~7.5	~27.0	NA
Average Oxidation Increase, %				
Hot Channel	0.70	0.43	0.42	0.063
Average Channel	0.066	0.037	0.038	0.0001
Whole-Core Hydrogen Generation, %	0.30	0.18	0.18	0.023
Average Channel Quench Time, s	232.2	200.3	204.1	111.4

Table A-16. Parameter Comparison for the CLPD Transition Break Cases.

Parameter	2-ft² LOCA	CLPD Transition LOCA Method Cases 2-ft²	1.5-ft²	1-ft²	0.75-ft²
CFT Flow Begins, s	33.0	33.0	42.0	64.0	84.0
End-of-Bypass, s	43.375	40.656	46.575	74.644	99.350
End-of-Blowdown (EOB),s	49.200	47.325	62.400	NA	NA
Bottom of Core Recovery, s	53.672	~52.0	~65.0	NA	NA
LPI Flow Begins, s	44.525	42.675	50.600	78.650	106.0
CFTs Empty,s	69.786	~28.0	140.0	NA	NA
Unruptured Segment:	13	12	13	15	15
PCT, F	1598.3	1555.2	1424.1	1095.1	1088.2
Time, s	71.055	75.919	90.406	9.0250	11.5000
Ave. Oxidation Increase, %					
Hot Channel	0.082	0.044	0.015	0.0002	0.0001
Average Channel	0.0001	0.0001	0.0003	0.0001	0.0001
Whole-Core Hydrogen Generation, %	0.031	0.016	0.006	0.0001	0.0001
Average Channel Quench Time, s	107.5	152.3	157.2	149.3	170.4

Table A-17. Hot Pin Initial Parameter Comparison for the Time-in-Life Cases.

Parameter	BOL	10,000 MWD/MTON	40,000 MWD/MTON	50,000 MWD/MTON
Hot Spot (6-ft) Average Fuel Temperature, F	2488.0	2266.6	2234.6	2381.1
Gas Pressure, psia	1004.12	1227.15	2491.65	3431.60
Hot Spot Inside Oxide Thickness, in	1.250×10^{-6}	2.004×10^{-4}	2.004×10^{-4}	2.004×10^{-4}
Hot Spot Outside Oxide Thickness, in	3.850×10^{-7}	2.564×10^{-5}	3.590×10^{-5}	4.104×10^{-5}

Table A-18. Parameter Comparison for the Time-in-Life Study.

Parameter	Base Case	10,000 MWD/MTON	40,000 MWD/MTON	50,000 MWD/MTON
CFT Flow Begins, s	12.8	12.8	12.8	12.8
End-of-Bypass, s	18.59	18.59	18.59	18.59
End-of-Blowdown (EOB),s	21.045	21.085	21.085	21.085
Liquid Mass in RV Lower Plenum at EOB, lbm	15799.8	15353.1	15403.7	15622.6
Integrated accumulator injection at EOB, lbm	48956.7	49191.9	49191.6	49190.0
Integrated Mass Removed at EOB, lbm				
Break	549268.	549349.	549355.	549367.
ECCS Bypass	47796.8	47824.5	47826.9	47813.1
Integrated energy out the break at EOB, BTU	$3.5151x10^8$	$3.5153X10^8$	$3.5151X10^8$	$3.5154X10^8$
RV Lower Plenum Filled, s	27.666	27.660	27.672	27.637
LPI Flow Begins, s	40.060	40.060	40.060	40.060
CFTs Empty,s	45.330	45.294	45.297	45.273
Clad Rupture Time, s	21.195	22.000	21.185	19.170
Unruptured Segment:	10	13	13	12
PCT, F	1958.8	1863.0	1881.3	2004.7
Time, s	~63.0	87.490	45.955	~31.0
Ruptured Segment:	11	10	11	11
PCT, F	1983.4	1714.9	1787.1	2046.7
Time, s	30.473	~29.0	~46.0	30.949
Average Oxidation Increase, %				
Hot Channel	0.70	0.38	0.37	0.52
Average Channel	0.066	0.066	0.067	0.066
Whole-Core Hydrogen Generation, %	0.30	0.18	0.12	0.23
Average Channel Quench Time, s	232.2	230.9	231.8	230.9

Table A-19. RELAP5/MOD2 Parameter Comparison for the 3-Pump, 75 Percent Power Study.

Parameter	Base Case	Pump 2B Locked	Pump 2A Locked	Pump 1A Locked
End-of-blowdown (EOB),s	19.460	21.380	22.645	21.415
Peak clad temperature at EOB, F	1613.5	1523.1	1598.6	1581.5
Amount of water in the reactor vessel and cold leg piping at EOB, ft^3	169.703	245.352	297.041	279.147
Integrated accumulator injection at EOB, lbm	48956.7	50176.3	52962.4	50079.5
Integrated mass out the break at EOB, lbm	578160.	549112.	549099.	548583.
Integrated energy out the break at EOB, mBTU	356.317	354.125	352.603	352.593

Table A-20. Parameter Comparison for the 3-Pump, 75 Percent Power Study.

Parameter	Base Case	Inoperable Pump In Broken Cold Leg
CFT Flow Begins, s	12.8	13.4
End-of-Bypass, s	18.59	19.45
End-of-Blowdown (EOB),s	21.045	22.645
Liquid Mass in RV Lower Plenum at EOB, lbm	15799.8	17331.5
Integrated accumulator injection at EOB, lbm	48956.7	52962.4
Integrated Mass Removed at EOB, lbm		
Break	549268.	549099.
ECCS Bypass	47796.8	52074.0
Integrated energy out the break at EOB, BTU	3.5151×10^8	3.5260×10^8
RV Lower Plenum Filled, s	27.666	28.998
LPI Flow Begins, s	40.060	40.060
CFTs Empty,s	45.330	46.204
Clad Rupture Time, s	21.195	25.095
Unruptured Segment:	10	10
PCT, F	1958.8	1886.2
Time, s	~63.0	58.805
Ruptured Segment:	11	11
PCT, F	1983.4	1752.9
Time, s	30.473	~30.6
Average Oxidation Increase, %		
Hot Channel	0.70	0.51
Average Channel	0.066	0.048
Whole-Core Hydrogen Generation, %	0.30	0.22
Average Channel Quench Time, s	232.2	162.2

Table A-21. Parameter Comparison for the 2-, 6-, and 10-ft LOCA Limit Demonstration Cases.

Parameter	2.865-ft	6.285-ft	9.705-ft
CFT Flow Begins, s	12.8	12.8	12.6
End-of-Bypass, s	18.67	18.59	18.50
End-of-Blowdown (EOB),s	21.130	21.045	20.985
Liquid Mass in RV Lower Plenum at EOB, lbm	15529.9	15799.8	15311.8
Integrated accumulator injection at EOB, lbm	49164.7	48956.7	49053.5
Integrated Mass Removed at EOB, lbm			
Break	549139.	549268.	549628.
ECCS Bypass	48004.0	47796.8	47687.4
Integrated energy out the break at EOB, BTU	3.5217×10^8	3.5151×10^8	3.5144×10^8
RV Lower Plenum Filled, s	27.694	27.666	27.588
LPI Flow Begins, s	40.060	40.060	40.060
CFTs Empty,s	44.333	45.330	45.213
Clad Rupture Time, s	20.070	21.195	21.585
Unruptured Segment:	7	10	16
PCT, F	1959.5	1958.8	2020.7
Time, s	~54.0	~63.0	71.140
Ruptured Segment:	6	11	18
PCT, F	1986.7	1983.4	1888.1
Time, s	30.002	30.473	~36.0
Average Oxidation Increase, %			
Hot Channel	0.68	0.70	0.67
Average Channel	0.039	0.066	0.091
Whole-Core Hydrogen Generation, %	0.28	0.30	0.30
Average Channel Quench Time, s	219.8	232.2	239.1

Table A-22. Blowdown Mass and Energy Releases for the Minimum Versus Maximum ECCS Cases.

	Maximum ECCS Injection		Minimum ECCS Injection	
Time, s	Int Mass (lbm)	Int Energy (BTU)	Int Mass (lbm)	Int Energy (BTU)
0.0	0.0	0.0	0.0	0.0
2.0	159343.	9.18×10^7	159343.	9.18×10^7
4.0	2.76×10^5	1.61×10^8	2.76×10^5	1.61×10^8
6.0	3.64×10^5	2.16×10^8	3.64×10^5	2.16×10^8
8.0	4.36×10^5	2.62×10^8	4.36×10^5	2.62×10^8
10.0	4.88×10^5	2.97×10^8	4.88×10^5	2.97×10^8
12.0	5.17×10^5	3.22×10^8	5.17×10^5	3.22×10^8
14.0	5.38×10^5	3.39×10^8	5.38×10^5	3.39×10^8
16.0	5.58×10^5	3.49×10^8	5.58×10^5	3.49×10^8
18.0	5.76×10^5	3.55×10^8	5.76×10^5	3.55×10^8
21.045	5.97×10^5	3.59×10^8	5.97×10^5	3.59×10^8

Table A-23. Reflood Mass and Energy Releases for the Minimum Versus Maximum ECCS Cases.

	Maximum ECCS Injection		Minimum ECCS Injection	
Time, s	Int Mass (lbm)	Int Energy (BTU)	Int Mass (lbm)	Int Energy (BTU)
28.278	0.0	0.0	0.0	0.0
35.04	1265.4	1.54×10^6	1265.4	1.54×10^6
40.04	14677.4	5.03×10^6	14677.4	5.03×10^6
46.04	40504.9	1.05×10^7	36502.0	1.01×10^7
50.04	44880.4	1.28×10^7	38548.2	1.27×10^7
55.04	50449.0	1.57×10^7	40358.5	1.49×10^7
60.04	56100.4	1.86×10^7	42512.0	1.76×10^7
65.04	61812.0	2.15×10^7	44683.0	2.02×10^7
70.04	67562.0	2.43×10^7	47044.0	2.29×10^7
81.04	80316.0	3.06×10^7	52353.0	2.87×10^7
91.04	91998.0	3.61×10^7	57278.0	3.38×10^7
101.04	103735.	4.16×10^7	62267.0	3.88×10^7
121.04	127299.	5.21×10^7	72345.0	4.84×10^7
141.04	150913.	6.04×10^7	82478.0	5.75×10^7
161.04	174535.	7.18×10^7	92640.0	6.62×10^7
181.04	198167.	8.12×10^7	102852.	7.44×10^7
201.04	221883.	9.02×10^7	113168.	8.24×10^7
221.04	245677.	9.91×10^7	123578.	9.00×10^7

Table A-24. Parameter Comparison for the Minimum Versus Maximum ECCS Cases.

Parameter	Base Case	Max ECCS	Min ECCS
CFT Flow Begins, s	12.8	12.8	12.8
End-of-Bypass, s	18.59	18.59	18.59
End-of-Blowdown (EOB),s	21.045	21.045	21.045
Liquid Mass in RV Lower Plenum at EOB, lbm	15799.8	15799.8	15799.8
Integrated accumulator injection at EOB, lbm	48956.7	48956.7	48956.7
Integrated Mass Removed at EOB, lbm			
Break	549268.	549268.	549268.
ECCS Bypass	47796.8	47796.8	47796.8
Integrated energy out the break at EOB, BTU	3.5151×10^8	3.5151×10^8	3.5151×10^8
RV Lower Plenum Filled, s	27.666	27.552	27.557
LPI Flow Begins, s	40.060	40.060	40.060
CFTs Empty,s	45.330	45.136	45.132
Clad Rupture Time, s	21.195	21.195	21.195
Unruptured Segment:	10	10	10
PCT, F	1958.8	2015.2	1980.5
Time, s	~63.0	66.245	63.710
Ruptured Segment:	11	11	11
PCT, F	1983.4	1967.2	1966.4
Time, s	30.473	~30.4	~30.4
Average Oxidation Increase, %			
Hot Channel	0.70	0.84	0.75
Average Channel	0.066	0.076	0.067
Whole-Core Hydrogen Generation, %	0.30	0.36	0.32
Average Channel Quench Time, s	232.2	253.4	232.1

Table A-25. Most Severe Break Case.

Parameter	Base Case
CFT Flow Begins, s	12.8
End-of-Bypass, s	18.59
End-of-Blowdown (EOB),s	21.045
Liquid Mass in RV Lower Plenum at EOB, lbm	15799.8
Integrated accumulator injection at EOB, lbm	48956.7
Integrated Mass Removed at EOB, lbm	
Break	549268.
ECCS Bypass	47796.8
Integrated energy out the break at EOB, BTU	3.5151×10^8
RV Lower Plenum Filled, s	27.552
LPI Flow Begins, s	40.060
CFTs Empty,s	45.136
Clad Rupture Time, s	21.195
Unruptured Segment:	10
PCT, F	2015.2
Time, s	66.245
Ruptured Segment:	11
PCT, F	1967.2
Time, s	~30.4
Average Oxidation Increase, %	
Hot Channel	0.84
Average Channel	0.076
Whole-Core Hydrogen Generation, %	0.36
Average Channel Quench Time, s	253.4

This page is intentionally left blank.

FIGURE A-1. RELAP5/MOD2 TIME STEP STUDY - REACTOR VESSEL UPPER PLENUM PRESSURE.

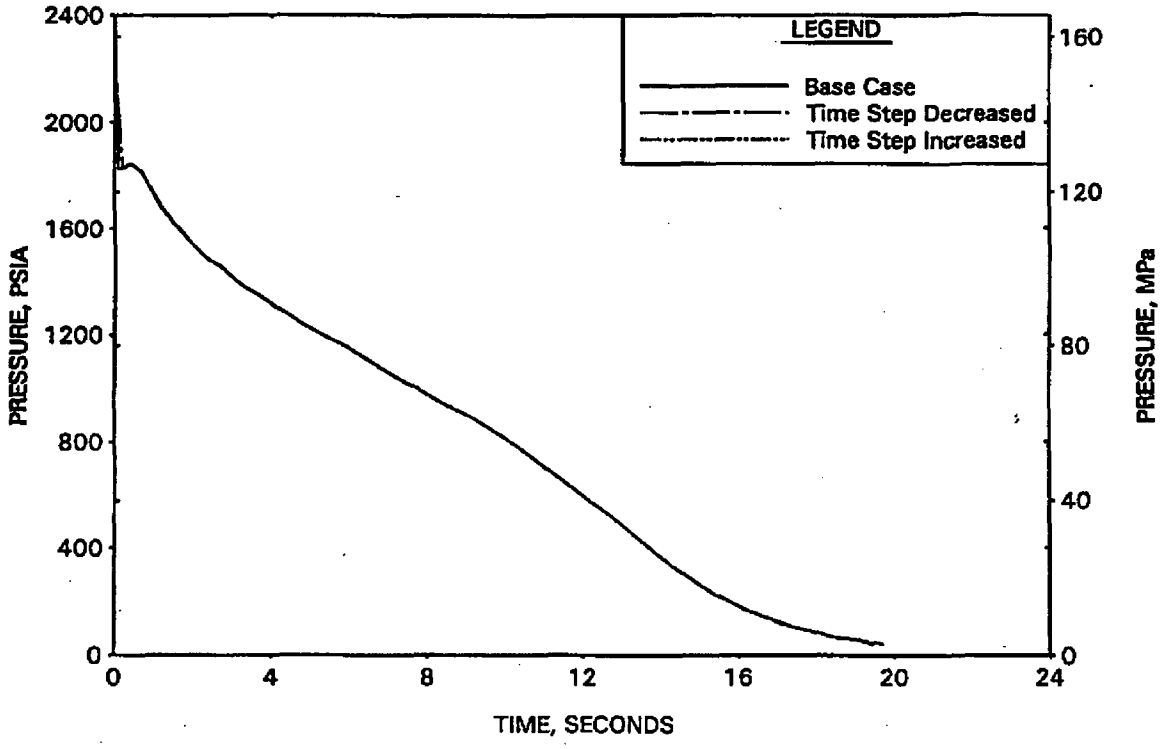

FIGURE A-2. RELAP5/MOD2 TIME STEP STUDY - HC CLAD TEMP AT PEAK POWER LOCATION.

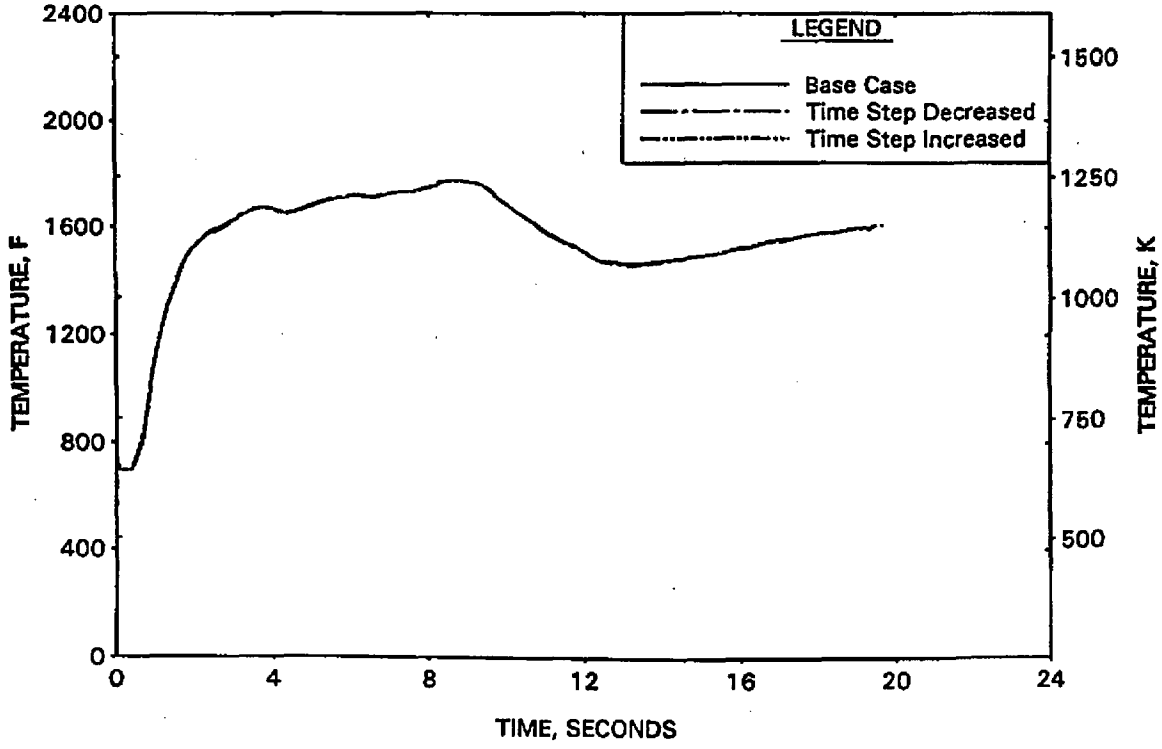

FIGURE A-3. RELAP5/MOD2 TIME STEP STUDY - RV SIDE BREAK MASS FLOW RATE.

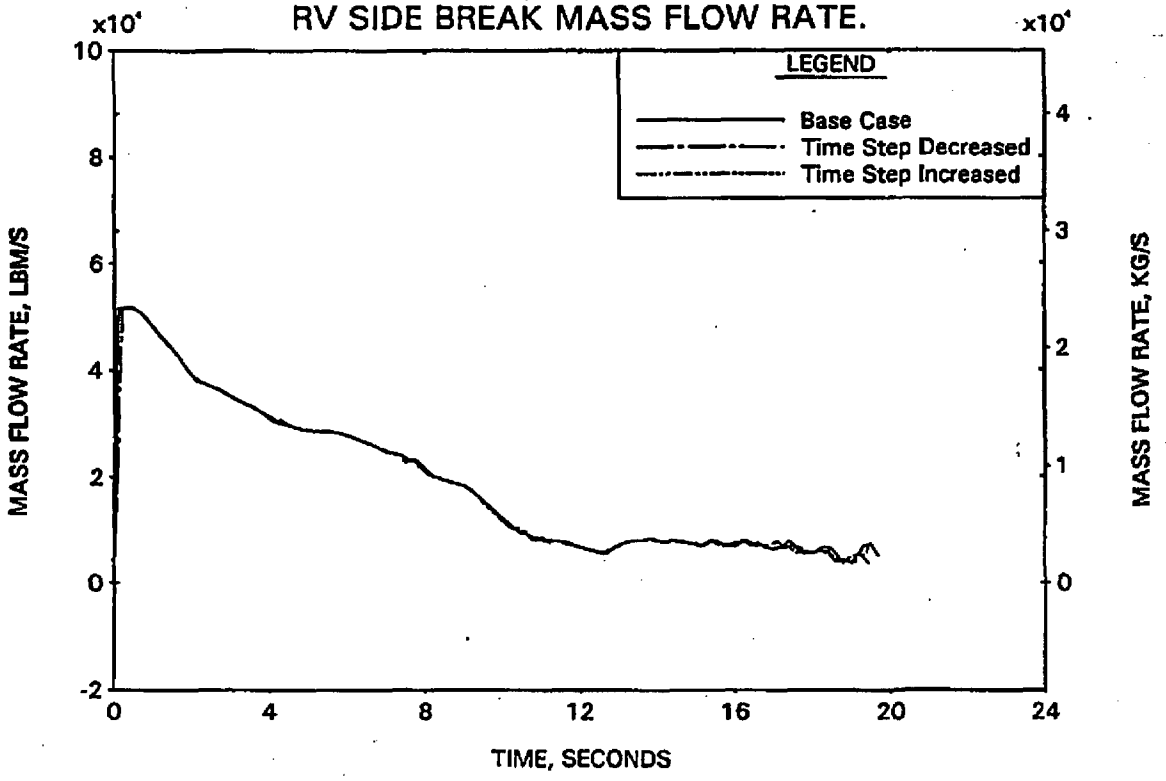

FIGURE A-4. RELAP5/MOD2 TIME STEP STUDY - PUMP SIDE BREAK MASS FLOW RATE.

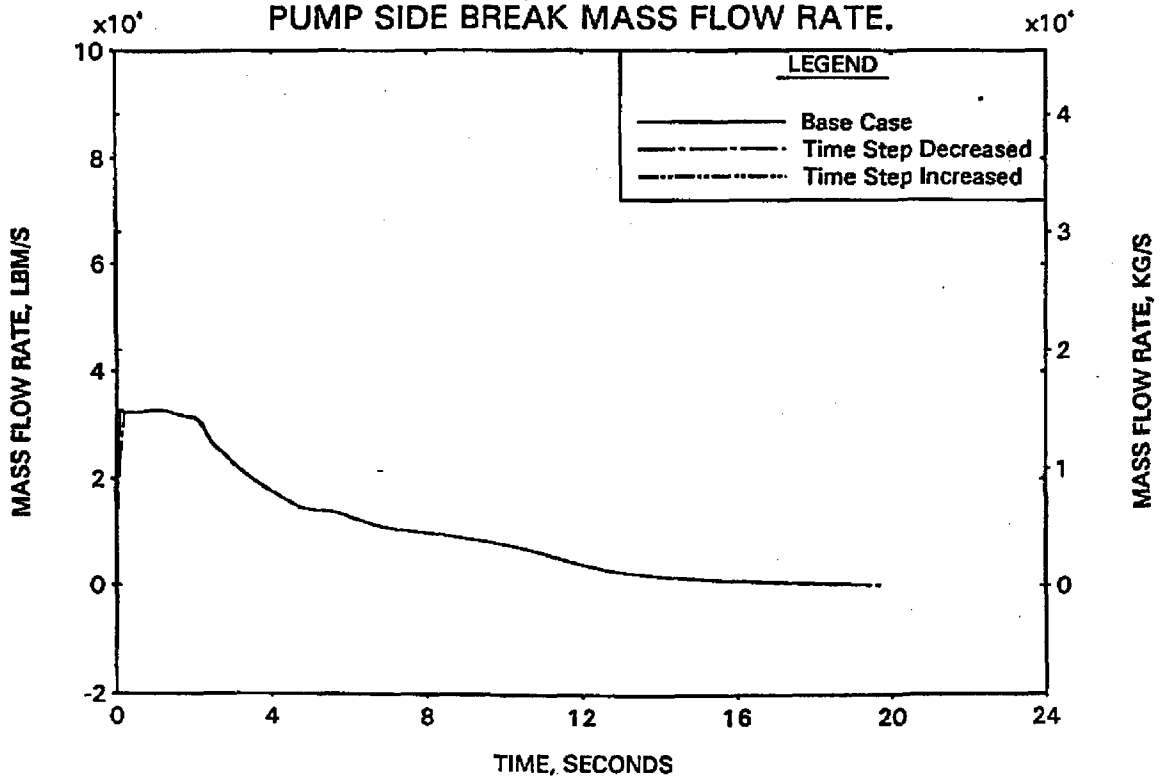

FIGURE A-5. RELAP5/MOD2 TIME STEP STUDY -
HC MASS FLOW RATE AT PEAK POWER LOCATION.

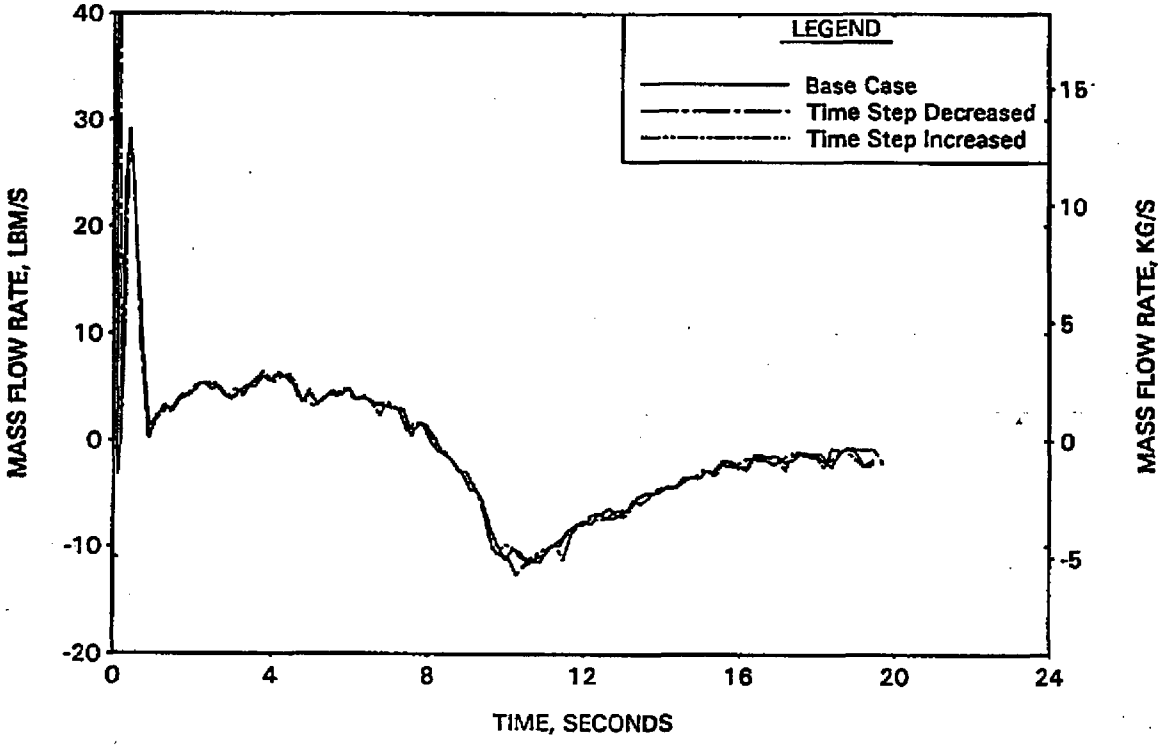

FIGURE A-6. RELAP5/MOD2 TIME STEP STUDY -
CODE TIME STEP ADVANCEMENTS.

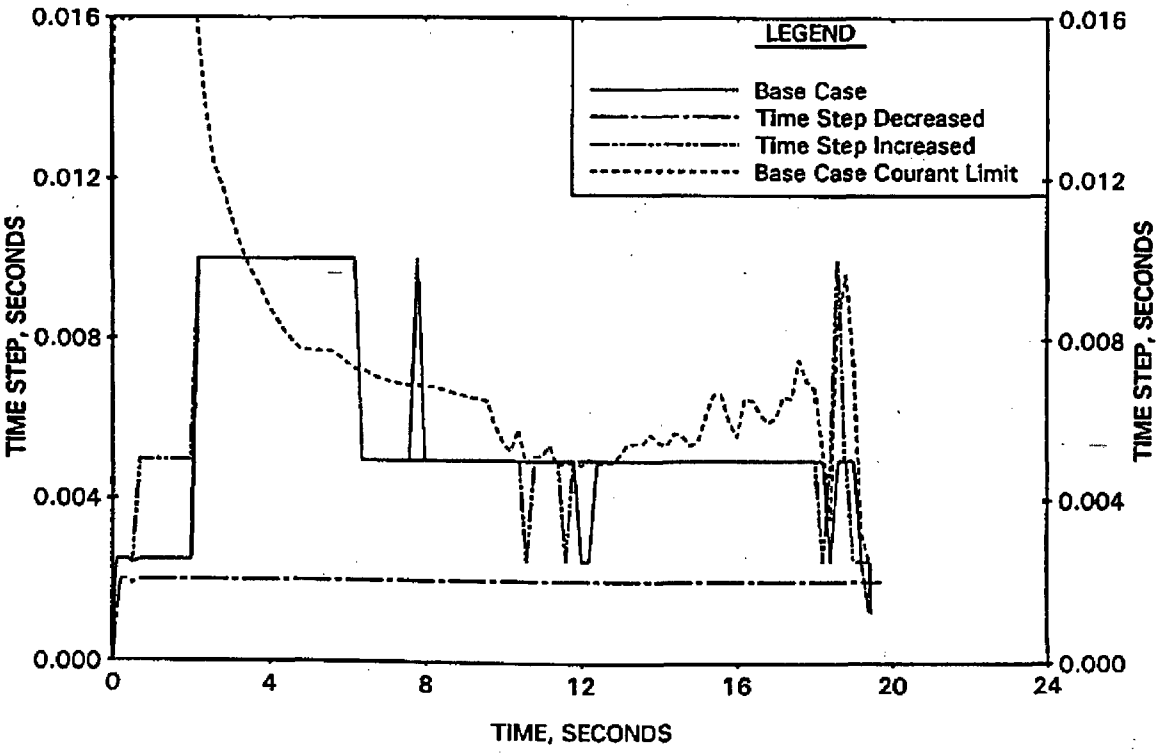

FIGURE A-7. RELAP5/MOD2 PRESSURIZER STUDY - REACTOR VESSEL UPPER PLENUM PRESSURE.

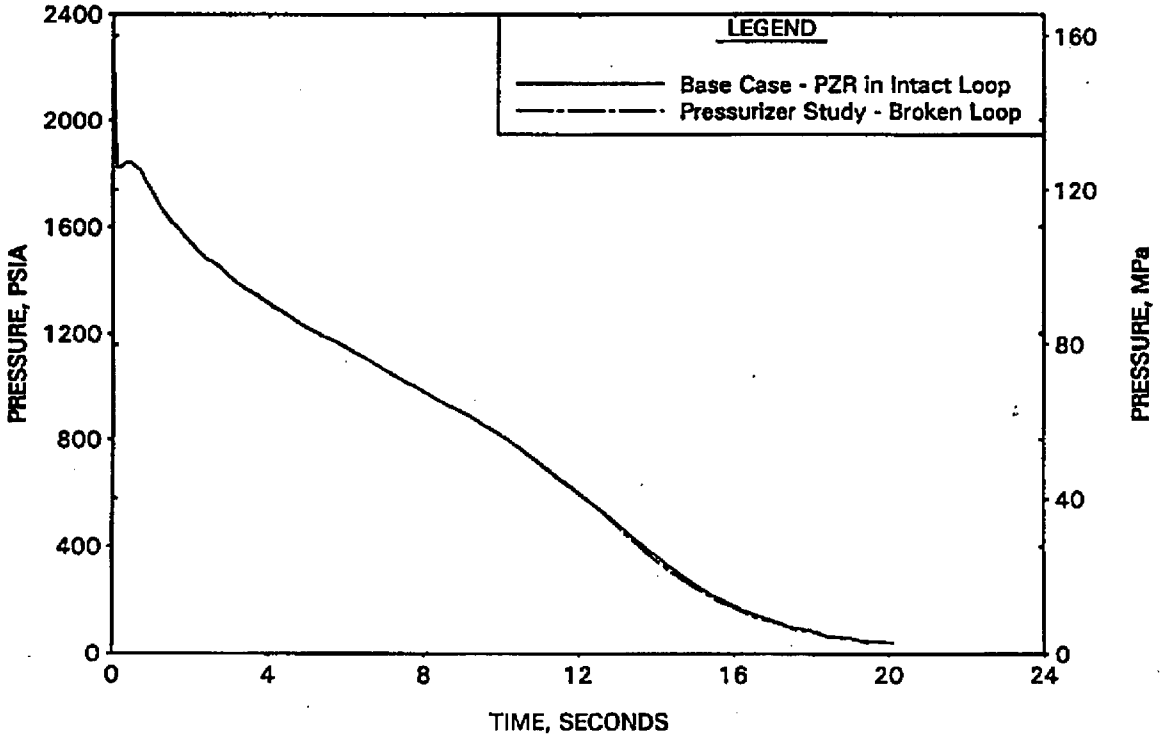

FIGURE A-8. RELAP5/MOD2 PRESSURIZER STUDY - HC CLAD TEMP AT PEAK POWER LOCATION.

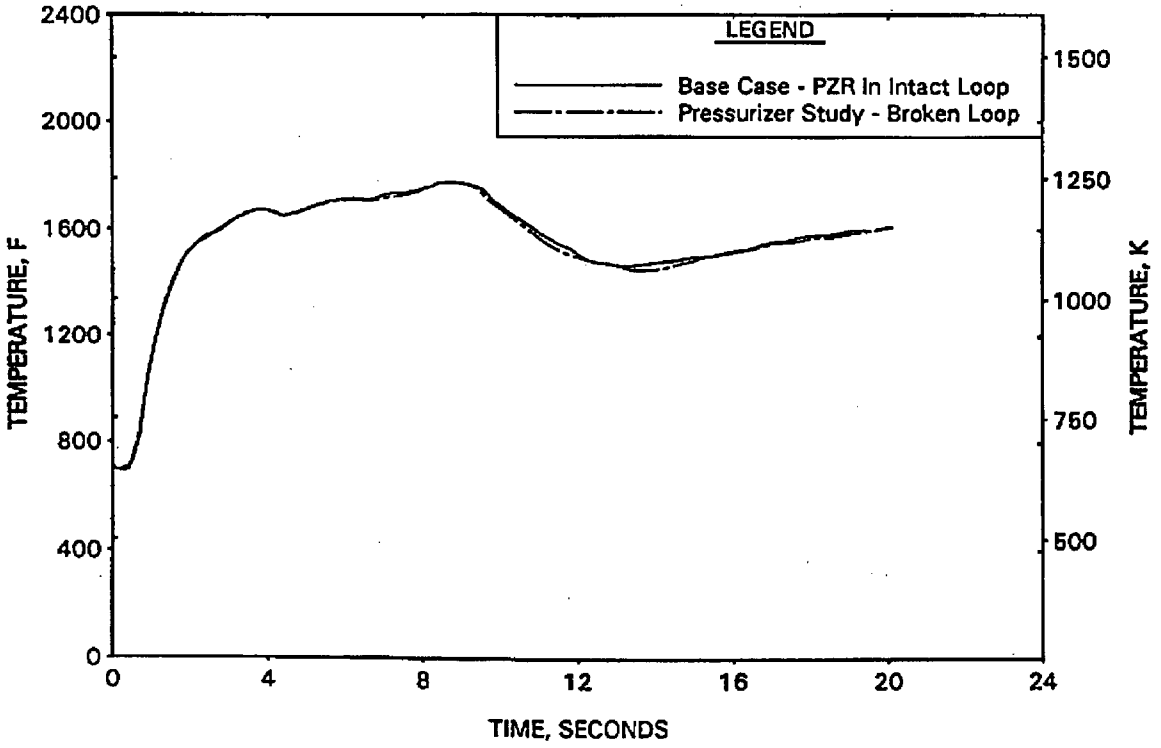

FIGURE A-9. RELAP5/MOD2 PRESSURIZER STUDY - RV SIDE BREAK MASS FLOW RATE.

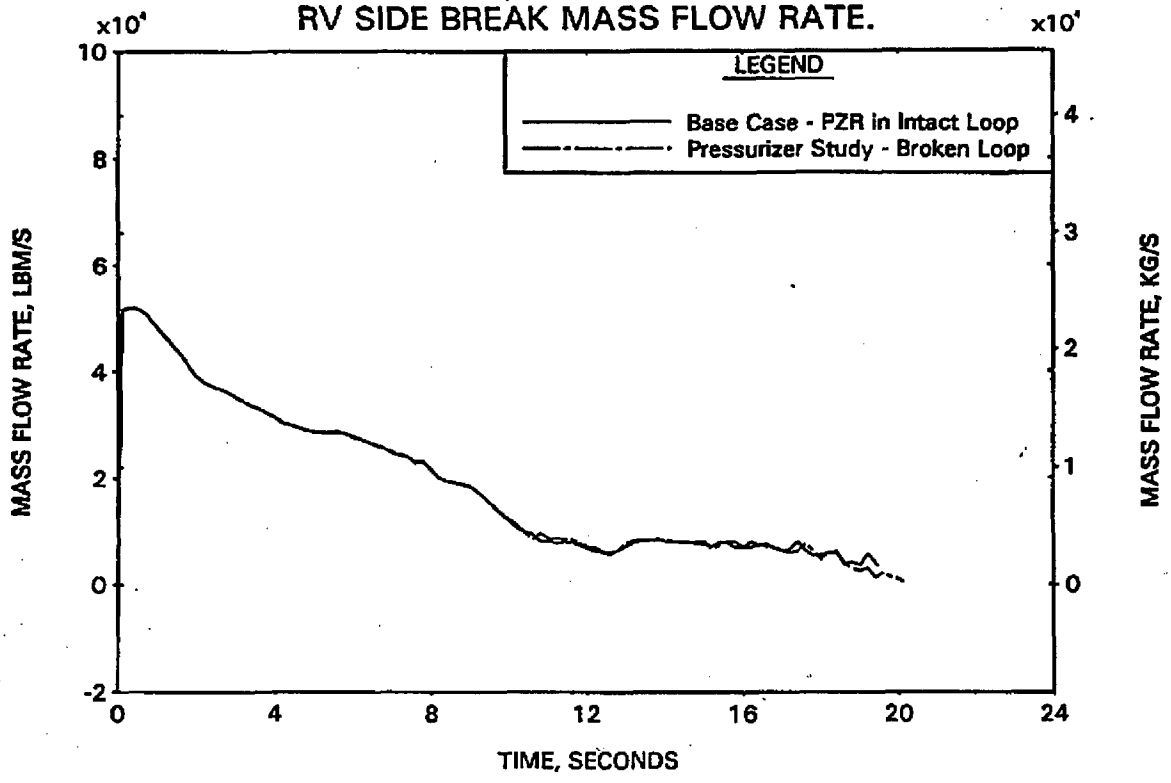

FIGURE A-10. RELAP5/MOD2 PRESSURIZER STUDY - PUMP SIDE BREAK MASS FLOW RATE.

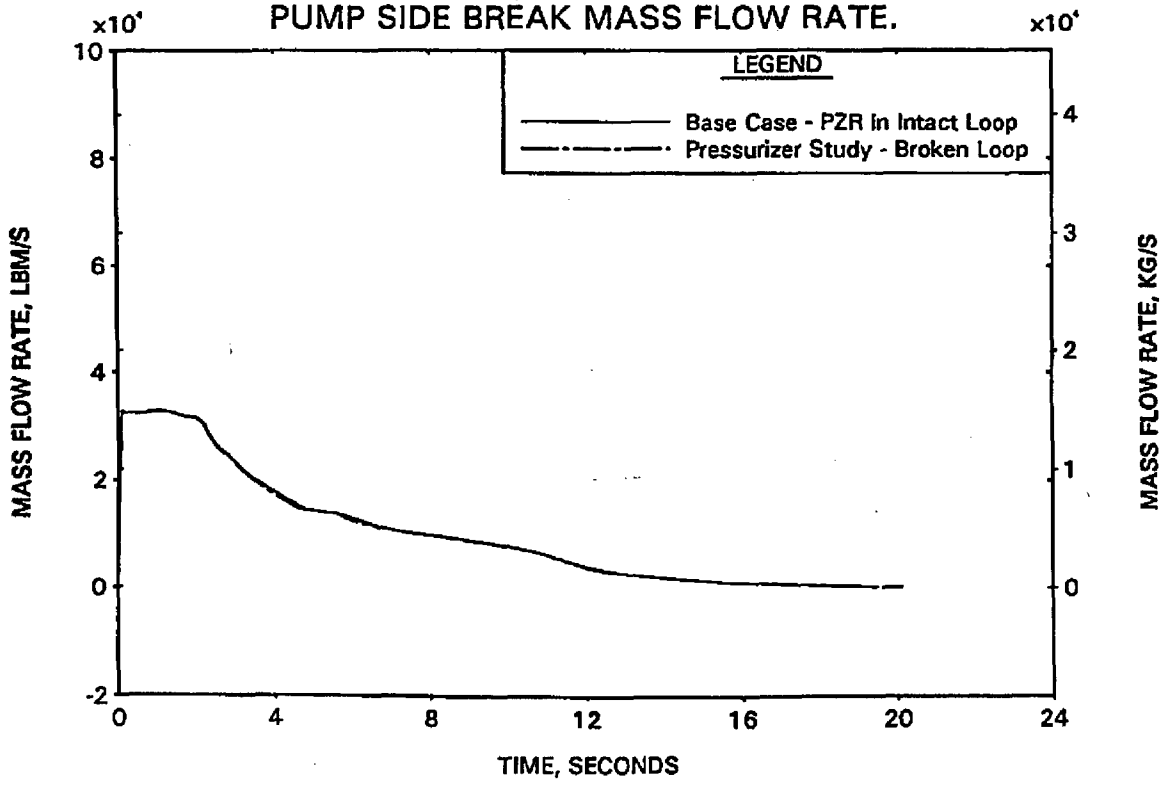

FIGURE A-11. RELAP5/MOD2 PRESSURIZER STUDY - HC MASS FLOW RATE AT PEAK POWER LOCATION.

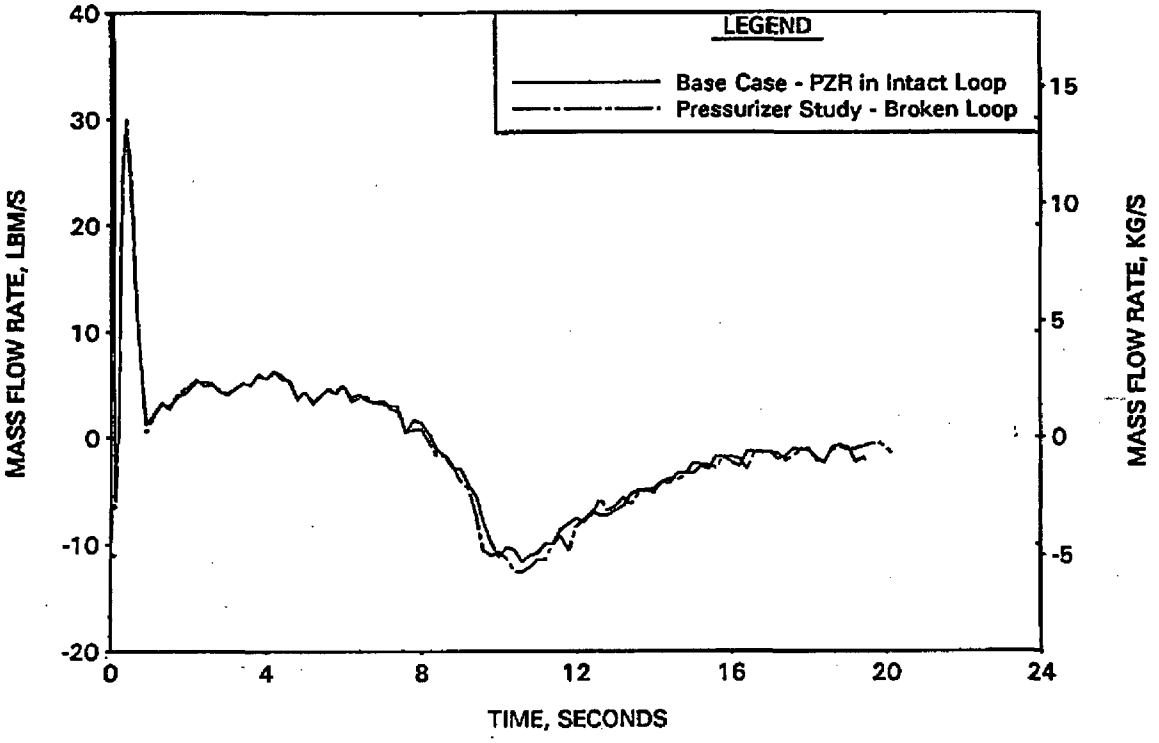

FIGURE A-12. DETAILED CLPD BREAK NODING ARRANGEMENT.

C,E

FIGURE A-13. RELAP5/MOD2 BREAK NODING STUDY - REACTOR VESSEL UPPER PLENUM PRESSURE.

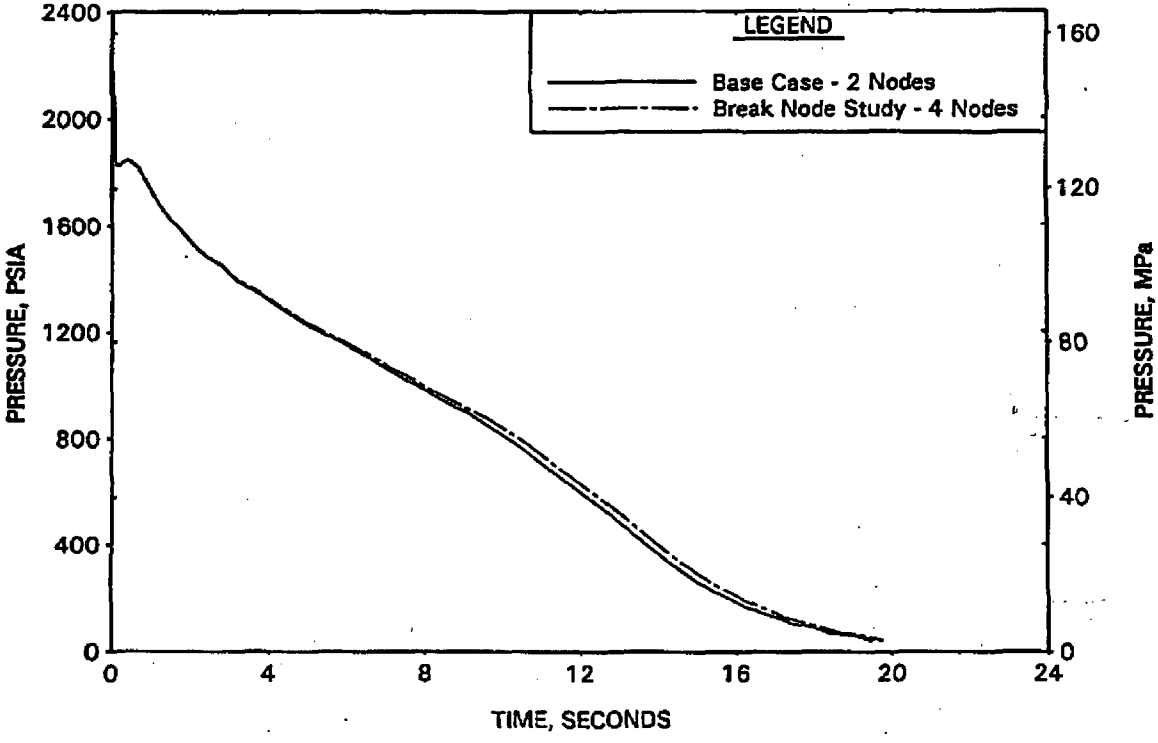

FIGURE A-14. RELAP5/MOD2 BREAK NODING STUDY - HC CLAD TEMP AT PEAK POWER LOCATION.

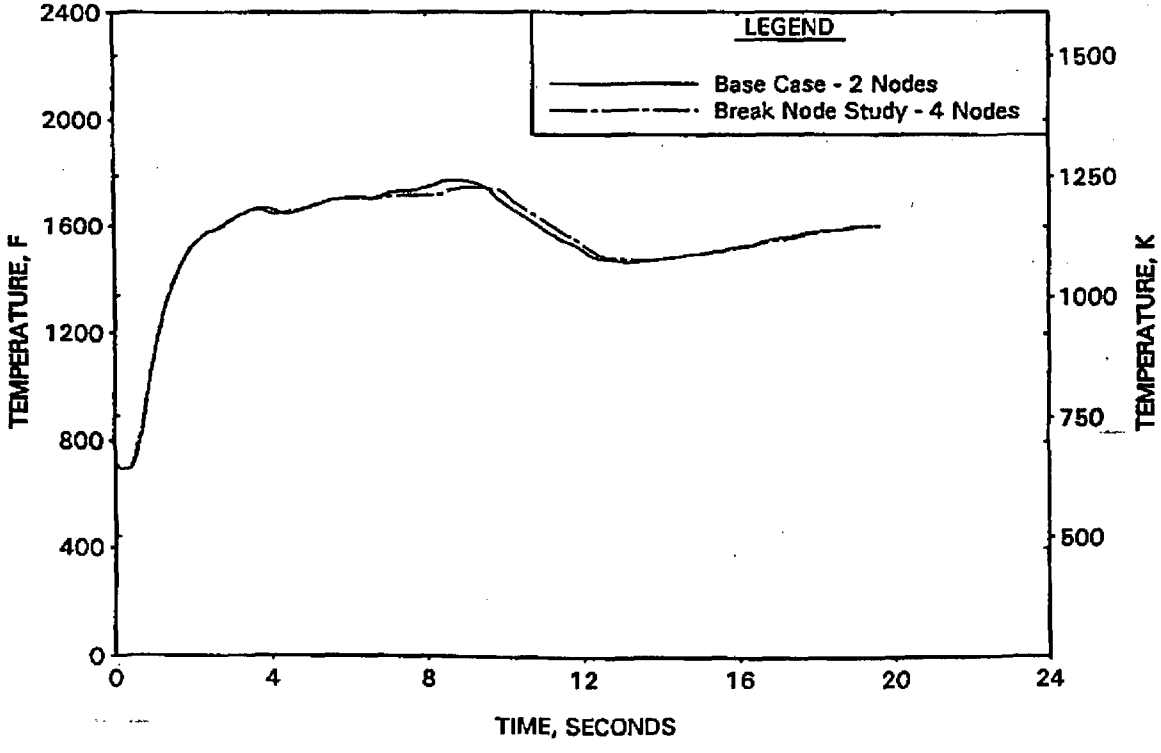

FIGURE A-15. RELAP5/MOD2 BREAK NODING STUDY - RV SIDE BREAK MASS FLOW RATE.

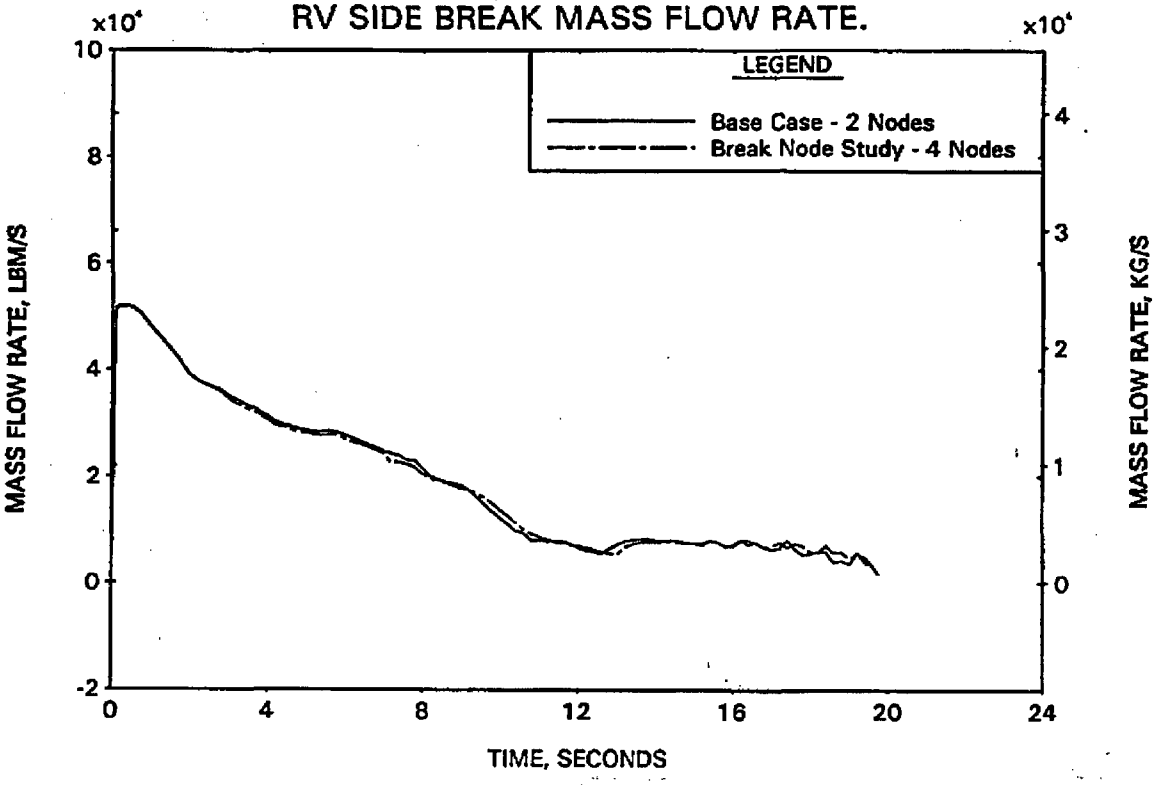

FIGURE A-16. RELAP5/MOD2 BREAK NODING STUDY - PUMP SIDE BREAK MASS FLOW RATE.

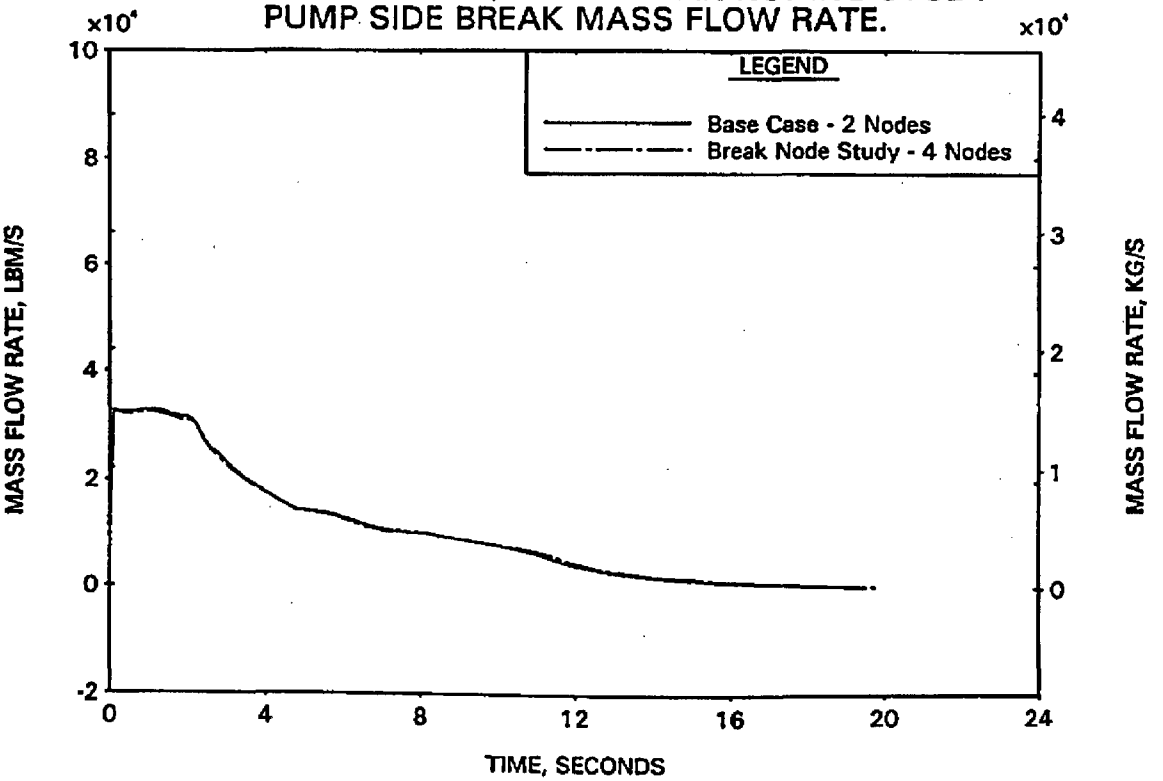

FIGURE A-17. RELAP5/MOD2 BREAK NODING STUDY - HC MASS FLOW RATE AT PEAK POWER LOCATION.

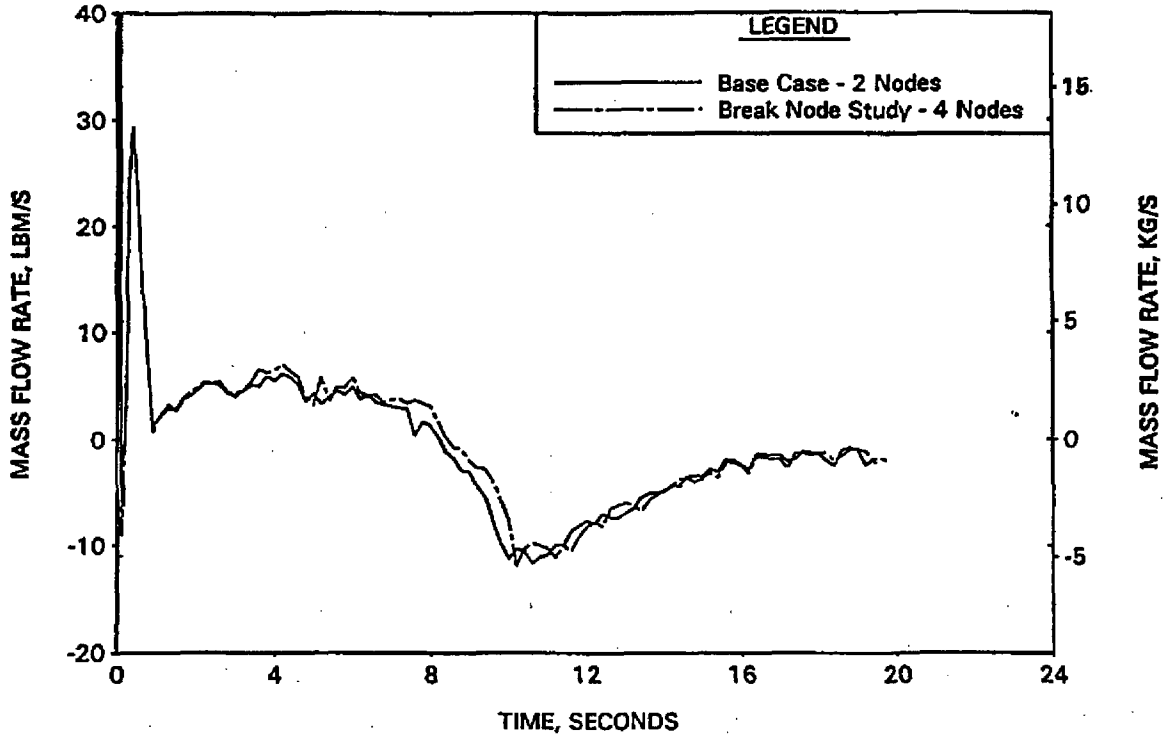

FIGURE A-18. RELAP5/MOD2 CROSSFLOW STUDY - REACTOR VESSEL UPPER PLENUM PRESSURE.

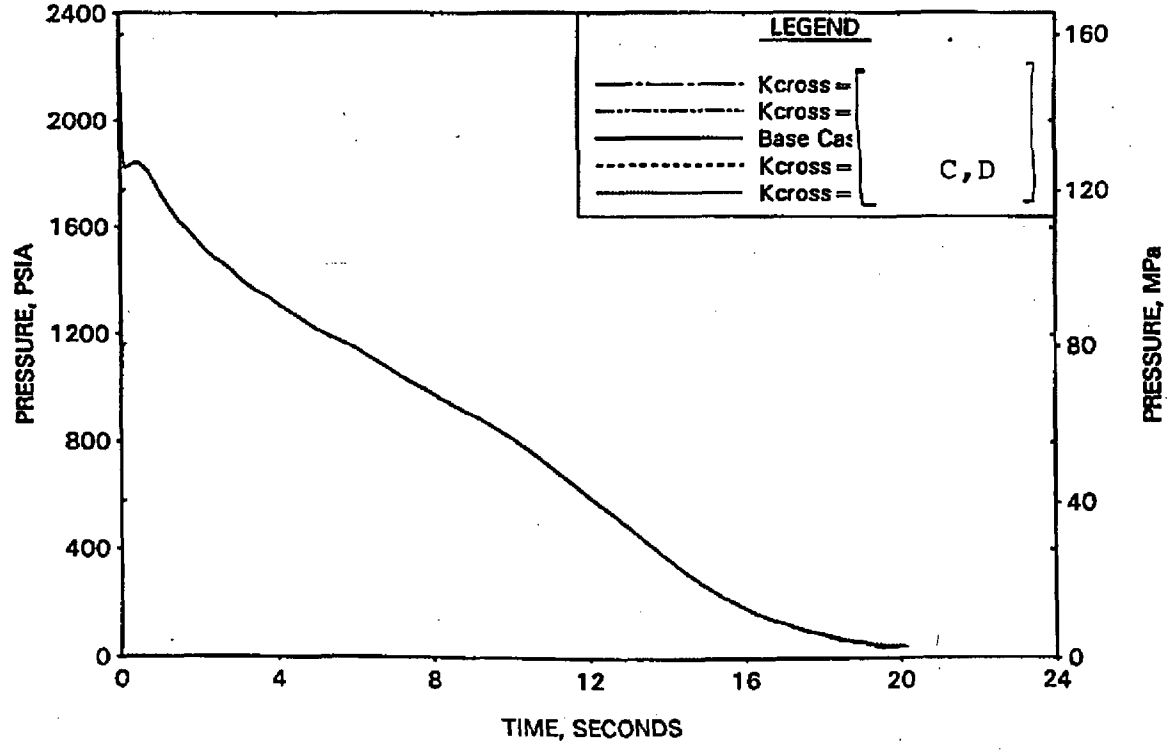

FIGURE A-19. RELAP5/MOD2 CROSSFLOW STUDY - HC CLAD AND FUEL TEMP AT PEAK POWER LOCATION.

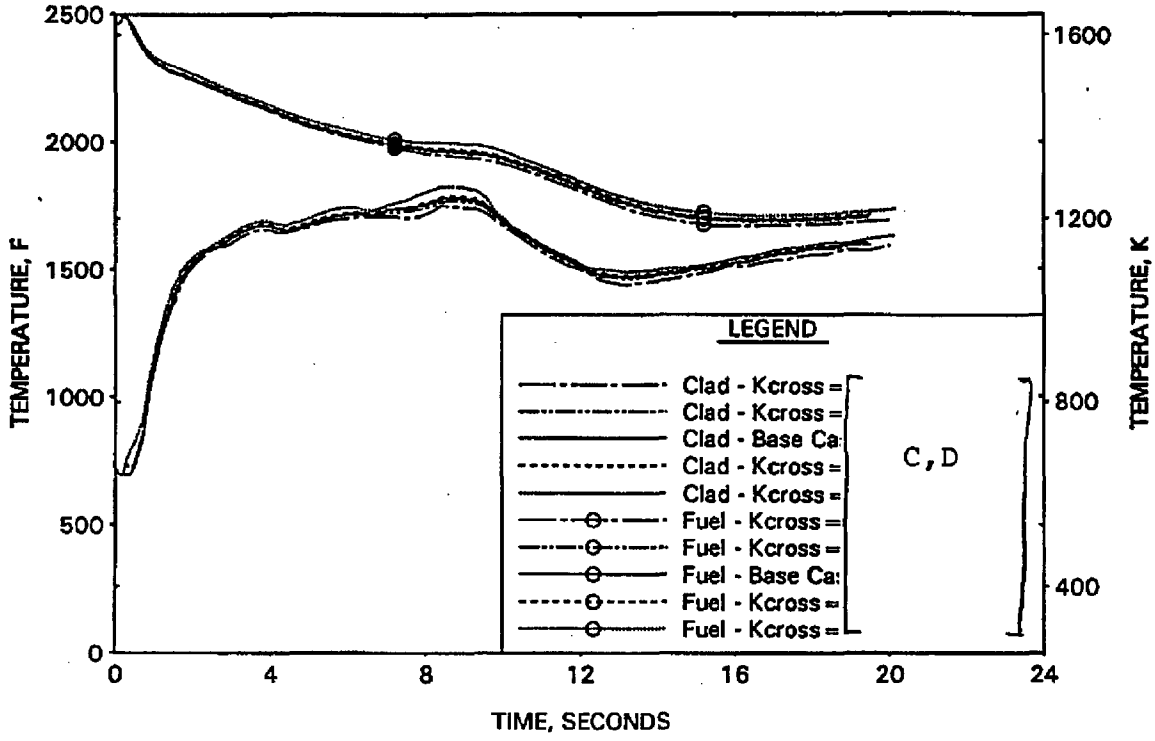

FIGURE A-20. RELAP5/MOD2 CROSSFLOW STUDY - RV SIDE BREAK MASS FLOW RATE.

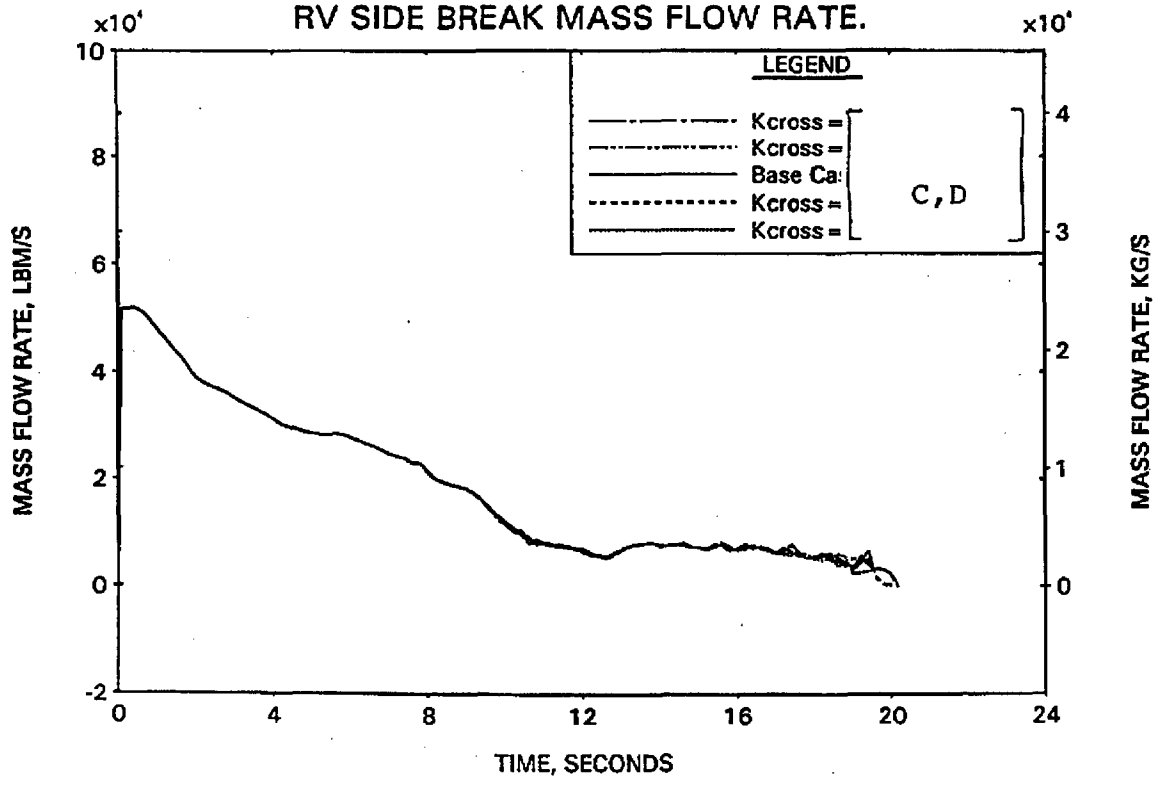

FIGURE A-21. RELAP5/MOD2 CROSSFLOW STUDY - PUMP SIDE BREAK MASS FLOW RATE.

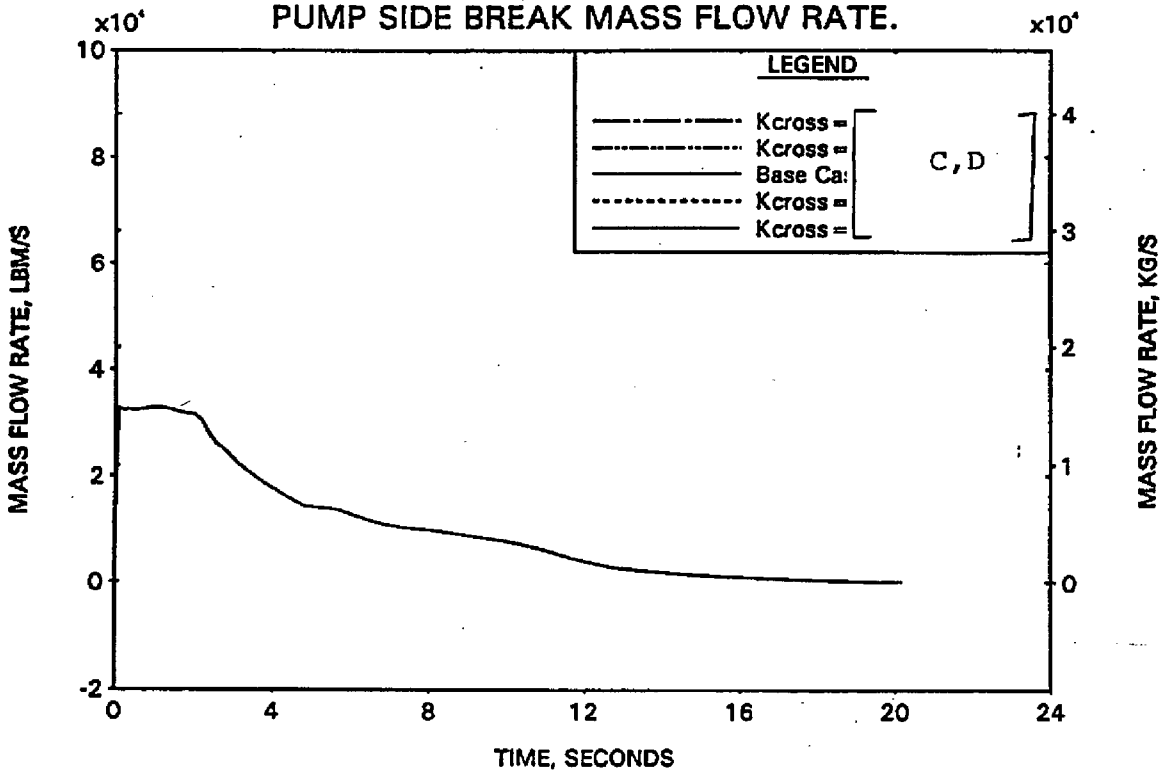

FIGURE A-22. RELAP5/MOD2 CROSSFLOW STUDY - HC MASS FLOW RATE AT PEAK POWER LOCATION.

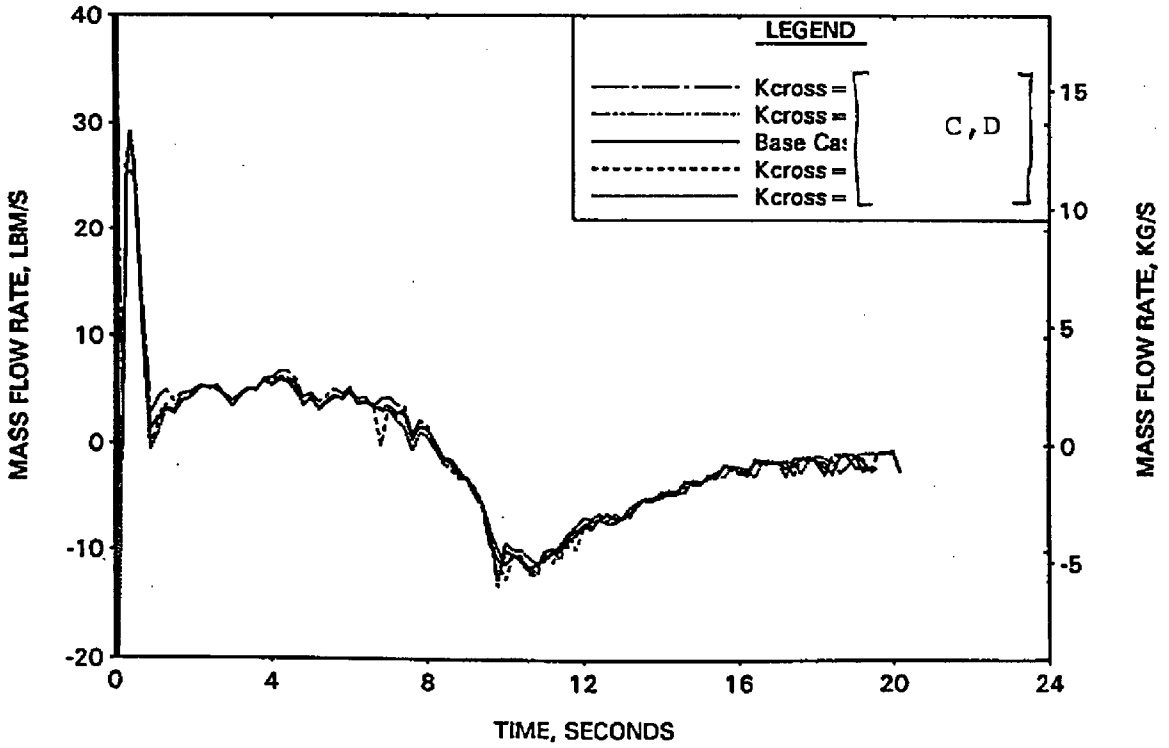

FIGURE A-23. RELAP5/MOD2 CROSSFLOW STUDY - AC-TO-HC CROSSFLOW RATE AT PEAK POWER LOCATION.

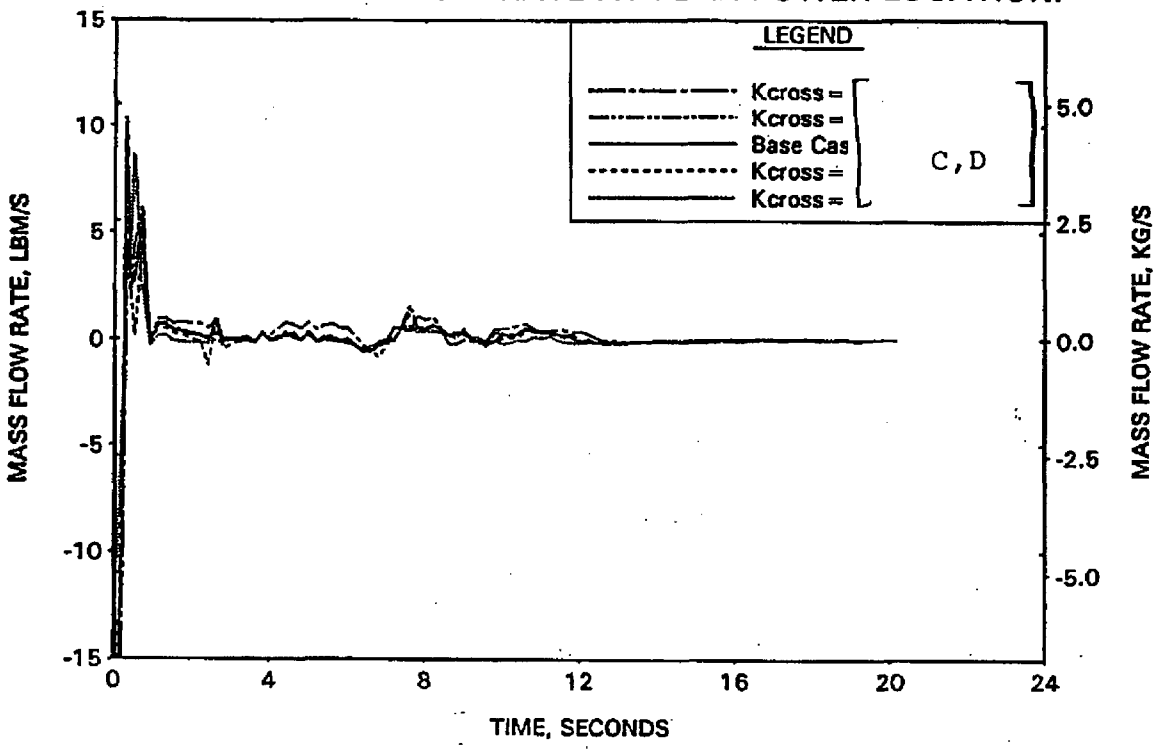

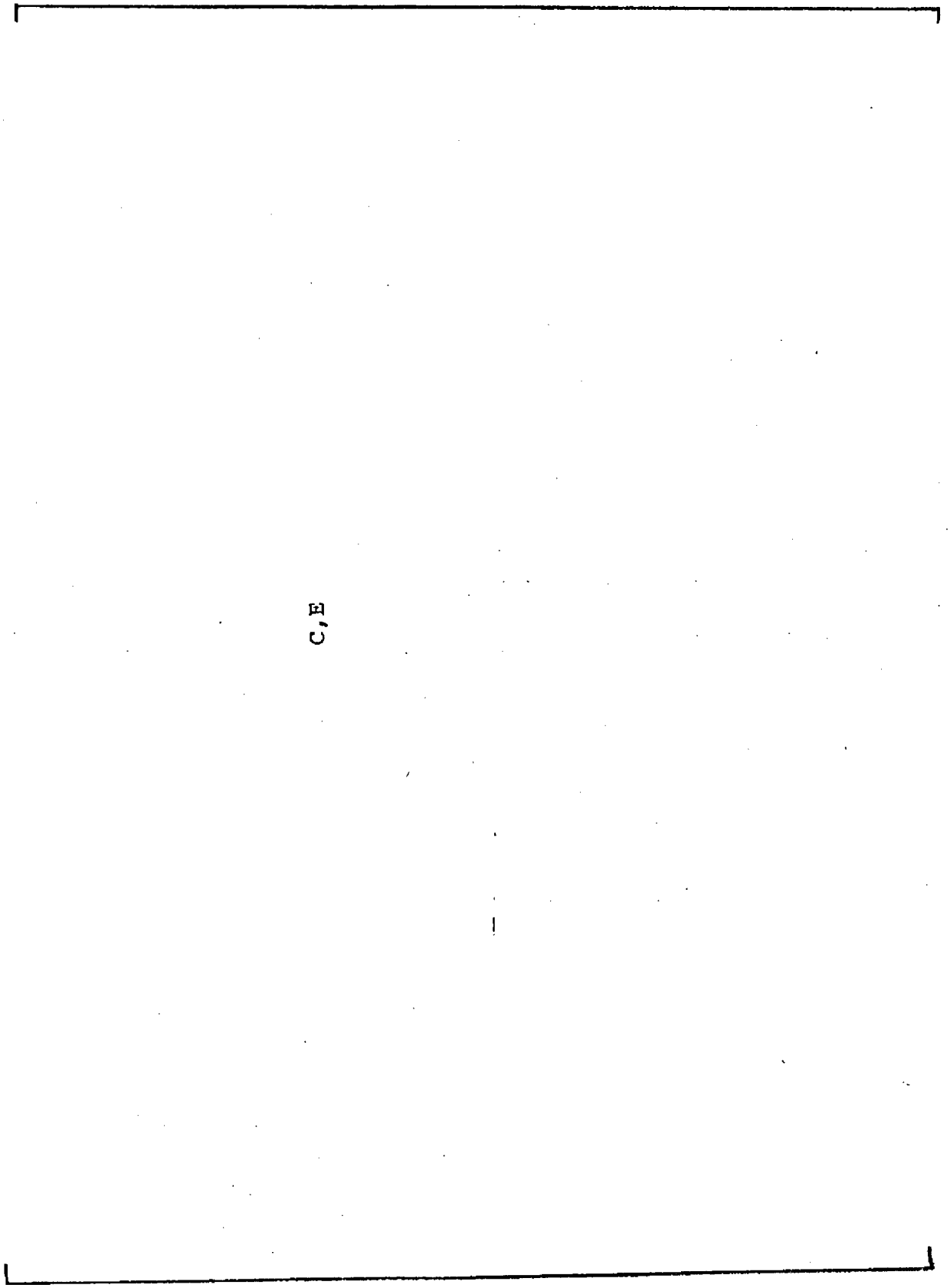

FIGURE A-24. REACTOR VESSEL ARRANGEMENT FOR THE CORE NODING STUDY.

FIGURE A-25. RELAP5/MOD2 CORE NODING STUDY - REACTOR VESSEL UPPER PLENUM PRESSURE.

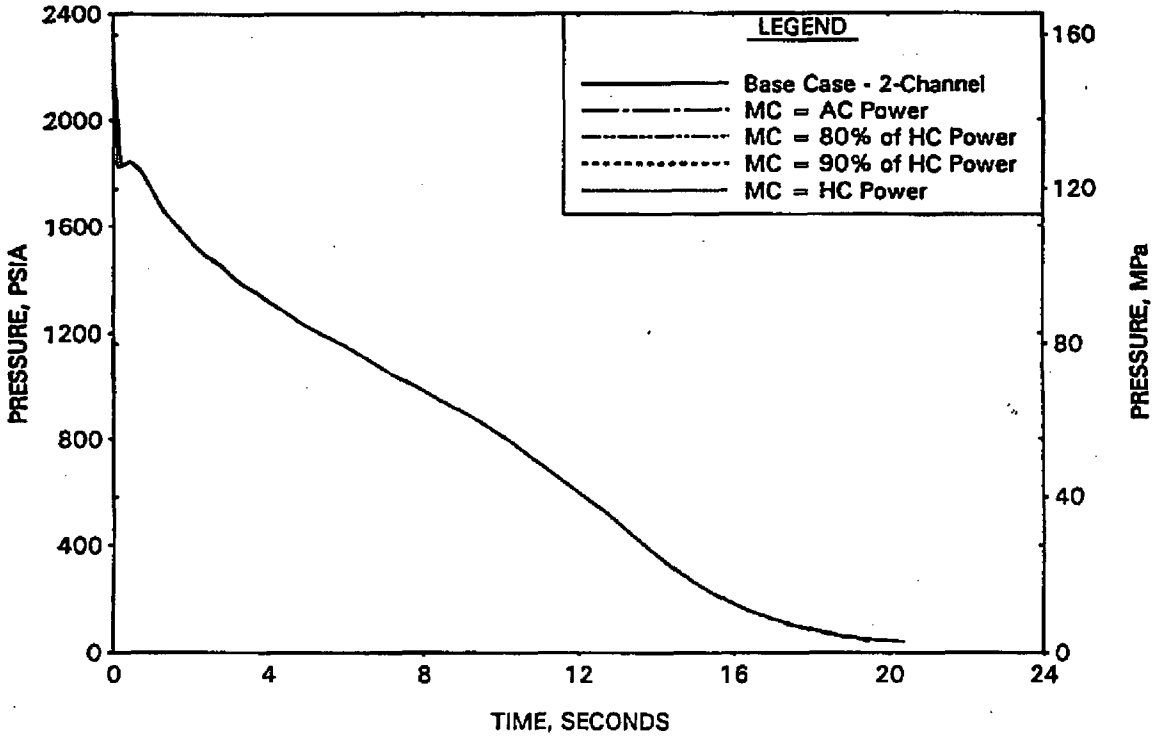

FIGURE A-26. RELAP5/MOD2 CORE NODING STUDY - HC CLAD AND FUEL TEMP AT PEAK POWER LOCATION.

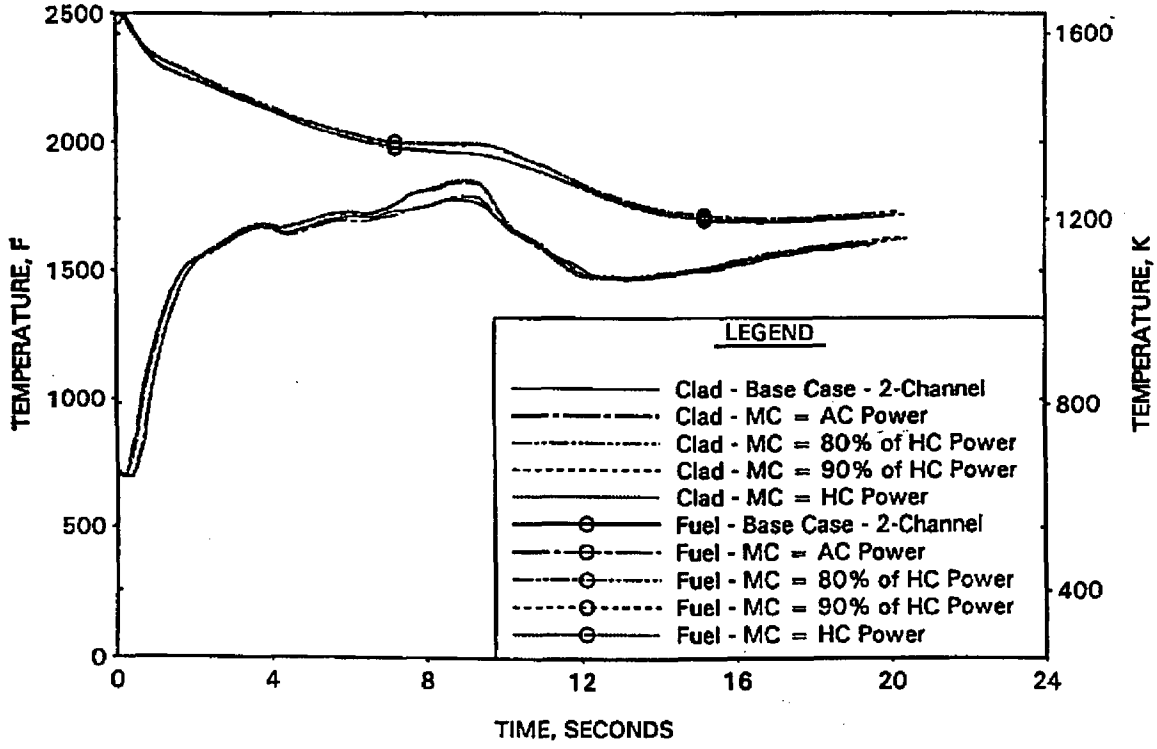

FIGURE A-27. RELAP5/MOD2 CORE NODING STUDY - RV SIDE BREAK MASS FLOW RATE.

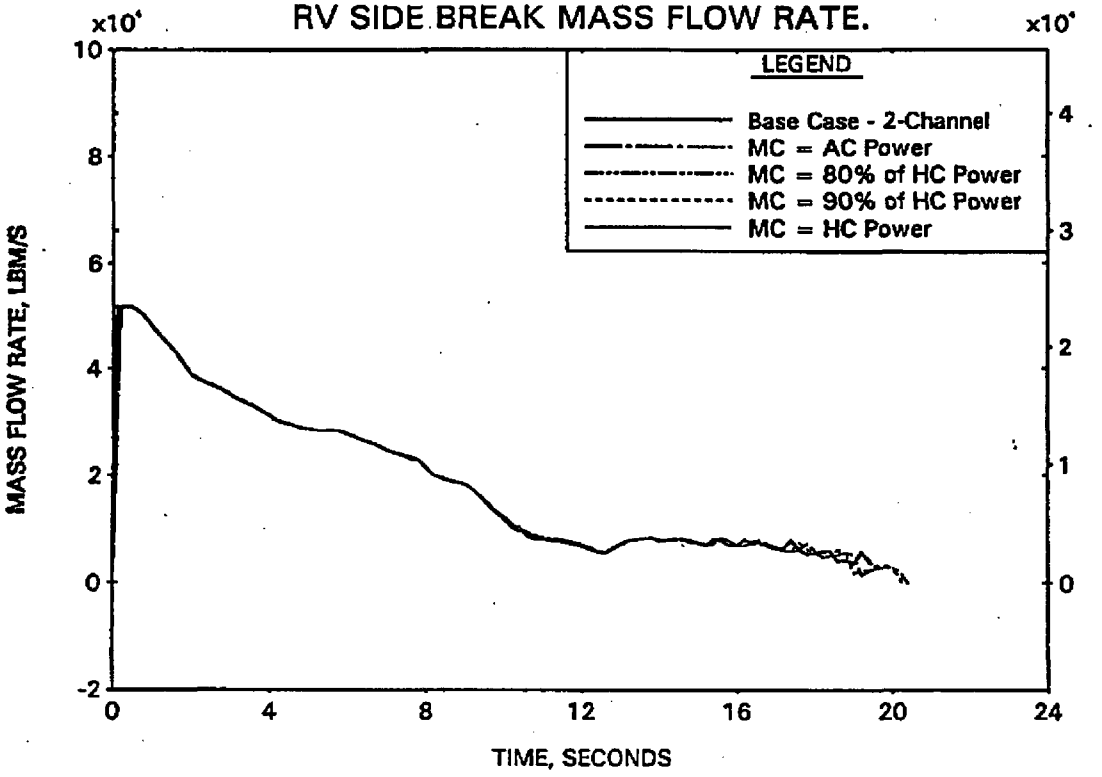

FIGURE A-28. RELAP5/MOD2 CORE NODING STUDY - PUMP SIDE BREAK MASS FLOW RATE.

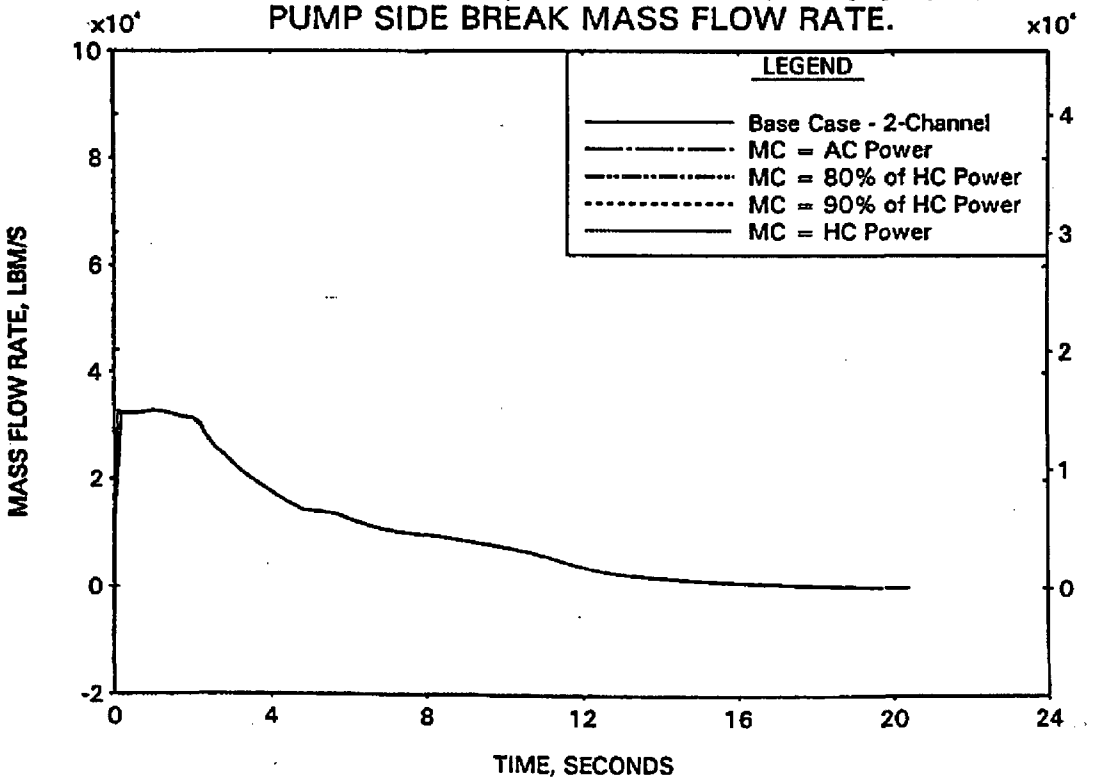

FIGURE A-29. RELAP5/MOD2 CORE NODING STUDY - HC MASS FLOW RATE AT PEAK POWER LOCATION.

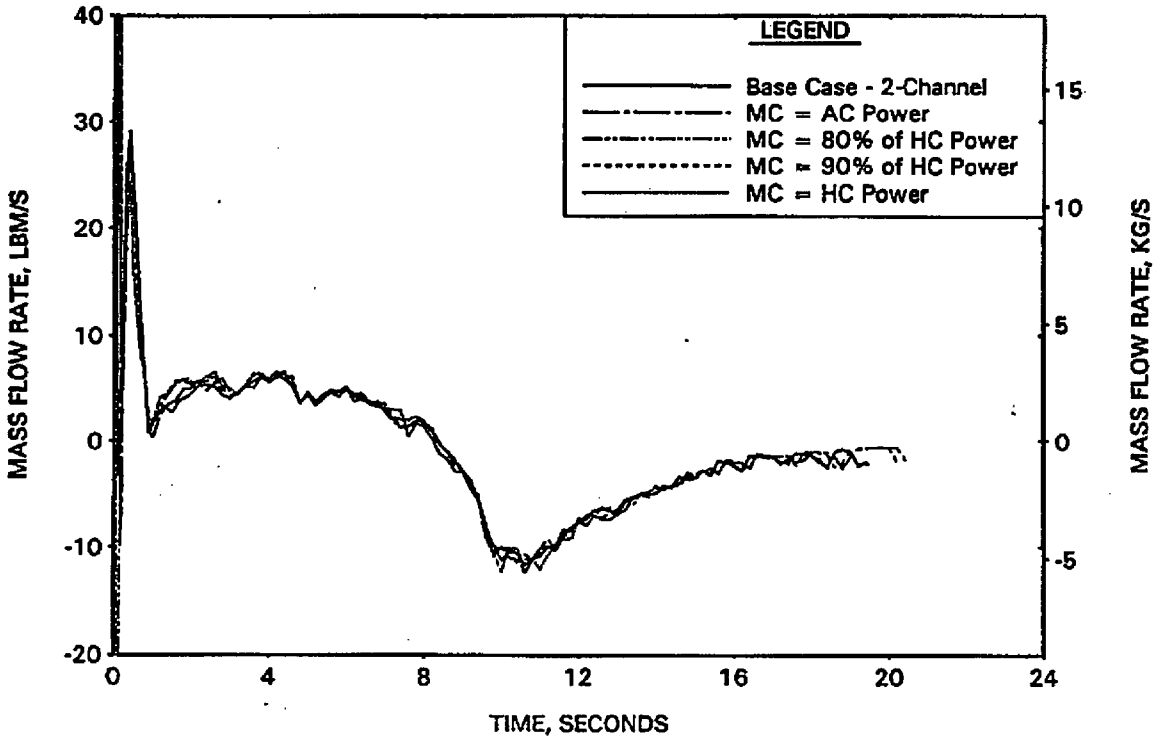

FIGURE A-30. RELAP5/MOD2 PUMP DEGRADATION STUDY - TWO-PHASE PUMP HEAD DEGRADATION MULTIPLIER CURVES.

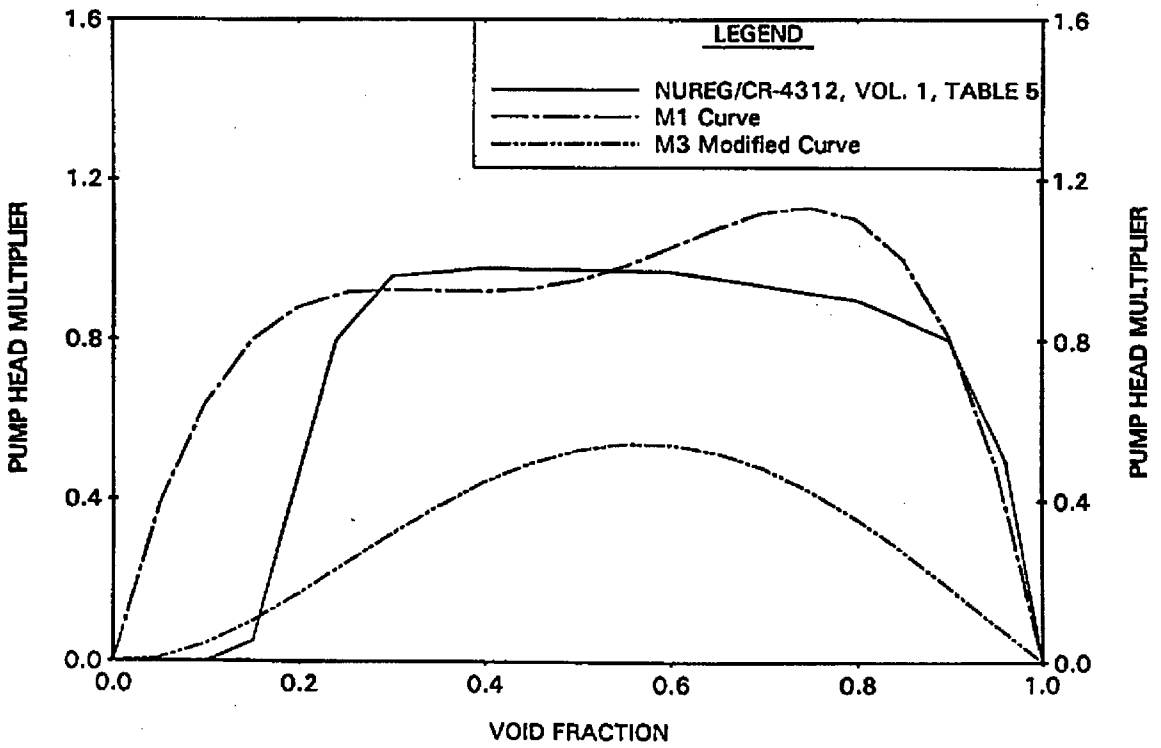

FIGURE A-31. RELAP5/MOD2 PUMP DEGRADATION STUDY - REACTOR VESSEL UPPER PLENUM PRESSURE.

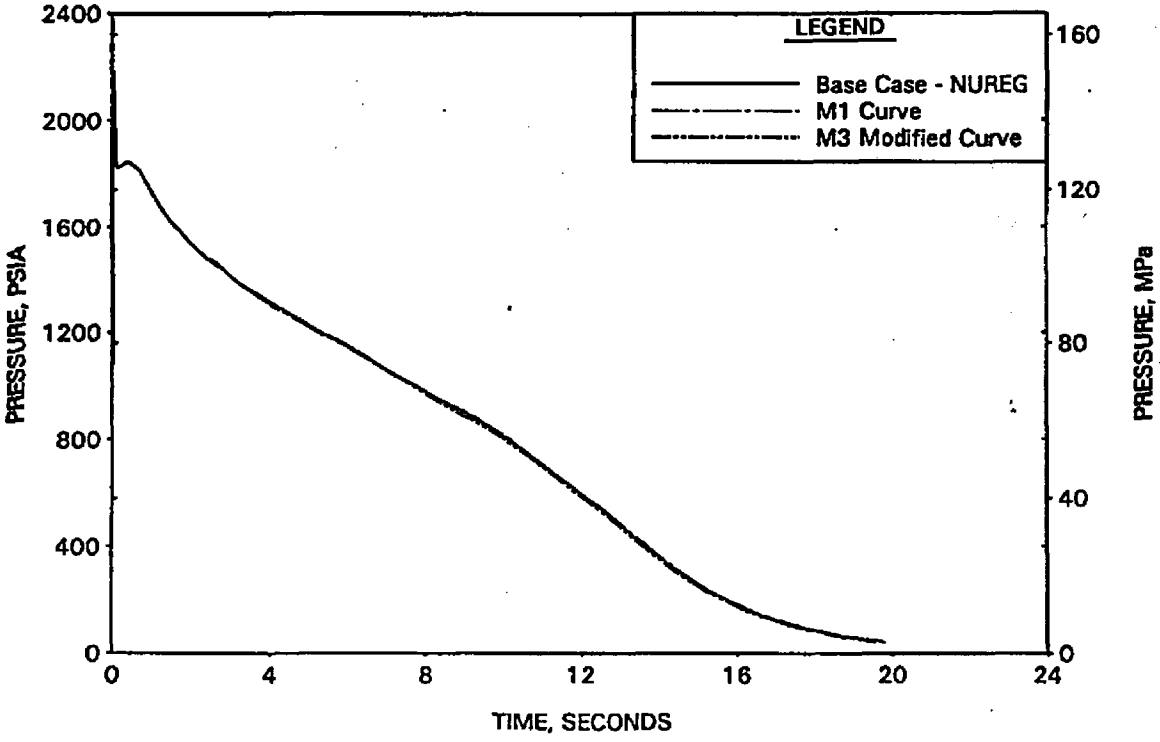

FIGURE A-32. RELAP5/MOD2 PUMP DEGRADATION STUDY - HC CLAD TEMP AT PEAK POWER LOCATION.

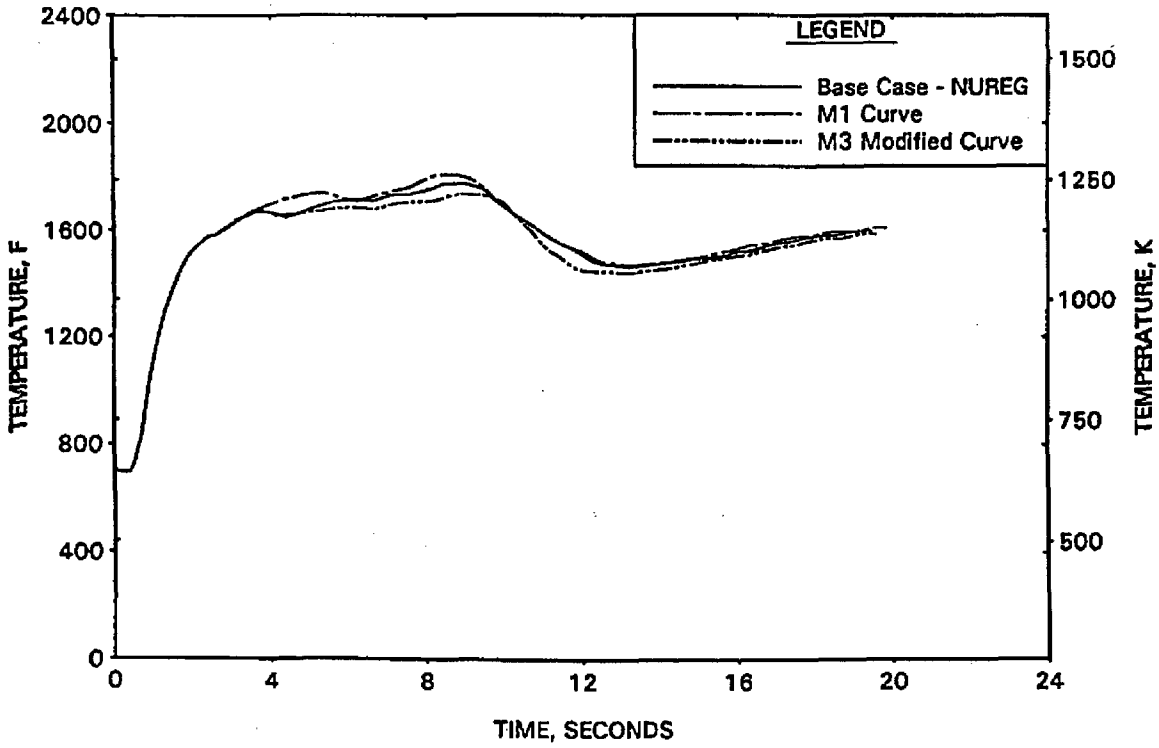

FIGURE A-33. RELAP5/MOD2 PUMP DEGRADATION STUDY - RV SIDE BREAK MASS FLOW RATE.

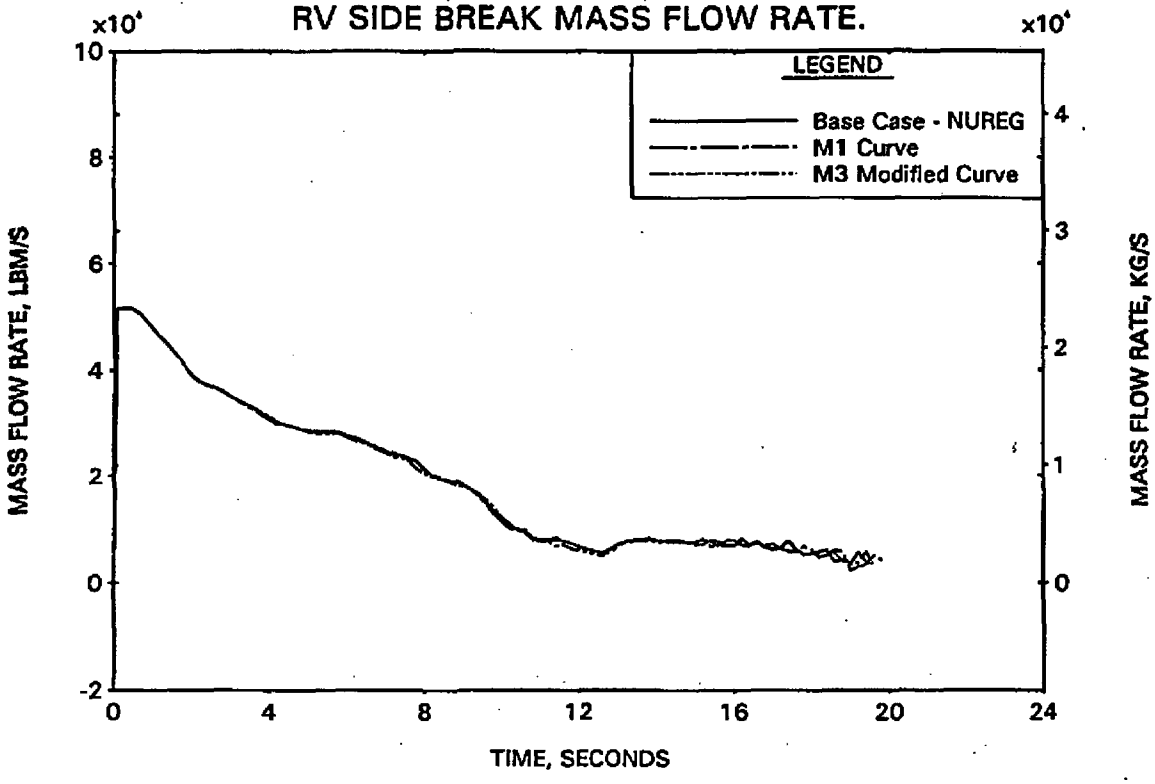

FIGURE A-34. RELAP5/MOD2 PUMP DEGRADATION STUDY - PUMP SIDE BREAK MASS FLOW RATE.

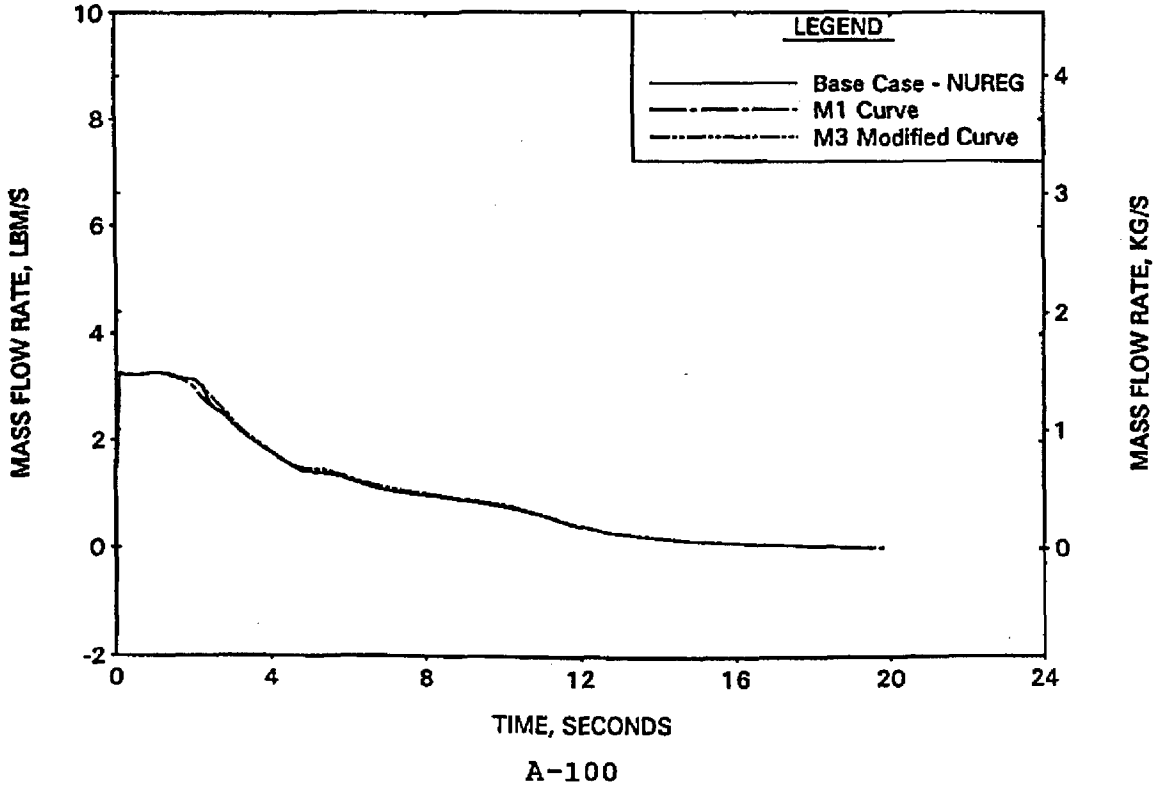

FIGURE A-35. RELAP5/MOD2 PUMP DEGRADATION STUDY - HC MASS FLOW RATE AT PEAK POWER LOCATION.

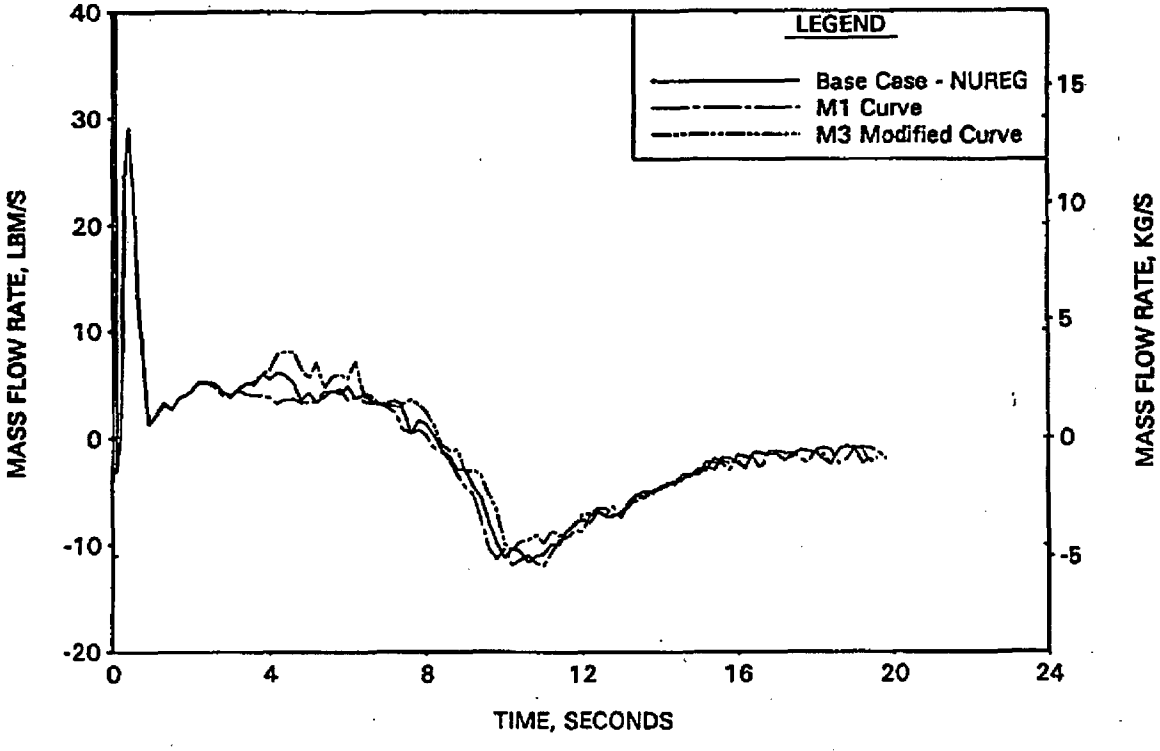

FIGURE A-36. RELAP5/MOD2 PUMP POWER STUDY - REACTOR VESSEL UPPER PLENUM PRESSURE.

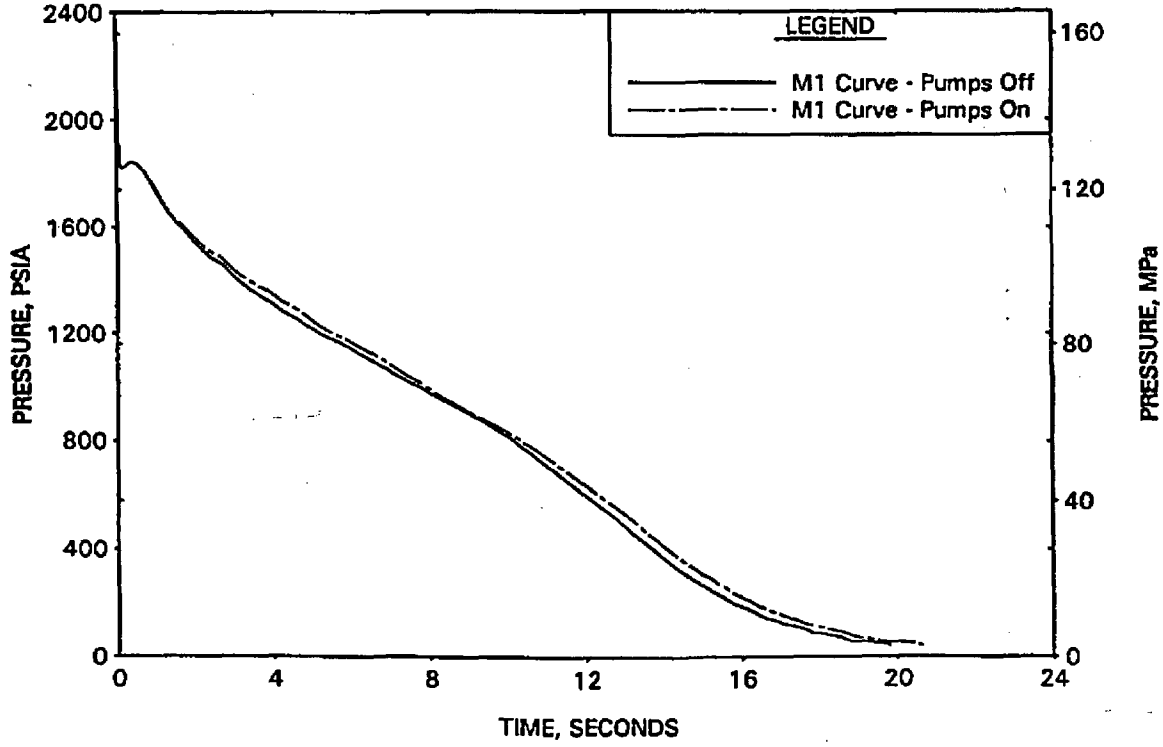

FIGURE A-37. RELAP5/MOD2 PUMP POWER STUDY - HC CLAD TEMP AT PEAK POWER LOCATION.

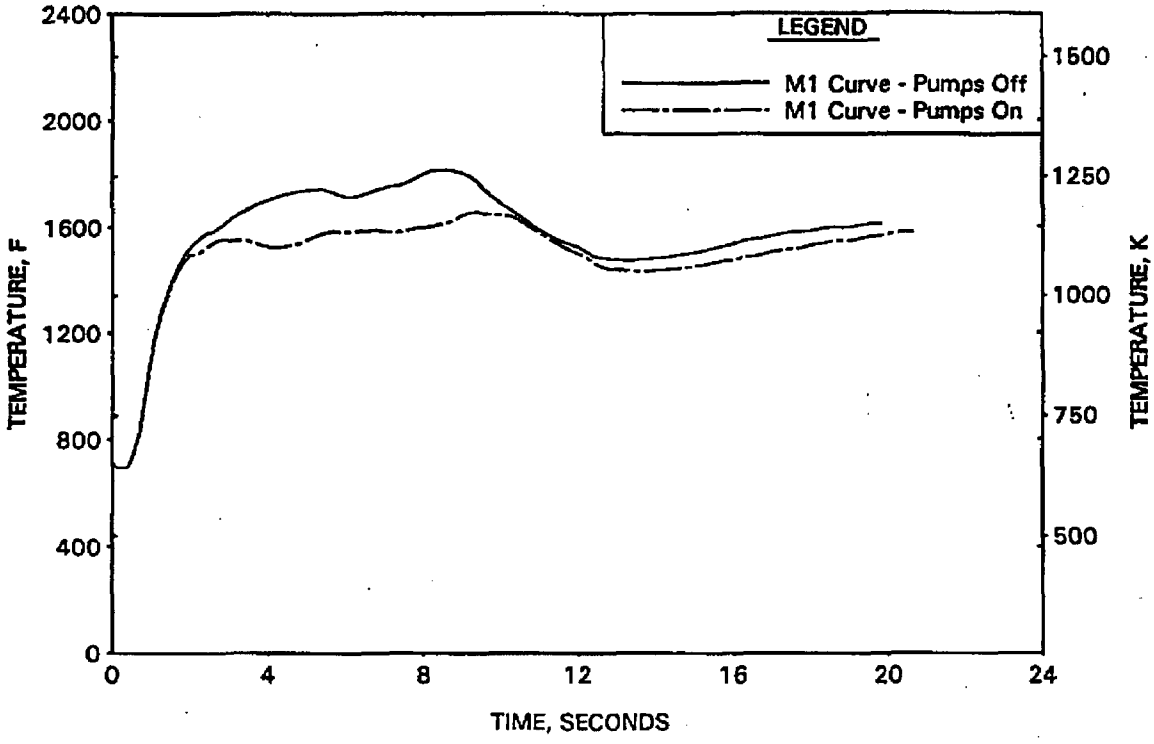

FIGURE A-38. RELAP5/MOD2 PUMP POWER STUDY - RV SIDE BREAK MASS FLOW RATE.

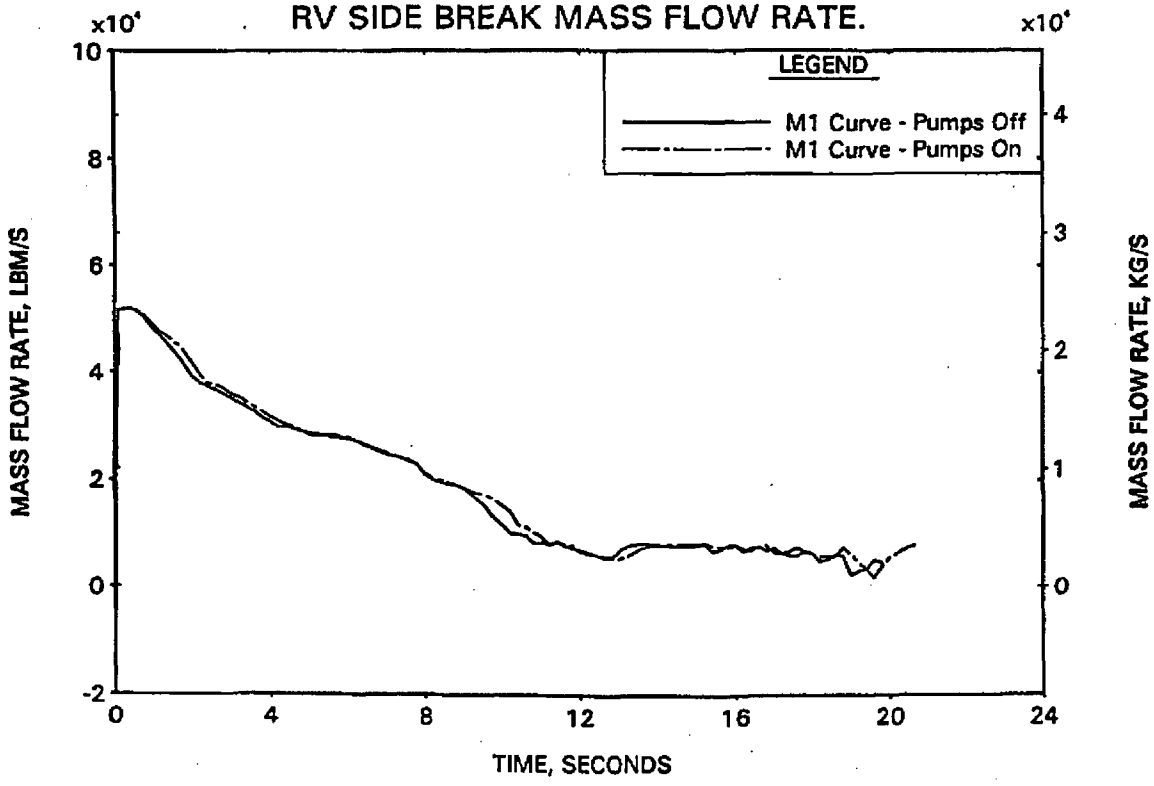

FIGURE A-39. RELAP5/MOD2 PUMP POWER STUDY - PUMP SIDE BREAK MASS FLOW RATE.

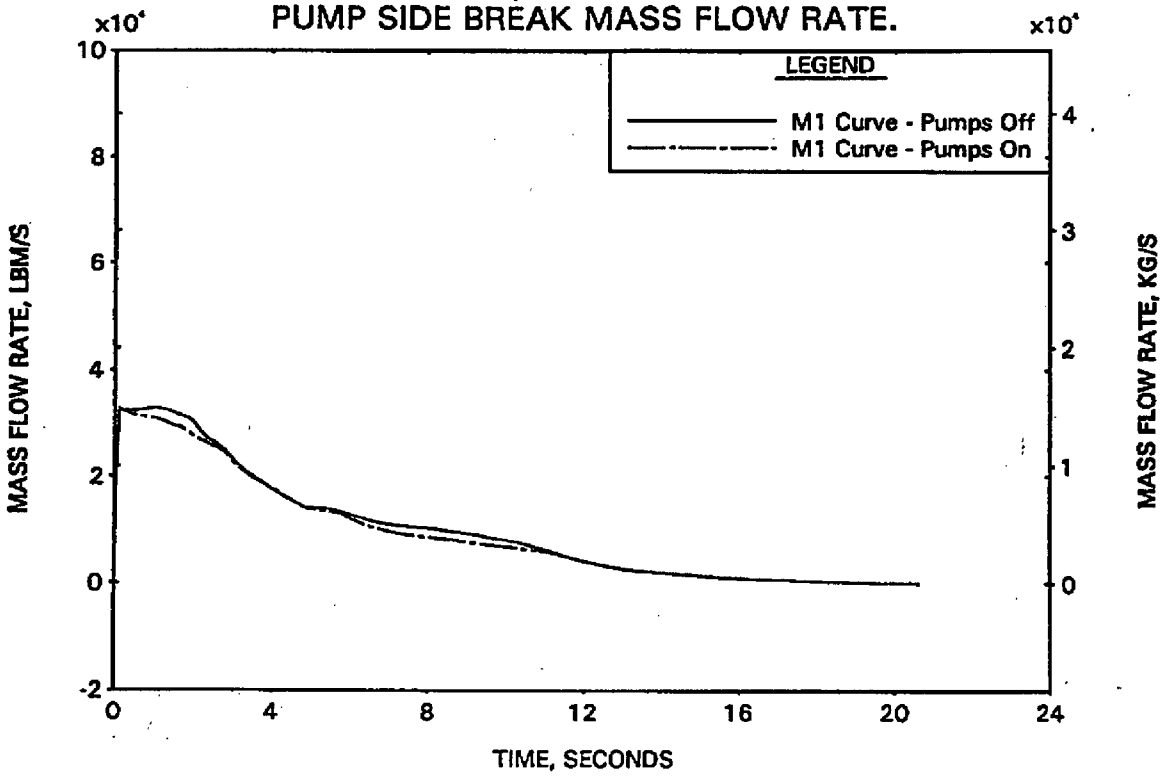

FIGURE A-40. RELAP5/MOD2 PUMP POWER STUDY - HC MASS FLOW RATE AT PEAK POWER LOCATION.

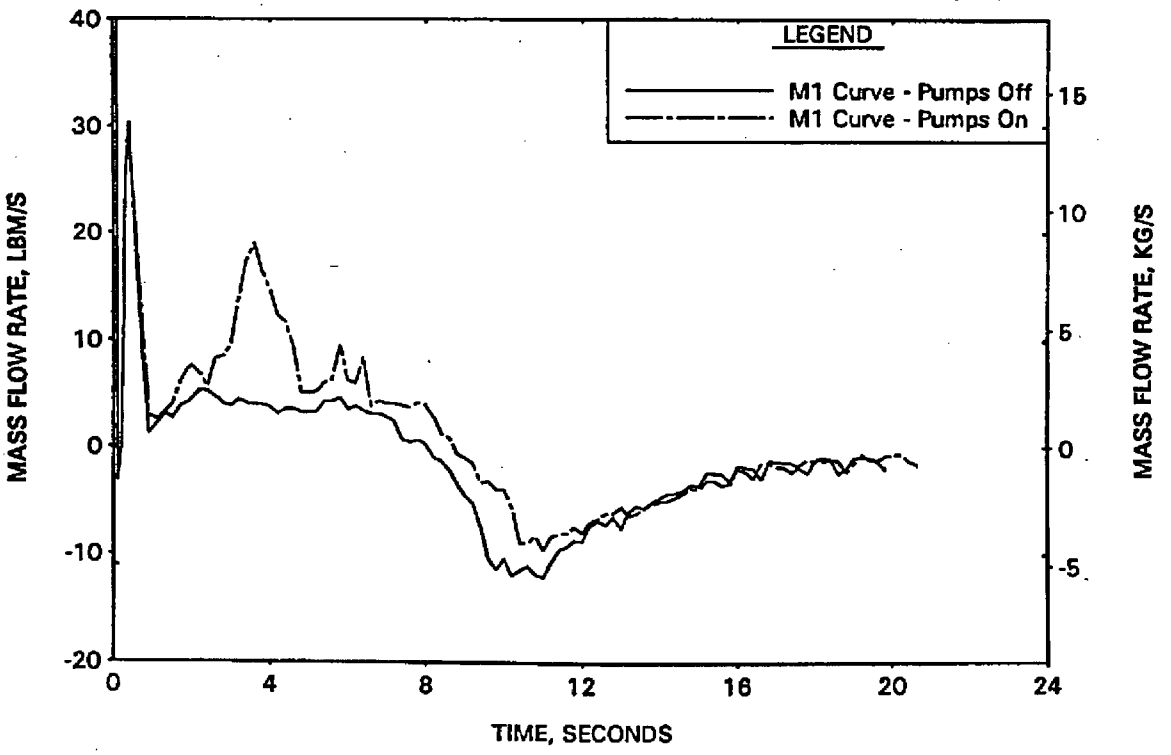

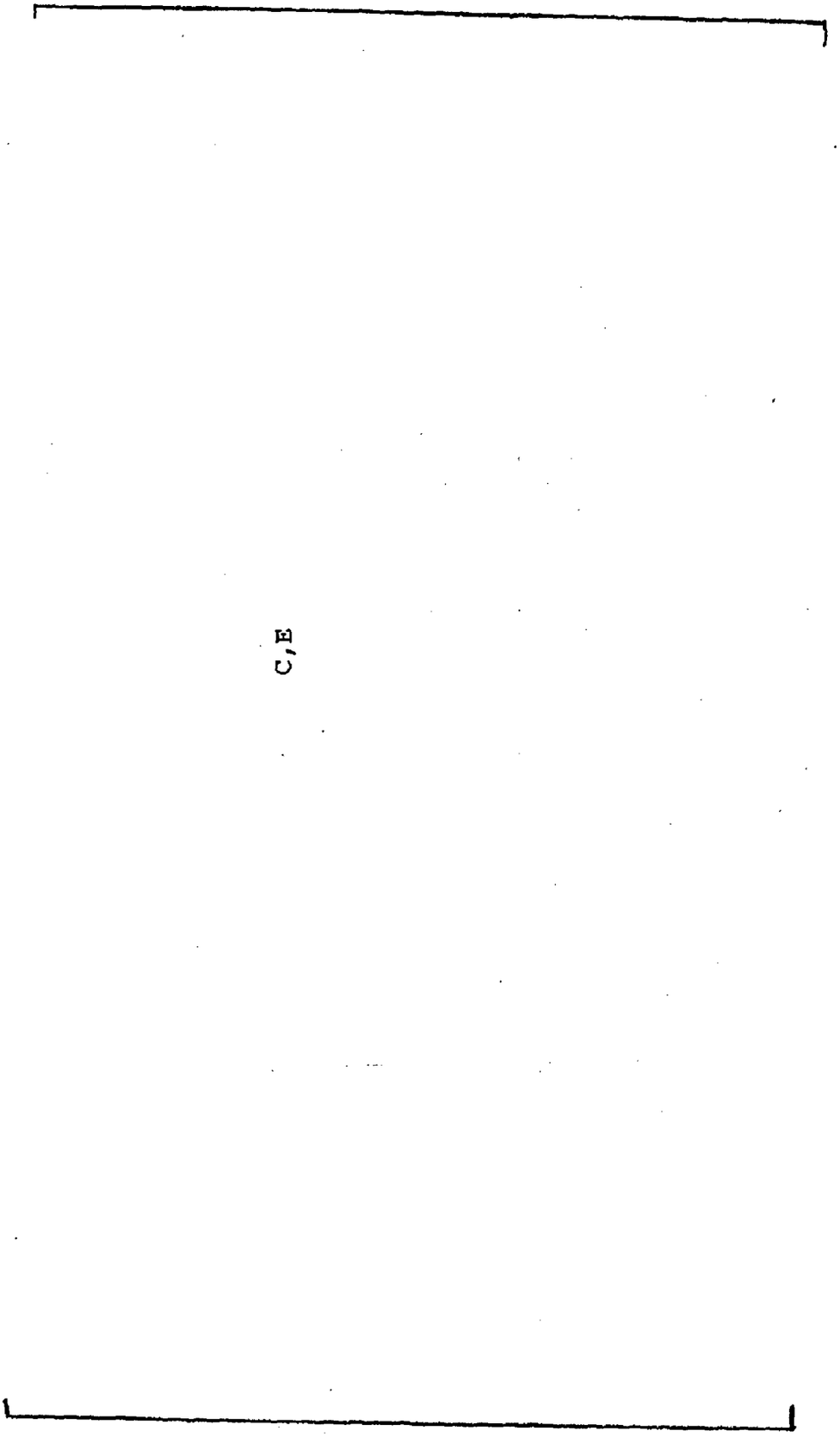

FIGURE A-41. REVISED RV NODING FOR ECCS BYPASS STUDY.

FIGURE A-42. RELAP5/MOD2 ECCS BYPASS MODEL - REACTOR VESSEL UPPER PLENUM PRESSURE.

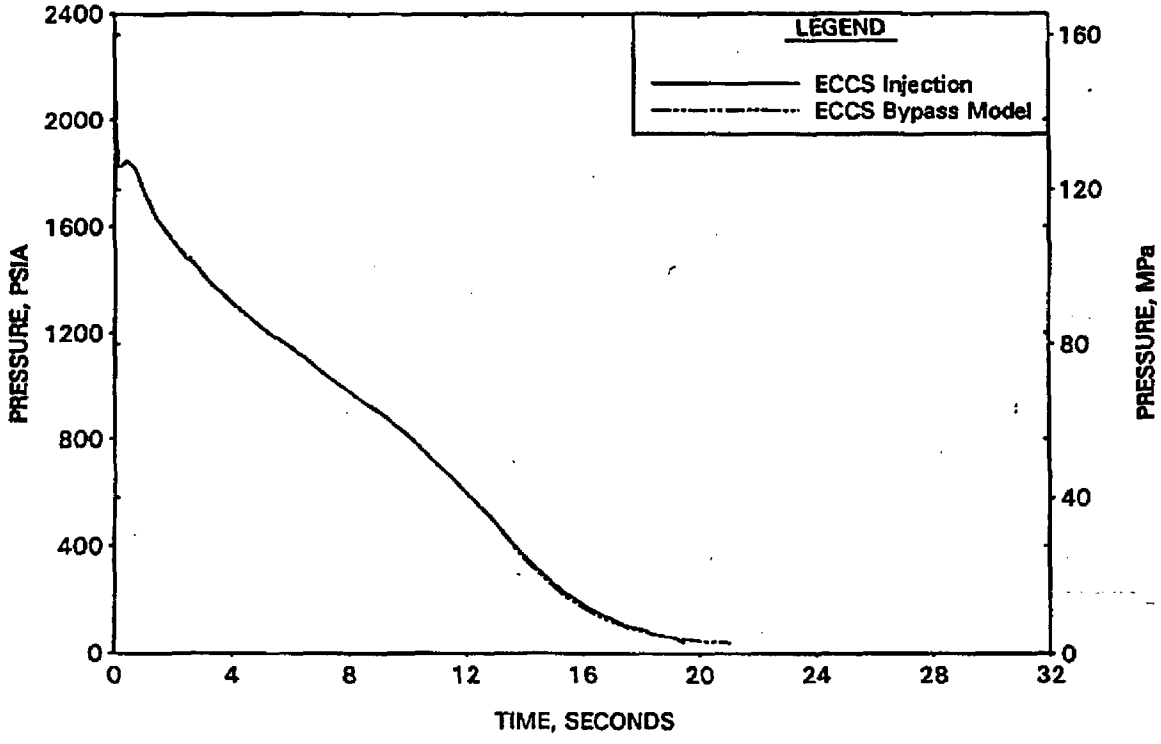

FIGURE A-43. RELAP5/MOD2 ECCS BYPASS MODEL - HC CLAD TEMP AT PEAK POWER LOCATION.

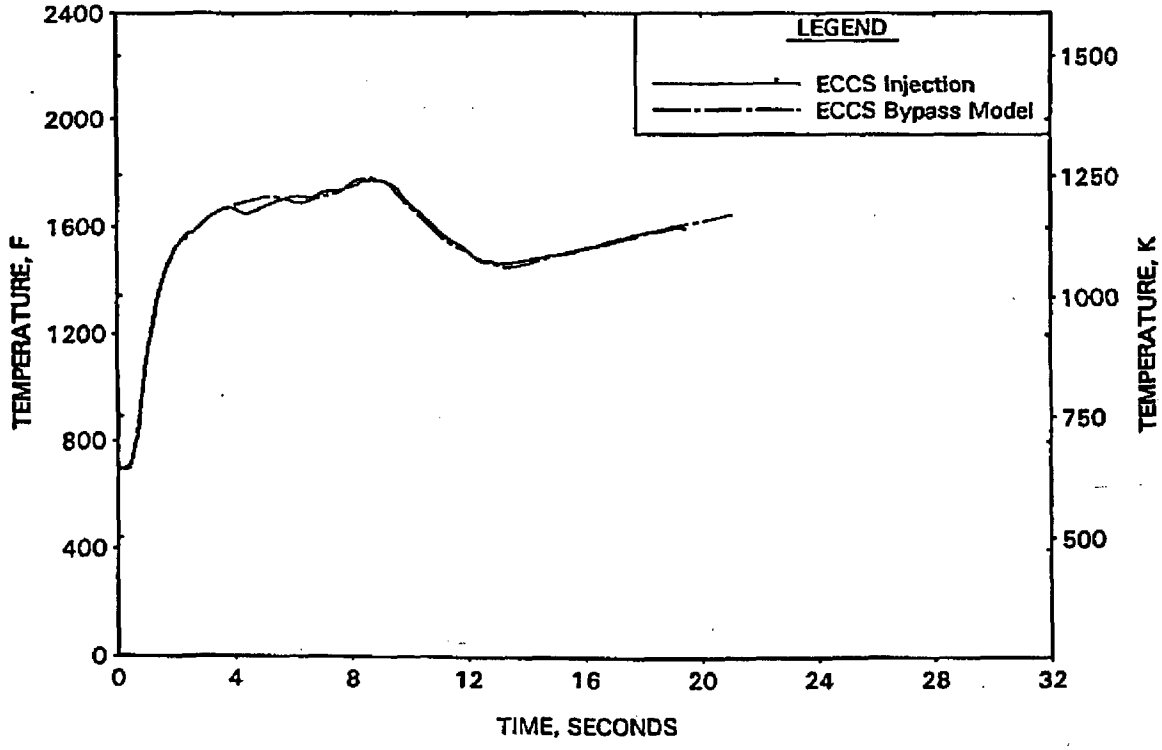

FIGURE A-44. RELAP5/MOD2 ECCS BYPASS MODEL - RV SIDE BREAK MASS FLOW RATE.

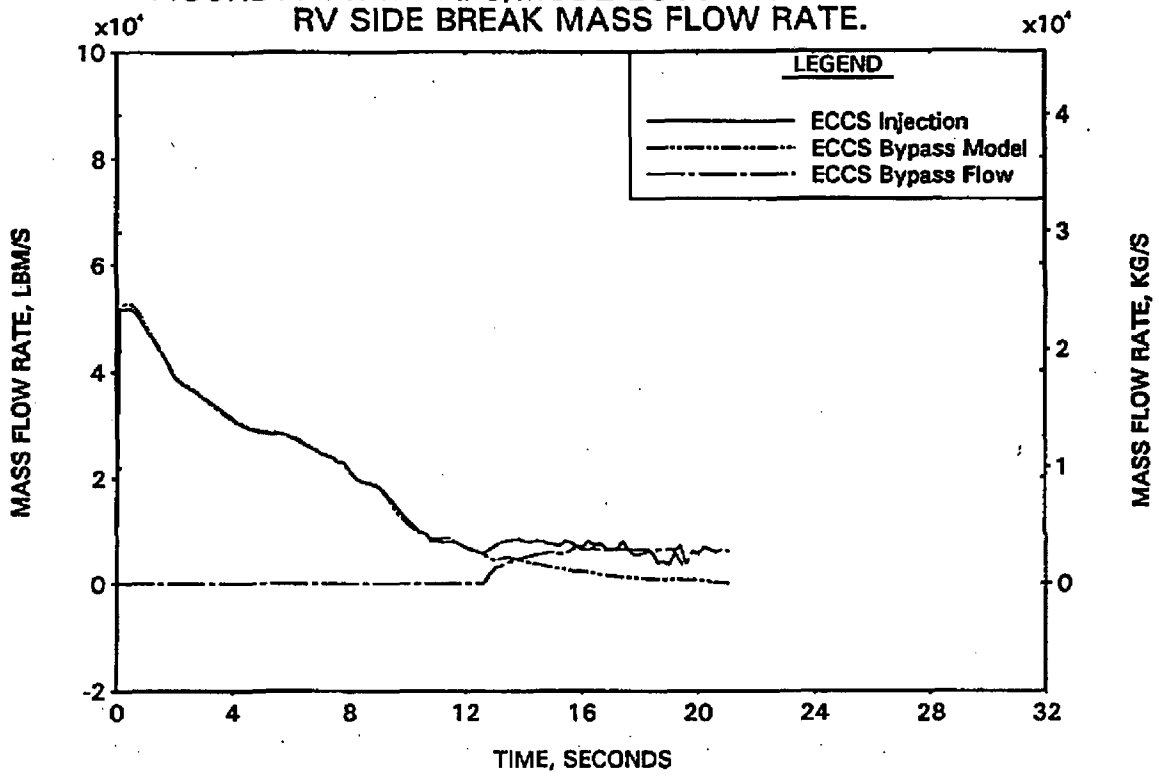

FIGURE A-45. RELAP5/MOD2 ECCS BYPASS MODEL - PUMP SIDE BREAK MASS FLOW RATE.

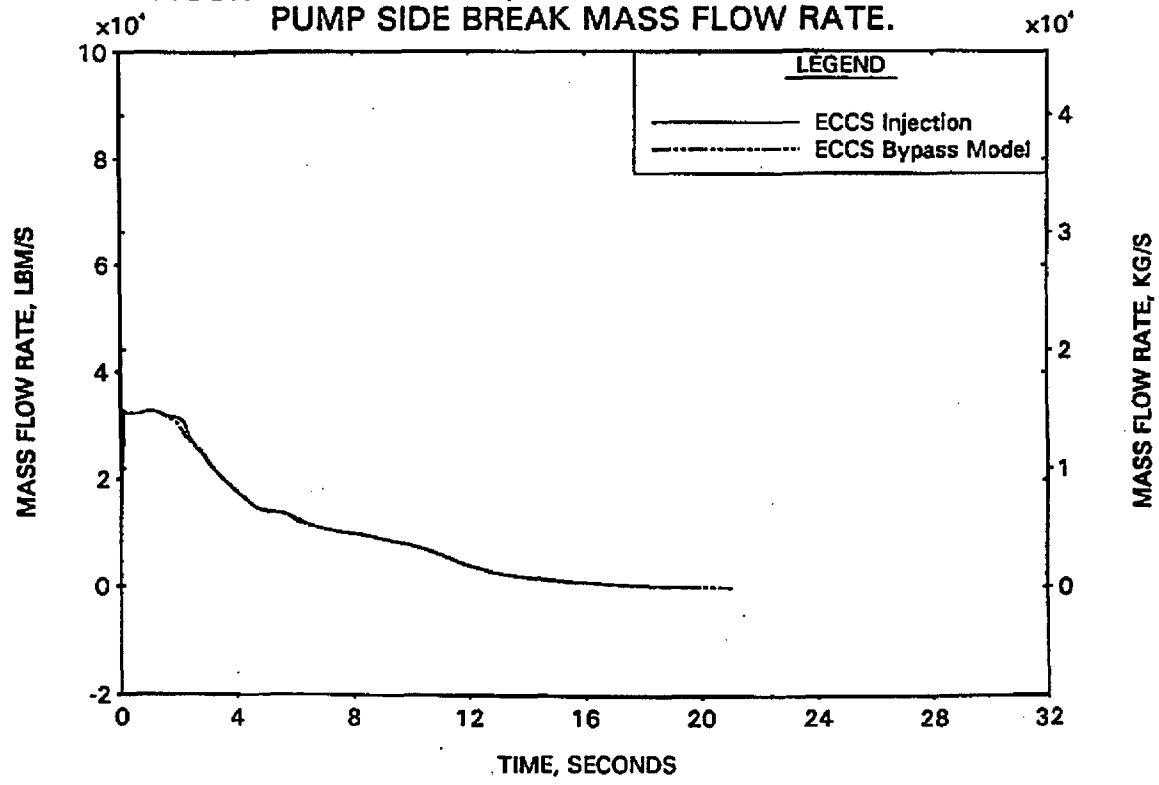

FIGURE A-46. RELAP5/MOD2 ECCS BYPASS MODEL - HC MASS FLOW RATE AT PEAK POWER LOCATION.

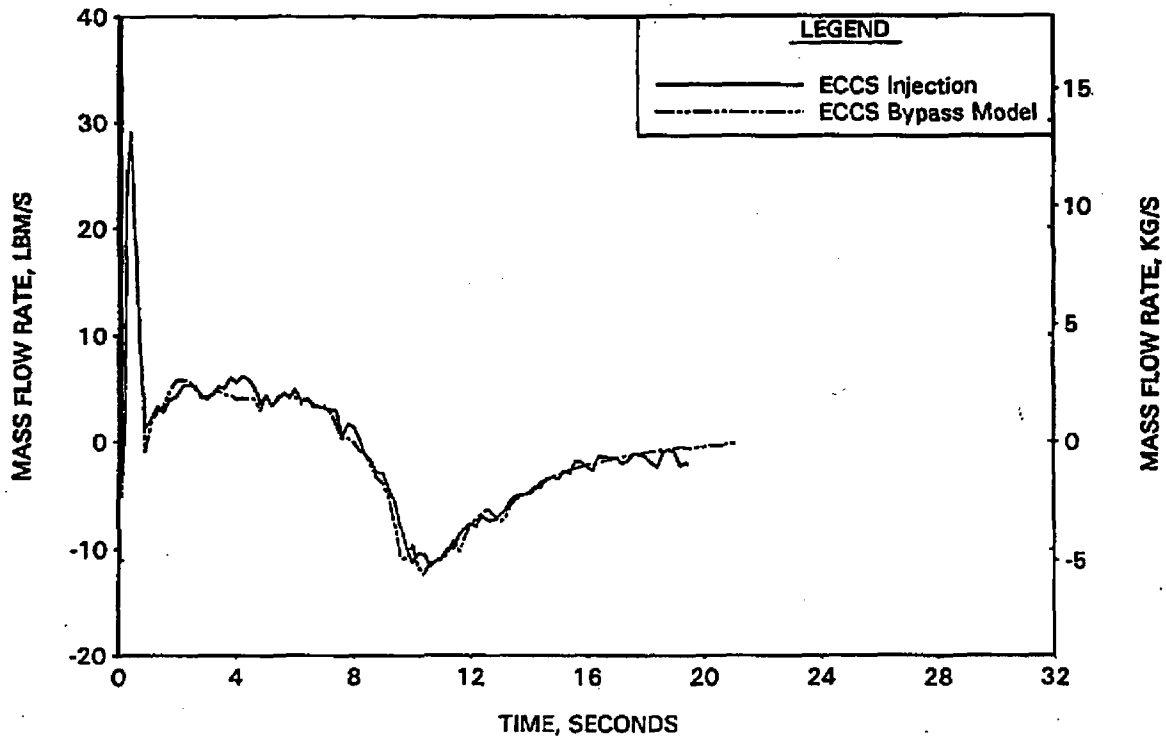

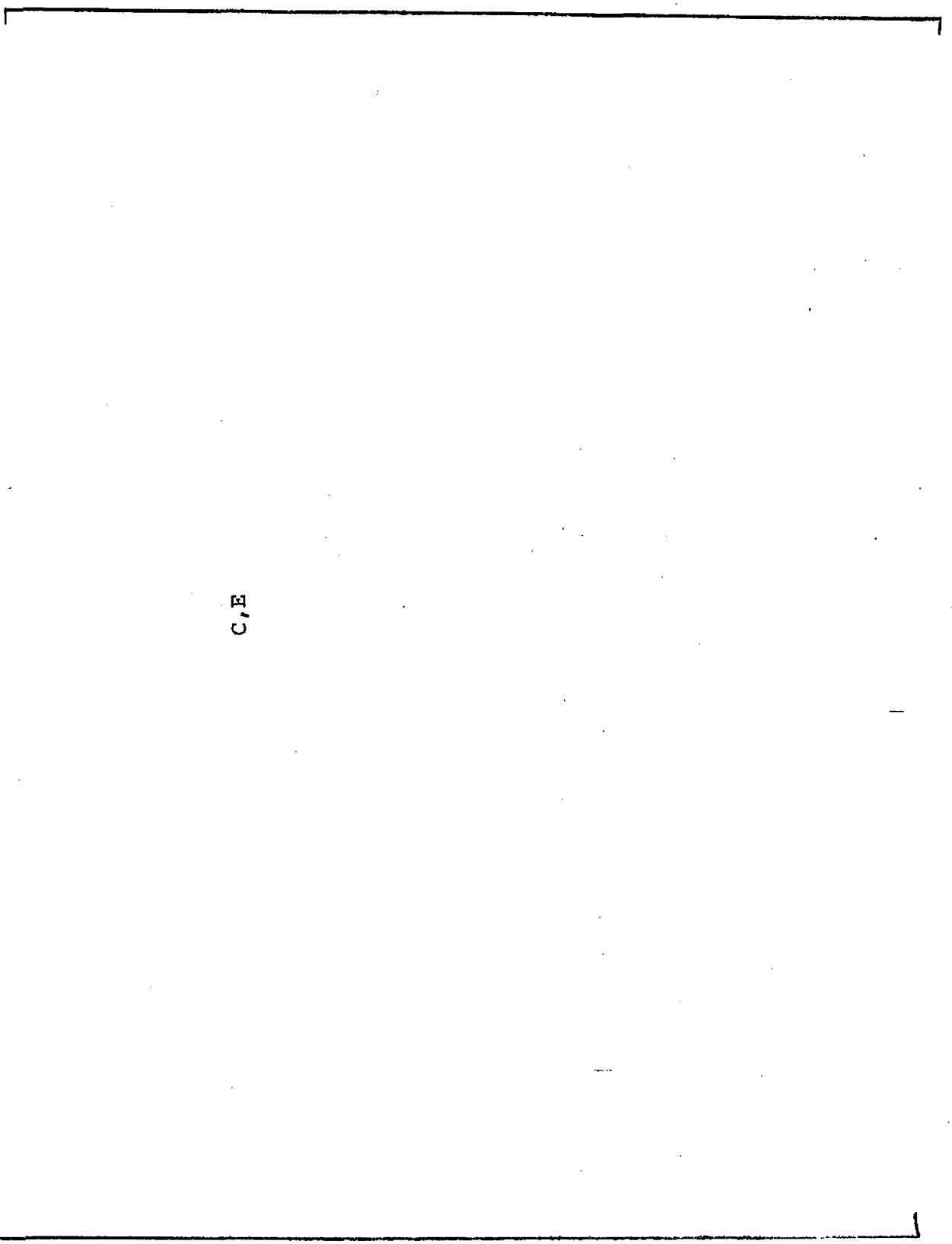

C,E

FIGURE A-47. REFLOOD3 DETAILED RCS LOOP NODING ARRANGEMENT.

FIGURE A-48. REFLOD3B LOOP NODING STUDY - CORE FLOODING RATE.

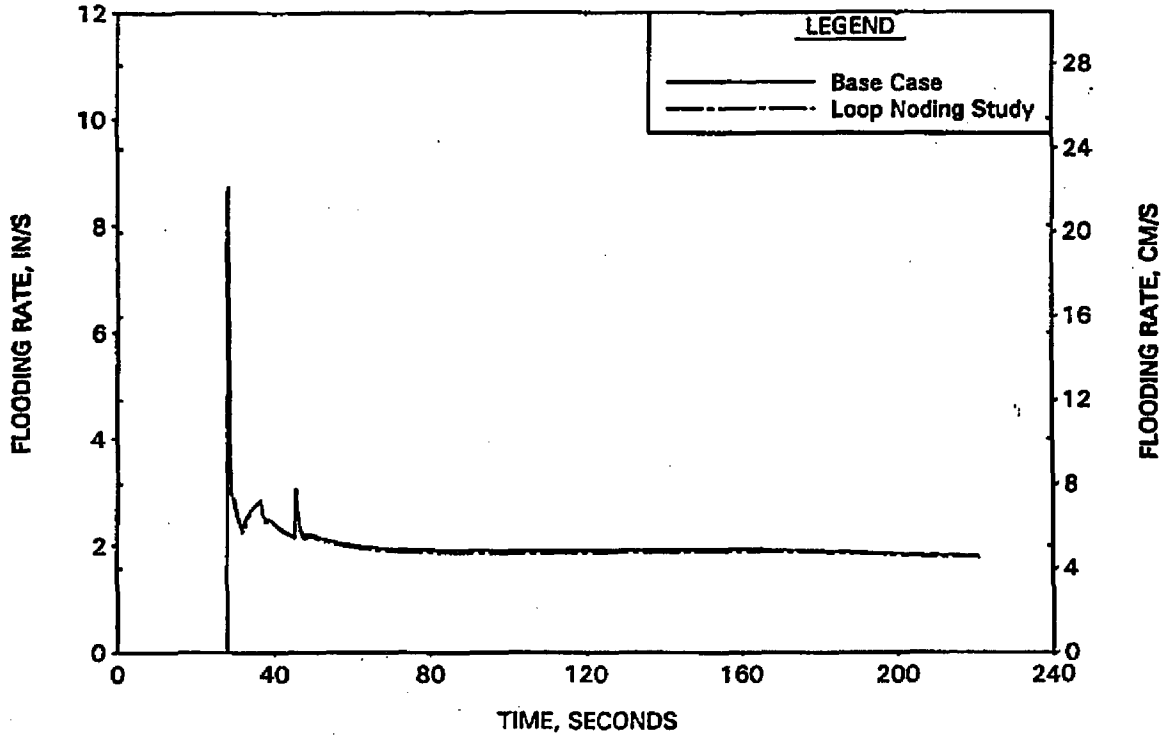

FIGURE A-49. REFLOD3B LOOP NODING STUDY - CORE WATER LEVEL.

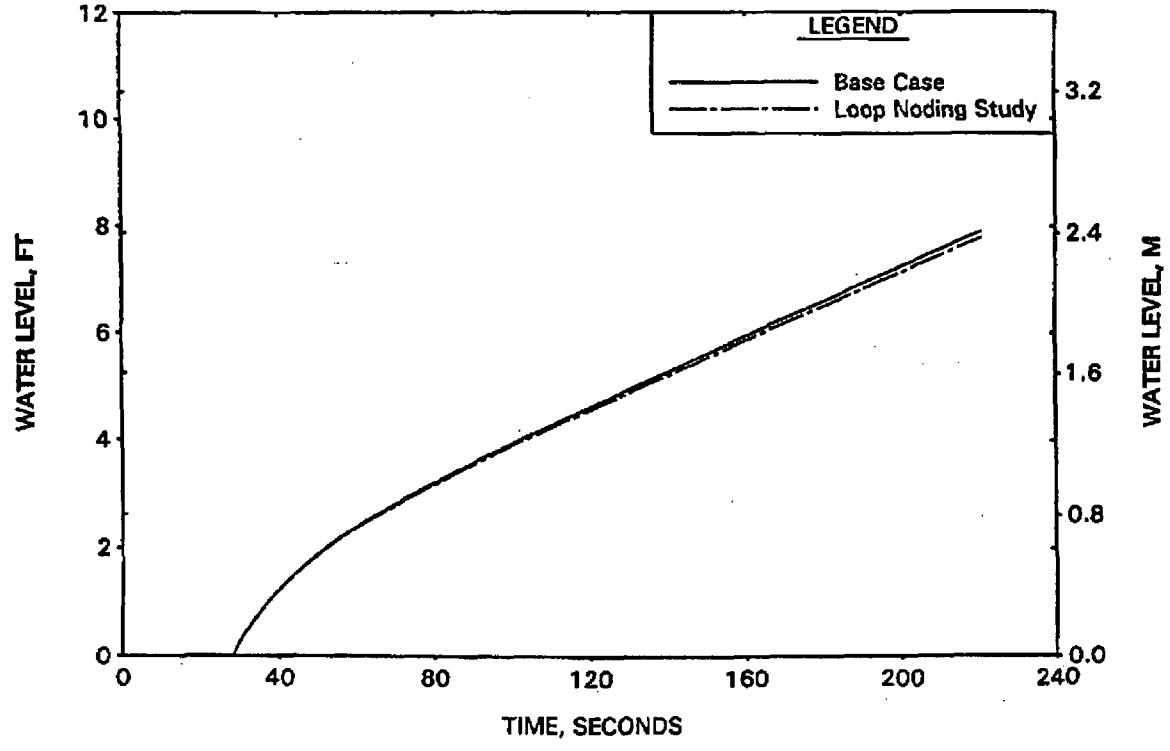

FIGURE A-50. REFLOD3B LOOP NODING STUDY - DOWNCOMER WATER LEVEL.

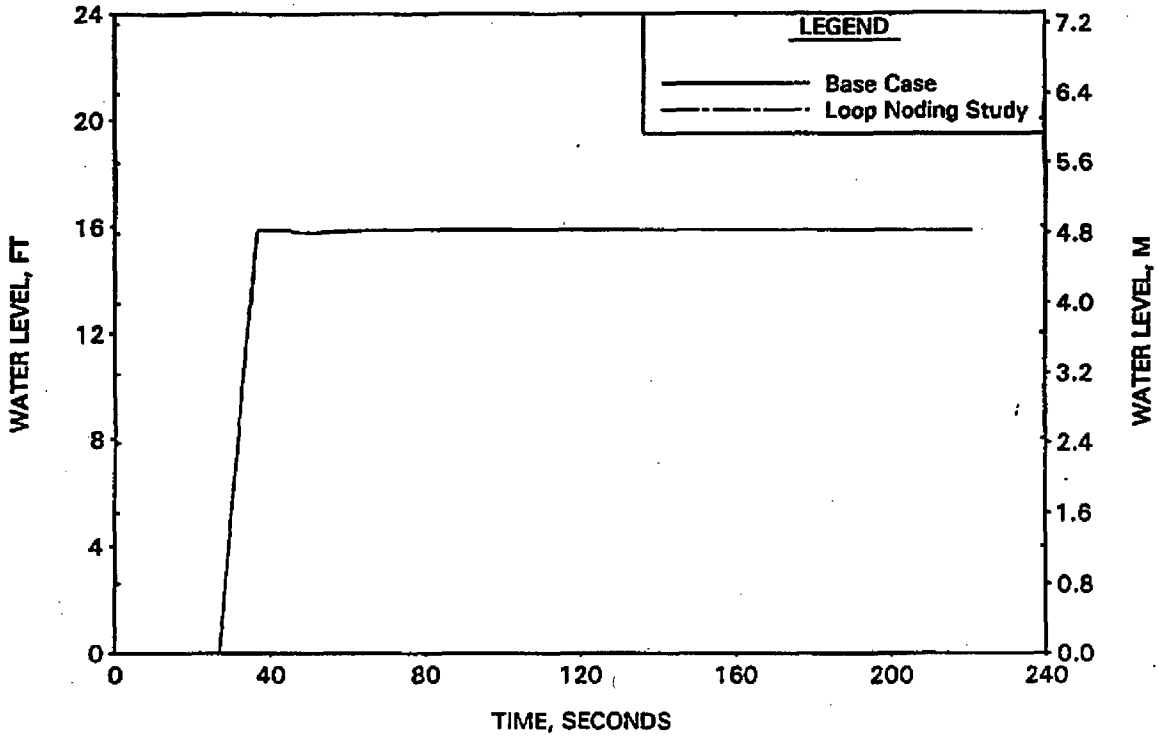

FIGURE A-51. REFLOD3B LOOP NODING STUDY - CARRYOUT RATE FRACTION.

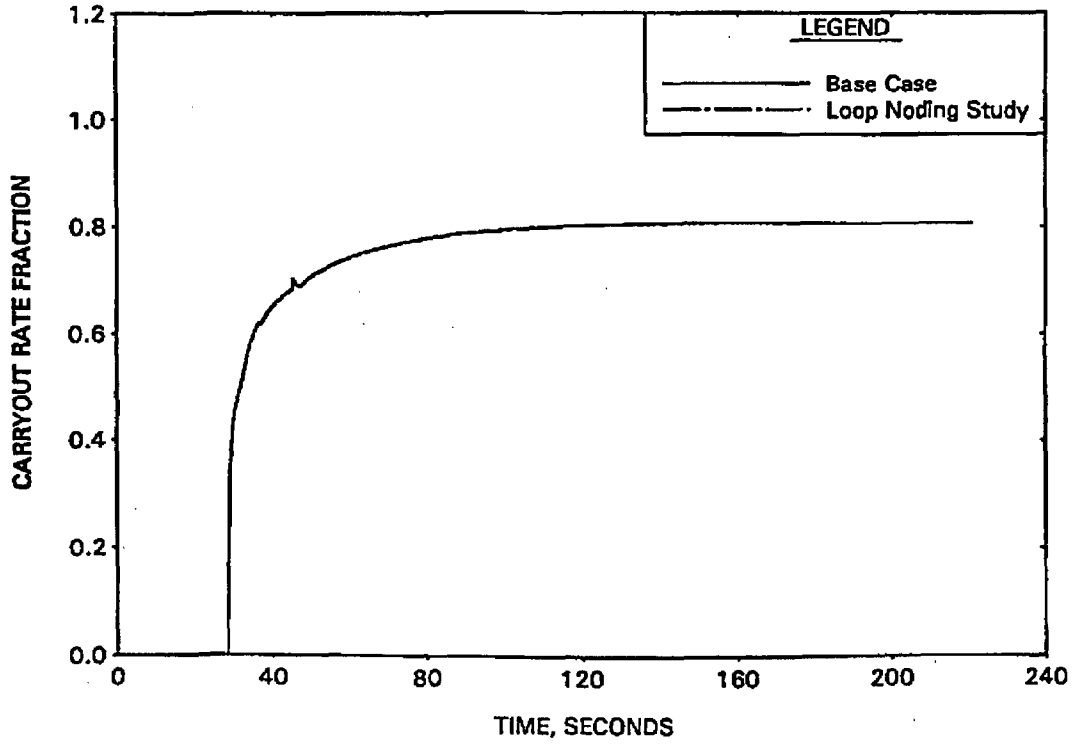

FIGURE A-52. REFLOD3B FREE-SPINNING ROTOR STUDY - CORE FLOODING RATE.

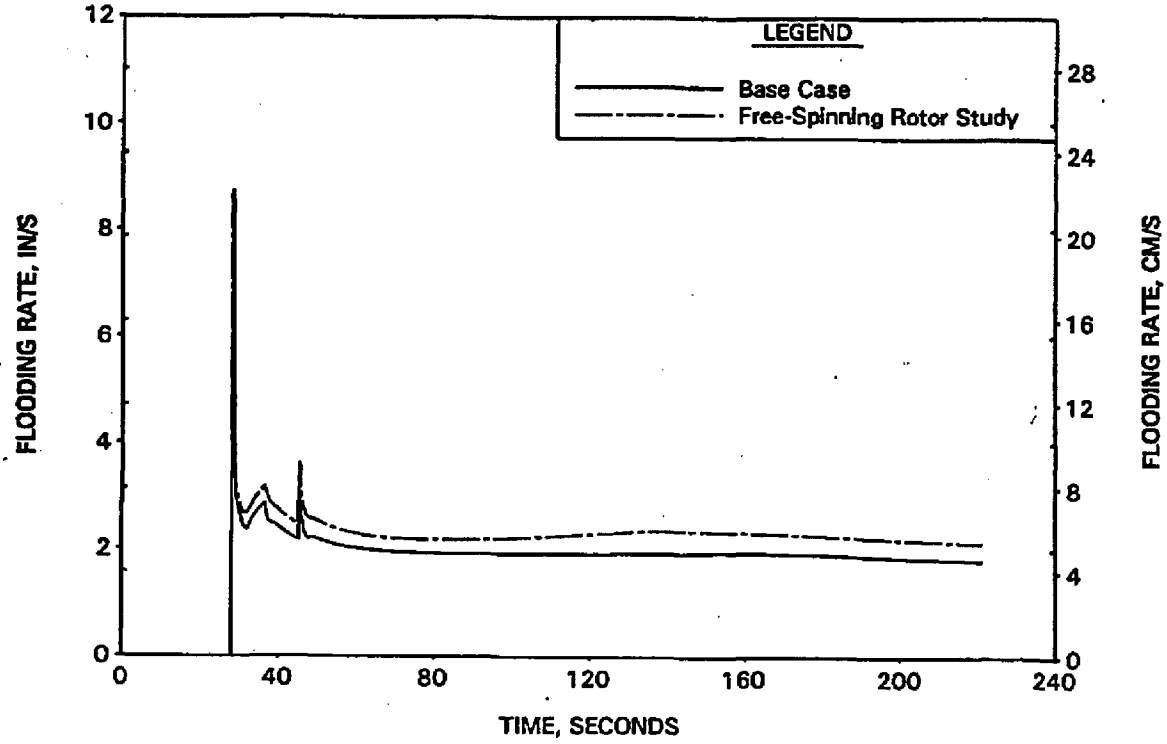

FIGURE A-53. REFLOD3B FREE-SPINNING ROTOR STUDY - CORE WATER LEVEL.

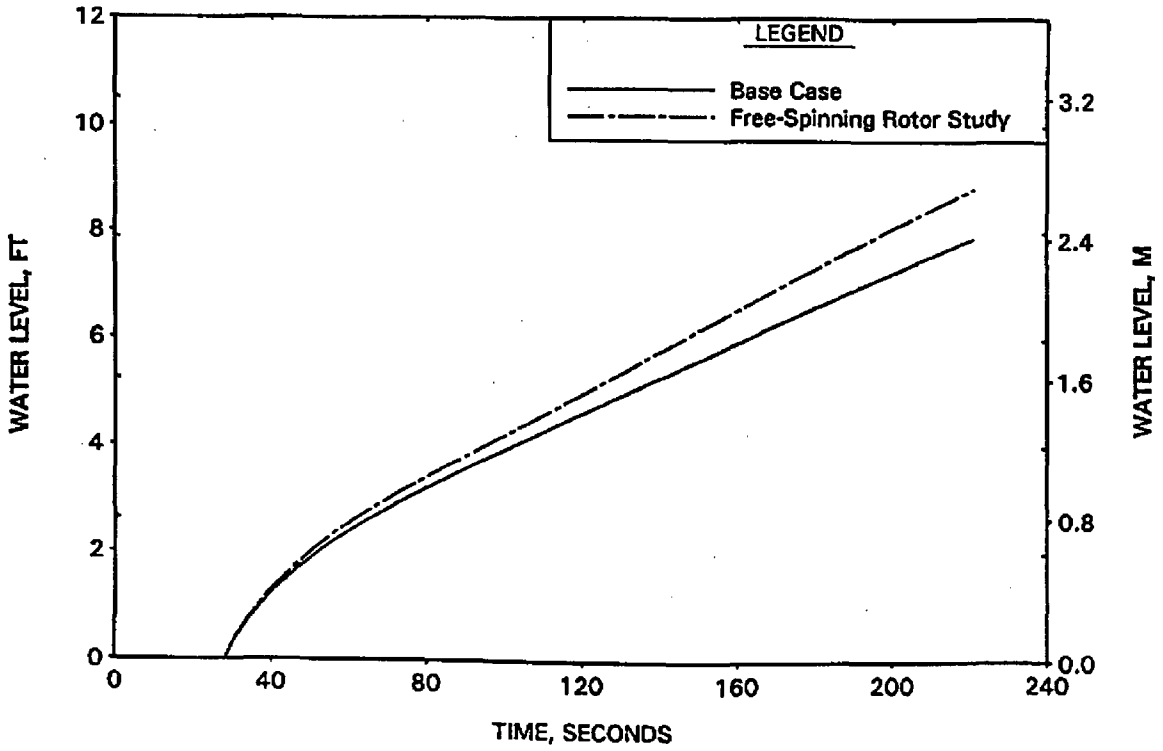

FIGURE A-54. REFLOD3B FREE-SPINNING ROTOR STUDY - DOWNCOMER WATER LEVEL.

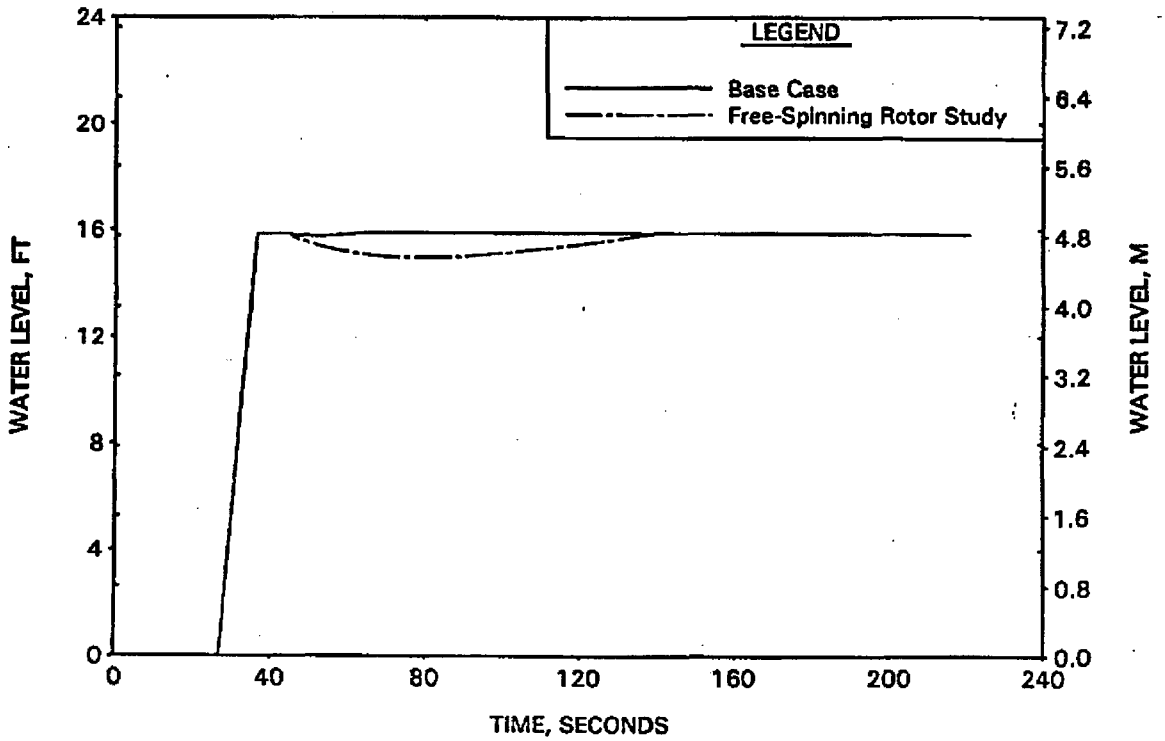

FIGURE A-55. REFLOD3B FREE-SPINNING ROTOR STUDY - CARRYOUT RATE FRACTION.

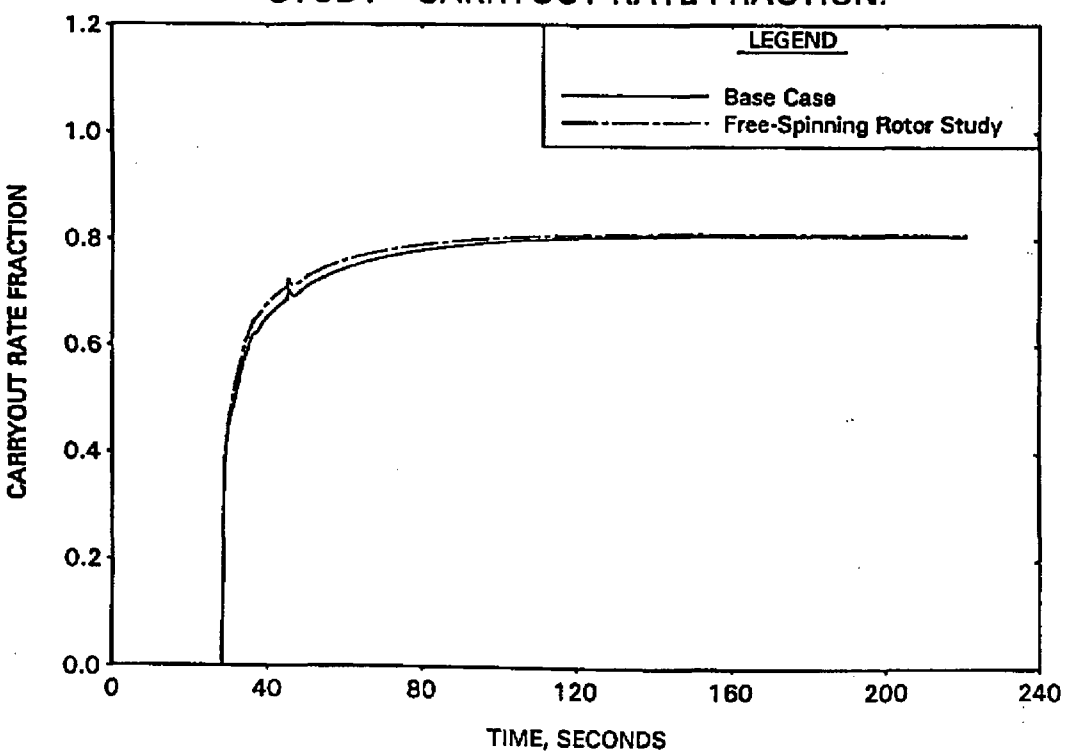

FIGURE A-56. BEACH NODING ARRANGEMENT (MARK-BW FUEL ASSEMBLY).

C,D,E

FIGURE A-57. BEACH TIME STEP STUDY - REQUESTED TIME STEP ADVANCEMENTS.

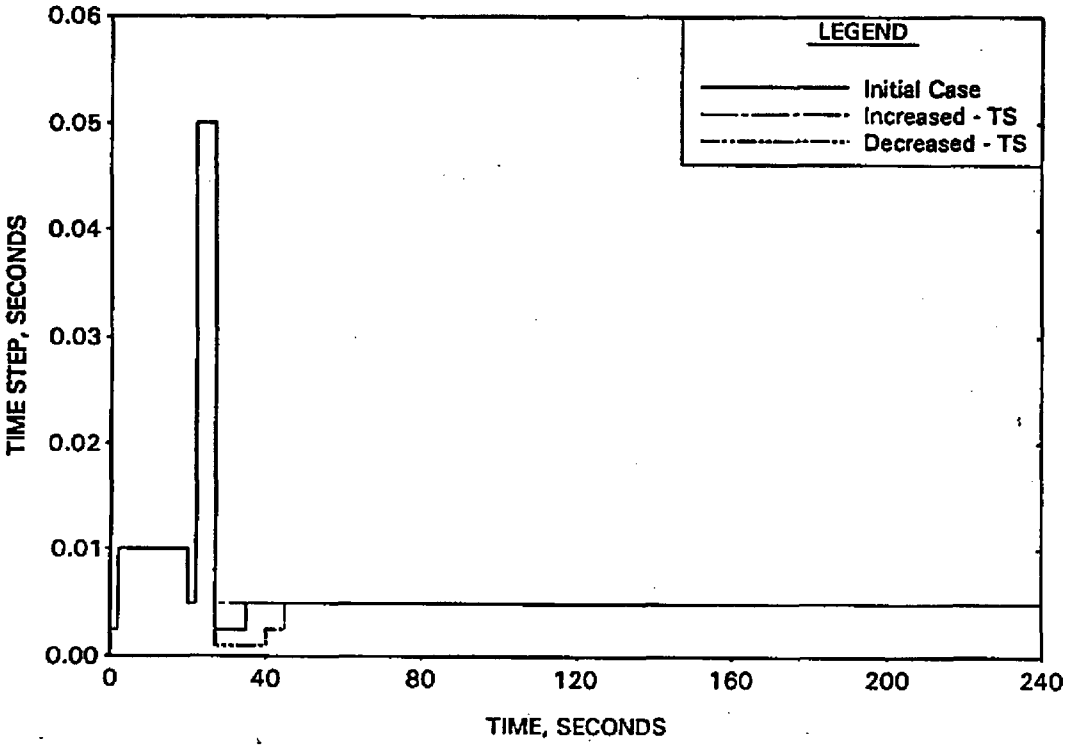

FIGURE A-58. BEACH TIME STEP STUDY - ACTUAL TIME STEP ADVANCEMENTS.

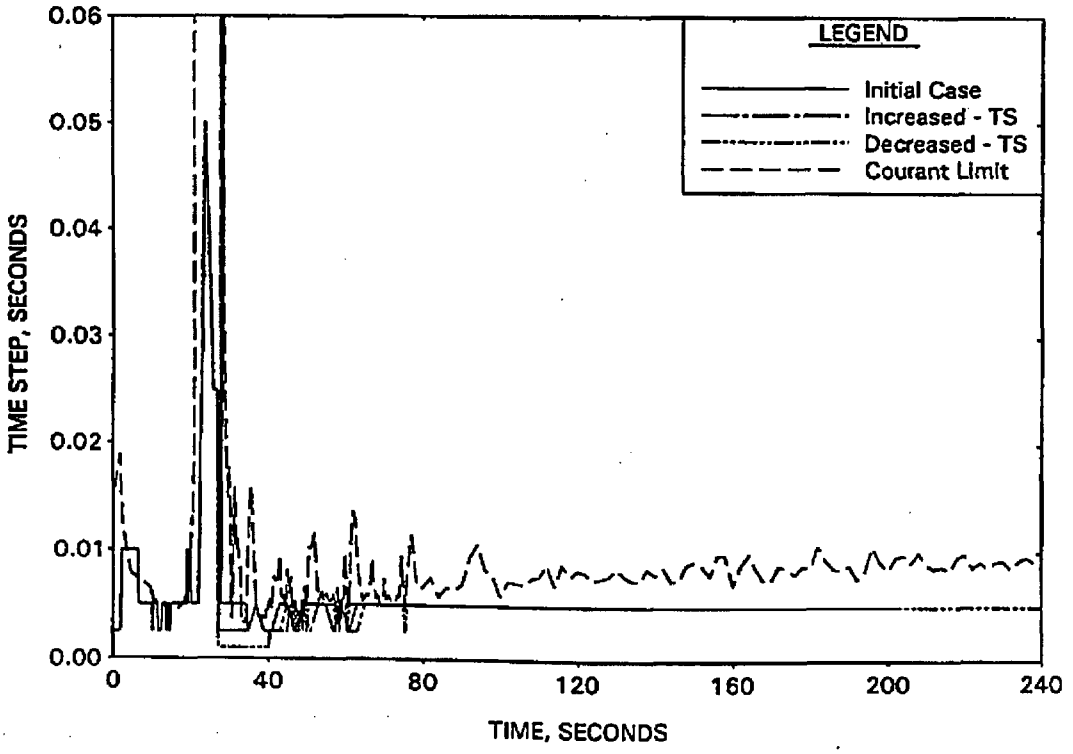

FIGURE A-59. BEACH TIME STEP STUDY -
HC CLAD TEMP AT RUPTURED LOCATION (SEGMENT 11).

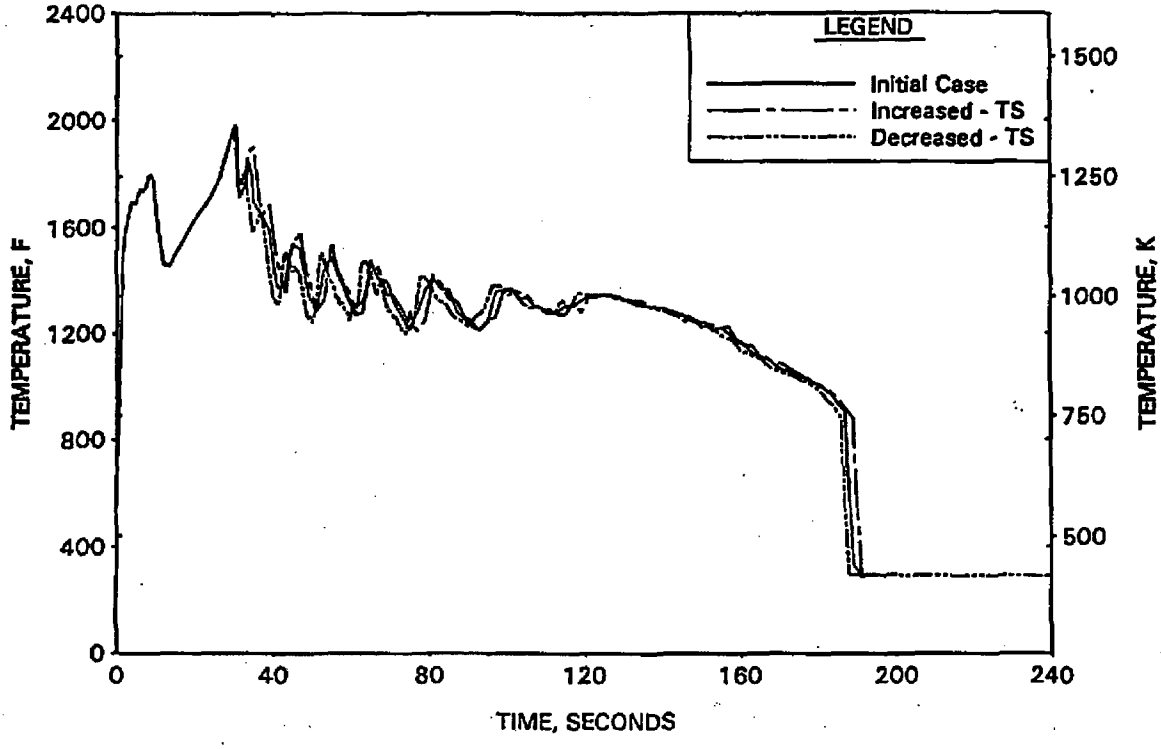

FIGURE A-60. BEACH TIME STEP STUDY -
HC CLAD TEMP AT PEAK UNRUPTURED LOCATION.

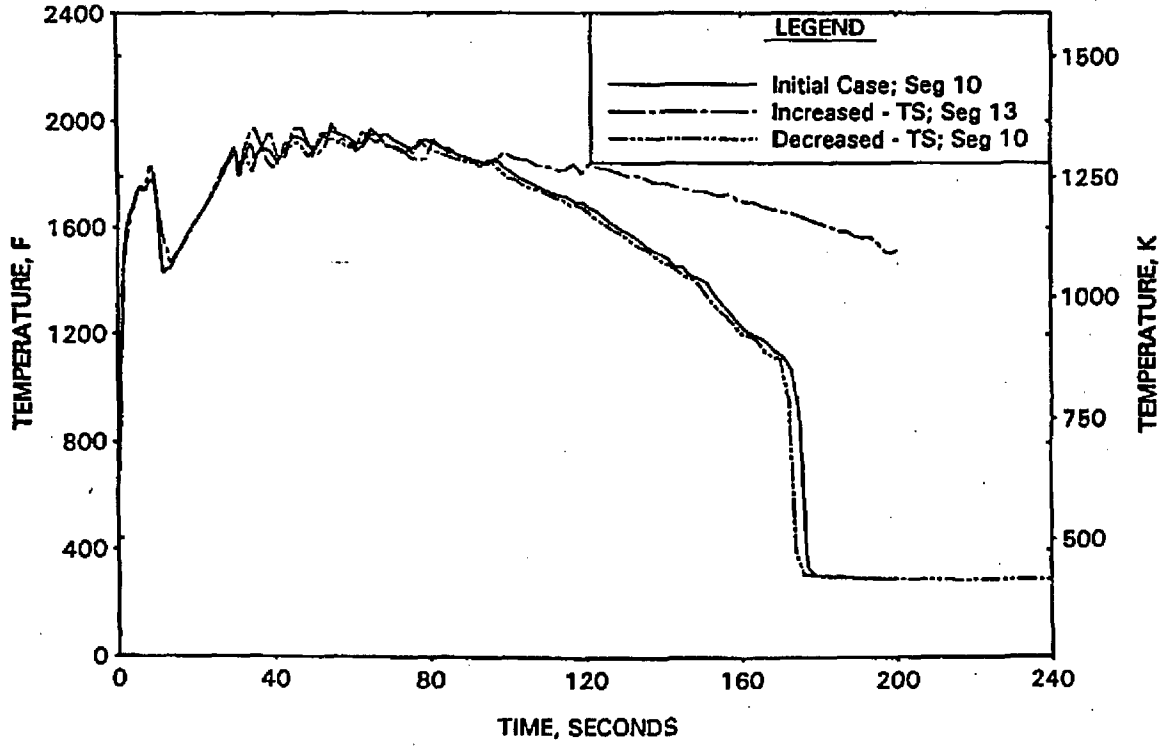

FIGURE A-61. BEACH TIME STEP STUDY - FILTERED HC HTC AT RUPTURED LOCATION (SEGMENT 11).

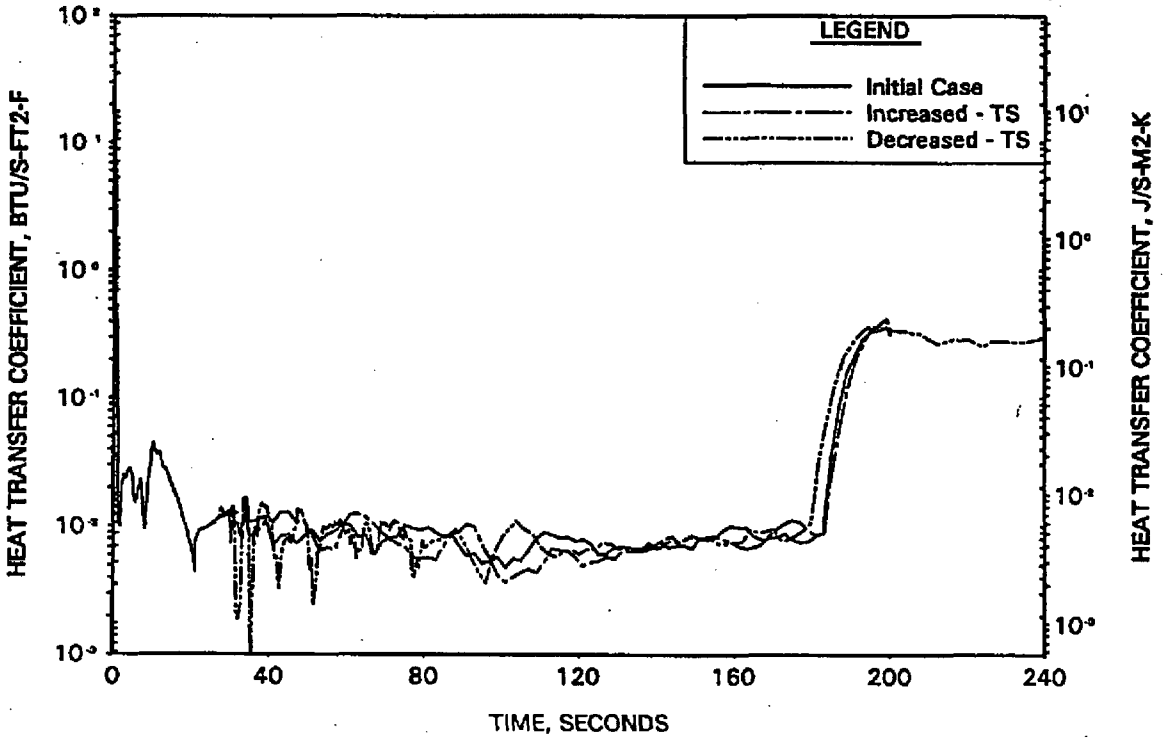

FIGURE A-62. BEACH TIME STEP STUDY - FILTERED HC HTC AT PEAK UNRUPTURED LOCATION.

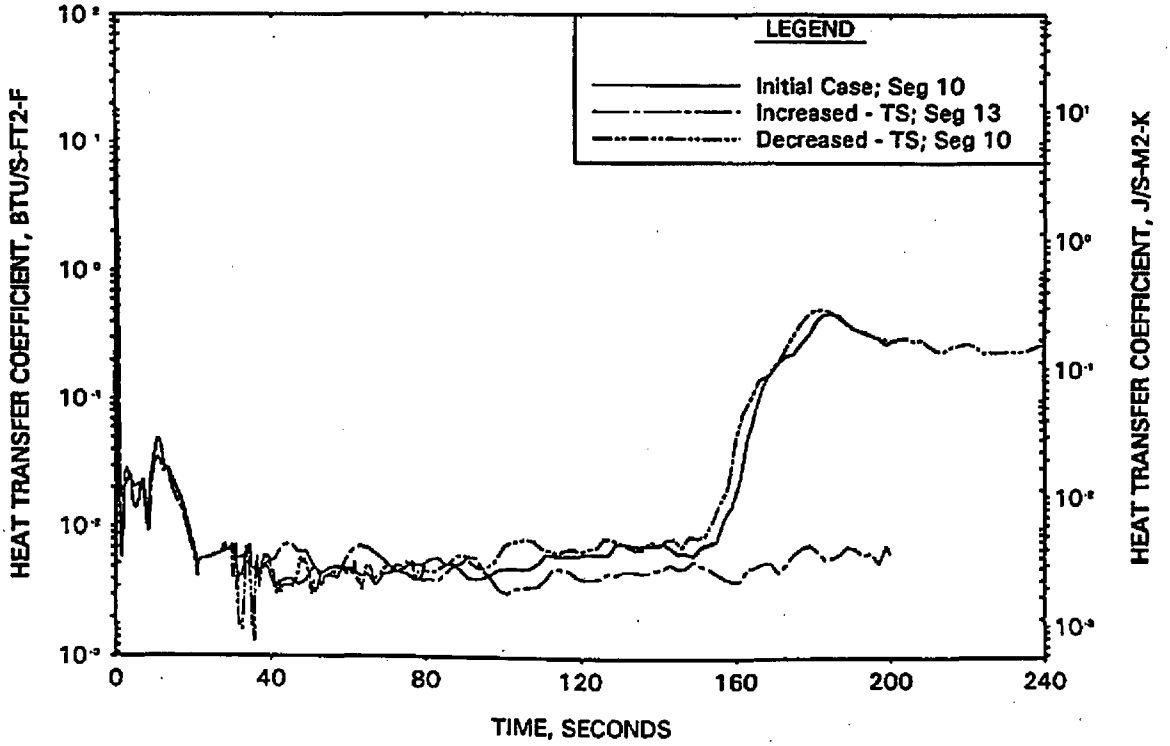

FIGURE A-63. BEACH TIME STEP STUDY -
HOT CHANNEL QUENCH FRONT ADVANCEMENT.

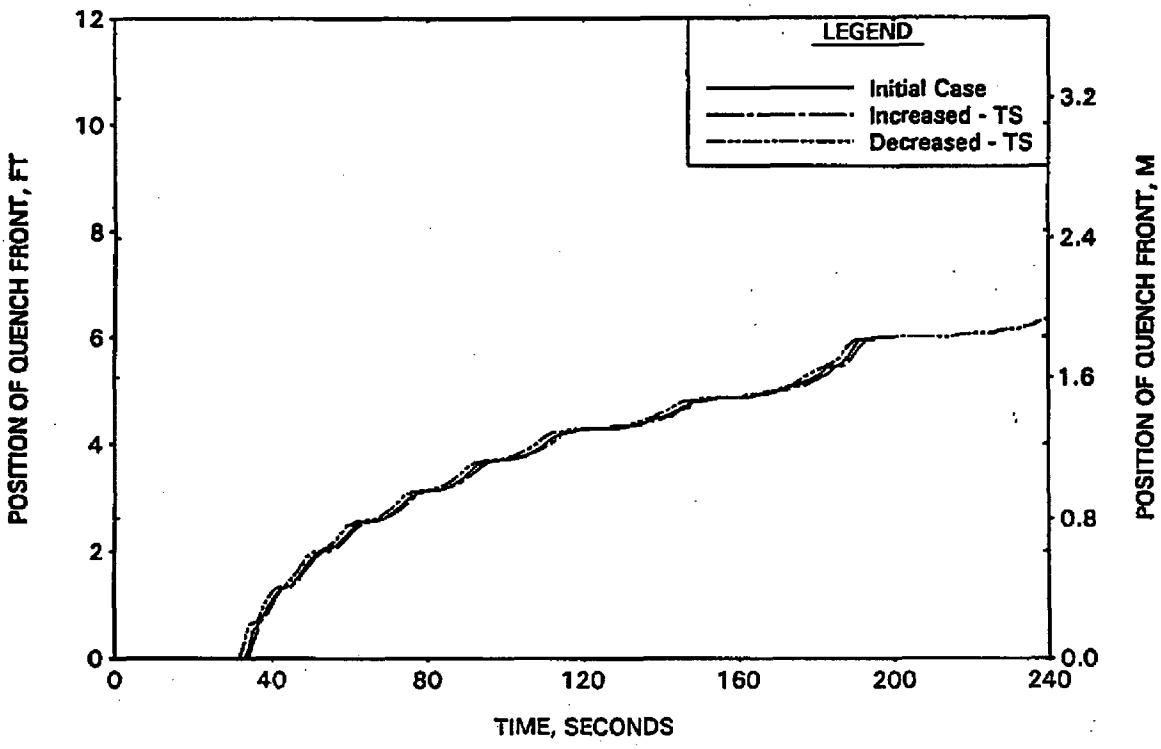

FIGURE A-64. BEACH TIME STEP STUDY -
AVERAGE CHANNEL QUENCH FRONT ADVANCEMENT.

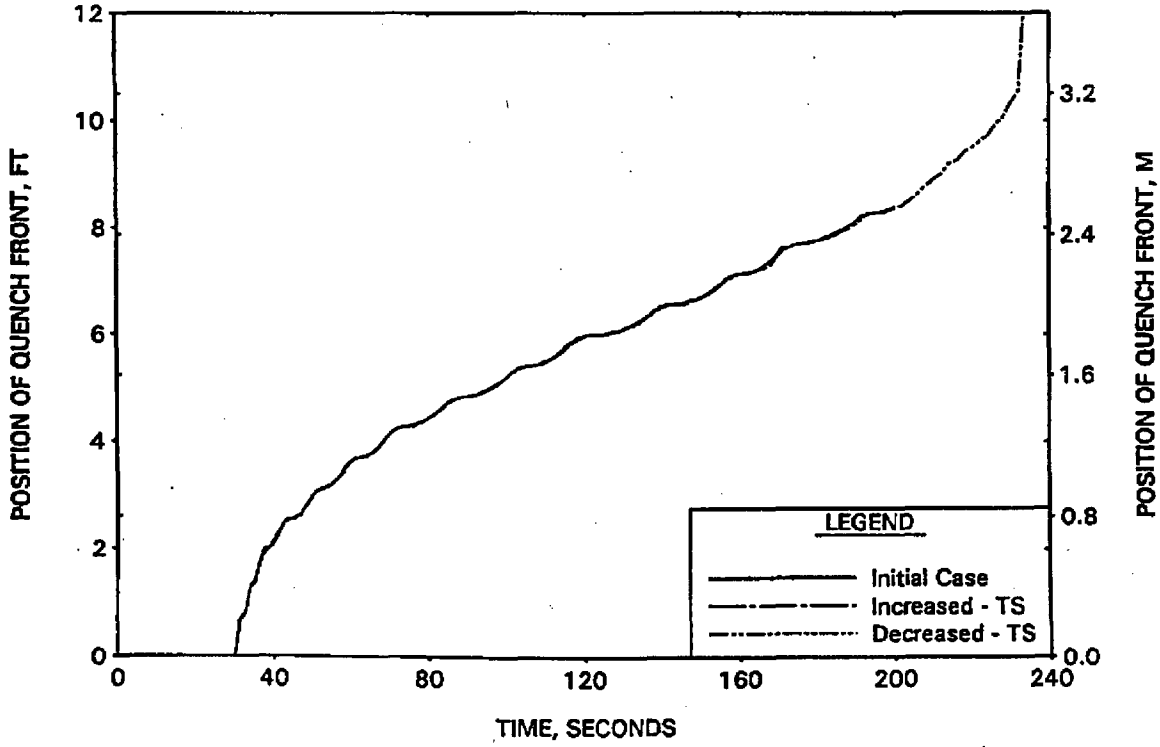

FIGURE A-65. BEACH AXIAL FUEL SEGMENTATION STUDY - HC CLAD TEMP AT RUPTURED LOCATION (SEGMENT 11).

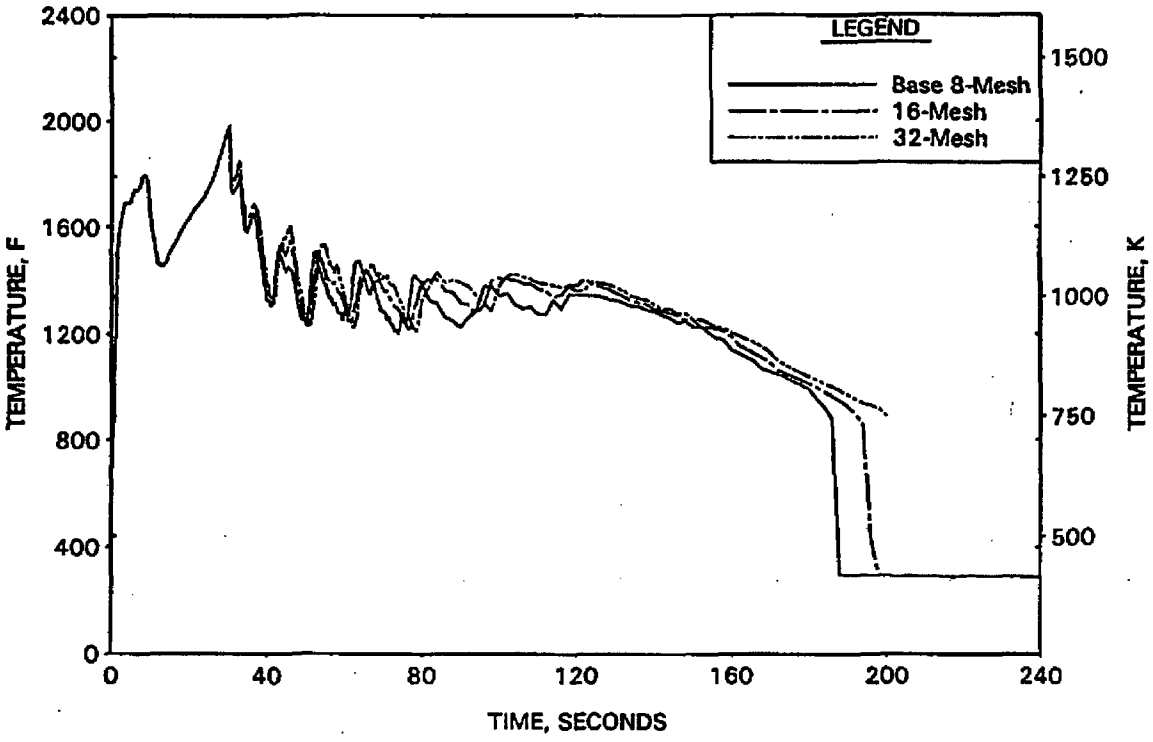

FIGURE A-66. BEACH AXIAL FUEL SEGMENTATION STUDY - HC CLAD TEMP AT PEAK UNRUPTURED LOCATION.

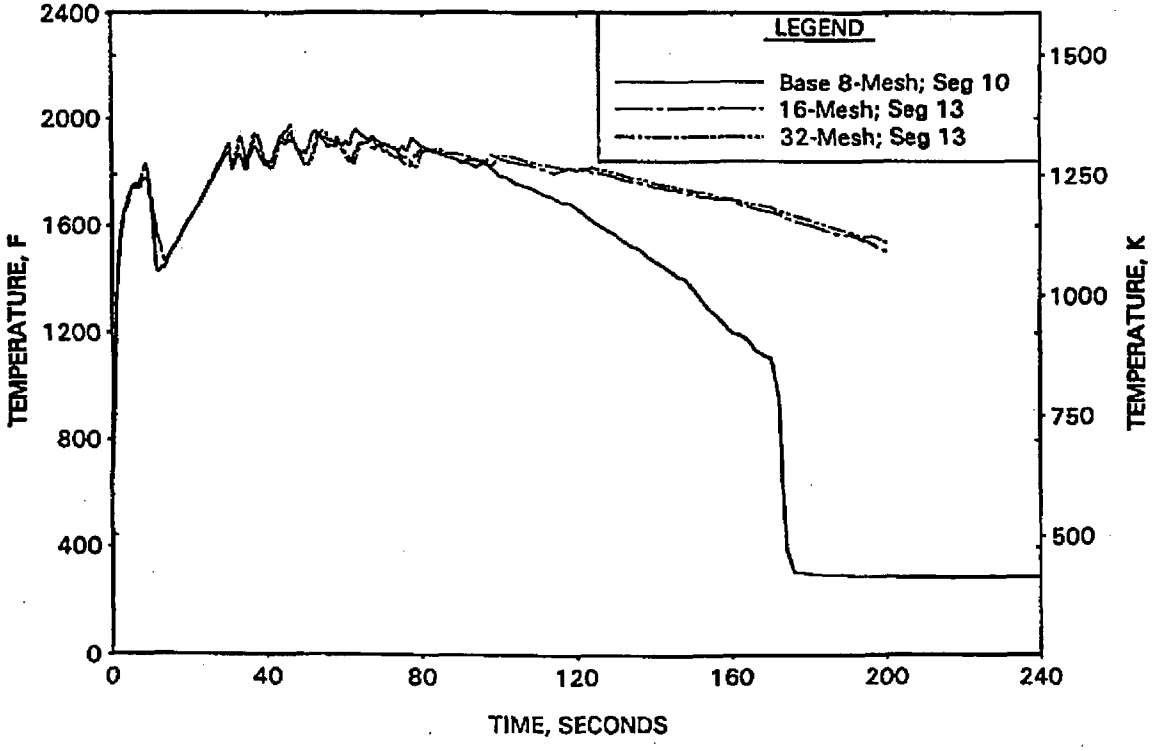

FIGURE A-67. BEACH AXIAL FUEL SEGMENTATION STUDY - HC FUEL TEMP AT RUPTURED LOCATION (SEGMENT 11).

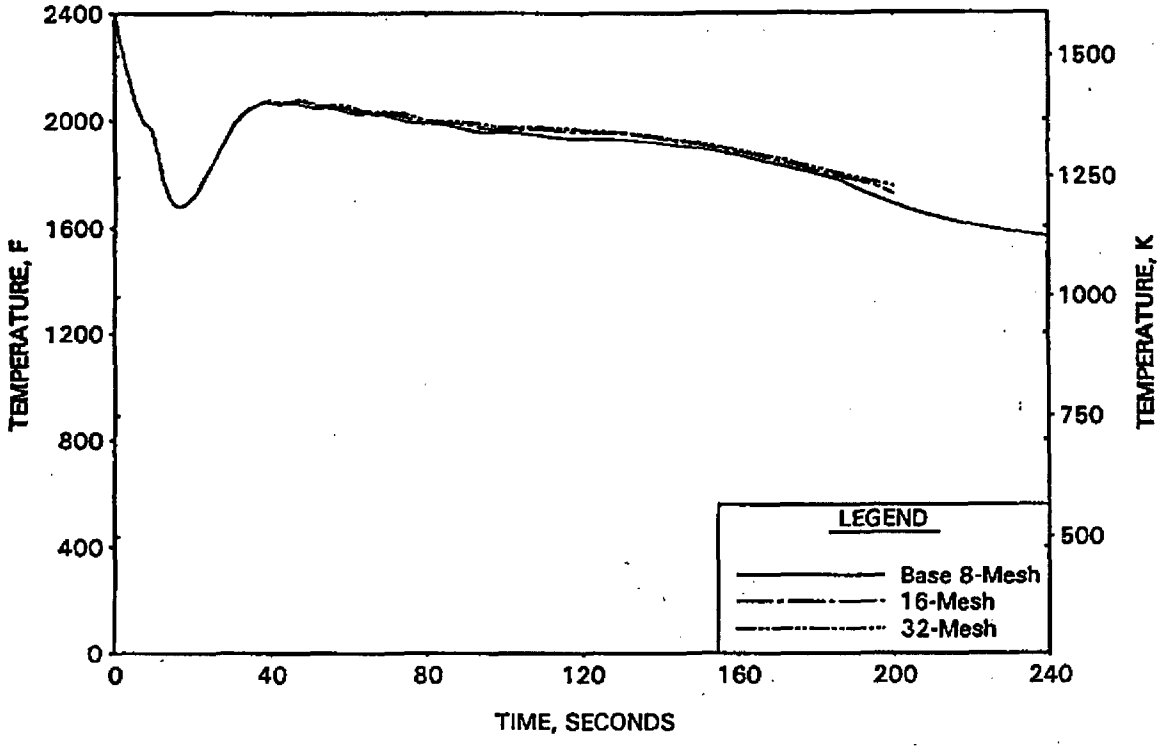

FIGURE A-68. BEACH AXIAL FUEL SEGMENTATION STUDY - HC FUEL TEMP AT PEAK UNRUPTURED LOCATION.

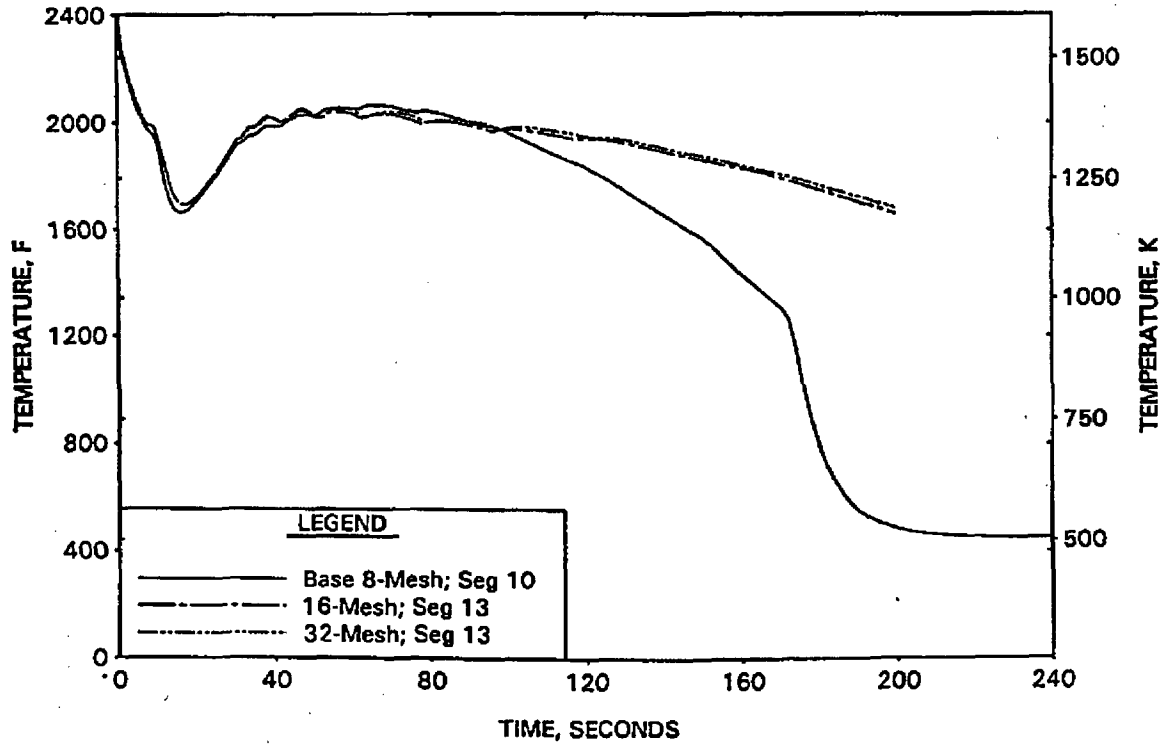

FIGURE A-69. BEACH AXIAL FUEL SEGMENTATION STUDY - HC FILTERED HTC AT RUPTURED LOCATION (SEGMENT 11).

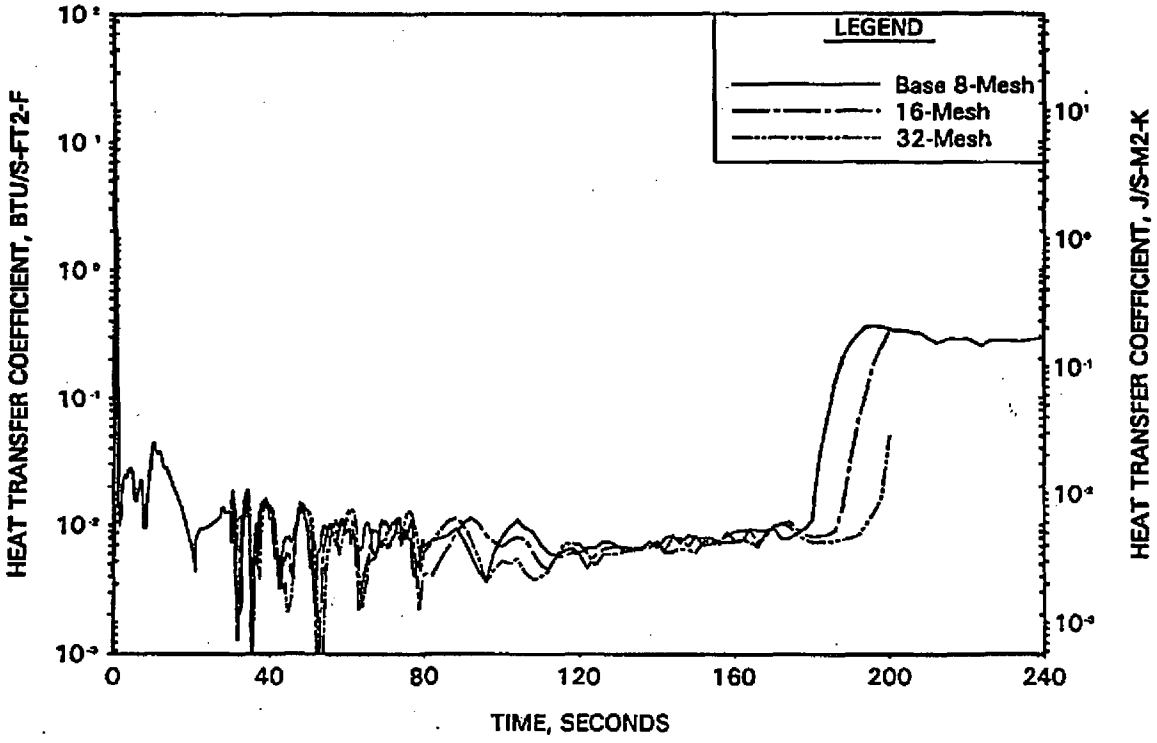

FIGURE A-70. BEACH AXIAL FUEL SEGMENTATION STUDY - HC FILTERED HTC AT PEAK UNRUPTURED LOCATION.

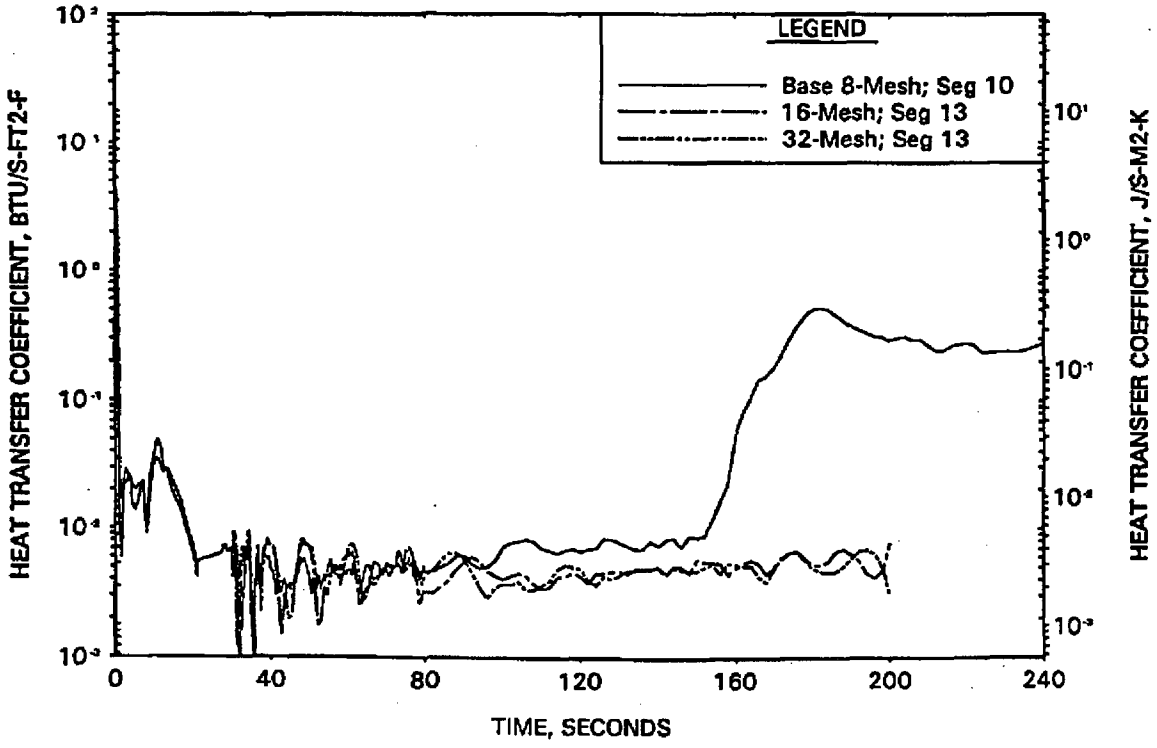

FIGURE A-71. BEACH AXIAL FUEL SEGMENTATION STUDY - HOT CHANNEL QUENCH FRONT ADVANCEMENT.

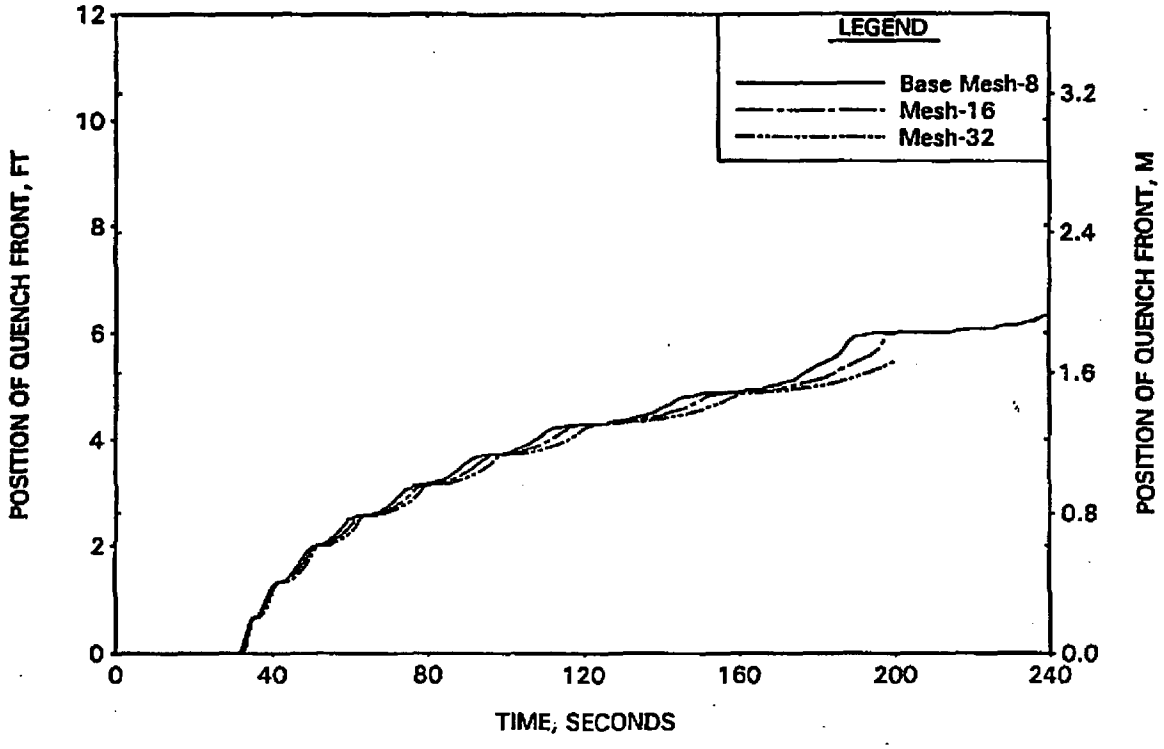

FIGURE A-72. BEACH AXIAL FUEL SEGMENTATION STUDY - AVERAGE CHANNEL QUENCH FRONT ADVANCEMENT.

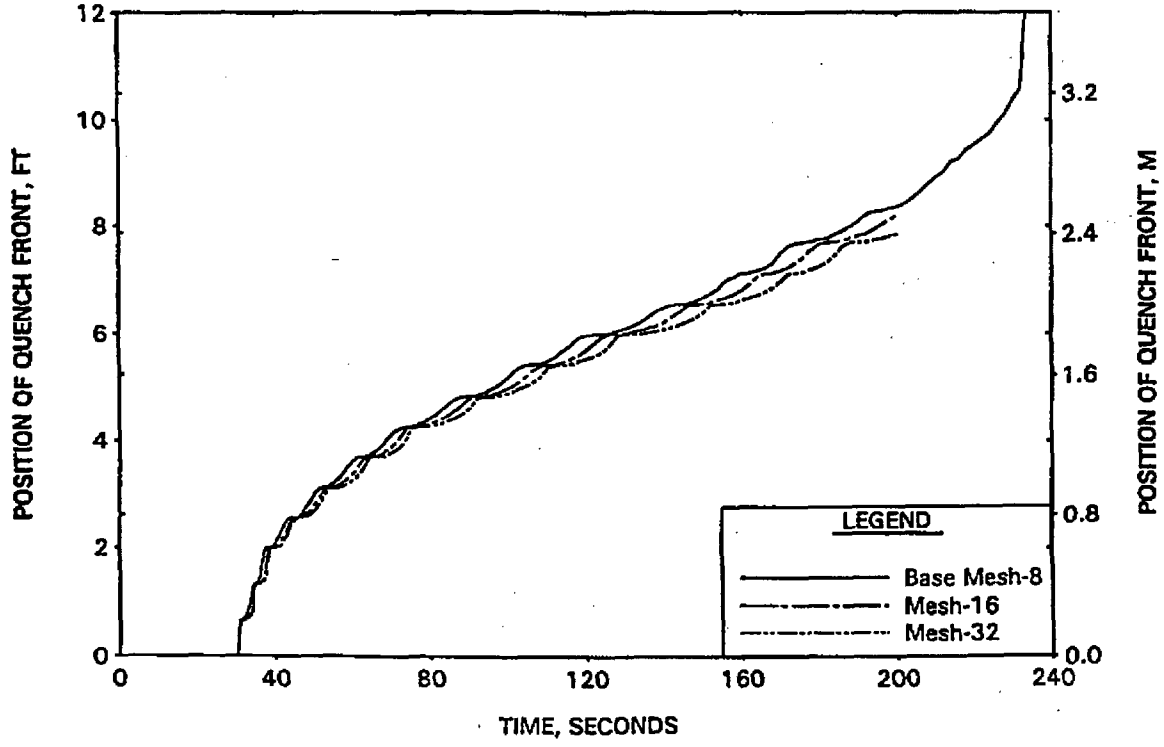

FIGURE A-73. AXIAL VS RADIAL CORE PEAKING FACTOR STUDY - 6.285-FT AXIAL POWER SHAPES.

C,D

FIGURE A-74. AXIAL VS RADIAL CORE PEAKING FACTOR STUDY - REACTOR VESSEL UPPER PLENUM PRESSURE.

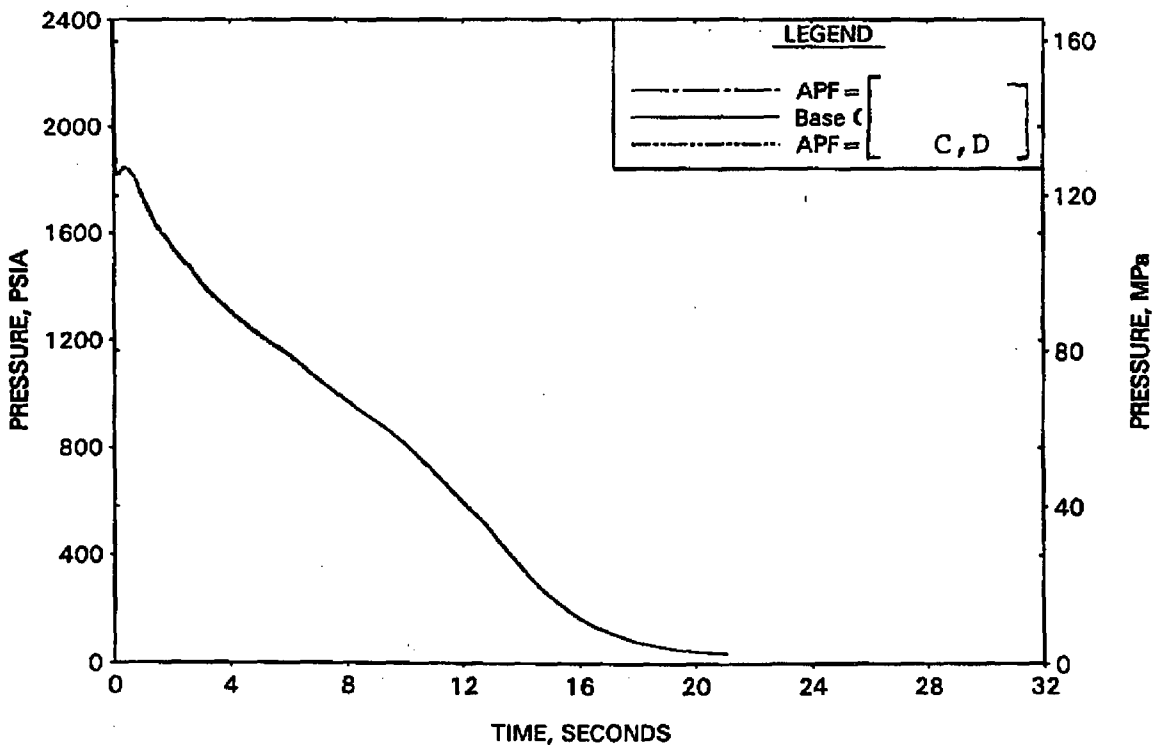

FIGURE A-75. AXIAL VS RADIAL CORE PEAKING FACTOR STUDY - RV SIDE BREAK MASS FLOW RATE.

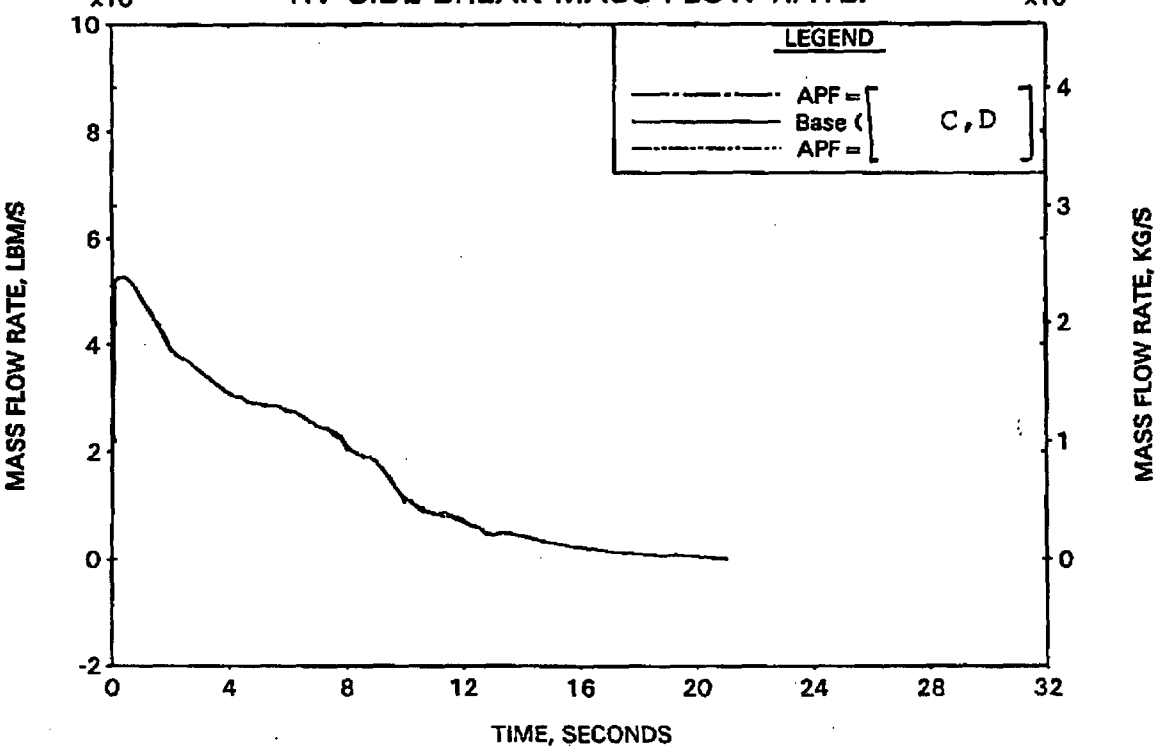

FIGURE A-76. AXIAL VS RADIAL CORE PEAKING FACTOR STUDY - PUMP SIDE BREAK MASS FLOW RATE.

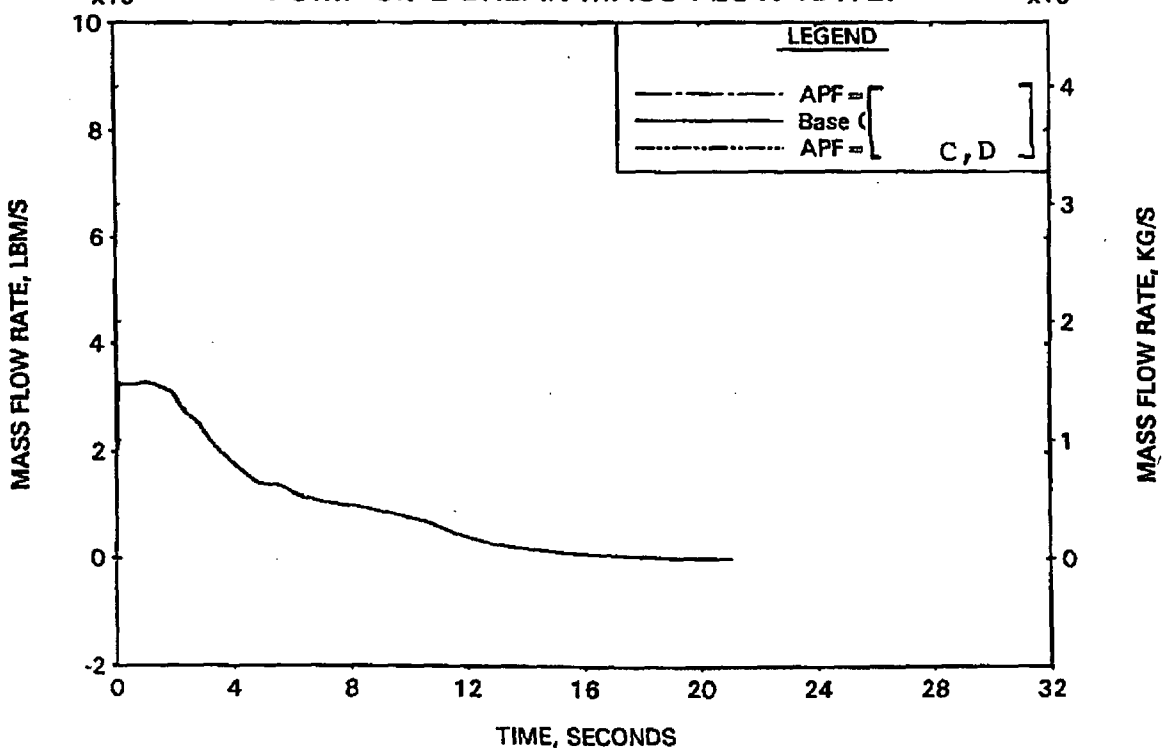

FIGURE A-77. AXIAL VS RADIAL CORE PEAKING FACTOR STUDY - HC MASS FLOW RATE AT PEAK POWER LOCATION.

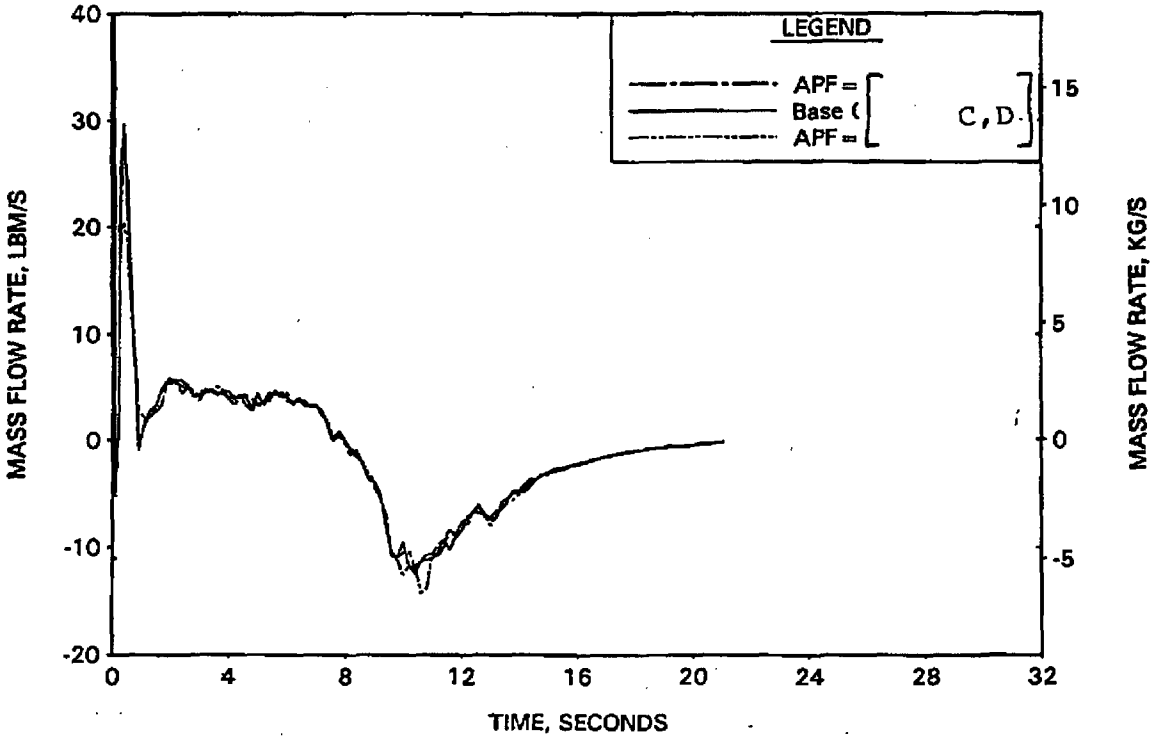

FIGURE A-78. AXIAL VS RADIAL CORE PEAKING FACTOR STUDY - CORE FLOODING RATE.

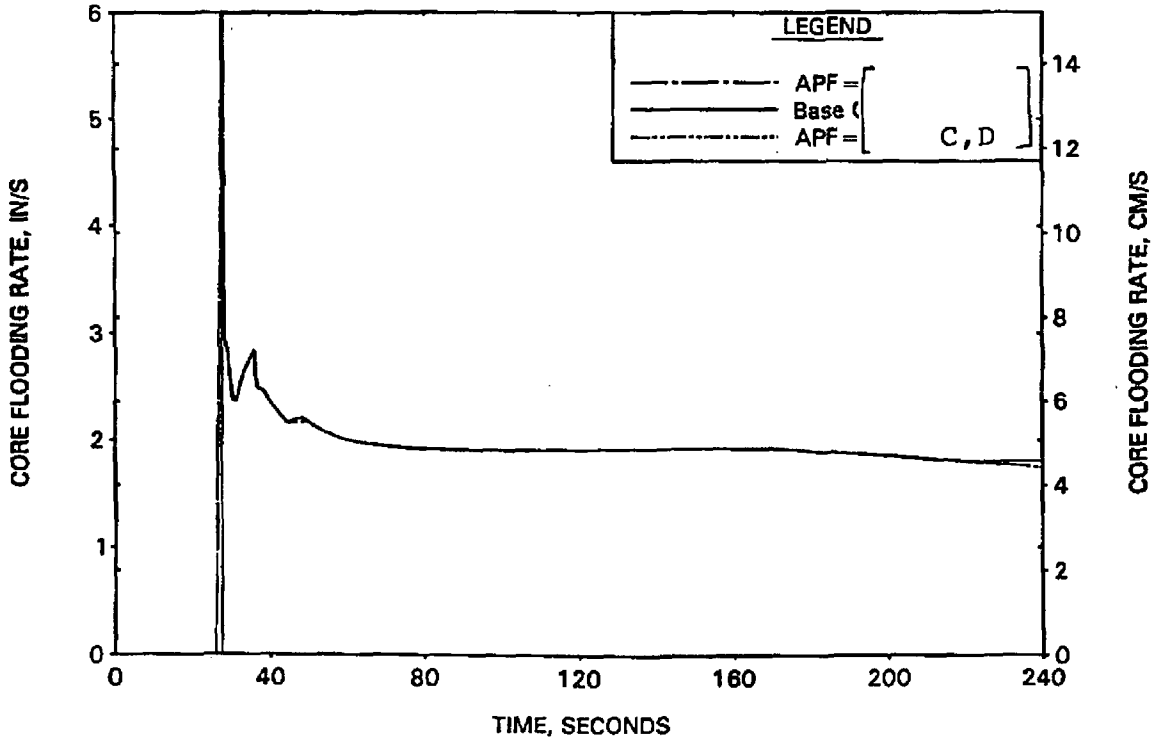

FIGURE A-79. AXIAL VS RADIAL CORE PEAKING FACTOR STUDY - HC CLAD TEMP AT RUPTURED LOCATION.

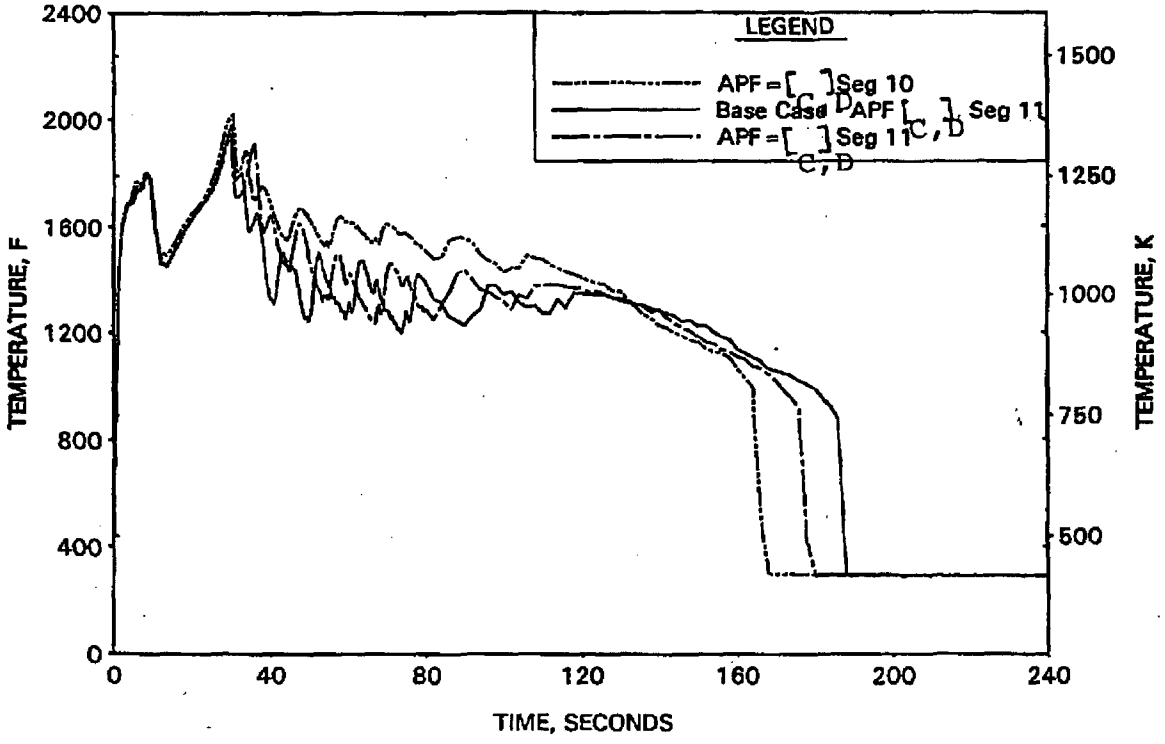

FIGURE A-80. AXIAL VS RADIAL CORE PEAKING FACTOR STUDY - HC CLAD TEMP AT PEAK UNRUPTURED LOCATION.

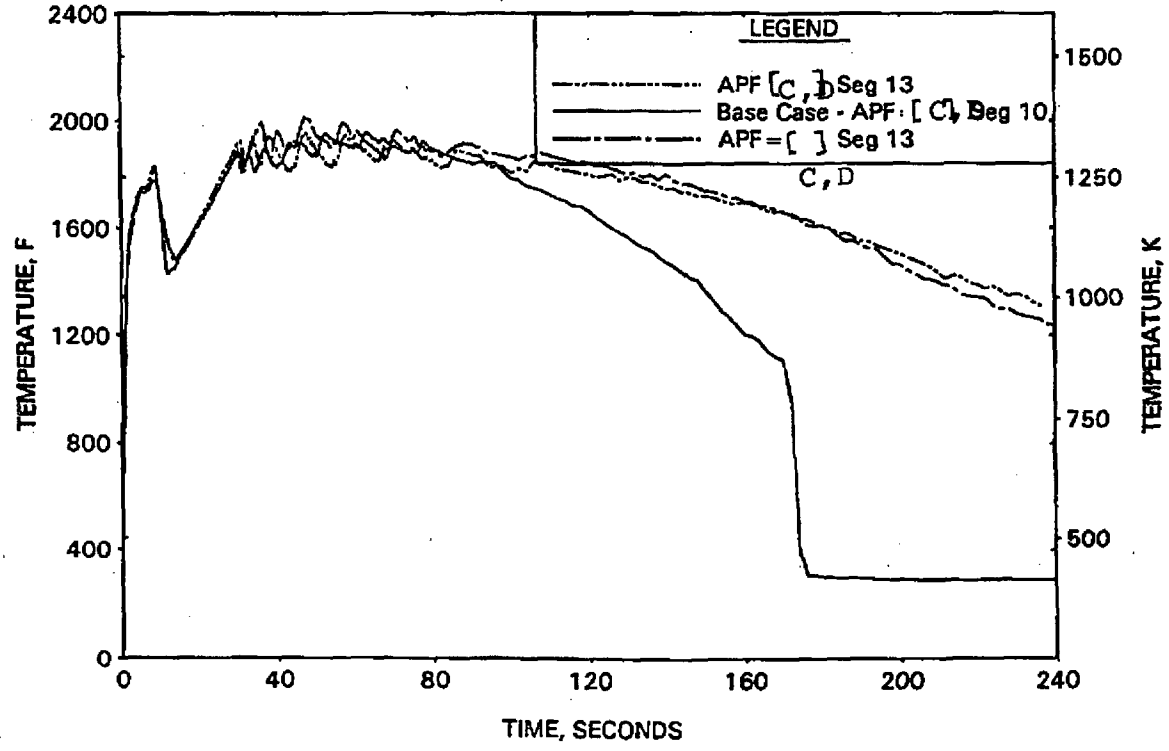

FIGURE A-81. AXIAL VS RADIAL CORE PEAKING FACTOR STUDY - HC FILTERED HTC AT RUPTURED LOCATION.

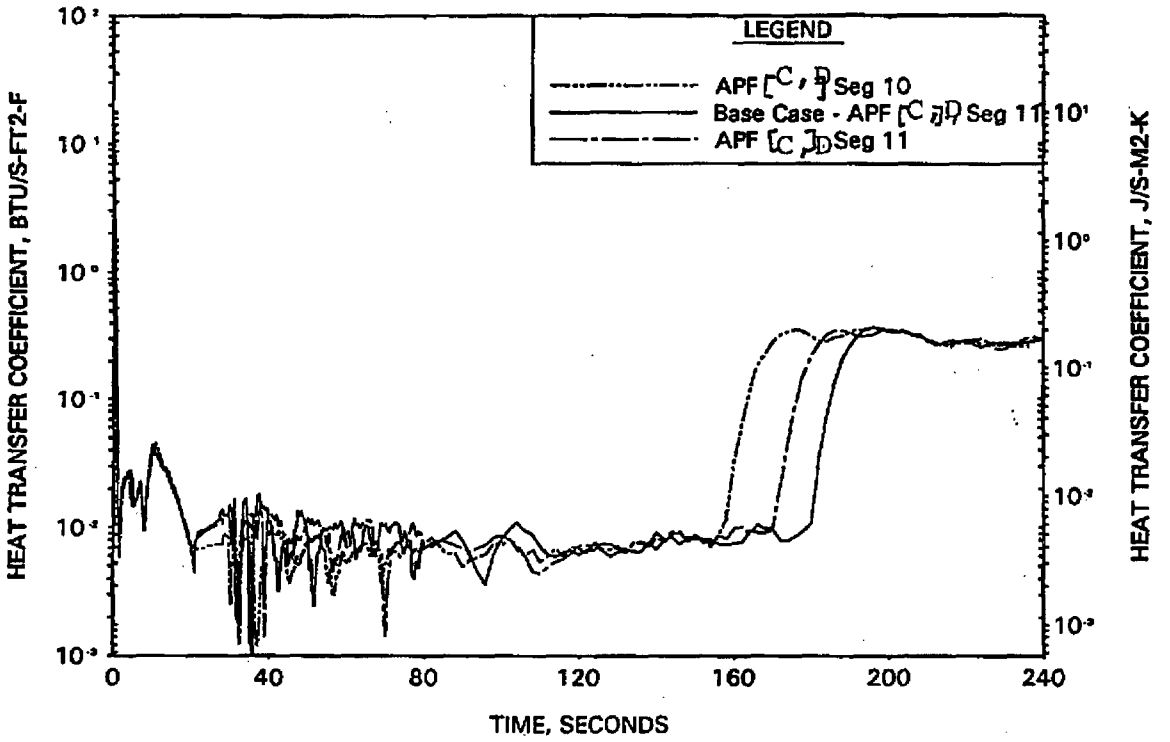

FIGURE A-82. AXIAL VS RADIAL CORE PEAKING FACTOR STUDY - HC FILTERED HTC AT PEAK UNRUPTURED LOCATION.

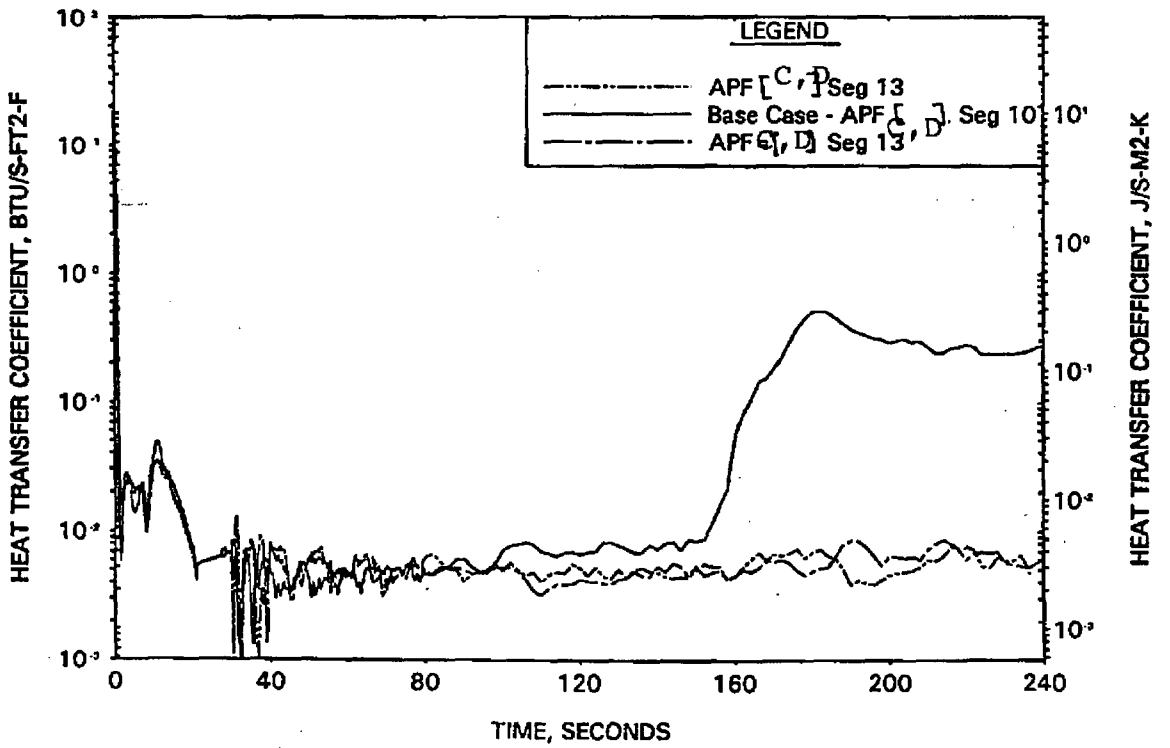

FIGURE A-83. BREAK SPECTRUM STUDY -
REACTOR VESSEL UPPER PLENUM PRESSURE.

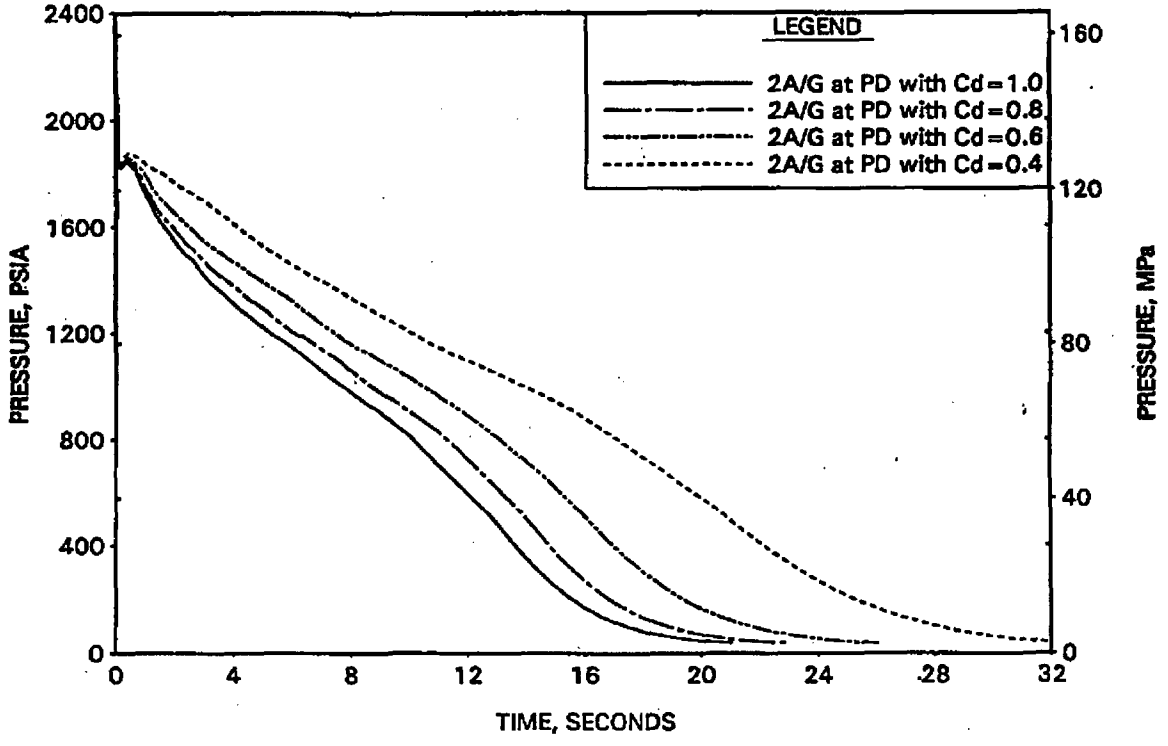

FIGURE A-84. BREAK SPECTRUM STUDY -
RV SIDE BREAK MASS FLOW RATE.

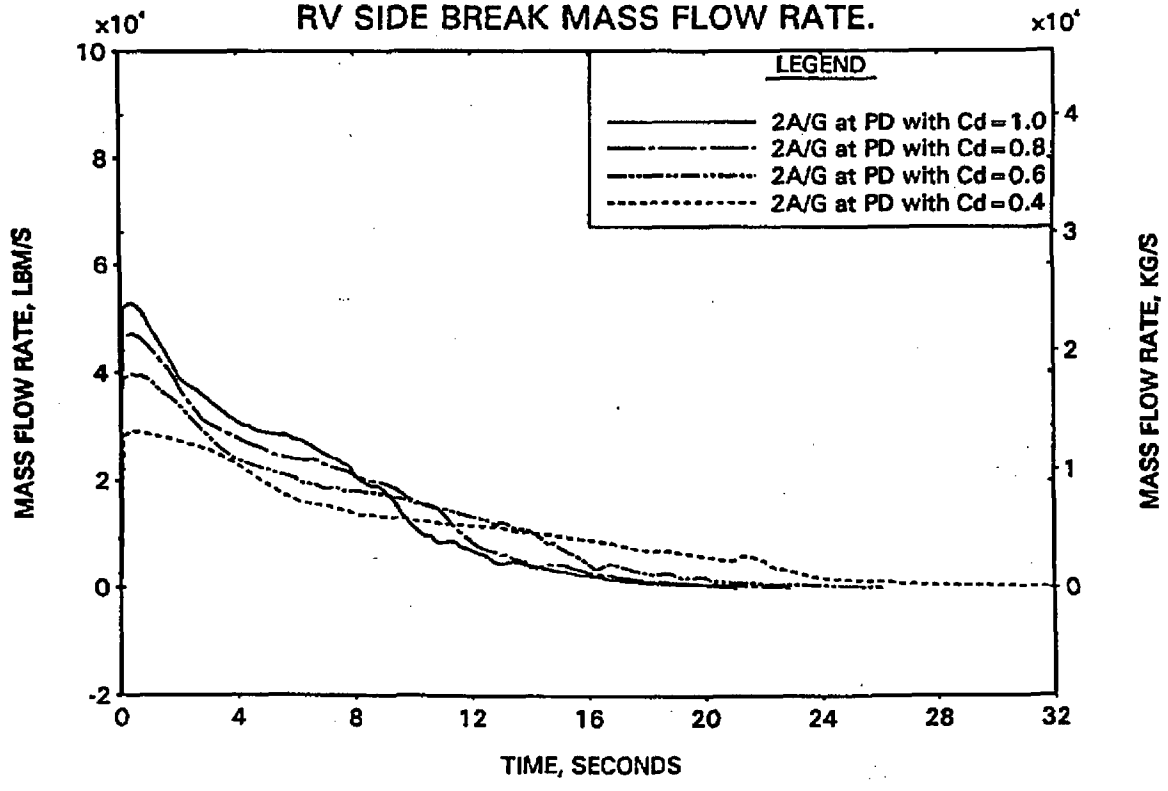

FIGURE A-85. BREAK SPECTRUM STUDY -
PUMP SIDE BREAK MASS FLOW RATE.

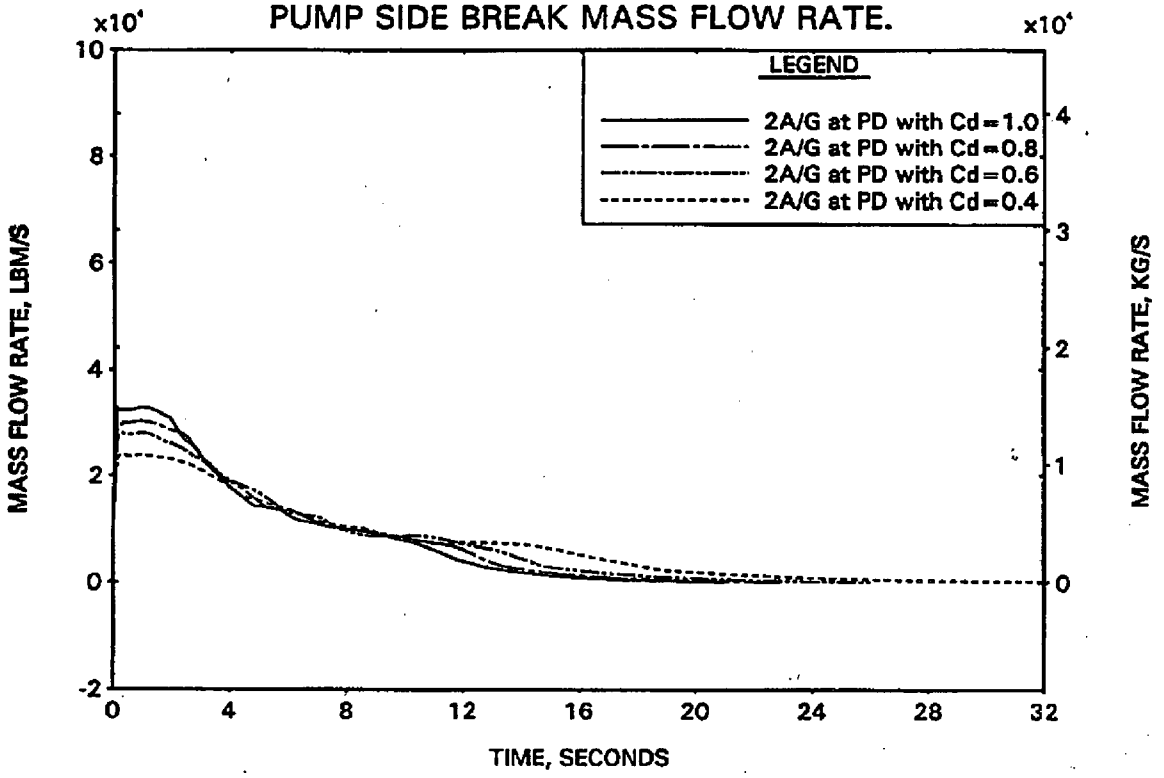

FIGURE A-86. BREAK SPECTRUM STUDY -
HC MASS FLOW RATE AT RUPTURED LOCATION.

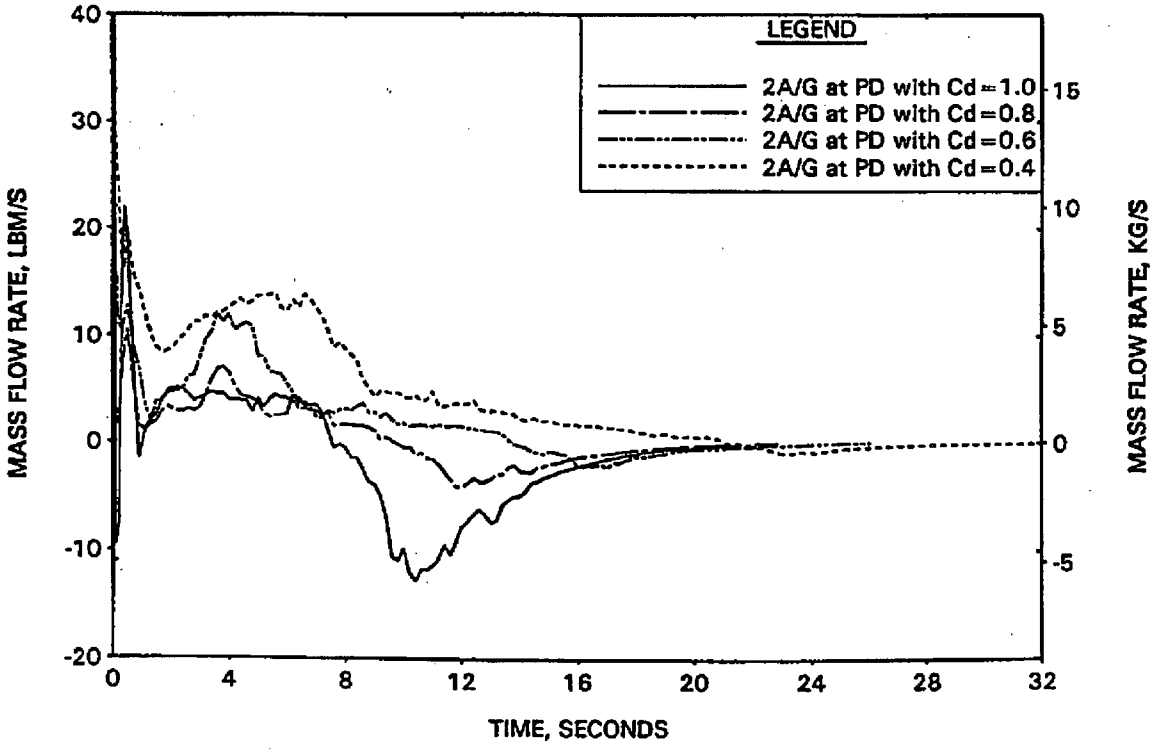

FIGURE A-87. BREAK SPECTRUM STUDY -
HC MASS FLOW RATE AT PEAK UNRUPTURED LOCATION.

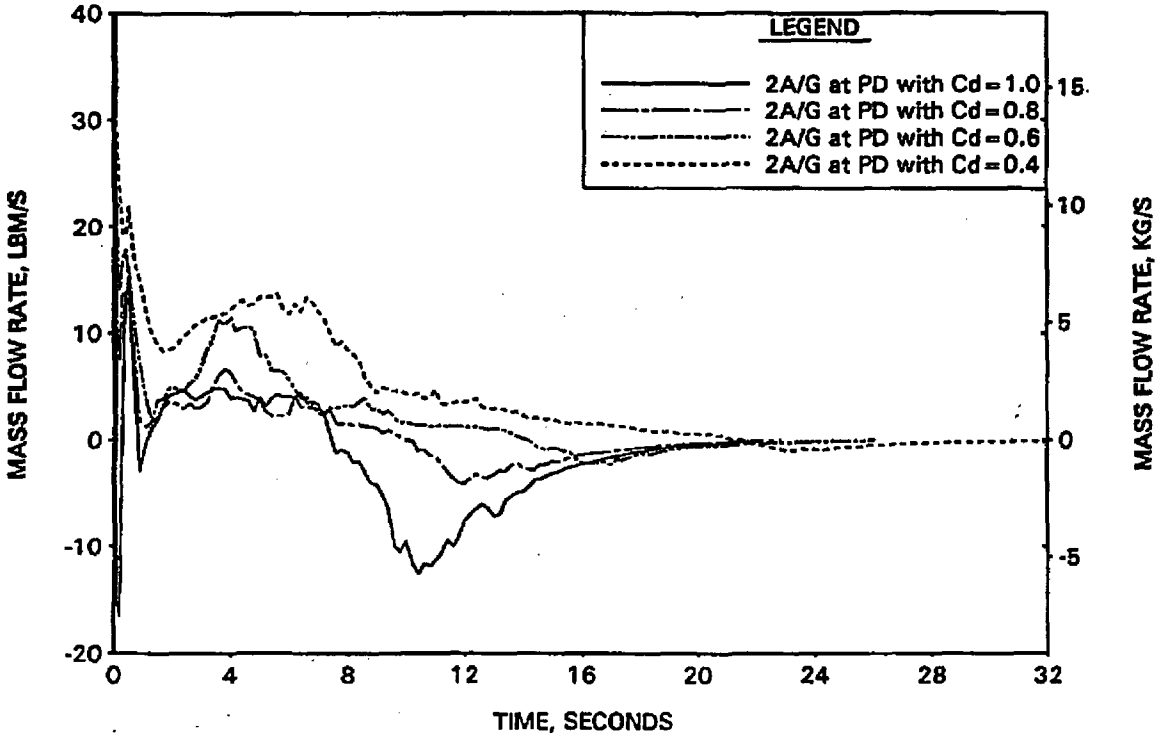

FIGURE A-88. BREAK SPECTRUM STUDY -
CORE FLOODING RATE.

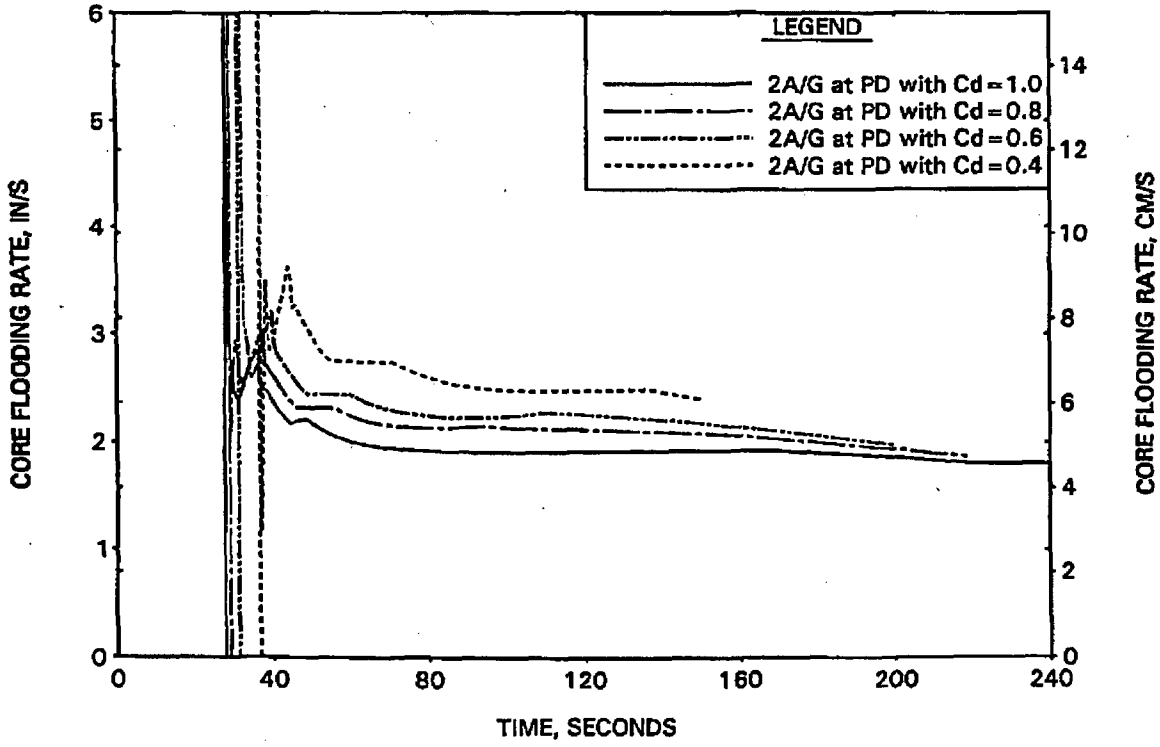

FIGURE A-89. BREAK SPECTRUM STUDY -
HC CLAD TEMP AT RUPTURED LOCATION.

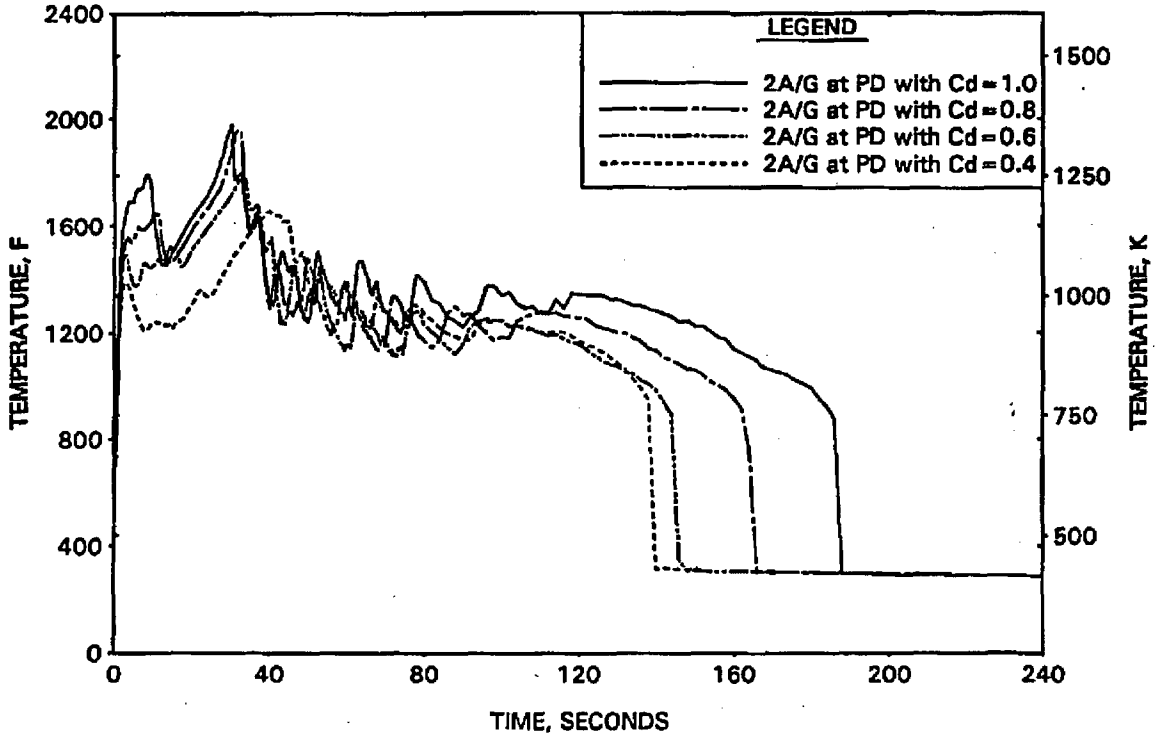

FIGURE A-90. BREAK SPECTRUM STUDY -
HC CLAD TEMP AT PEAK UNRUPTURED LOCATION.

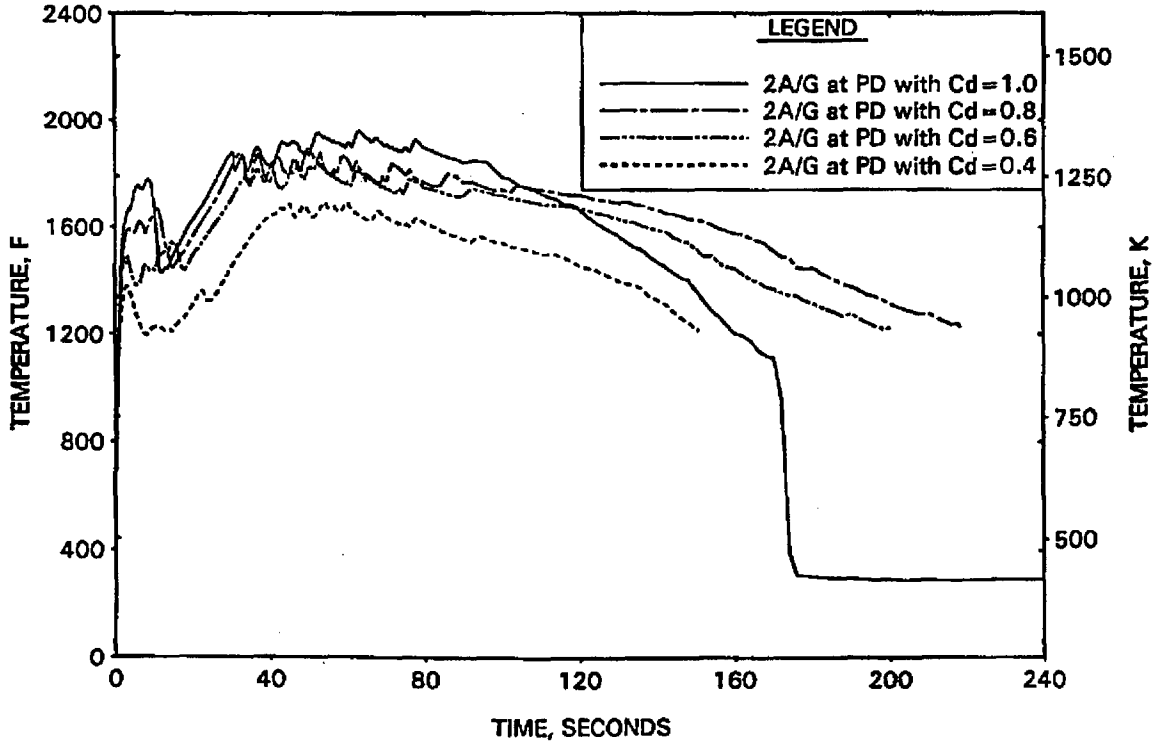

FIGURE A-91. BREAK SPECTRUM STUDY - FILTERED HC CLAD SURFACE HTC; 2A/G AT PD WITH CD=1.0

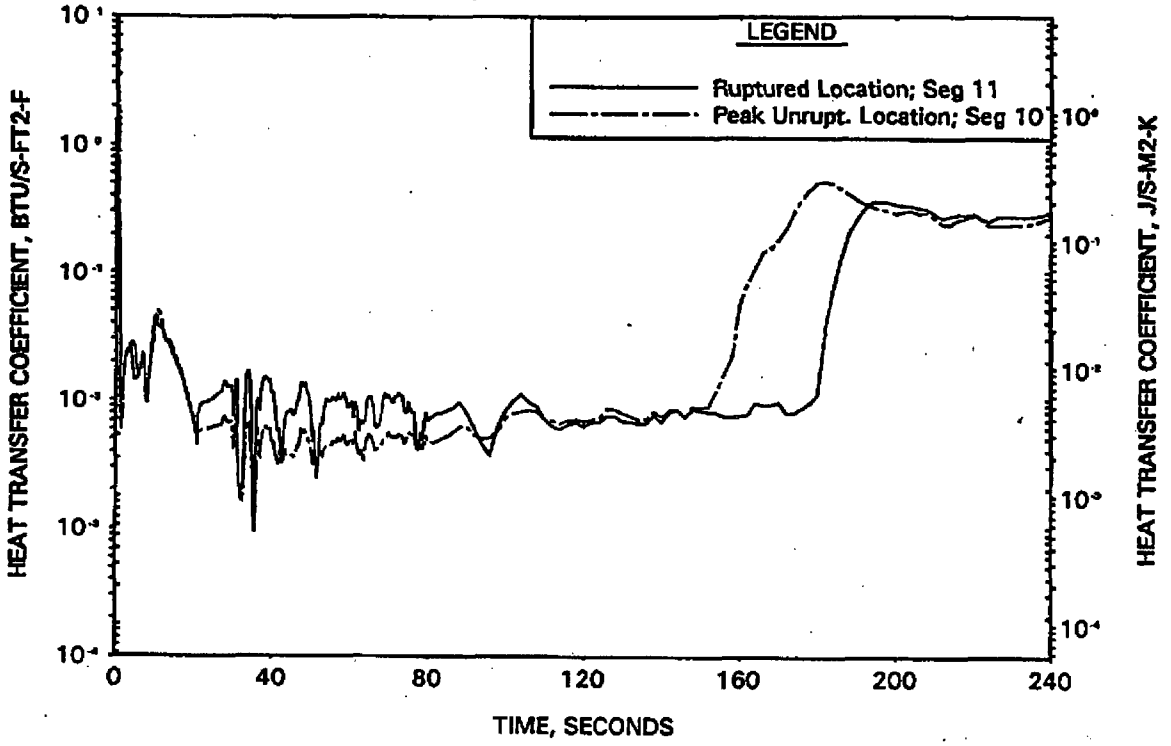

FIGURE A-92. BREAK SPECTRUM STUDY - FILTERED HC CLAD SURFACE HTC; 2A/G AT PD WITH CD=0.8

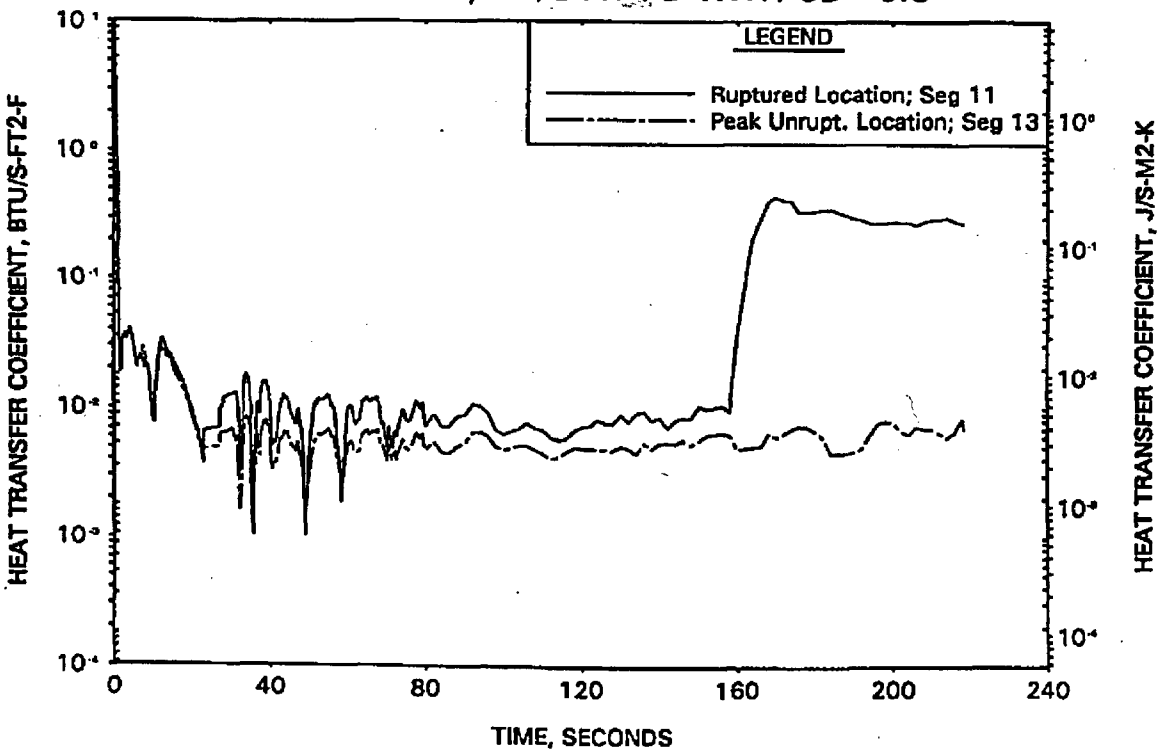

FIGURE A-93. BREAK SPECTRUM STUDY - FILTERED HC CLAD SURFACE HTC; 2A/G AT PD WITH CD = 0.6

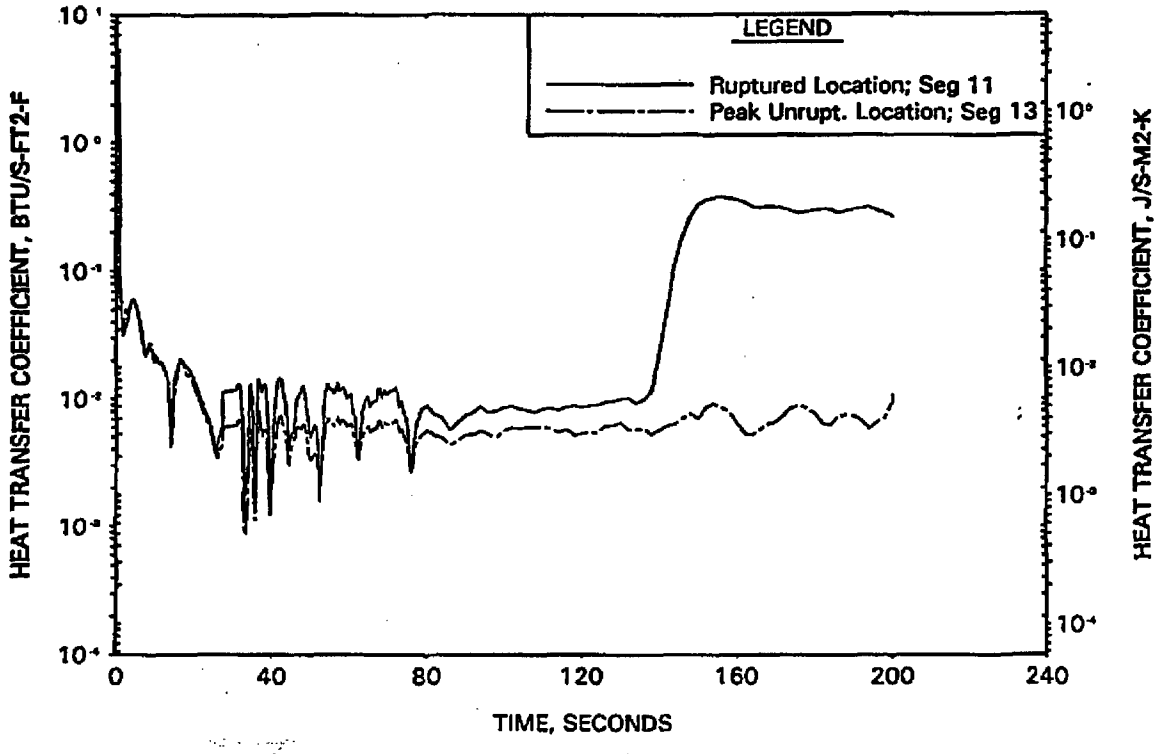

FIGURE A-94. BREAK SPECTRUM STUDY - FILTERED HC CLAD SURFACE HTC; 2A/G AT PD WITH CD = 0.4

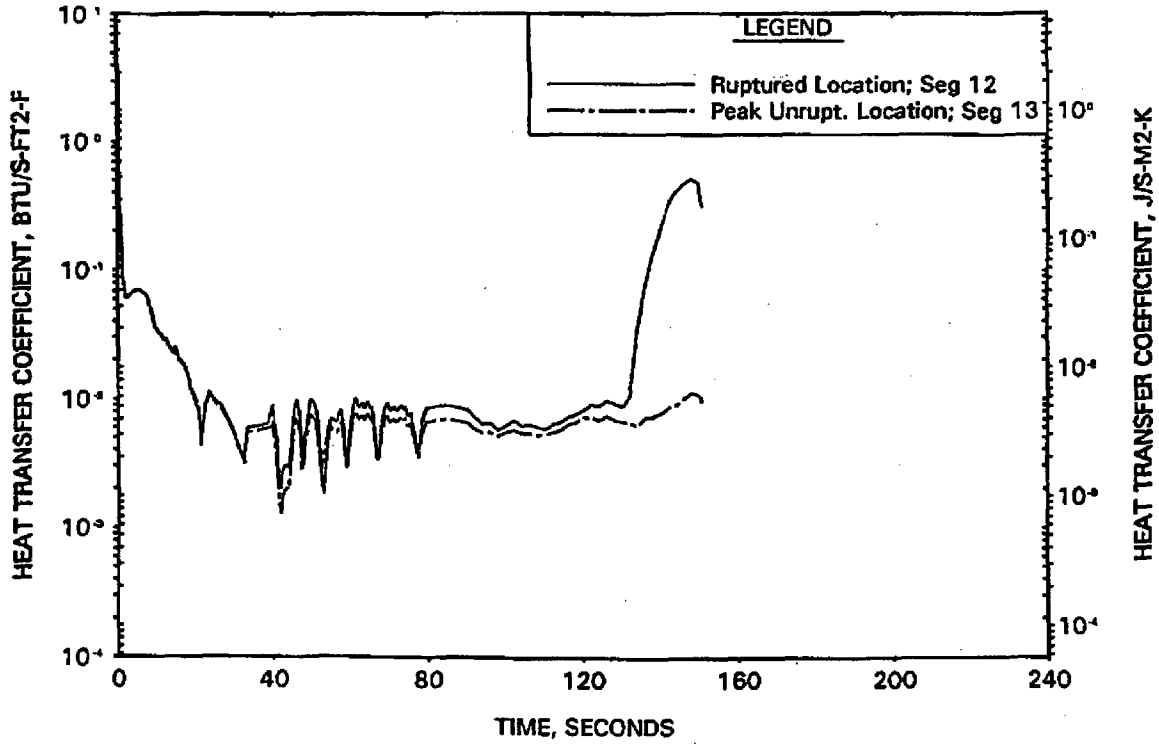

FIGURE A-95. COLD LEG PUMP SUCTION BREAK NODING ARRANGEMENT.

C,E

FIGURE A-96. BREAK SPECTRUM STUDY -
REACTOR VESSEL UPPER PLENUM PRESSURE.

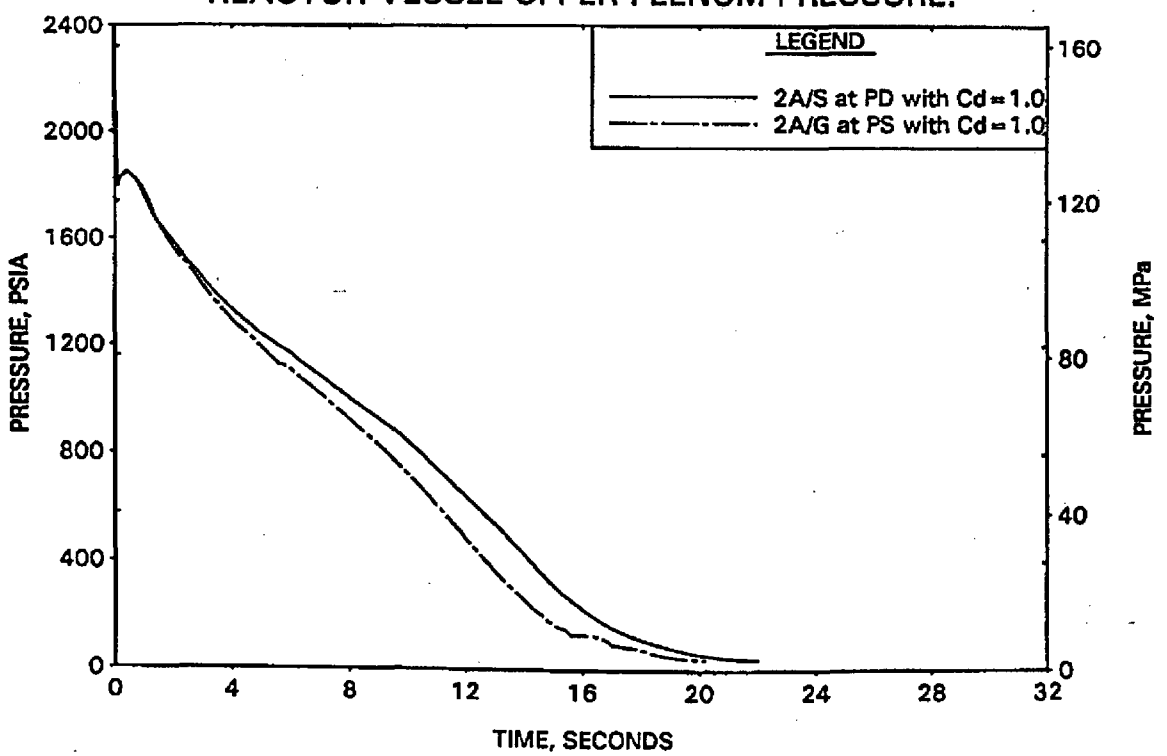

FIGURE A-97. BREAK SPECTRUM STUDY - TOTAL BREAK MASS FLOW RATE.

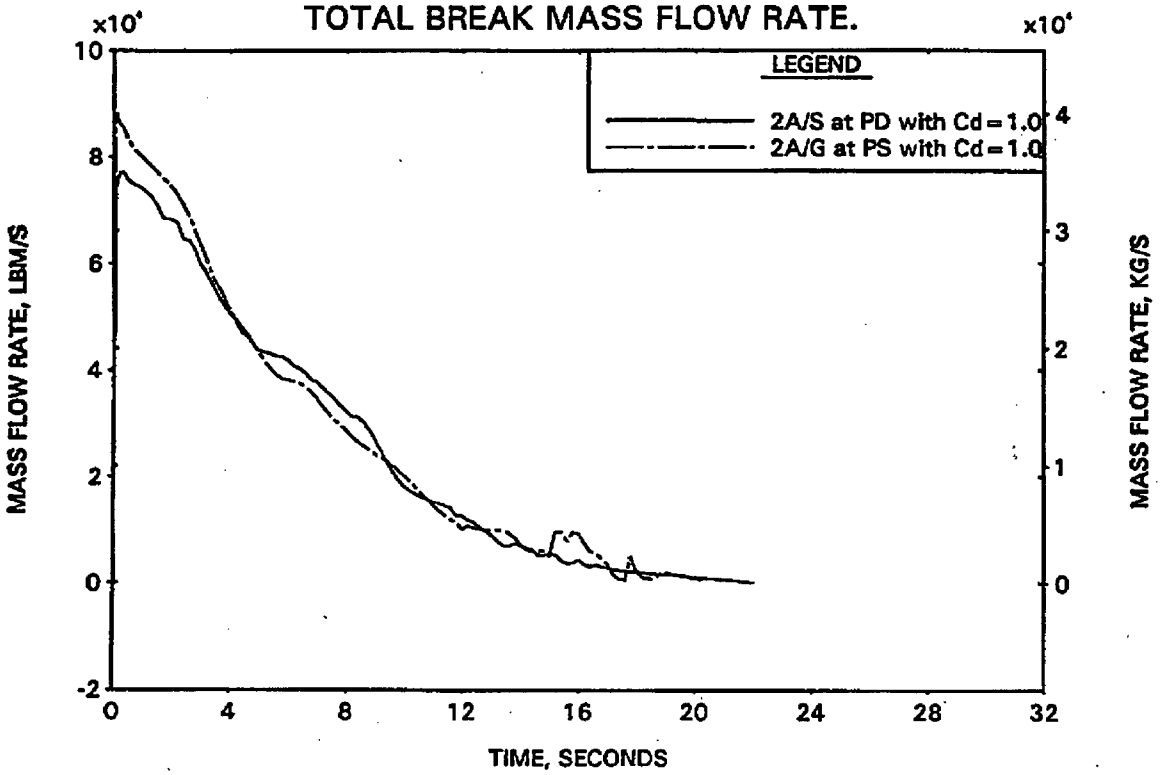

FIGURE A-98. BREAK SPECTRUM STUDY - BREAK MASS FLOW RATE COMPONENTS.

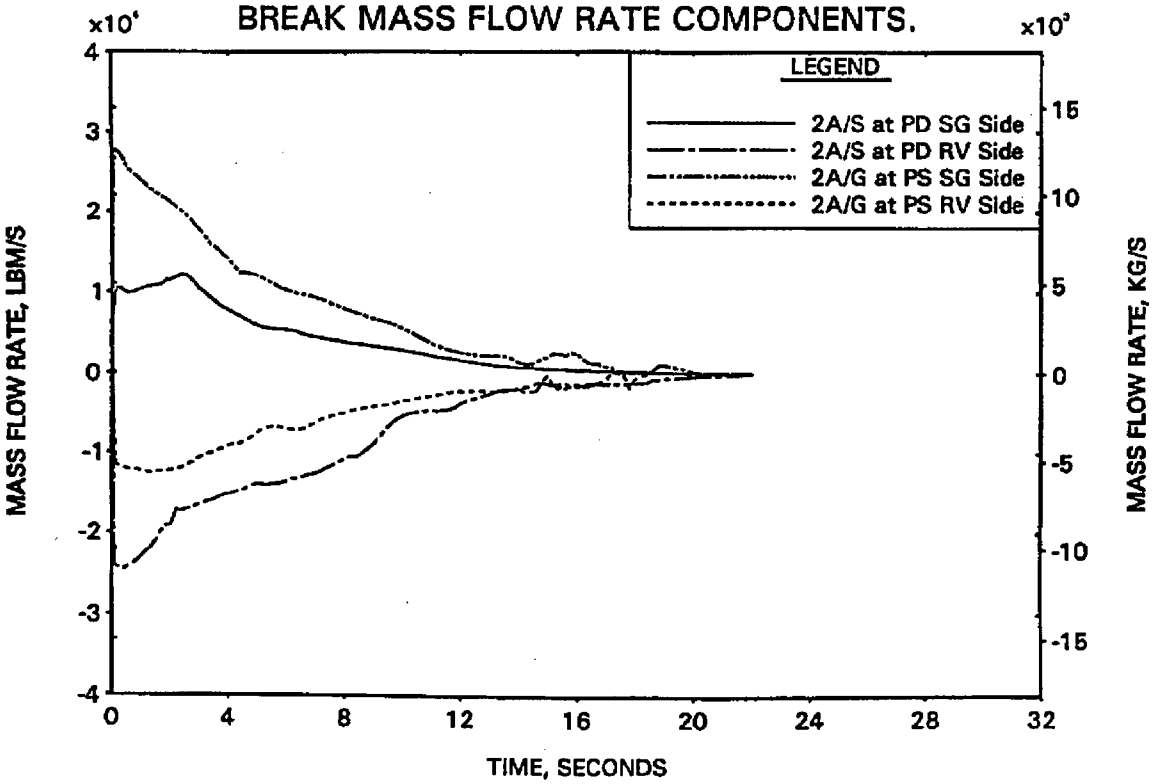

FIGURE A-99. BREAK SPECTRUM STUDY -
HC MASS FLOW RATE AT PEAK POWER LOCATION.

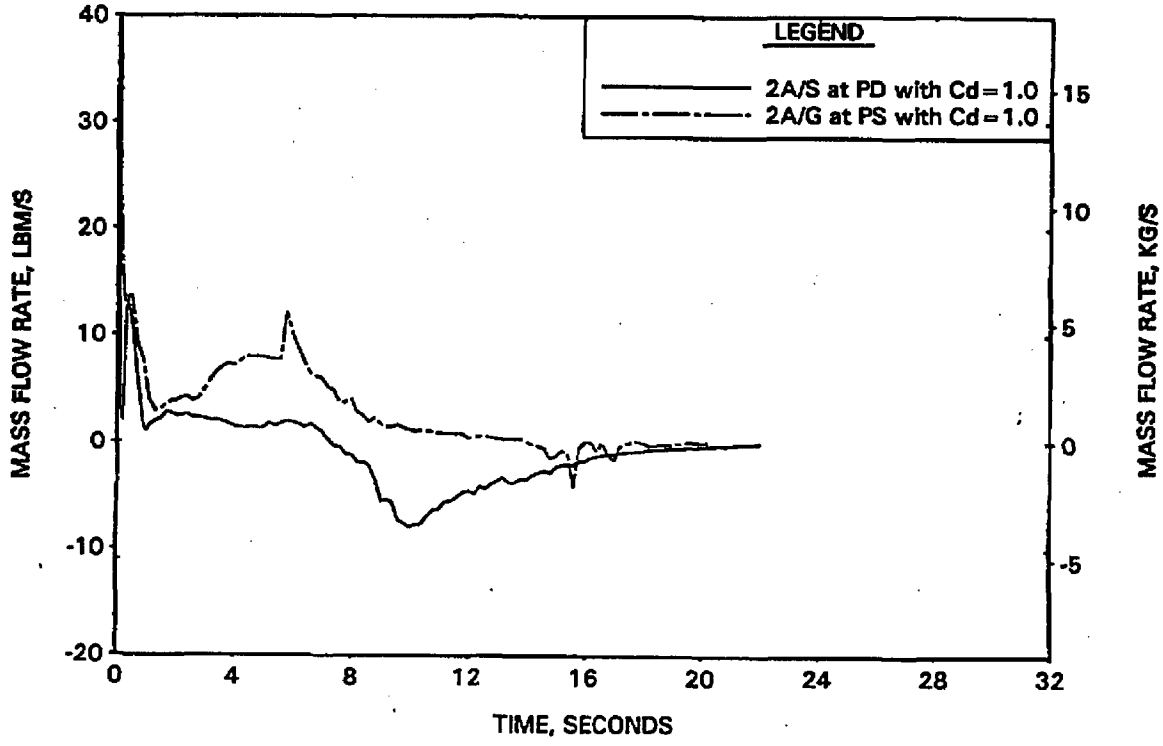

FIGURE A-100. BREAK SPECTRUM STUDY -
CORE FLOODING RATE.

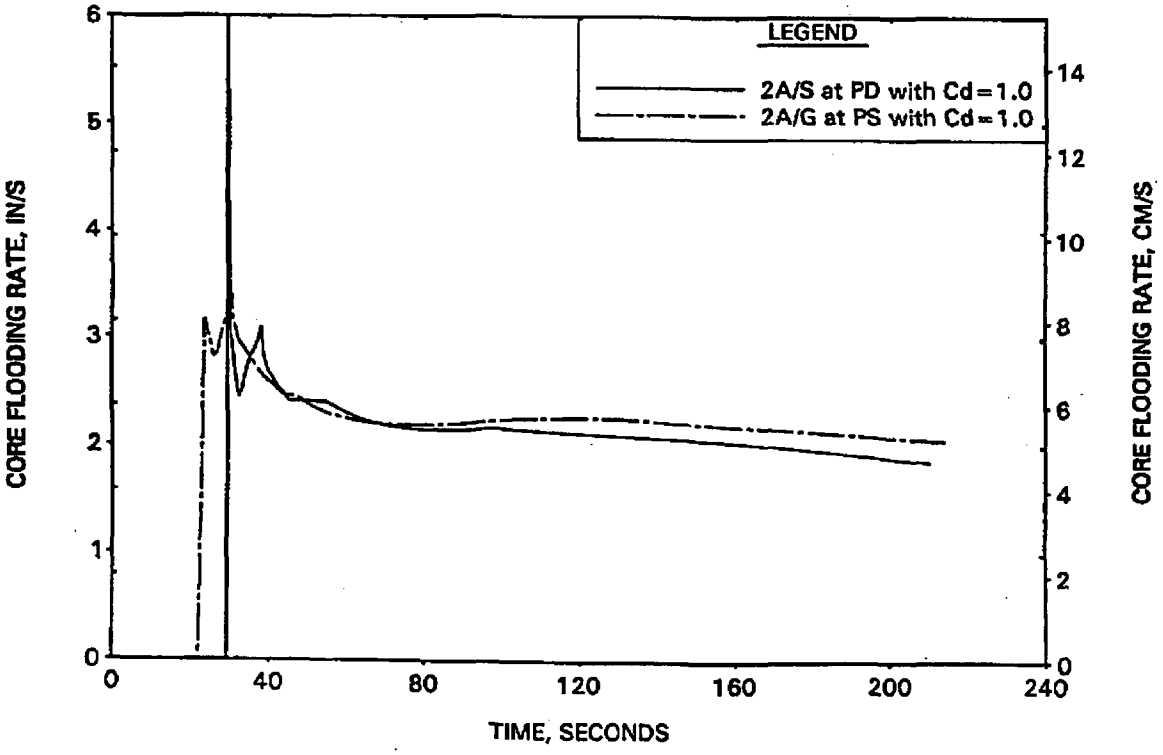

FIGURE A-101. BREAK SPECTRUM STUDY -
HC CLAD TEMP AT RUPTURED LOCATION.

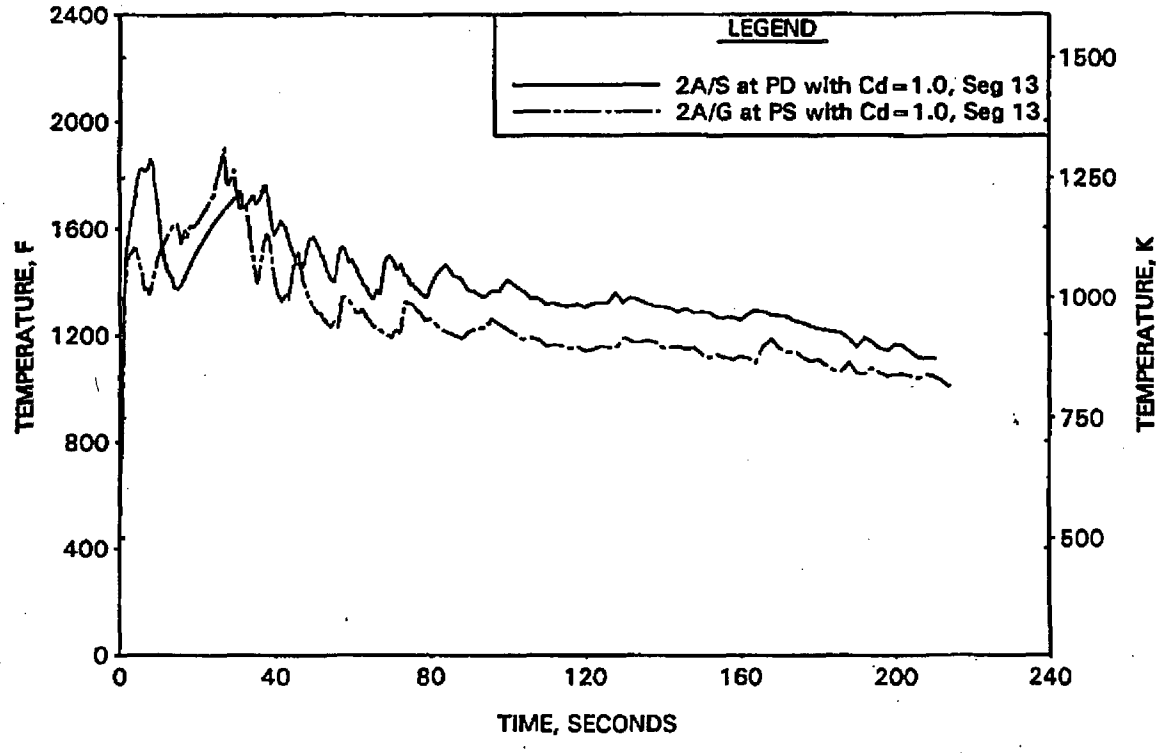

FIGURE A-102. BREAK SPECTRUM STUDY -
HC CLAD TEMP AT PEAK UNRUPTURED LOCATION.

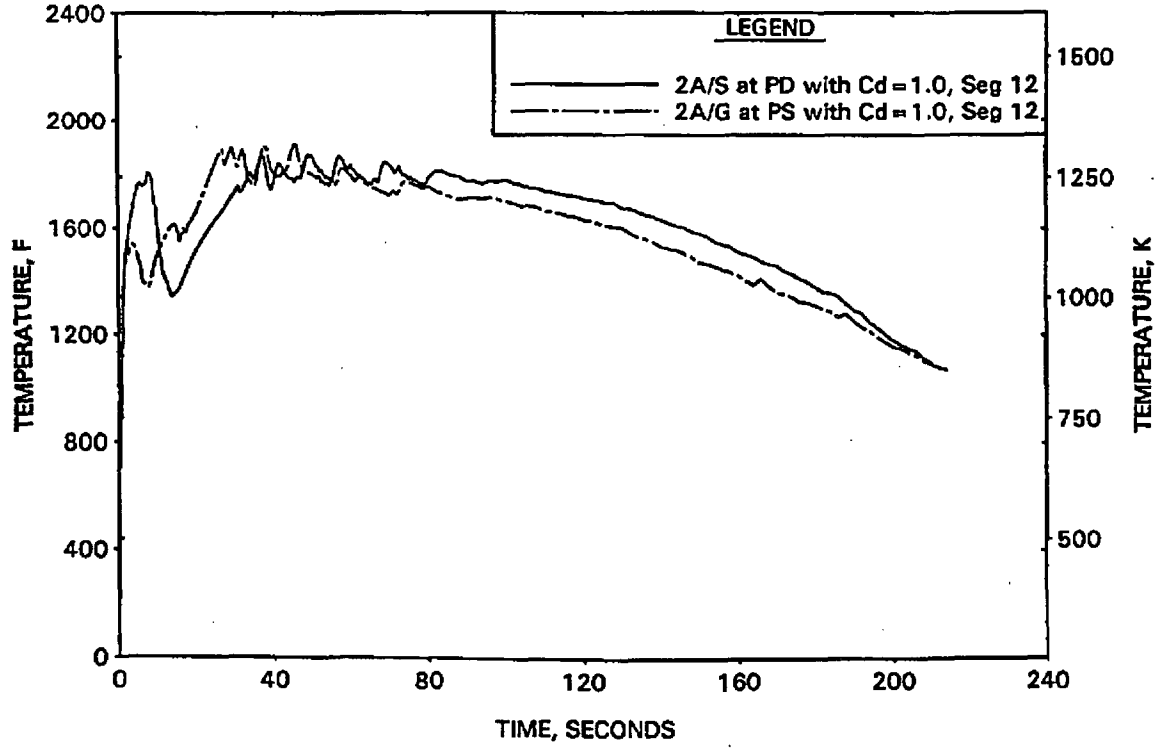

FIGURE A-103. BREAK SPECTRUM STUDY - FILTERED HC CLAD SURFACE HTC; 2A/S AT PD WITH CD = 1.0

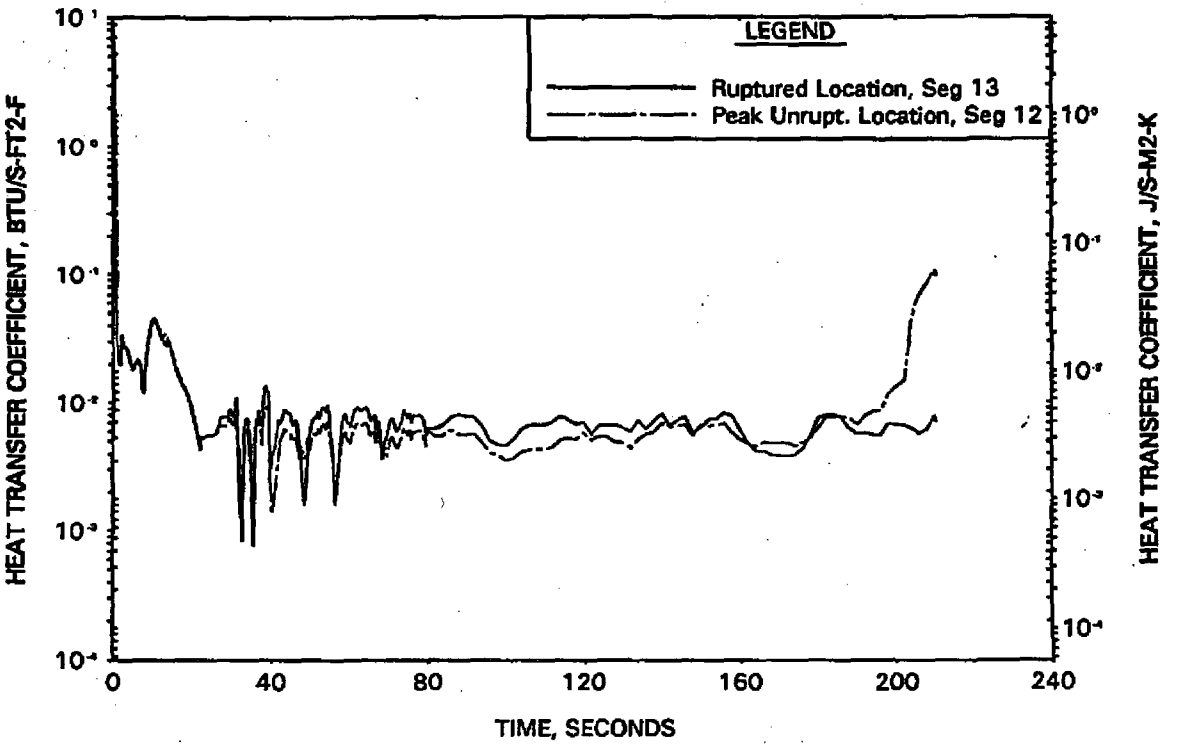

FIGURE A-104. BREAK SPECTRUM STUDY - FILTERED HC CLAD SURFACE HTC; 2A/G AT PS WITH CD = 1.0

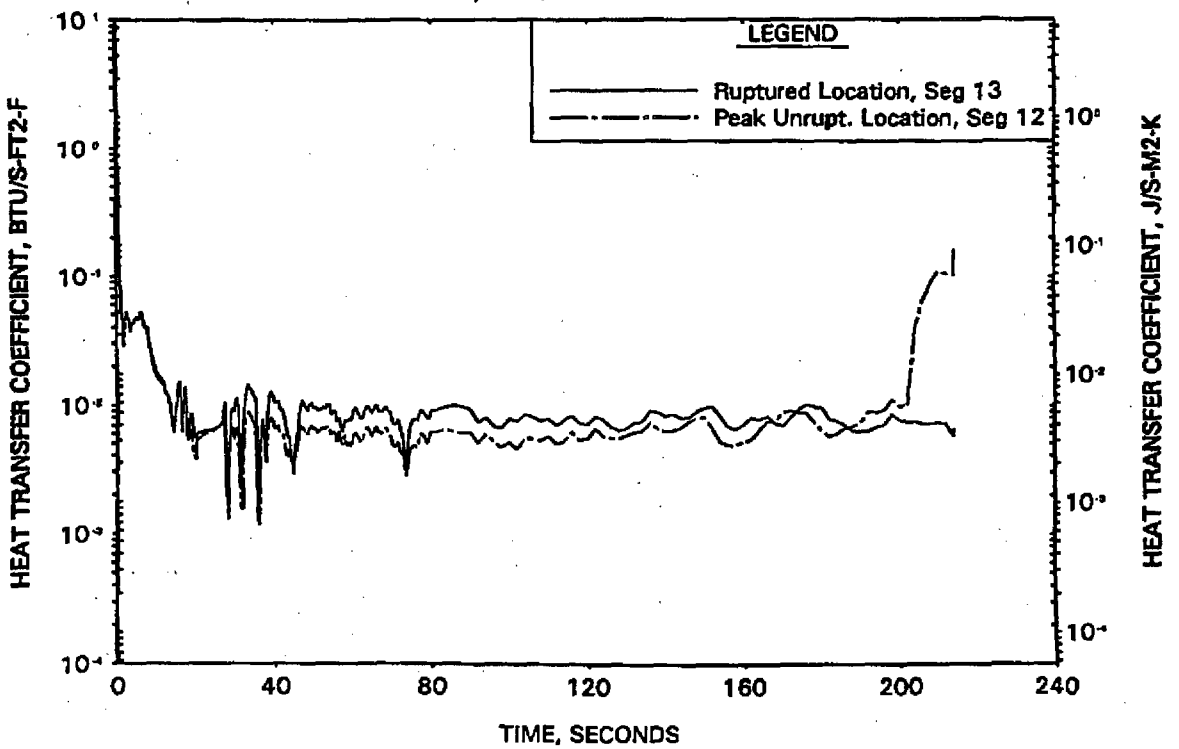

FIGURE A-105. 2.0-FT2 TRANSITION LOCA STUDY - REACTOR VESSEL UPPER PLENUM PRESSURE.

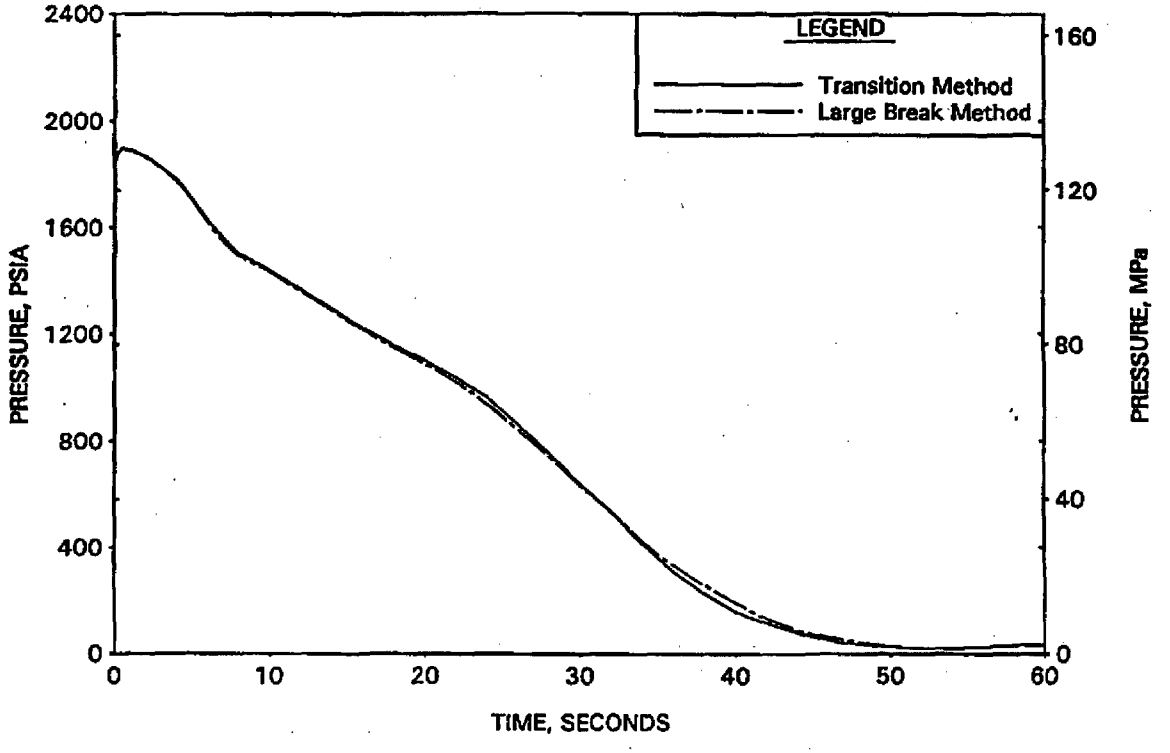

FIGURE A-106. 2.0-FT2 TRANSITION LOCA STUDY - BREAK MASS FLOW RATE.

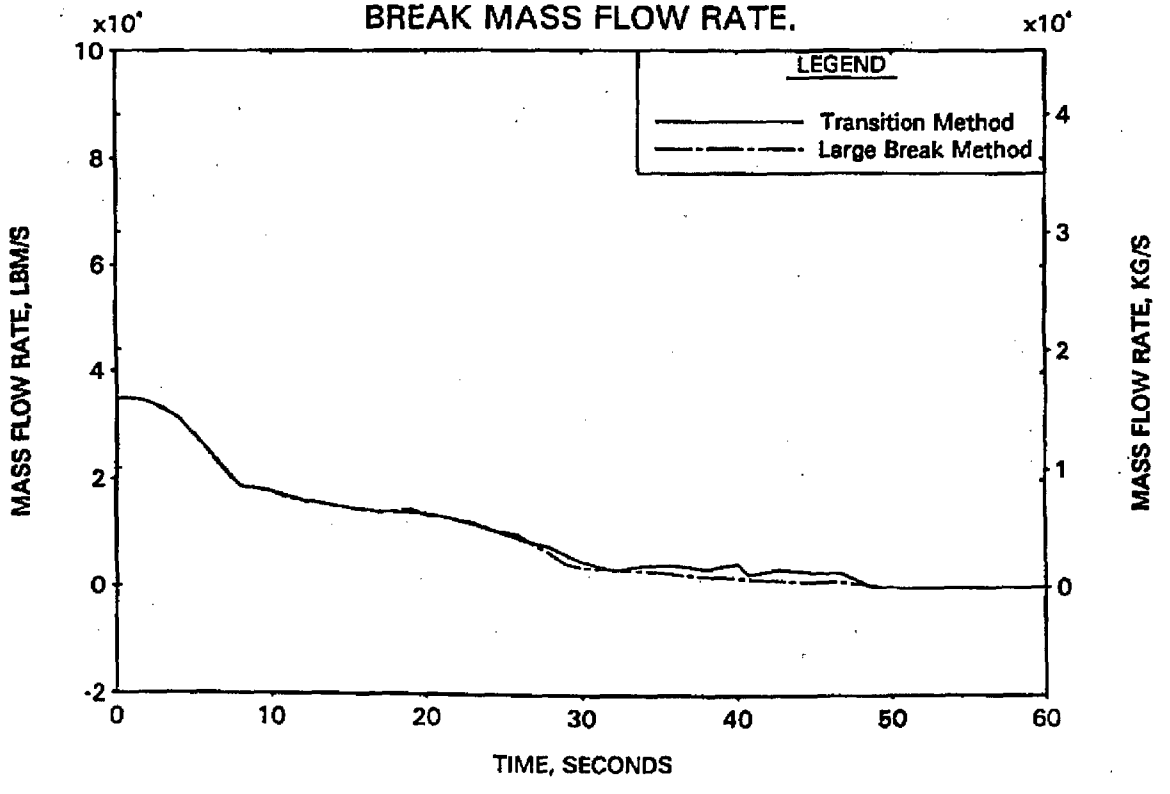

FIGURE A-107. 2.0-FT2 TRANSITION LOCA STUDY - FILTERED HC MASS FLOW RATE AT PEAK POWER LOCATION.

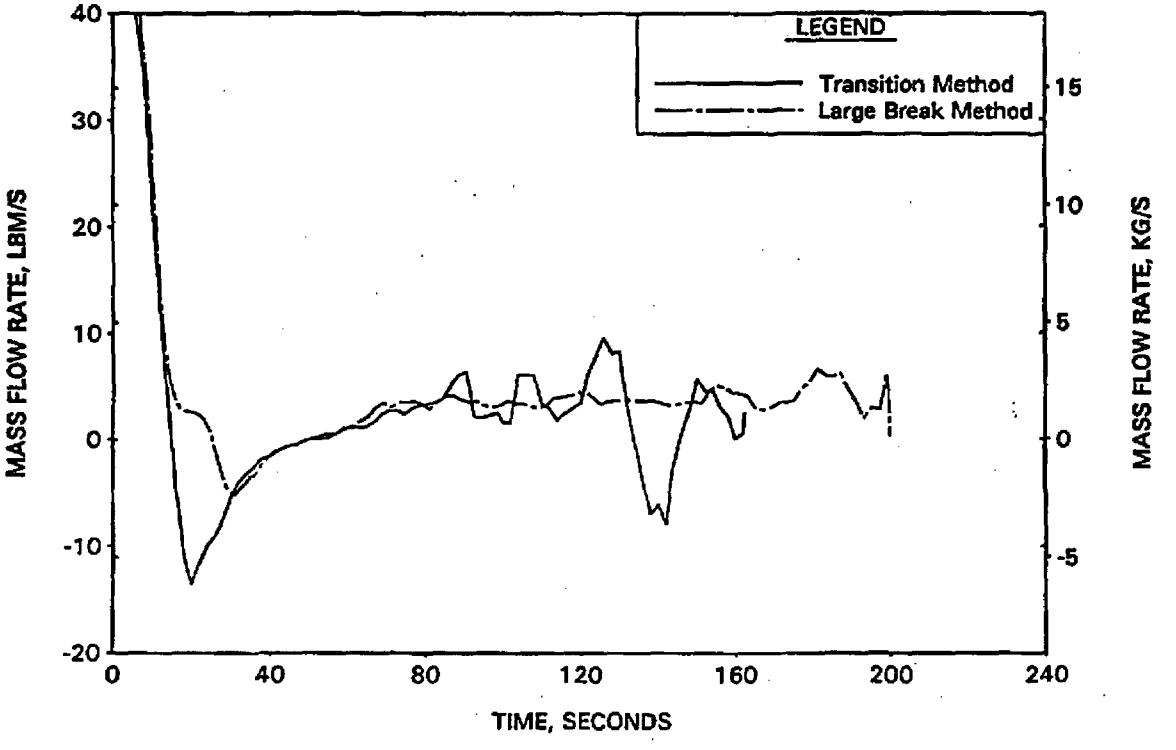

FIGURE A-108. 2.0-FT2 TRANSITION LOCA STUDY - COLLAPSED LIQUID LEVEL IN HC.

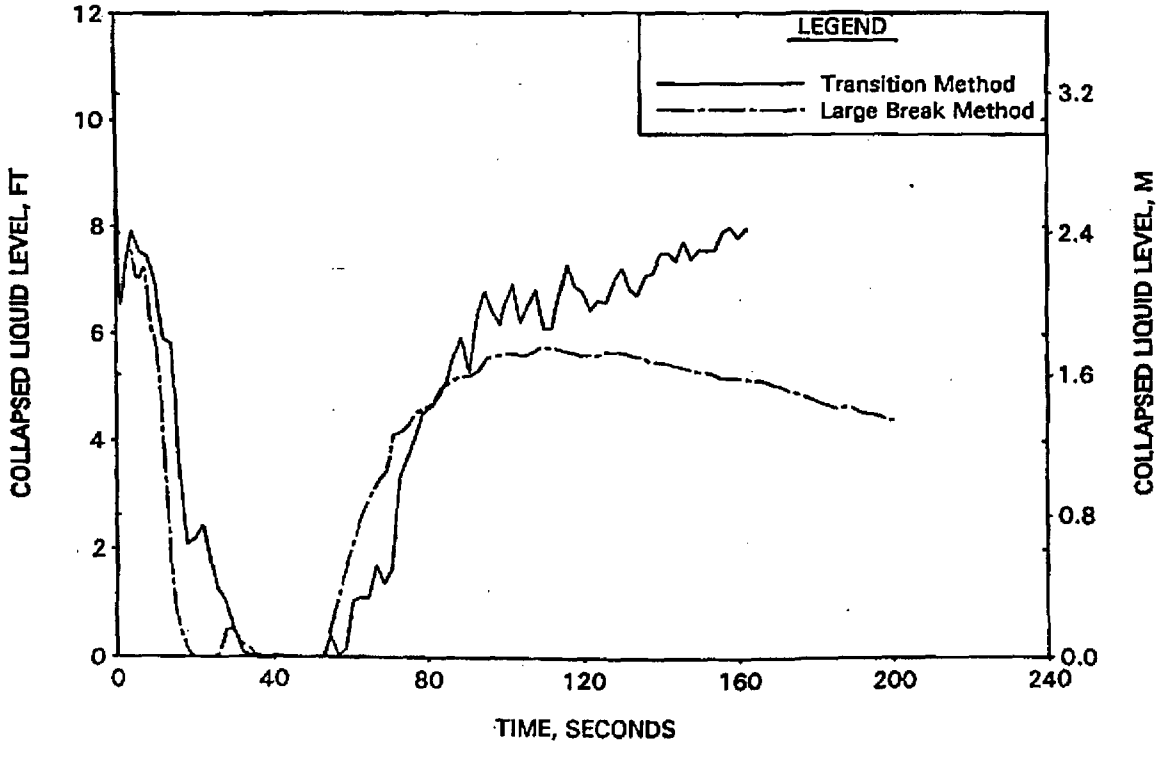

FIGURE A-109. 2.0-FT2 TRANSITION LOCA STUDY - HC CLAD TEMP AT PEAK POWER LOCATION.

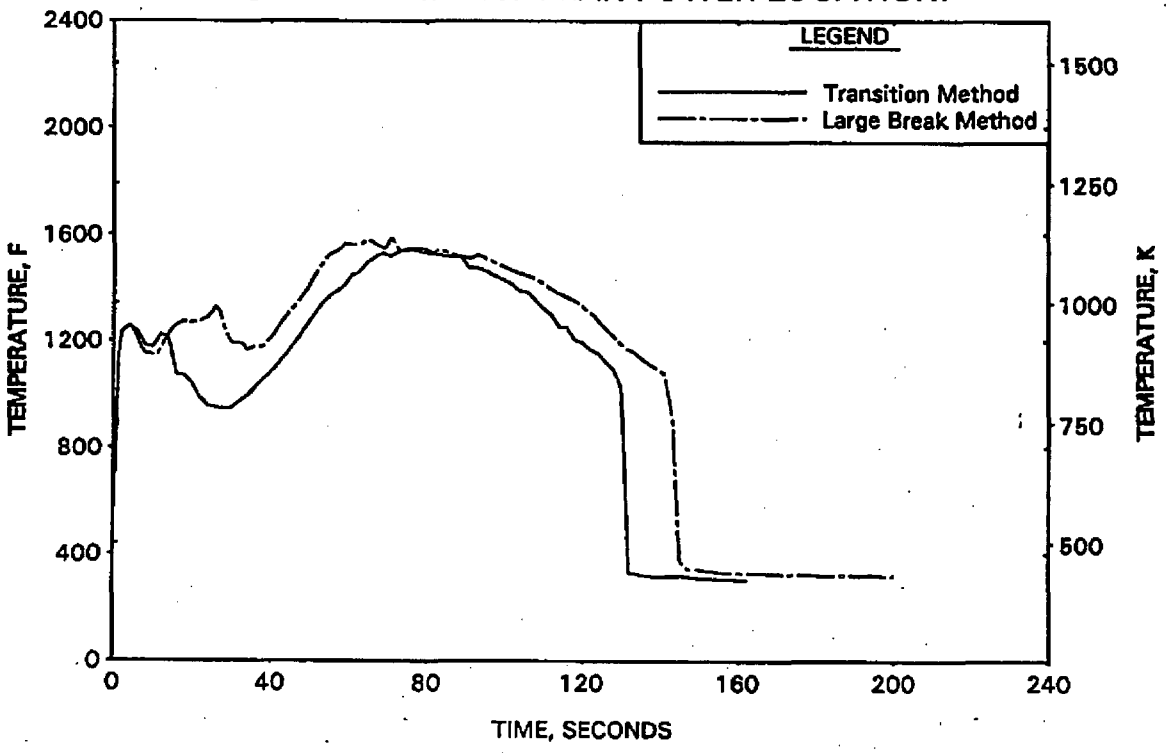

FIGURE A-110. 2.0-FT2 TRANSITION LOCA STUDY - FILTERED HC HTC AT PEAK POWER LOCATION.

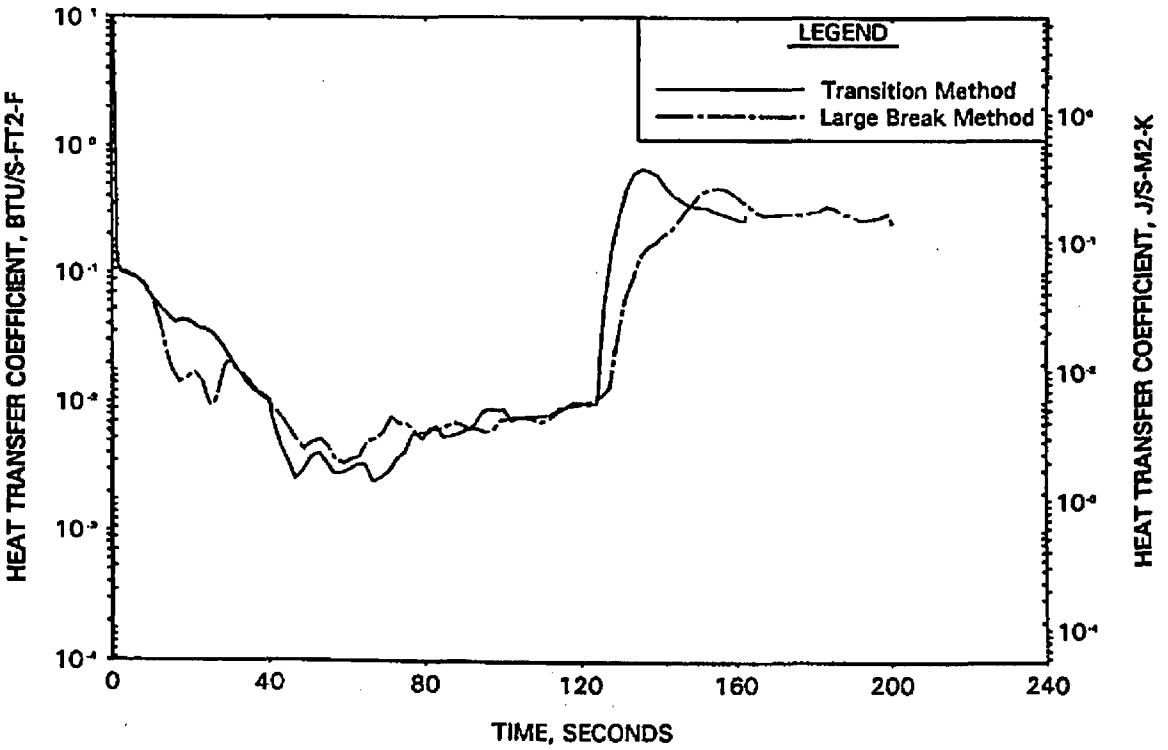

FIGURE A-111. TRANSITION LOCA STUDY - REACTOR VESSEL UPPER PLENUM PRESSURE.

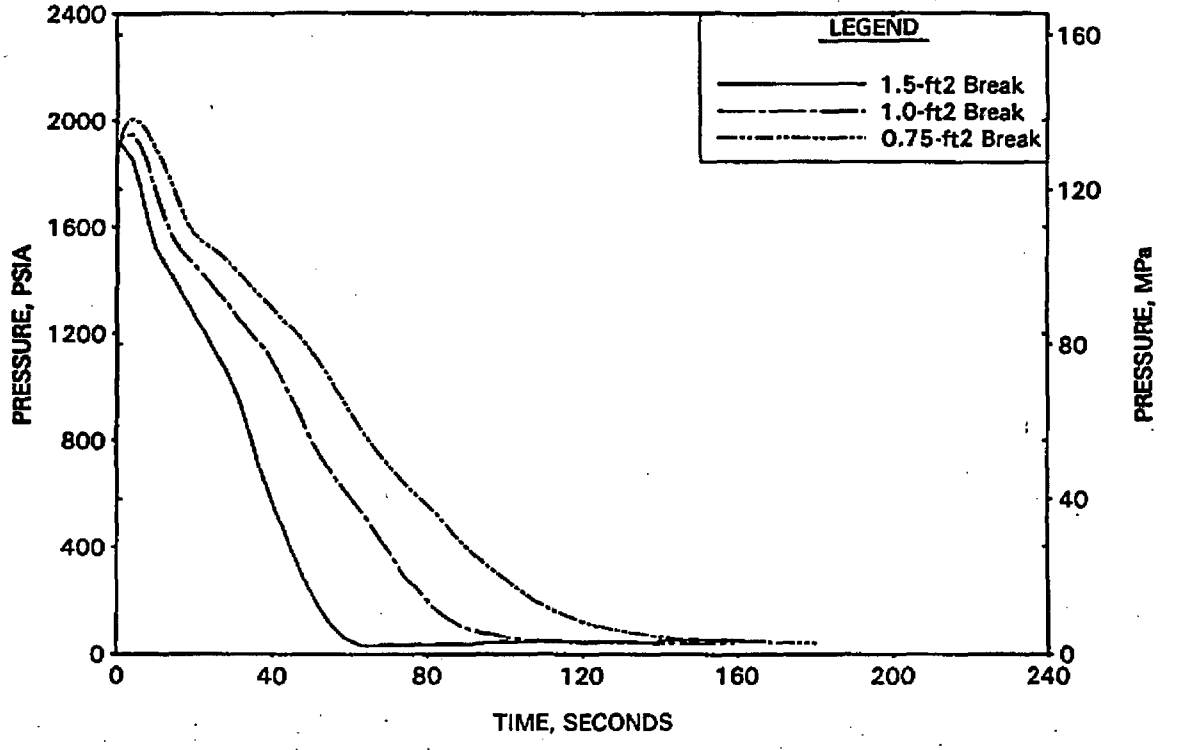

FIGURE A-112. TRANSITION LOCA STUDY - BREAK MASS FLOW RATE.

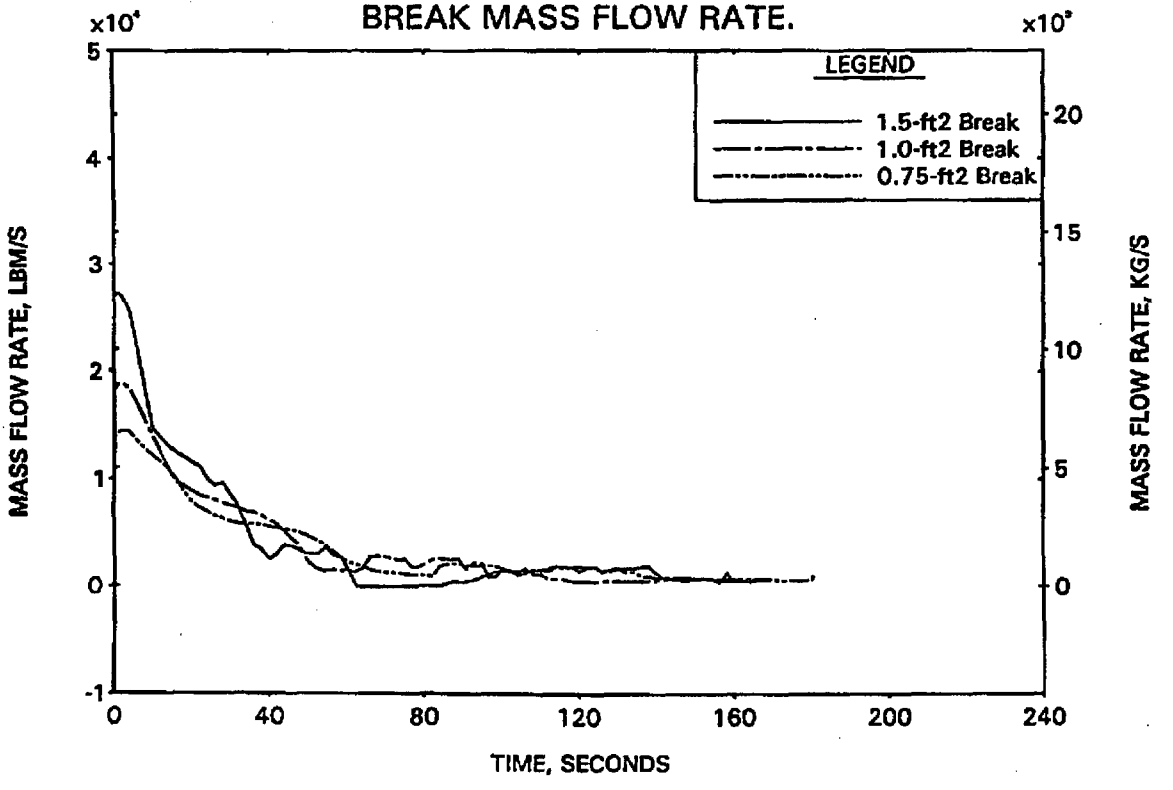

FIGURE A-113. TRANSITION LOCA STUDY - FILTERED HC MASS FLOW RATE AT PEAK POWER LOCATION.

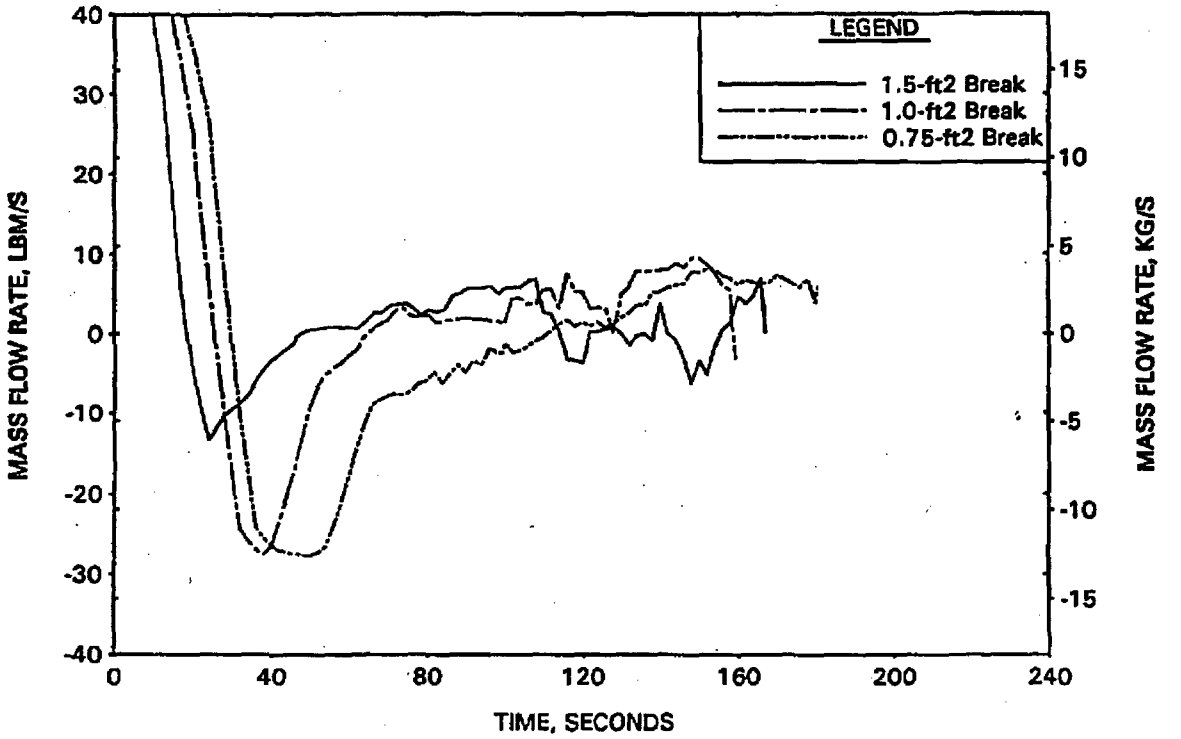

FIGURE A-114. TRANSITION LOCA STUDY - COLLAPSED LIQUID LEVEL IN HC.

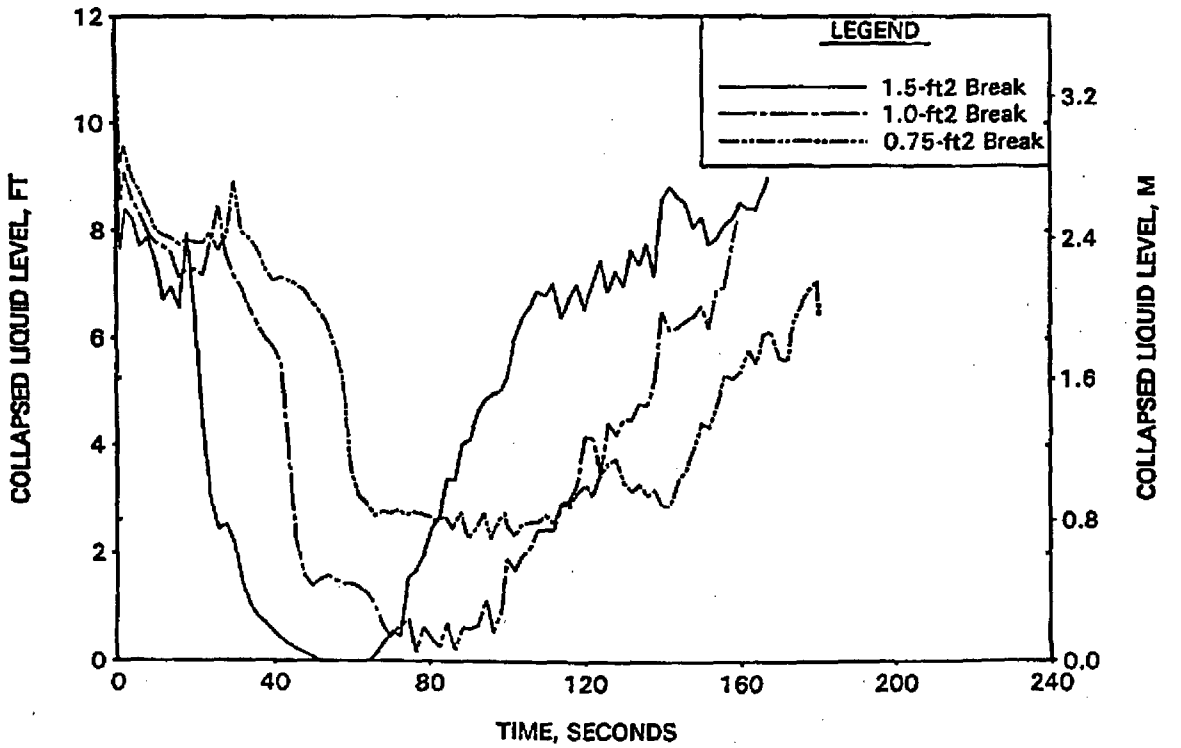

FIGURE A-115. TRANSITION LOCA STUDY - HC CLAD TEMP AT PCT LOCATION.

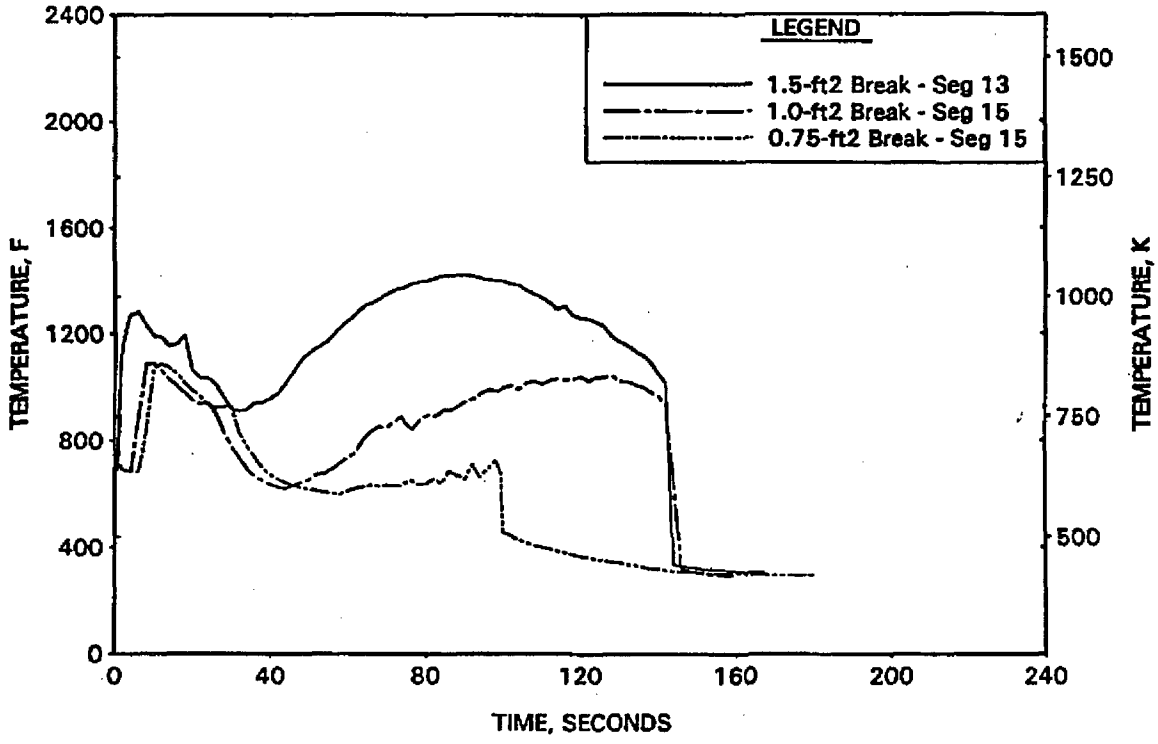

FIGURE A-116. TRANSITION LOCA STUDY - FILTERED HC CLAD SURFACE HTC AT PCT LOCATION; 1.5-FT2 CASE.

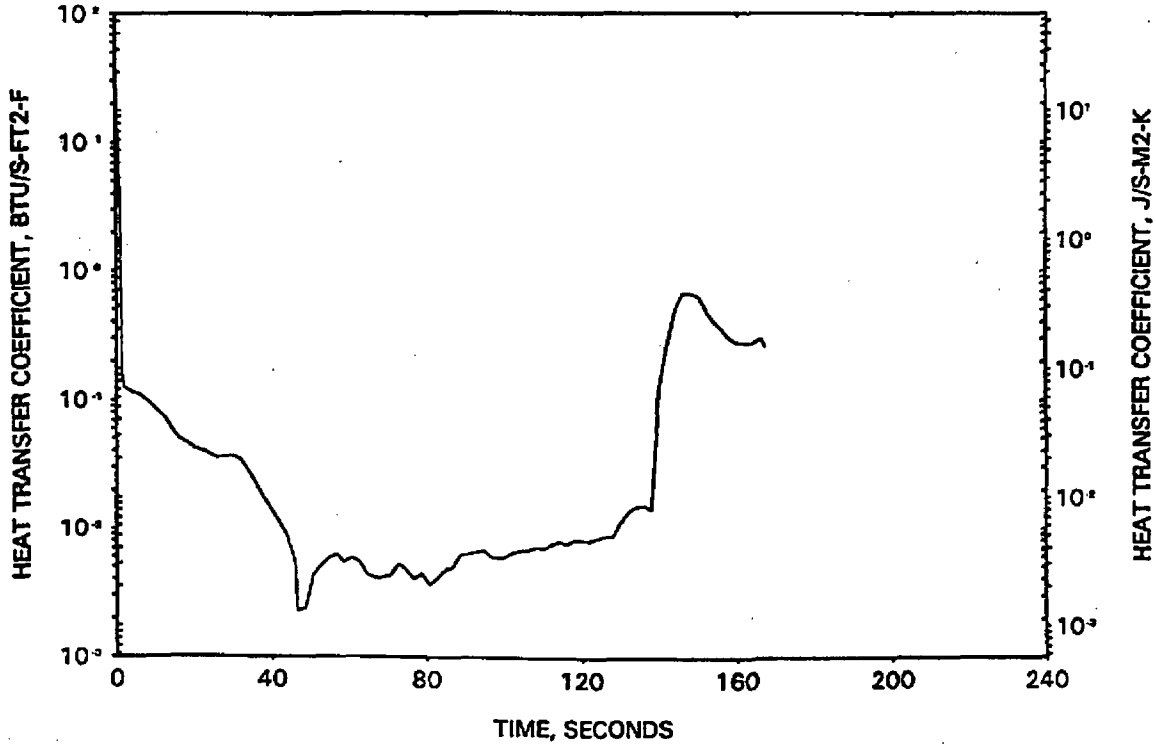

FIGURE A-117. TRANSITION LOCA STUDY - FILTERED HC CLAD SURFACE HTC AT PCT LOCATION; 1.0-FT2 CASE.

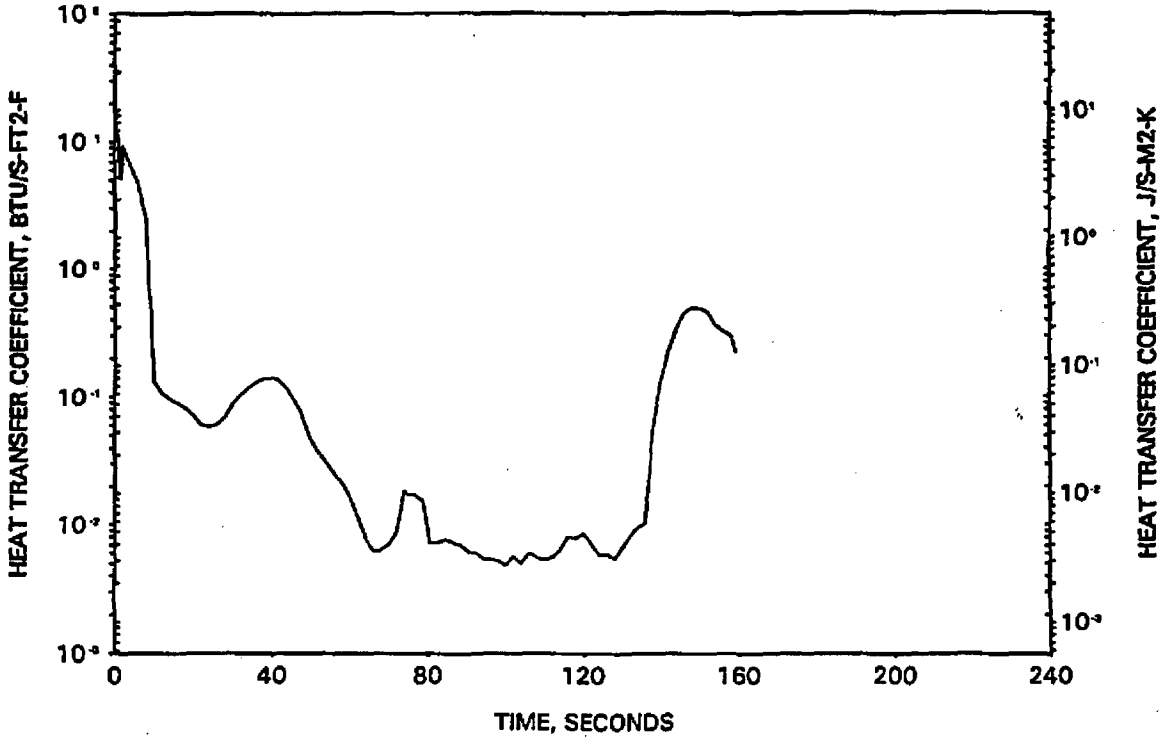

FIGURE A-118. TRANSITION LOCA STUDY - FILTERED HC CLAD SURFACE HTC AT PCT LOCATION; 0.75-FT2 CASE.

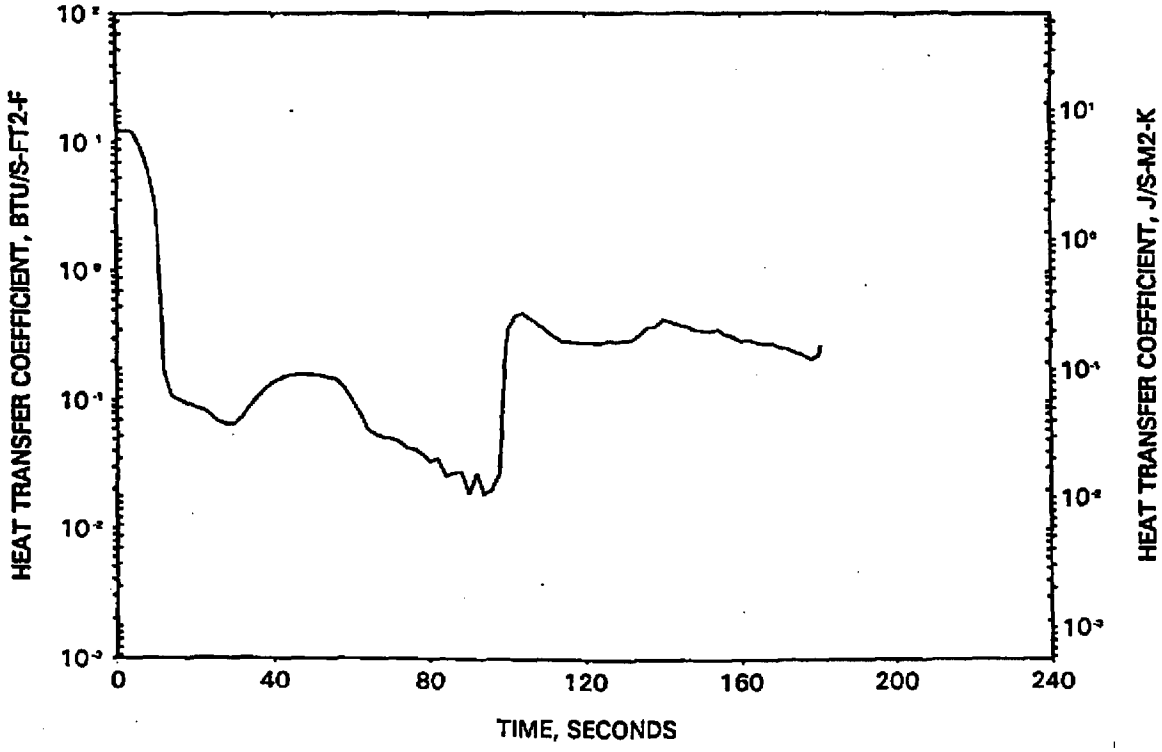

FIGURE A-119. HOT LEG BREAK NODING ARRANGEMENT.

C,E

FIGURE A-120. HOT LEG BREAK STUDY -
REACTOR VESSEL UPPER PLENUM PRESSURE.

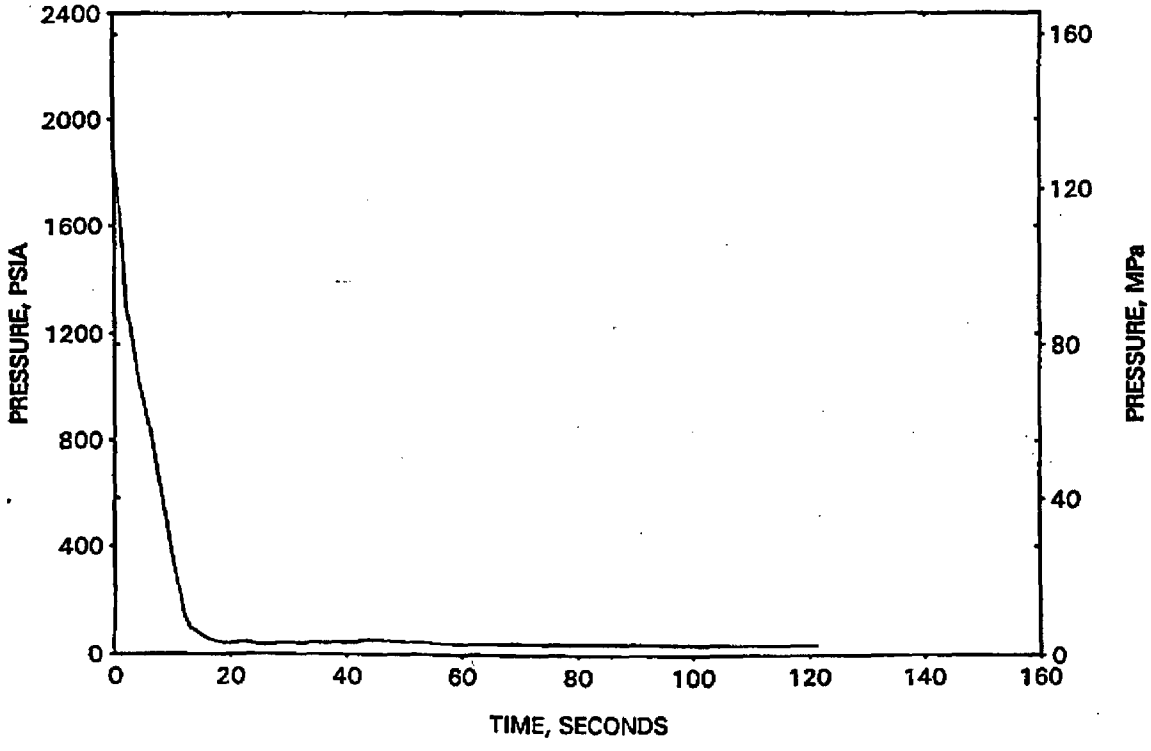

FIGURE A-121. HOT LEG BREAK STUDY - BREAK MASS FLOW RATE.

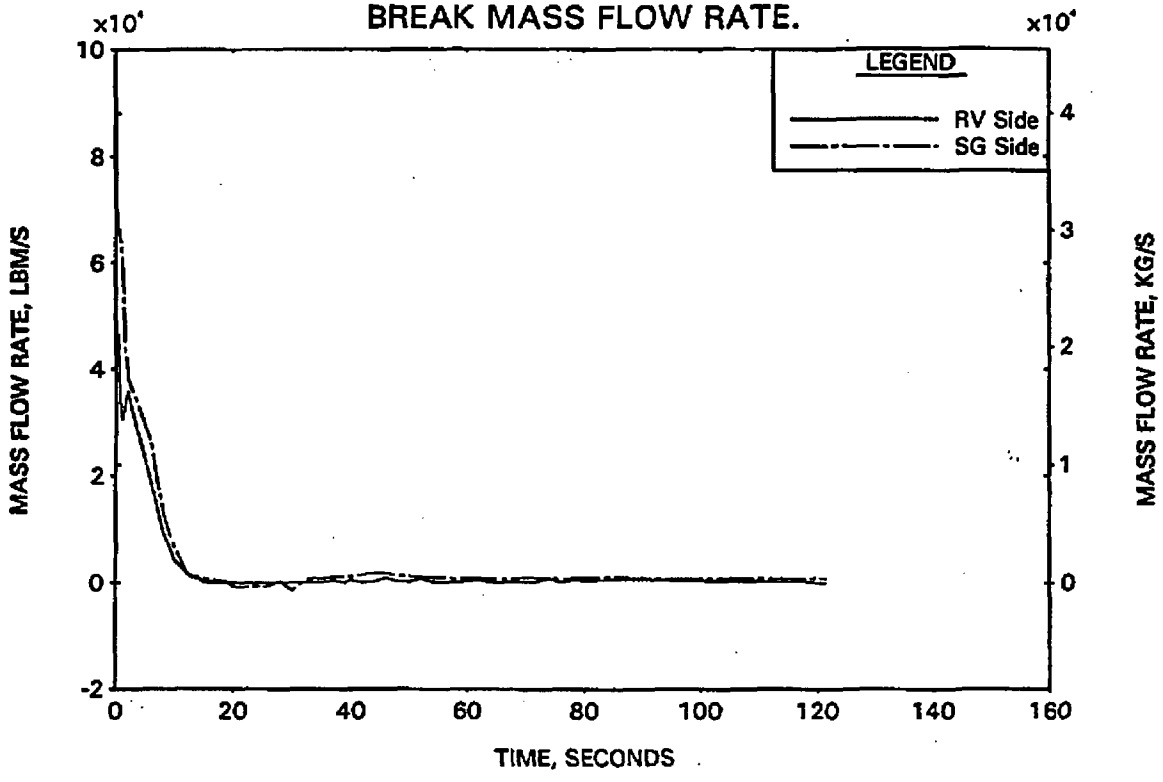

FIGURE A-122. HOT LEG BREAK STUDY - FILTERED HC MASS FLOW RATE AT PCT LOCATION (SEGMENT 12).

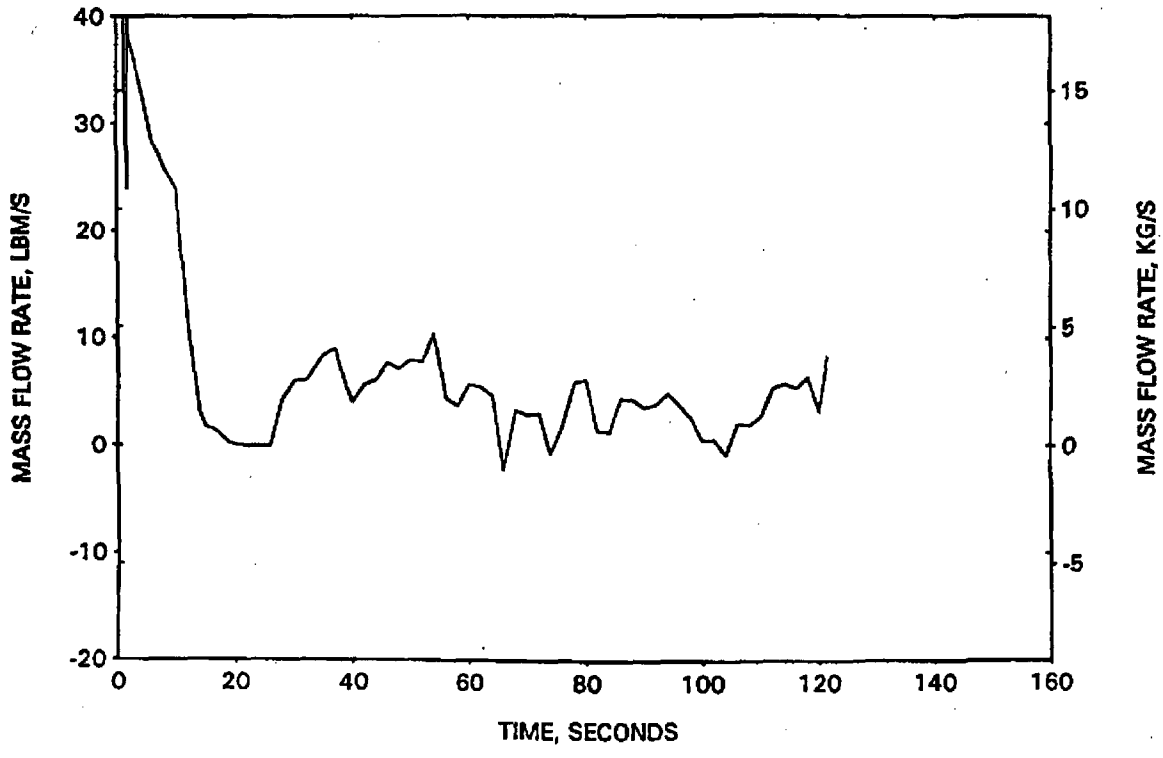

FIGURE A-123. HOT LEG BREAK STUDY -
HC CLAD TEMP AT PCT LOCATION (SEGMENT 12).

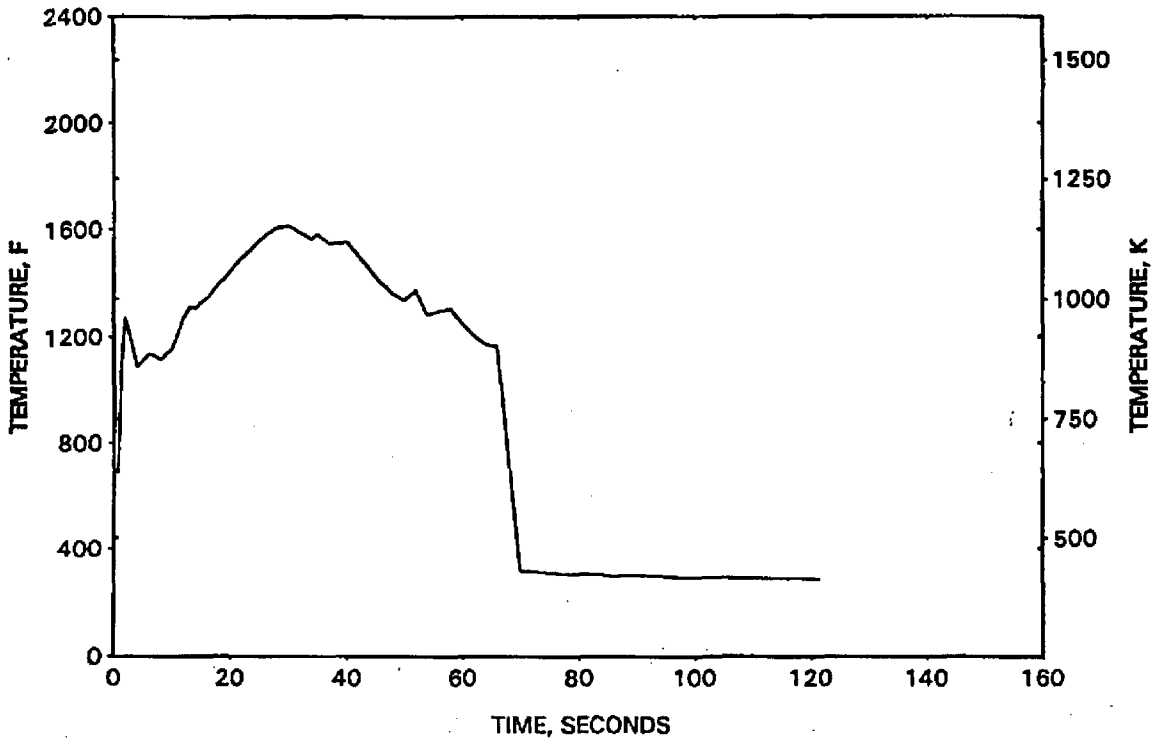

FIGURE A-124. HOT LEG BREAK STUDY -
FILTERED HC HTC AT PCT LOCATION (SEGMENT 12).

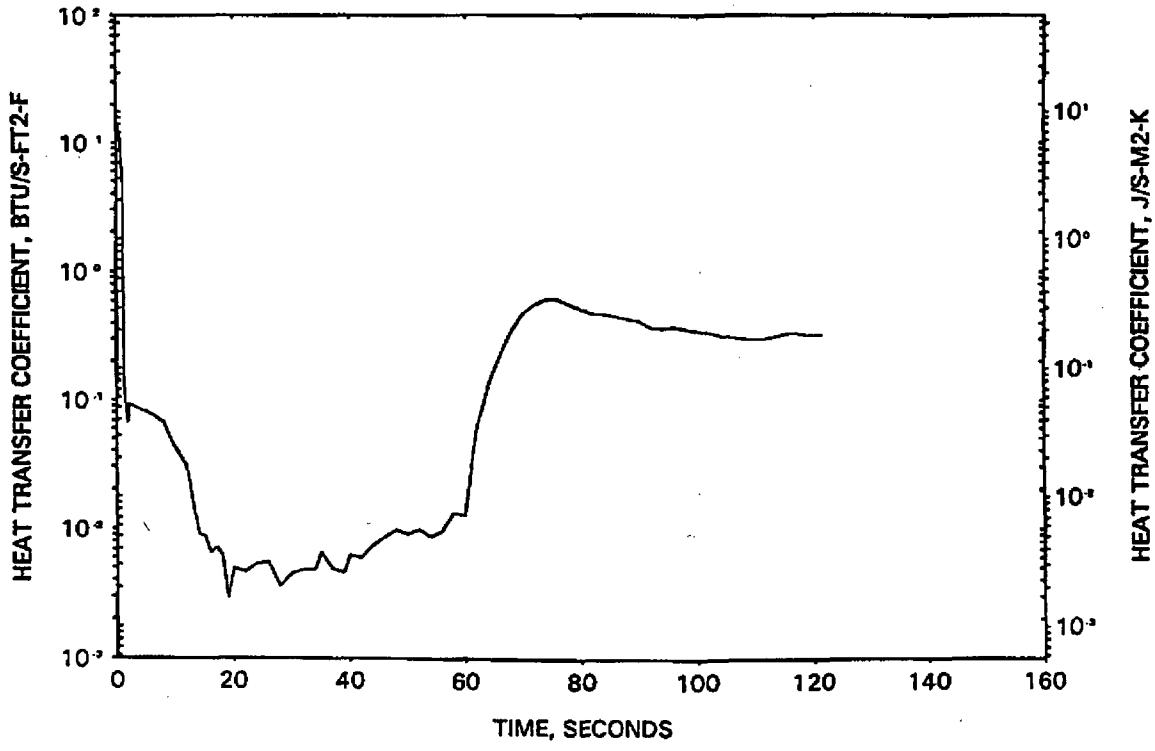

FIGURE A-125. TIME-IN-LIFE STUDY -
REACTOR VESSEL UPPER PLENUM PRESSURE.

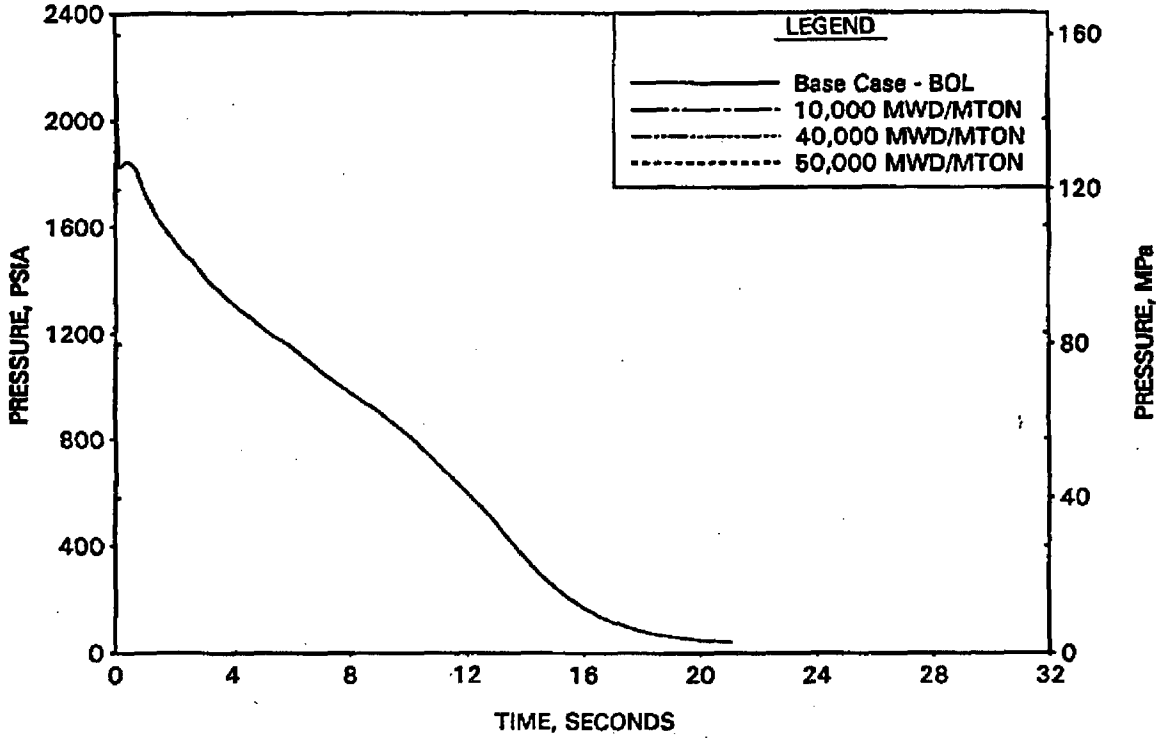

FIGURE A-126. TIME-IN-LIFE STUDY -
RV SIDE BREAK MASS FLOW RATE.

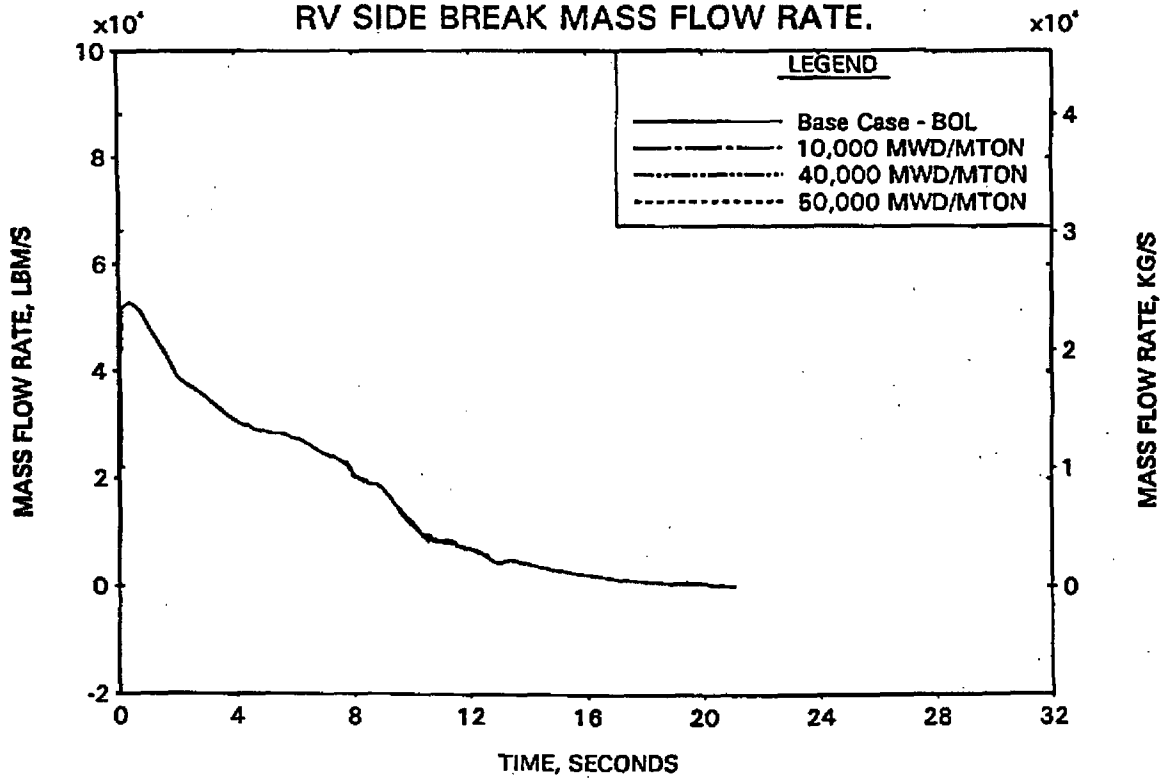

FIGURE A-127. TIME-IN-LIFE STUDY -
PUMP SIDE BREAK MASS FLOW RATE.

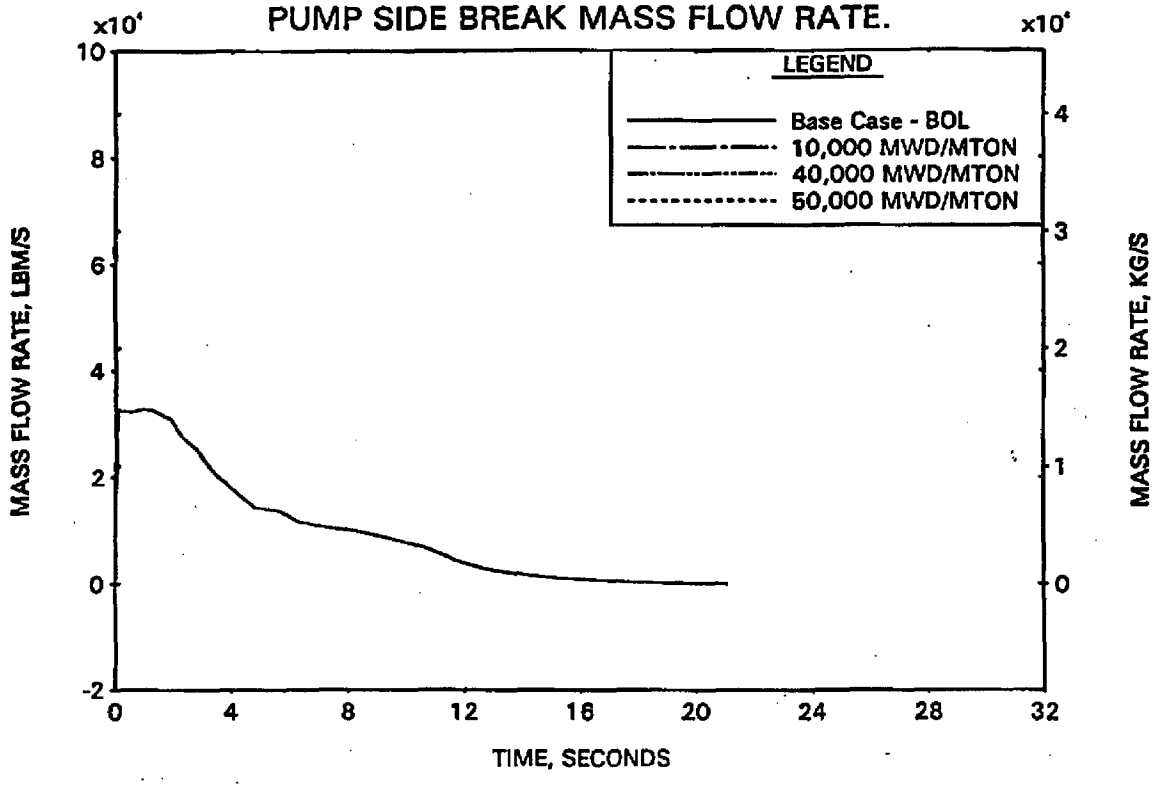

FIGURE A-128. TIME-IN-LIFE STUDY -
HC MASS FLOW RATE AT RUPTURED LOCATION.

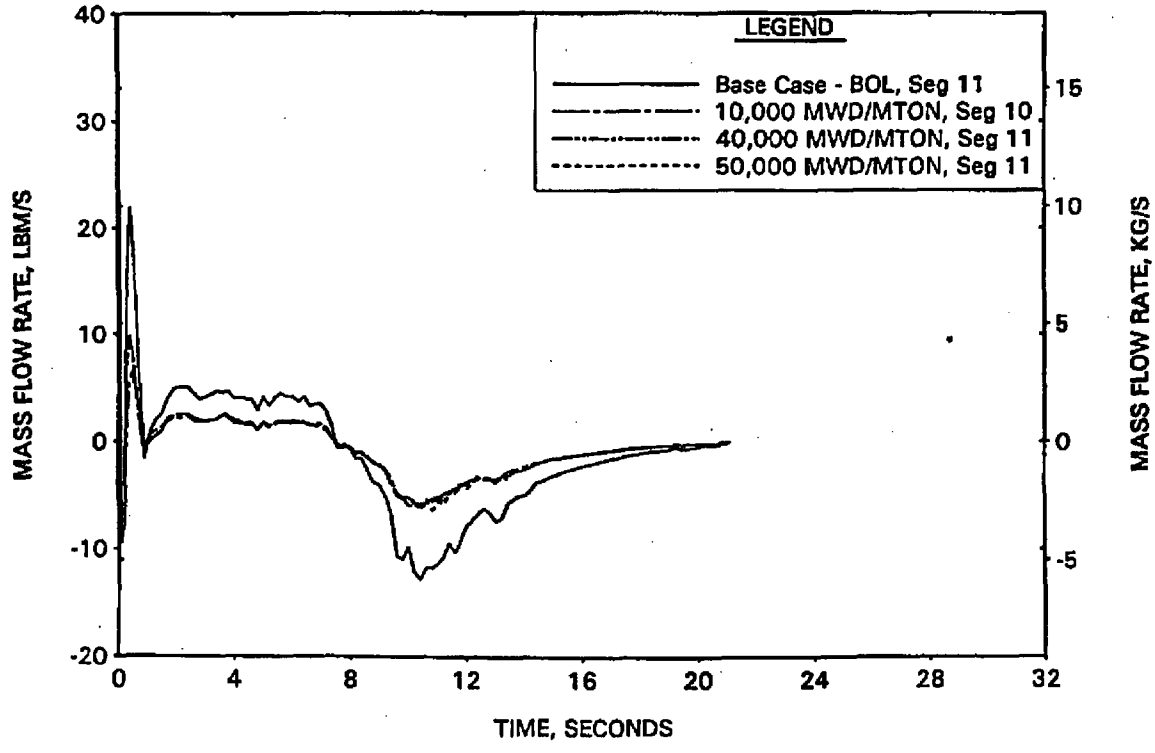

FIGURE A-129. TIME-IN-LIFE STUDY -
HC MASS FLOW RATE AT PEAK UNRUPTURED LOCATION.

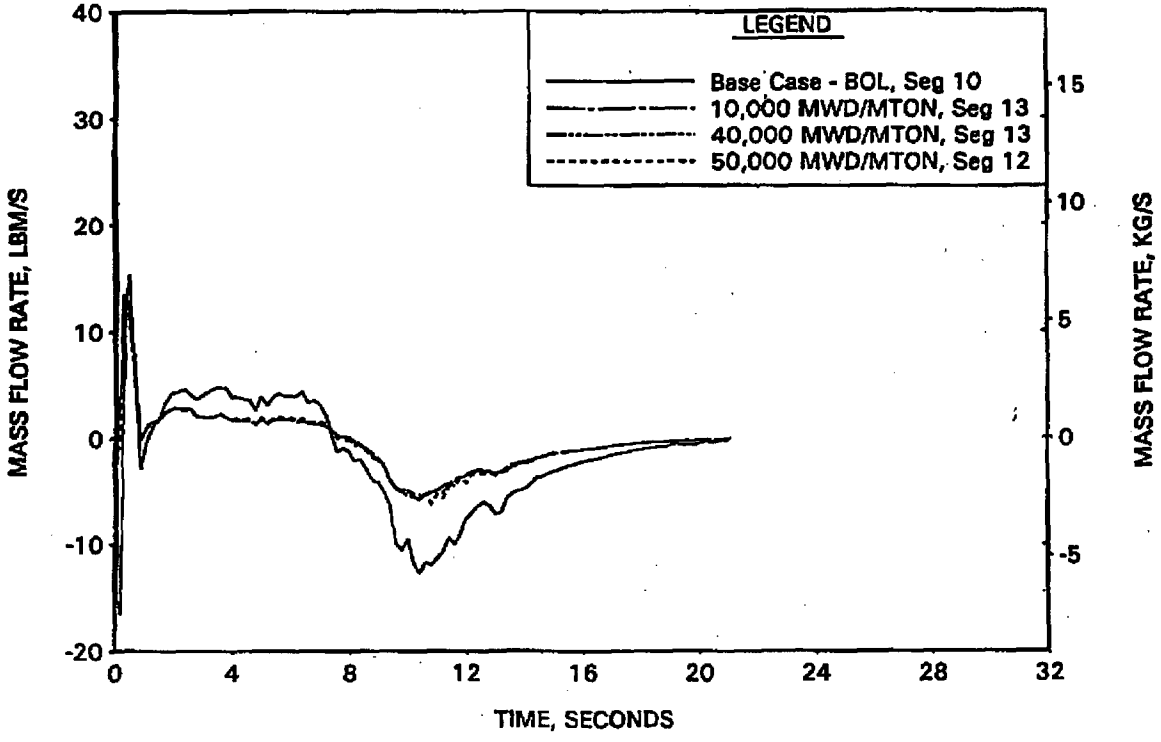

FIGURE A-130. TIME-IN-LIFE STUDY -
CORE FLOODING RATE.

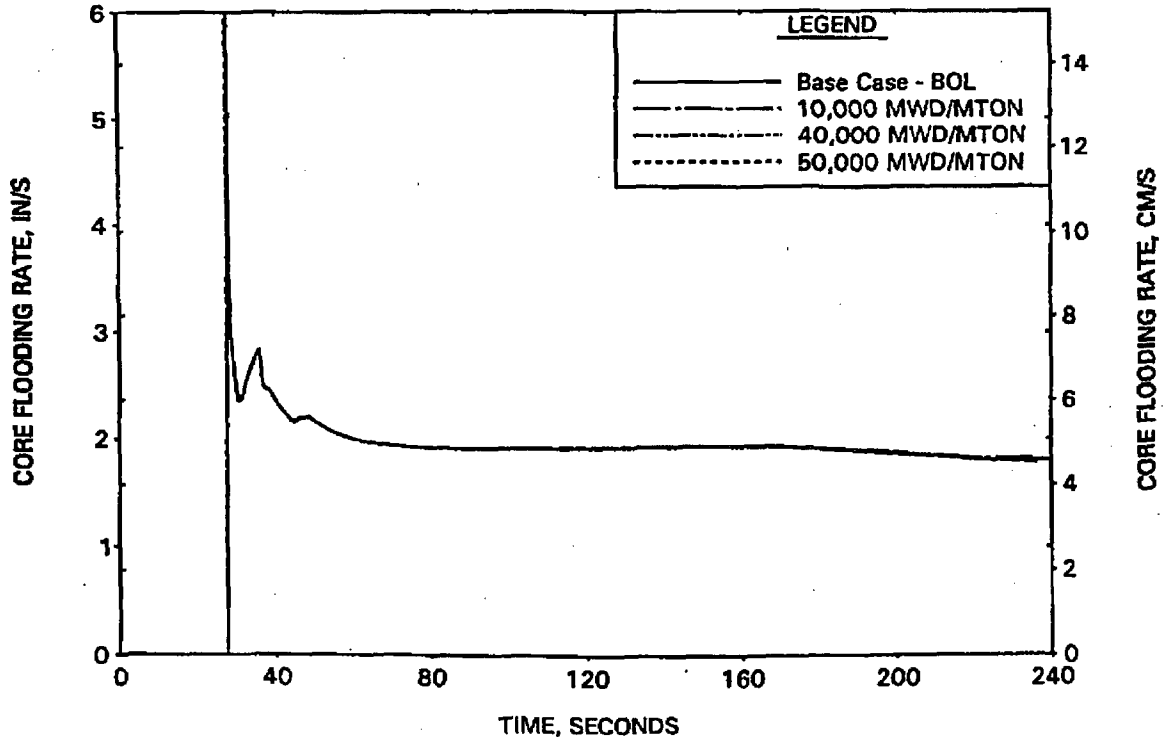

FIGURE A-131. TIME-IN-LIFE STUDY -
HC CLAD TEMP AT RUPTURED LOCATION.

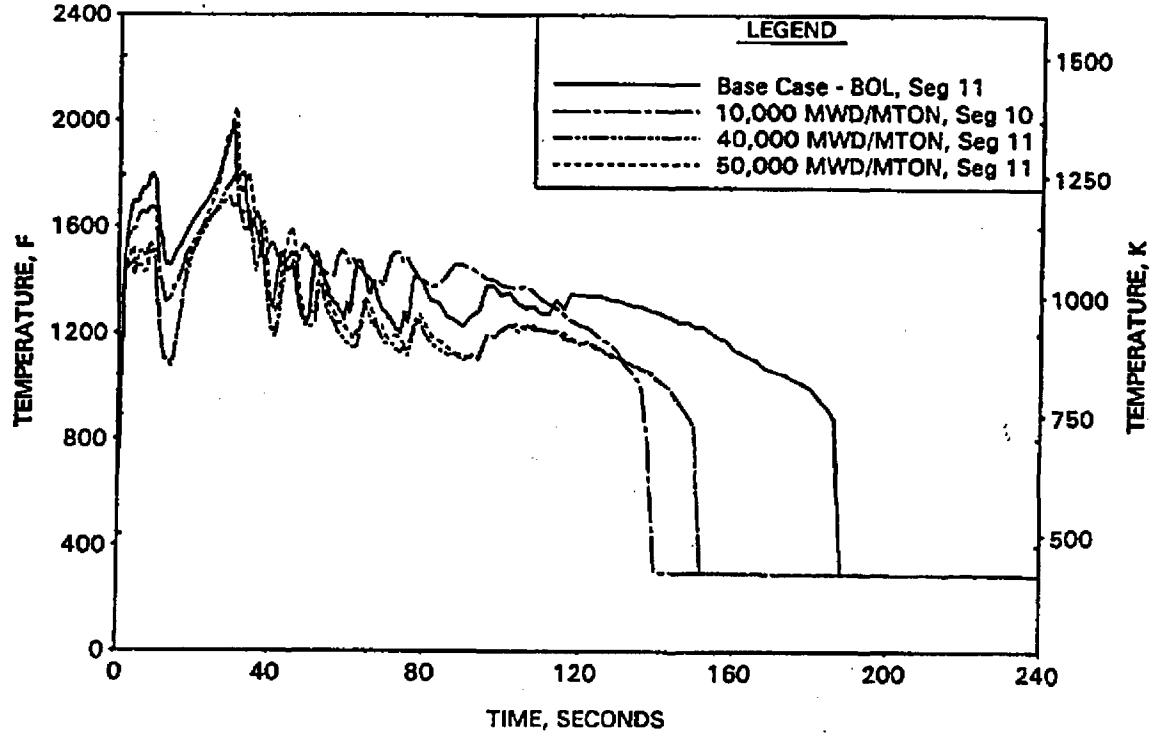

FIGURE A-132. TIME-IN-LIFE STUDY -
HC CLAD TEMP AT PEAK UNRUPTURED LOCATION.

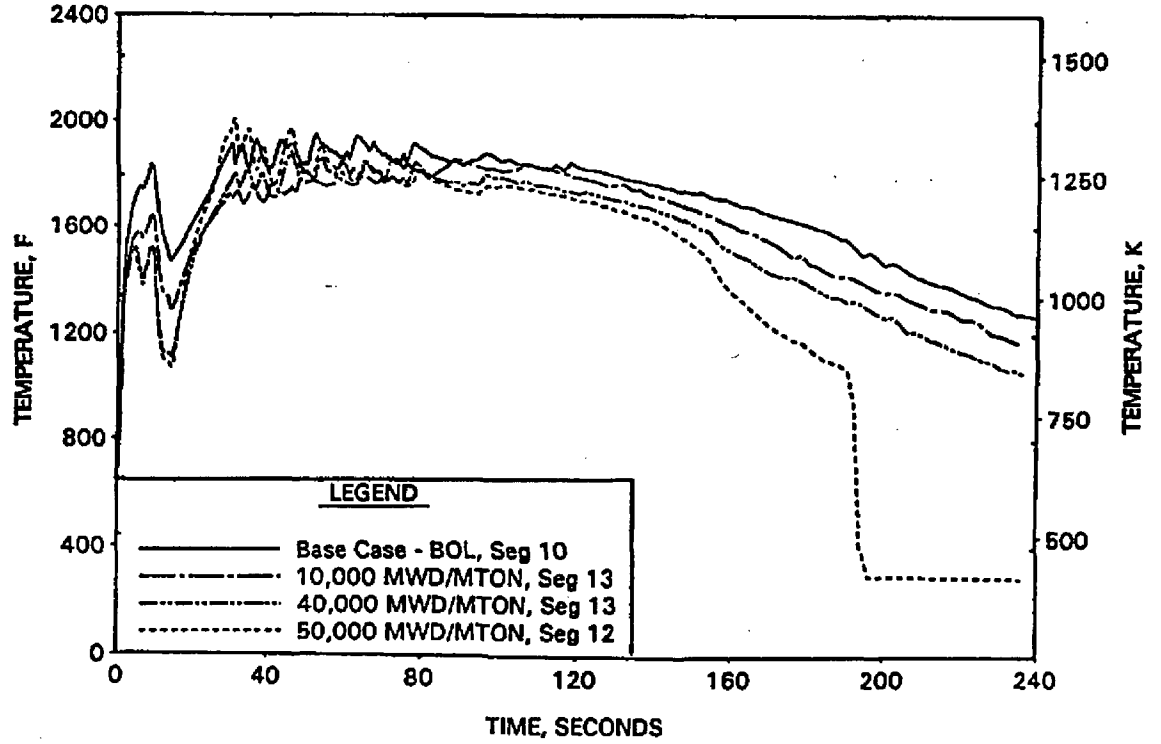

FIGURE A-133. TIME-IN-LIFE STUDY -
FILTERED HC HTC AT RUPTURED LOCATION.

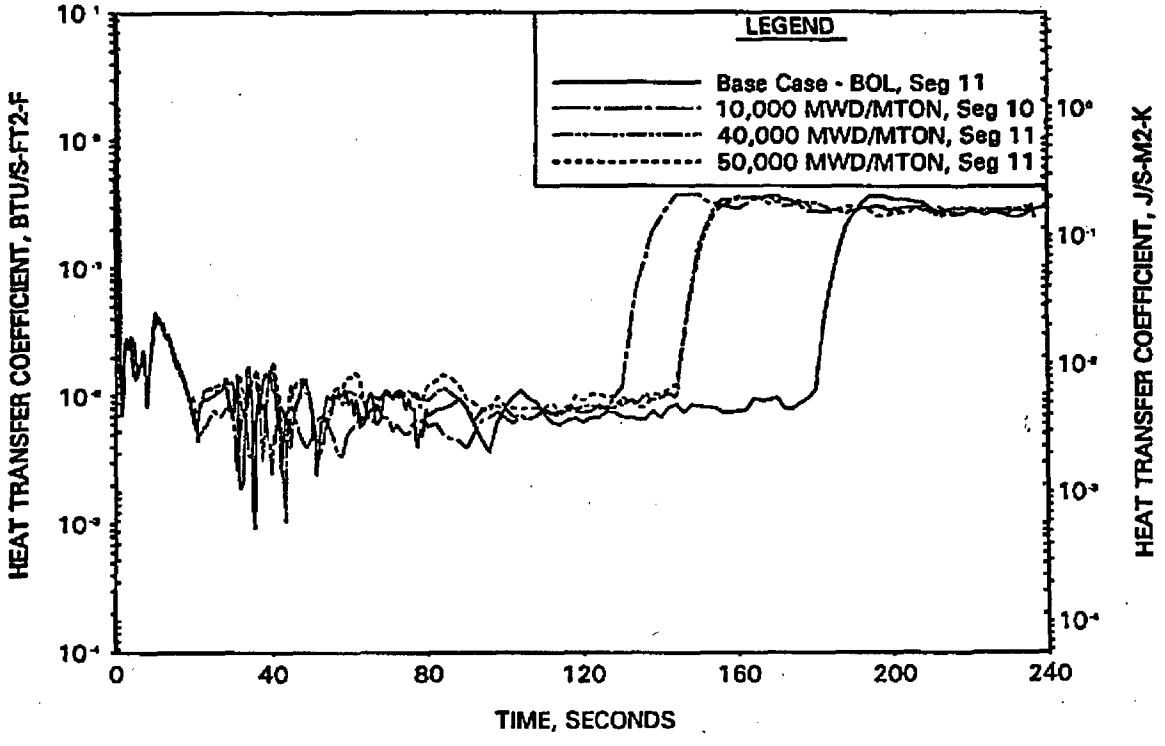

FIGURE A-134. TIME-IN-LIFE STUDY -
FILTERED HC HTC AT PEAK UNRUPTURED LOCATION.

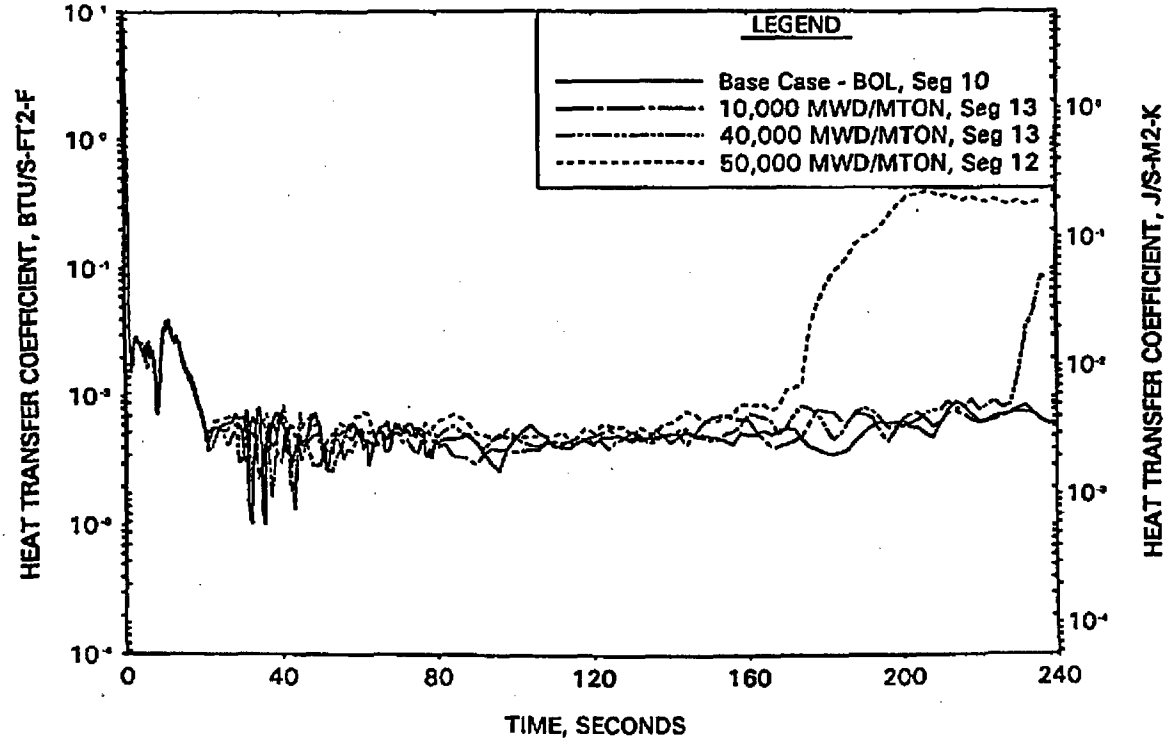

FIGURE A-135. TIME-IN-LIFE STUDY -
HC GAP HTC AT RUPTURED LOCATION.

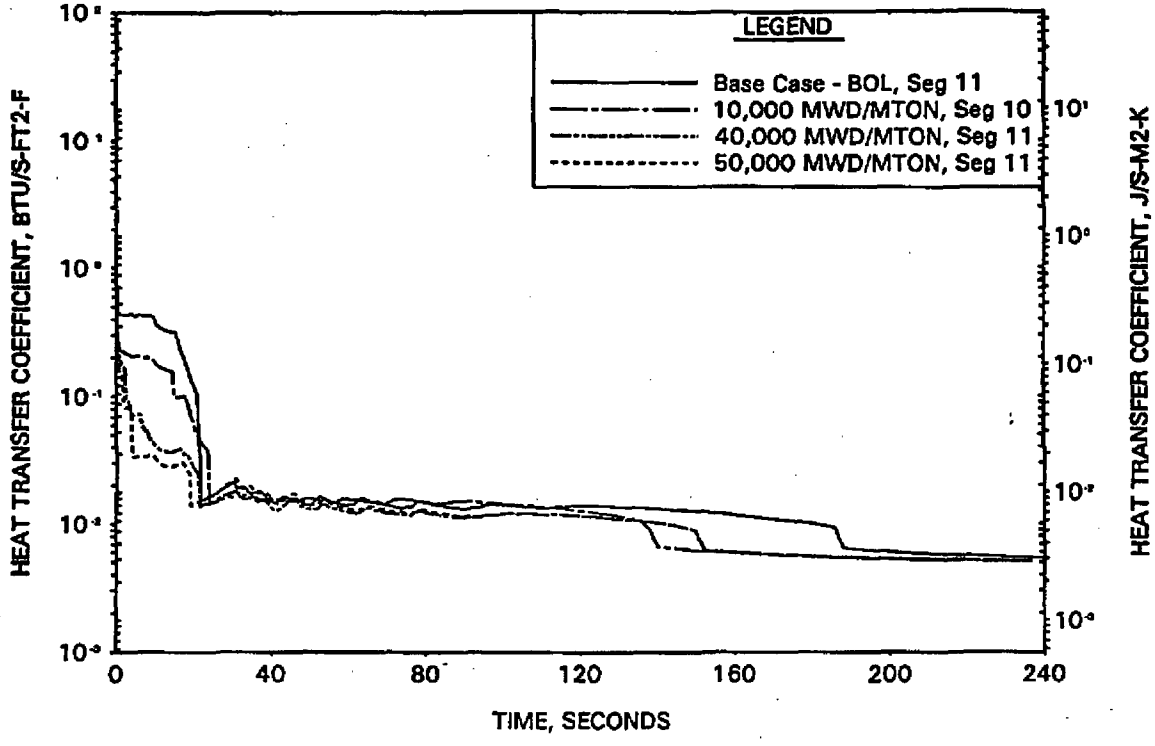

FIGURE A-136. TIME-IN-LIFE STUDY -
HC GAP HTC AT PEAK UNRUPTURED LOCATION.

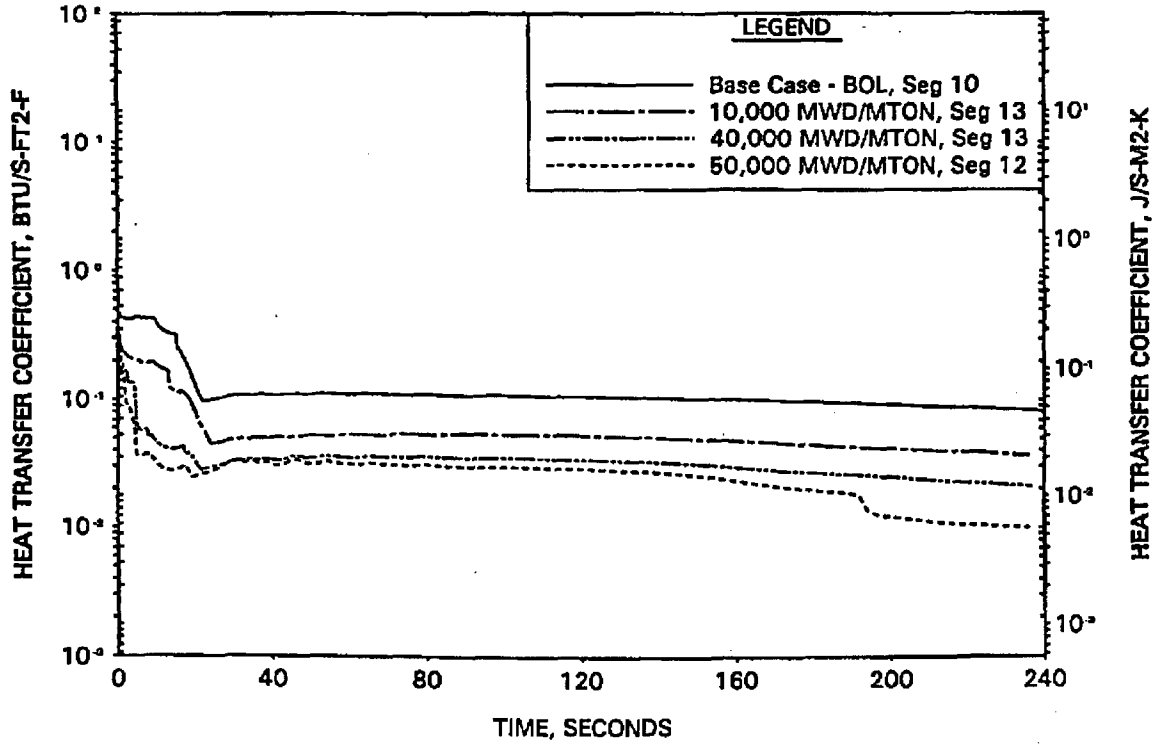

FIGURE A-137. 3-PUMP/75% POWER STUDY - REACTOR VESSEL UPPER PLENUM PRESSURE.

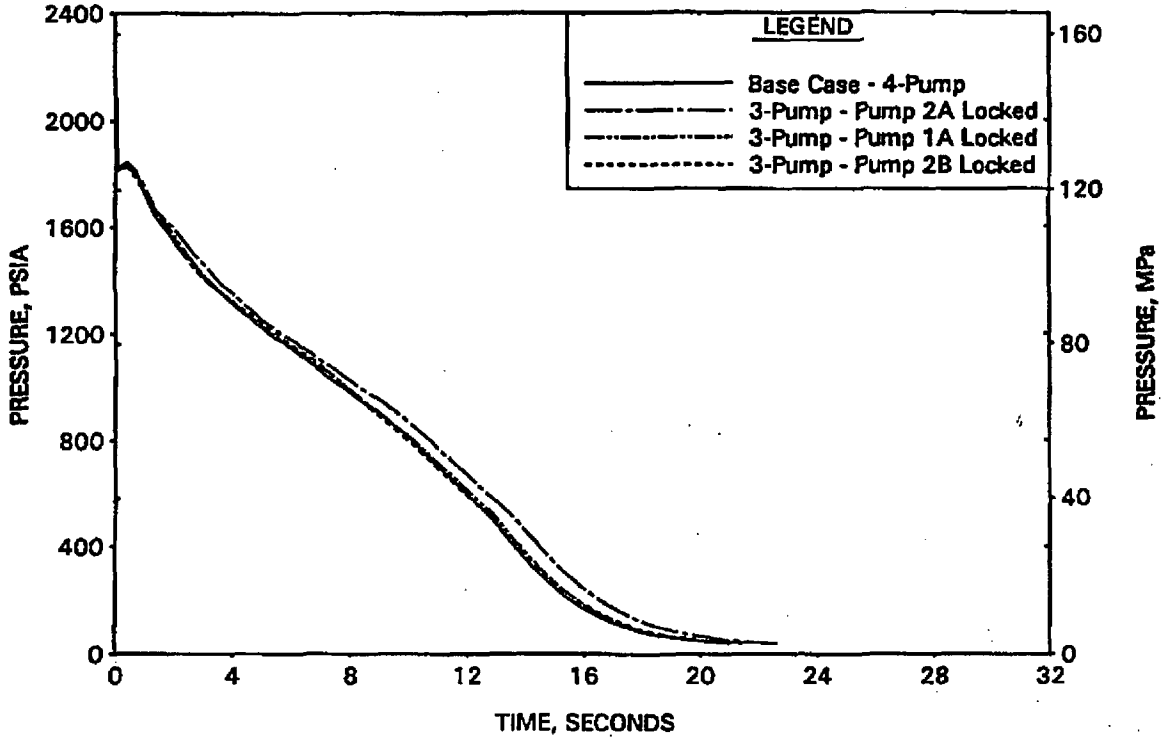

FIGURE A-138. 3-PUMP/75% POWER STUDY - RV SIDE BREAK MASS FLOW RATE.

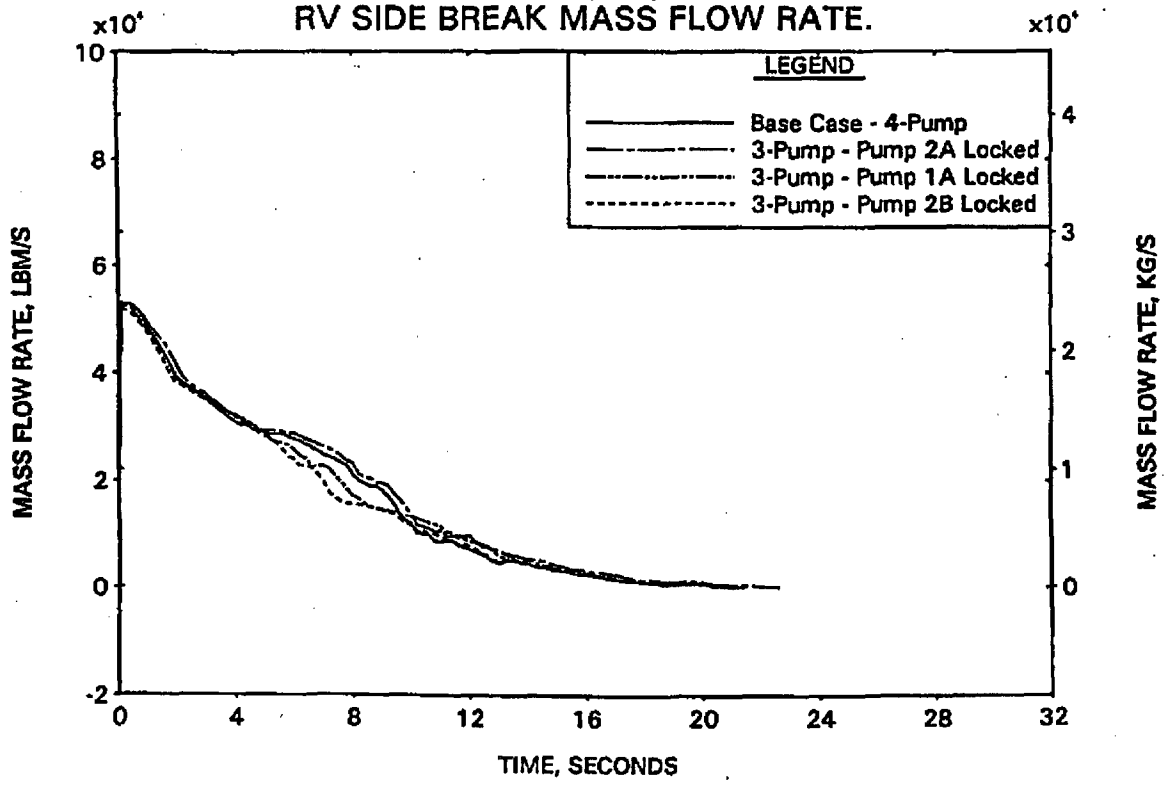

FIGURE A-139. 3-PUMP/75% POWER STUDY - PUMP SIDE BREAK MASS FLOW RATE.

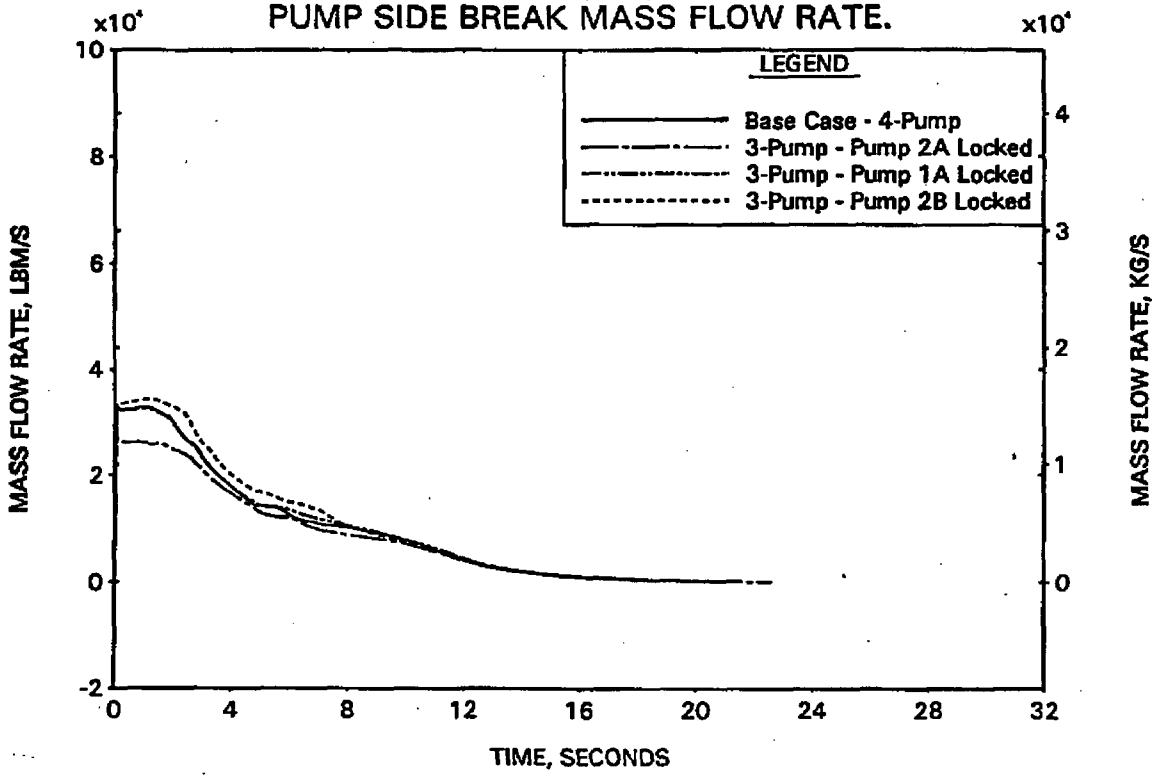

FIGURE A-140. 3-PUMP/75% POWER STUDY - HC MASS FLOW RATE AT RUPTURED LOCATION.

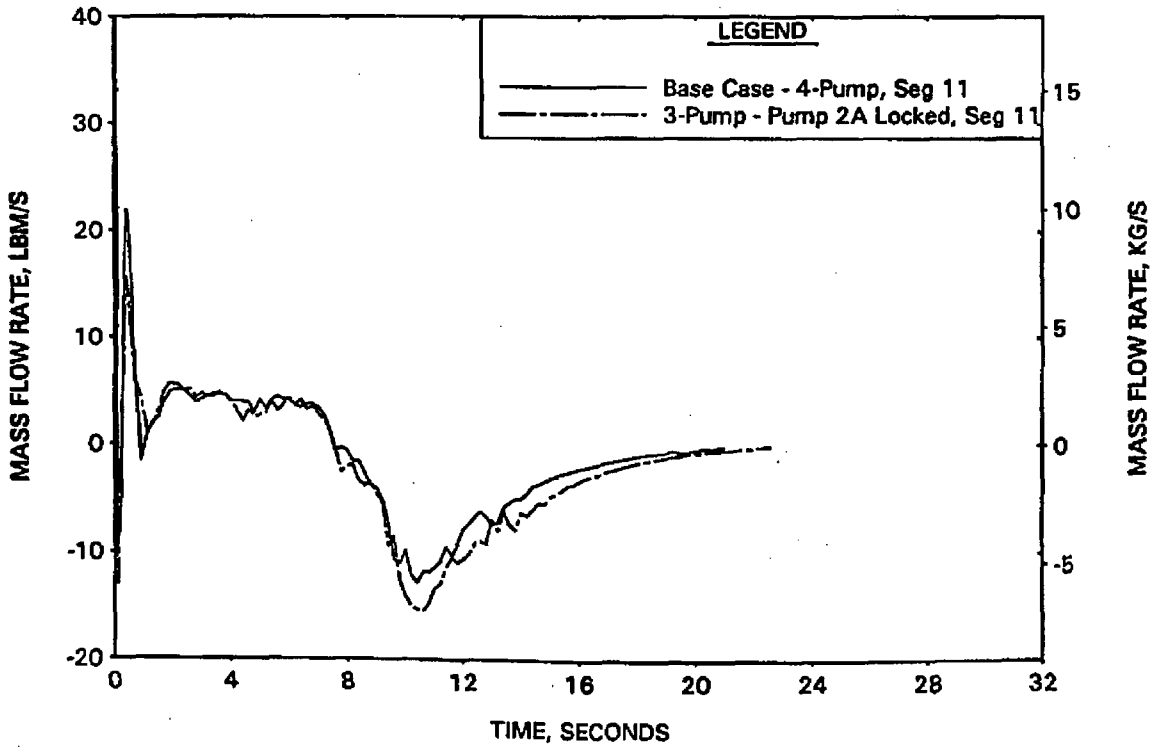

FIGURE A-141. 3-PUMP/75% POWER STUDY -
HC MASS FLOW RATE AT PEAK UNRUPTURED LOCATION.

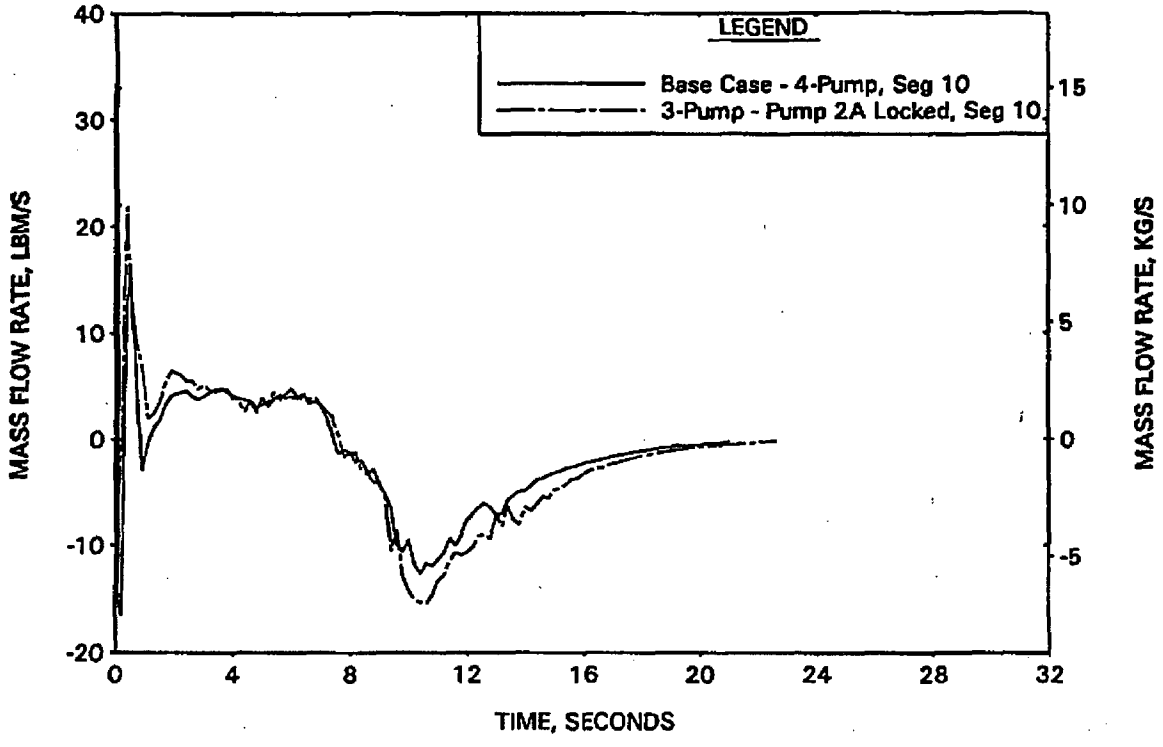

FIGURE A-142. 3-PUMP/75% POWER STUDY -
CORE FLOODING RATE.

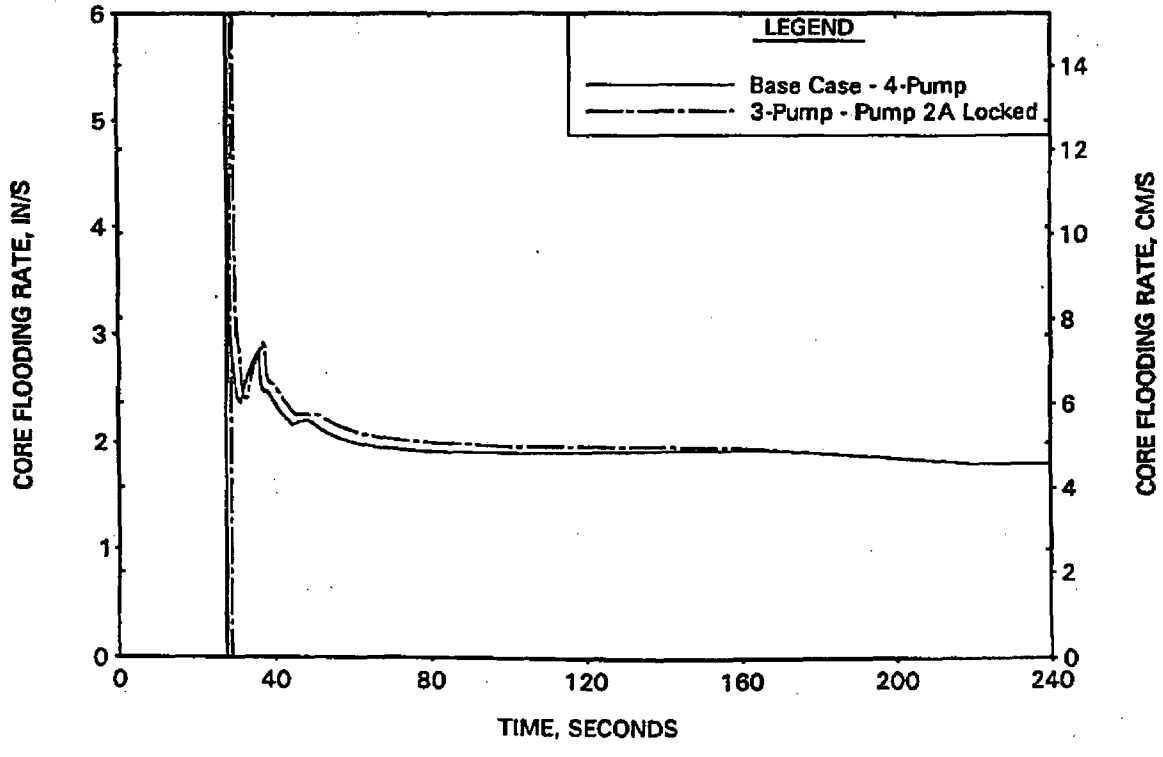

FIGURE A-143. 3-PUMP/75% POWER STUDY -
HC CLAD TEMP AT RUPTURED LOCATION.

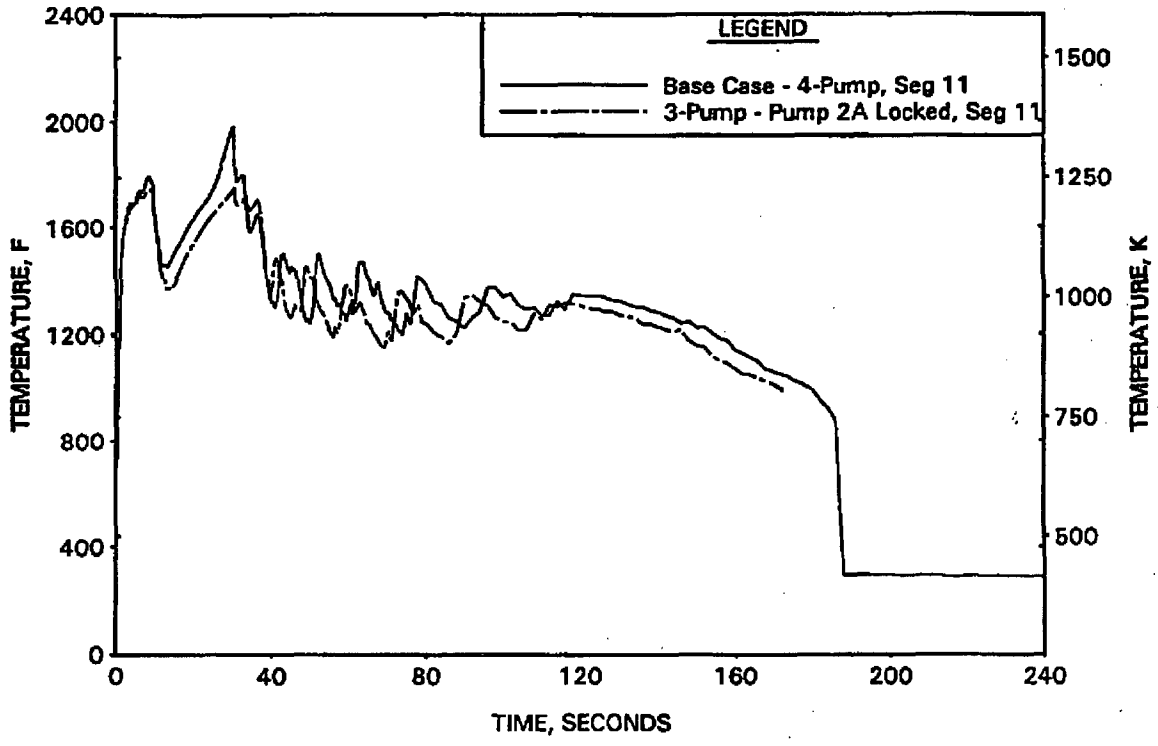

FIGURE A-144. 3-PUMP/75% POWER STUDY -
HC CLAD TEMP AT PEAK UNRUPTURED LOCATION.

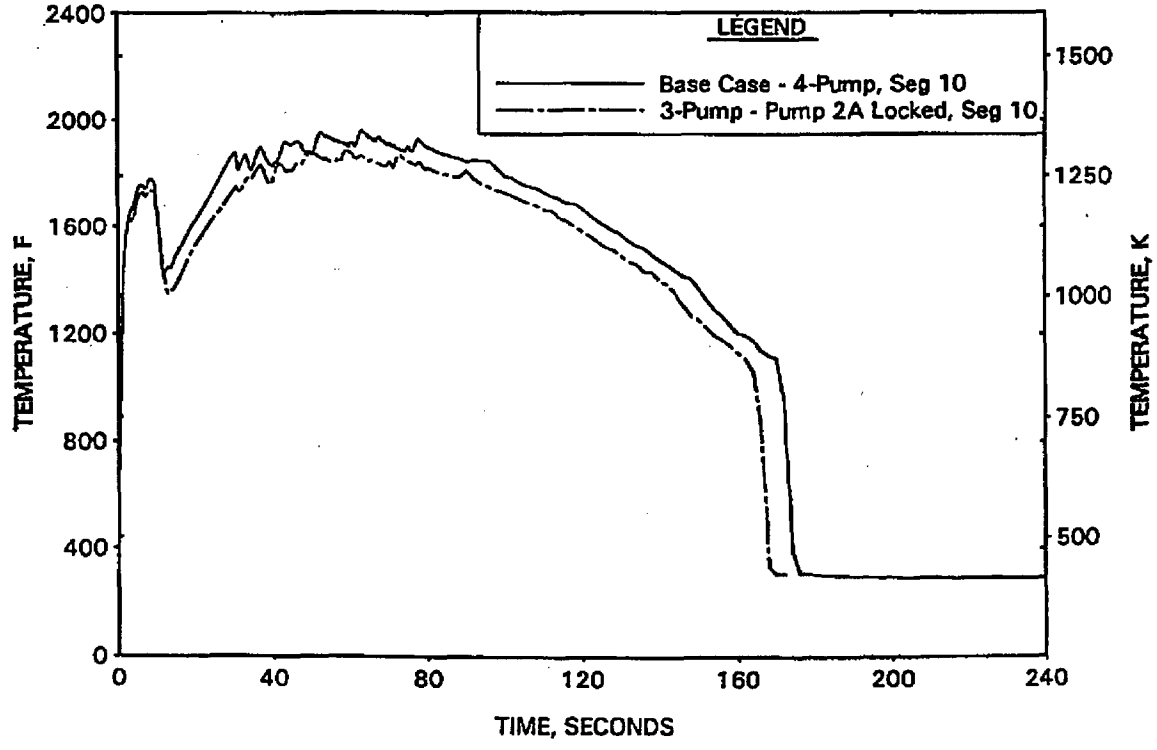

FIGURE A-145. 3-PUMP/75% POWER STUDY - FILTERED HC HTC AT RUPTURED LOCATION.

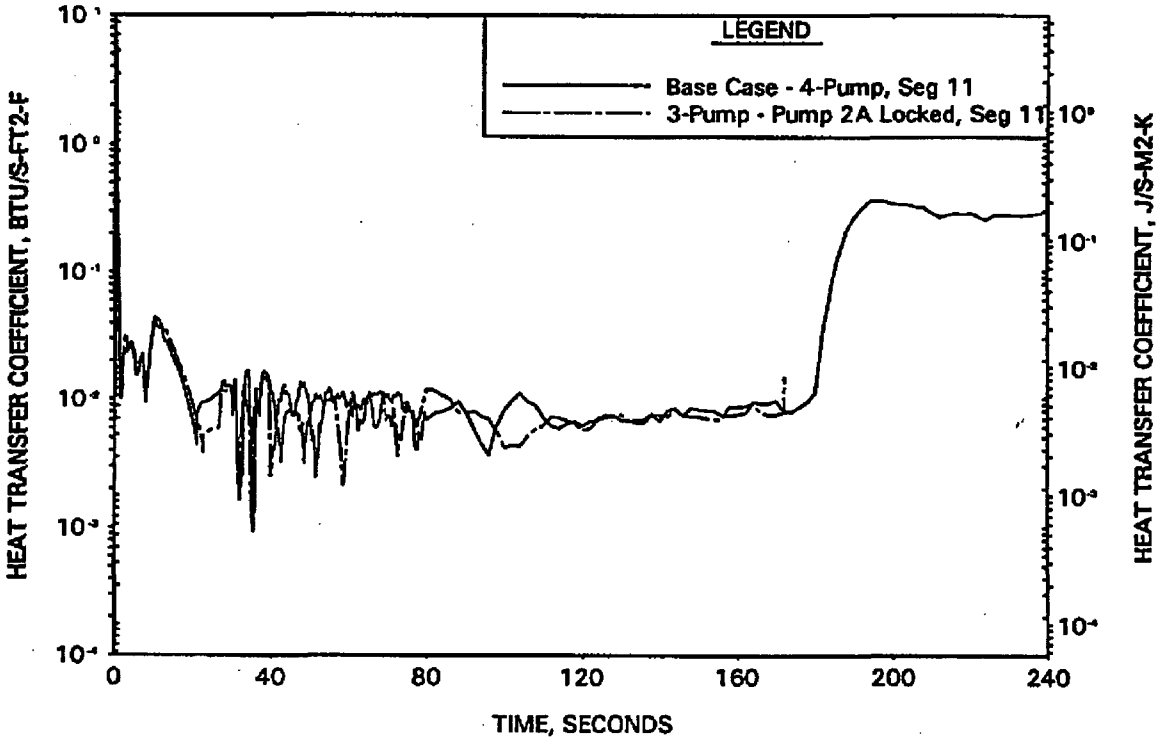

FIGURE A-146. 3-PUMP/75% POWER STUDY - FILTERED HC HTC AT PEAK UNRUPTURED LOCATION.

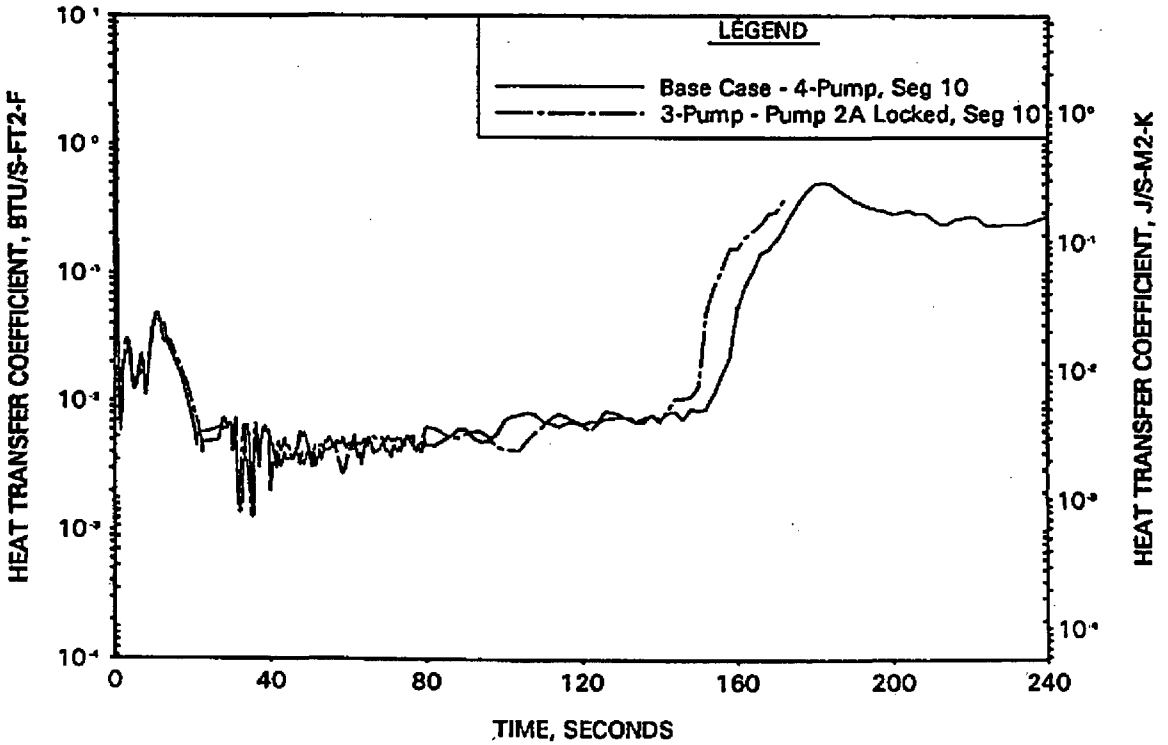

FIGURE A-147. LOCA LIMIT AXIAL POWER SHAPES.

C,D

FIGURE A-148. 2.865-FT LOCA LIMIT CASE - REACTOR VESSEL UPPER PLENUM PRESSURE.

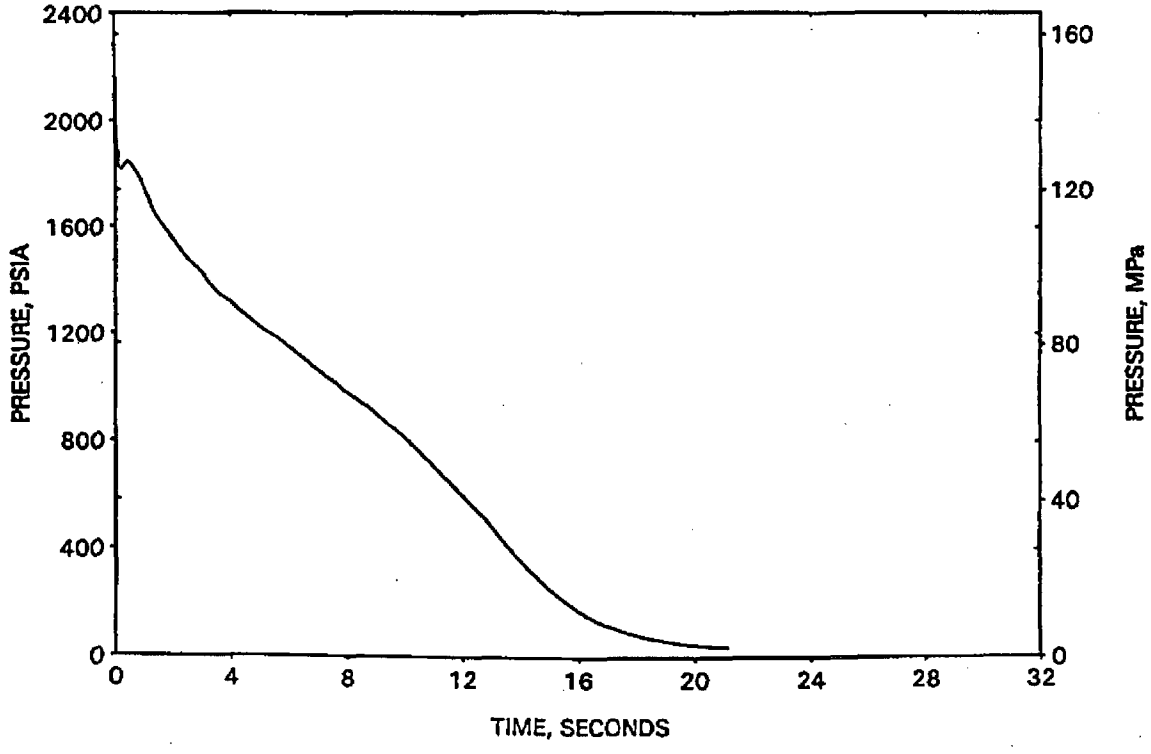

FIGURE A-149. 2.865-FT LOCA LIMIT CASE - BREAK MASS FLOW RATE.

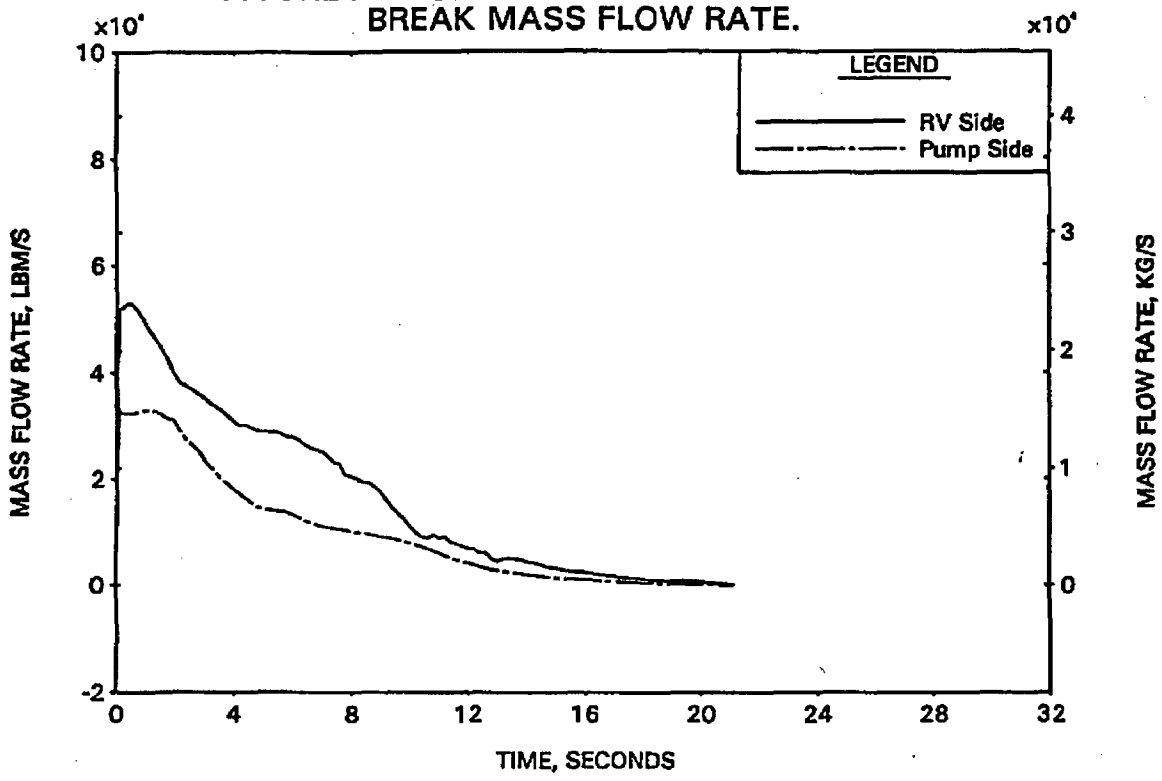

FIGURE A-150. 2.865-FT LOCA LIMIT CASE - HC MASS FLOW RATES AT RUPTURED AND PEAK UNRUPTURED LOCATIONS.

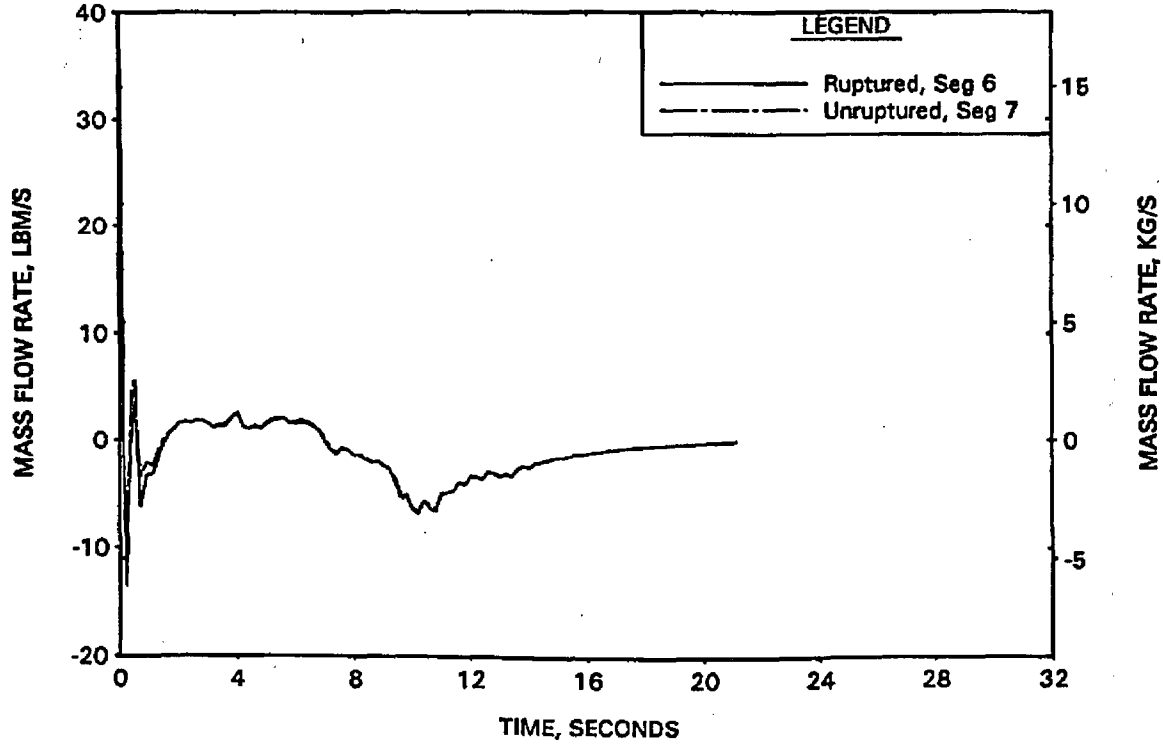

FIGURE A-151. 2.865-FT LOCA LIMIT CASE - CORE FLOODING RATE.

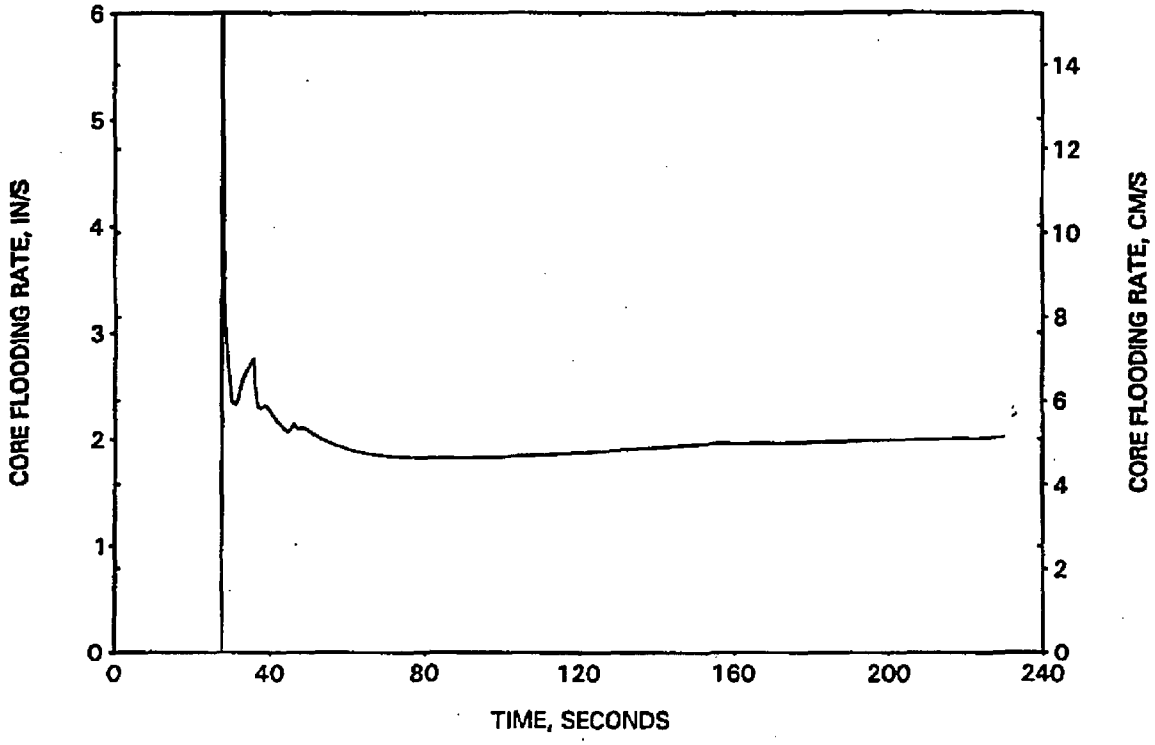

FIGURE A-152. 2.865-FT LOCA LIMIT CASE - HC CLAD TEMP AT RUPTURED AND PEAK UNRUPTURED LOCATIONS.

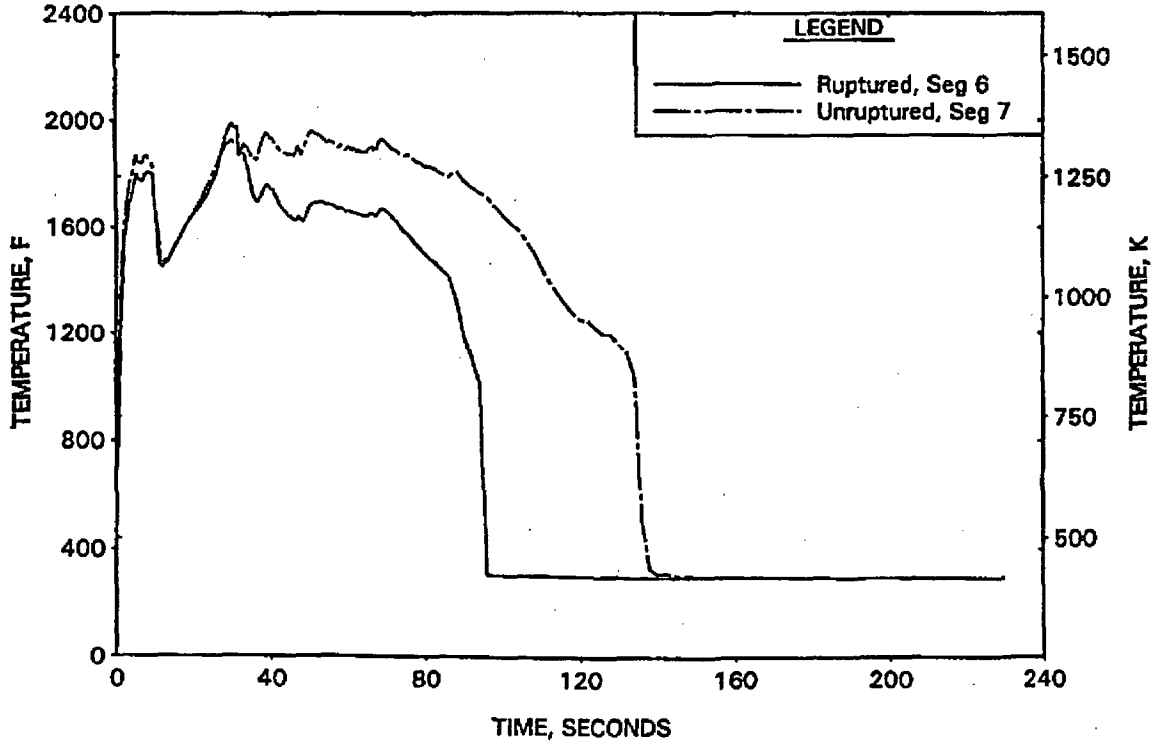

FIGURE A-153. 2.865-FT LOCA LIMIT CASE - FILTERED HC HTC AT RUPTURED AND PEAK UNRUPTURED LOCATIONS.

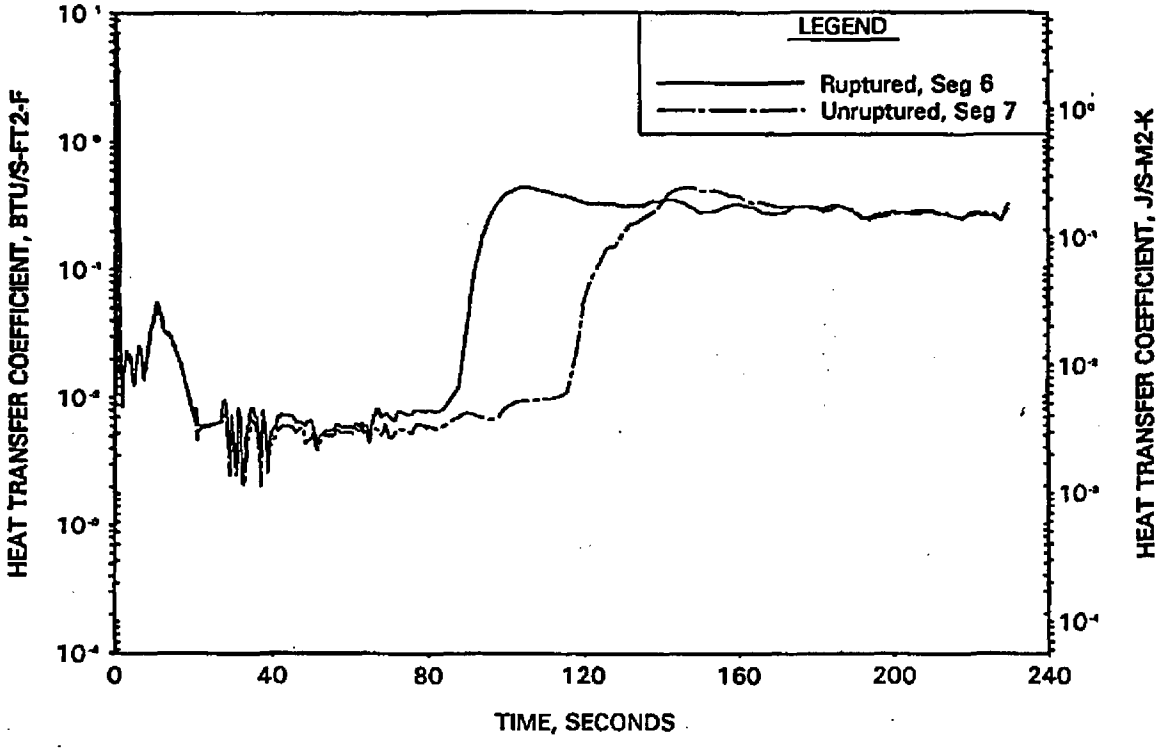

FIGURE A-154. 6.285-FT LOCA LIMIT CASE - REACTOR VESSEL UPPER PLENUM PRESSURE.

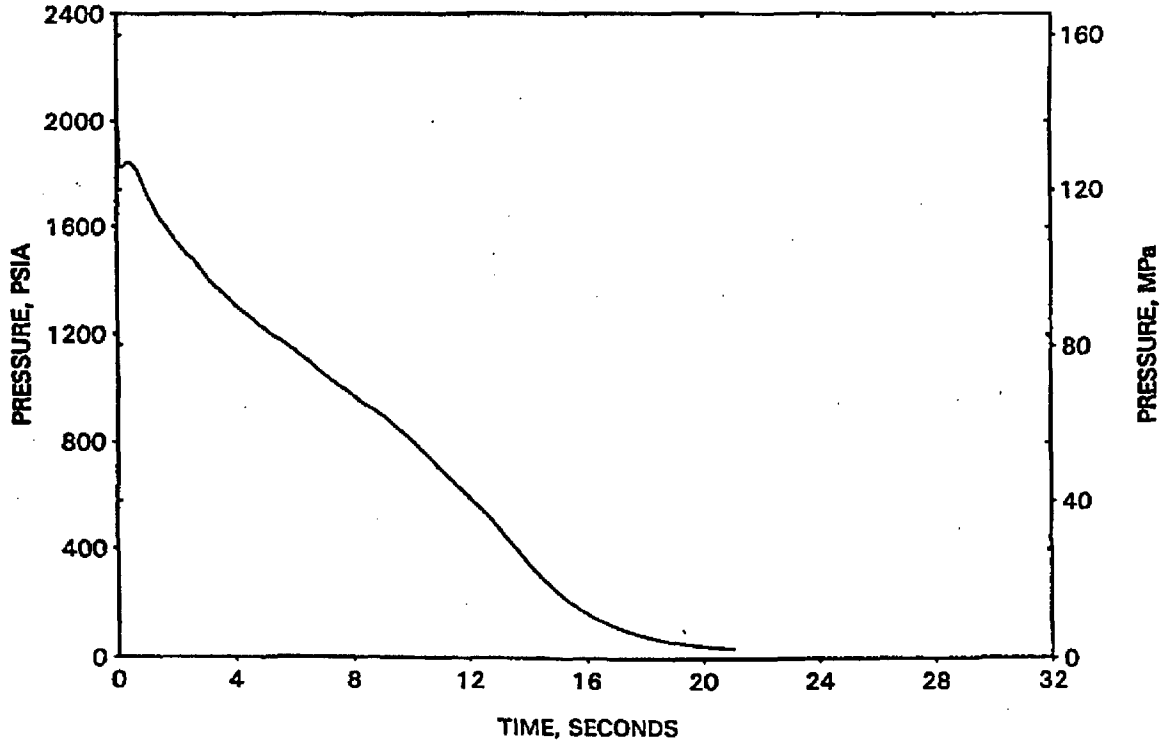

FIGURE A-155. 6.285-FT LOCA LIMIT CASE - BREAK MASS FLOW RATE.

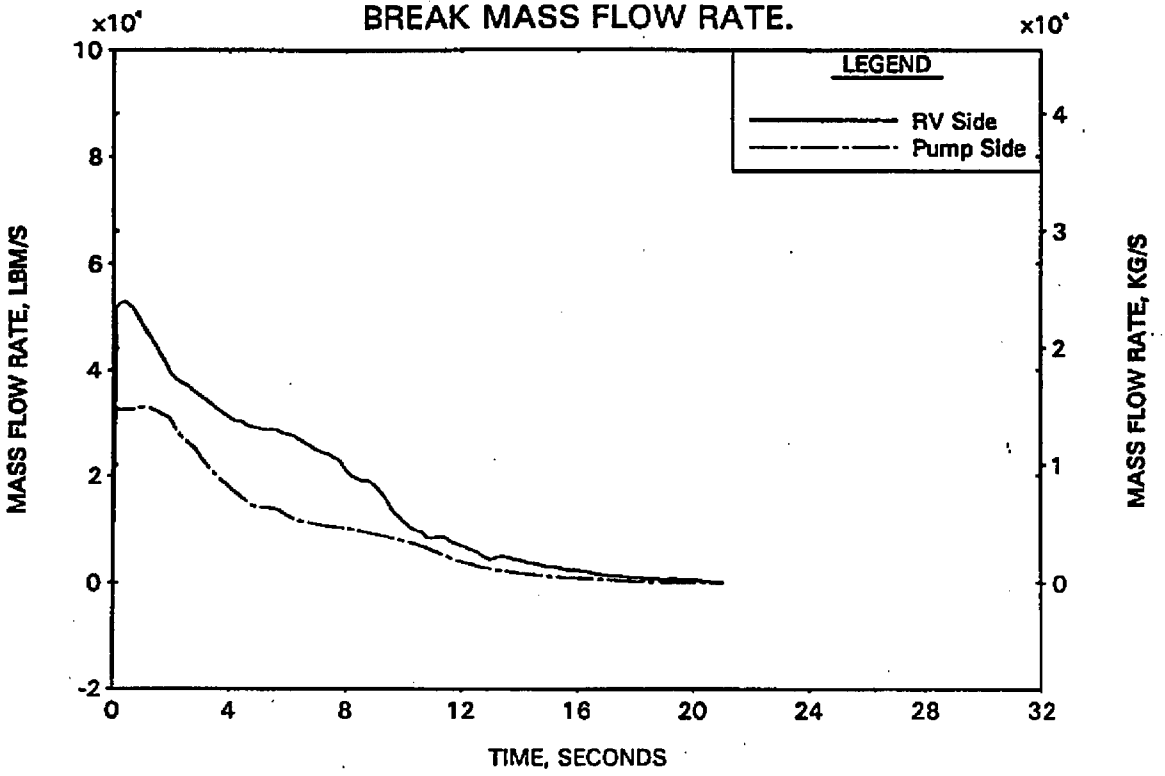

FIGURE A-156. 6.285-FT LOCA LIMIT CASE - HC MASS FLOW RATES AT RUPTURED AND PEAK UNRUPTURED LOCATIONS.

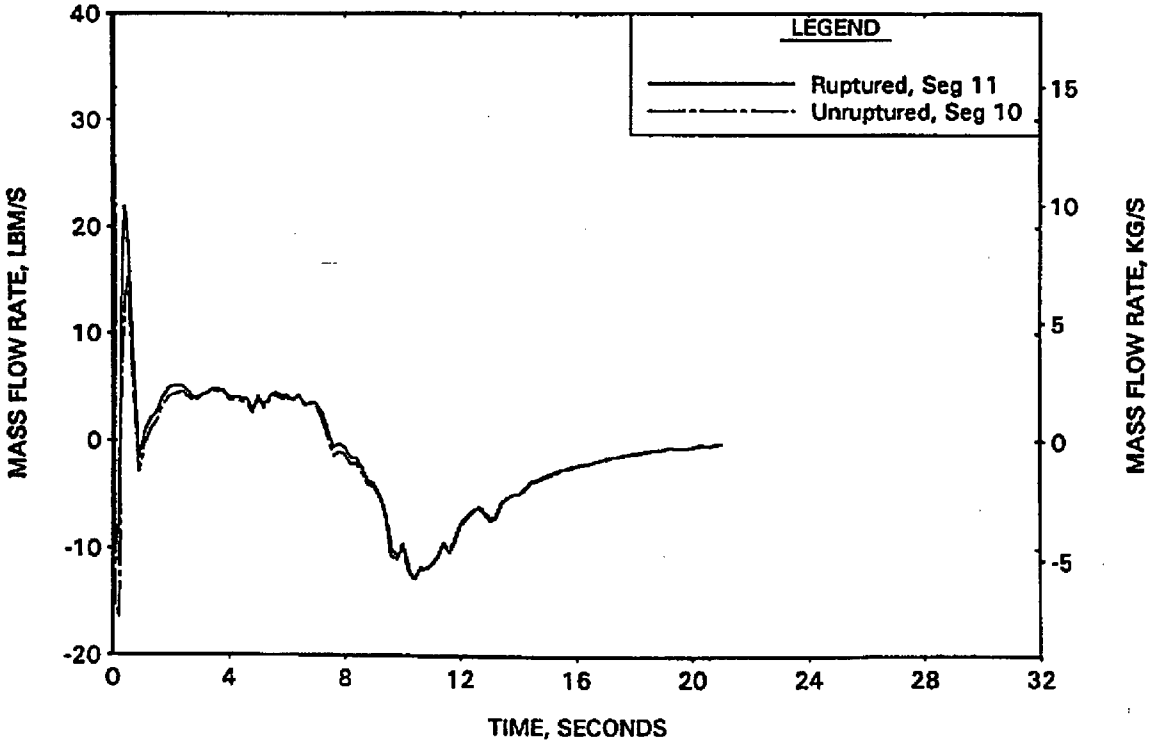

FIGURE A-157. 6.285-FT LOCA LIMIT CASE - CORE FLOODING RATE.

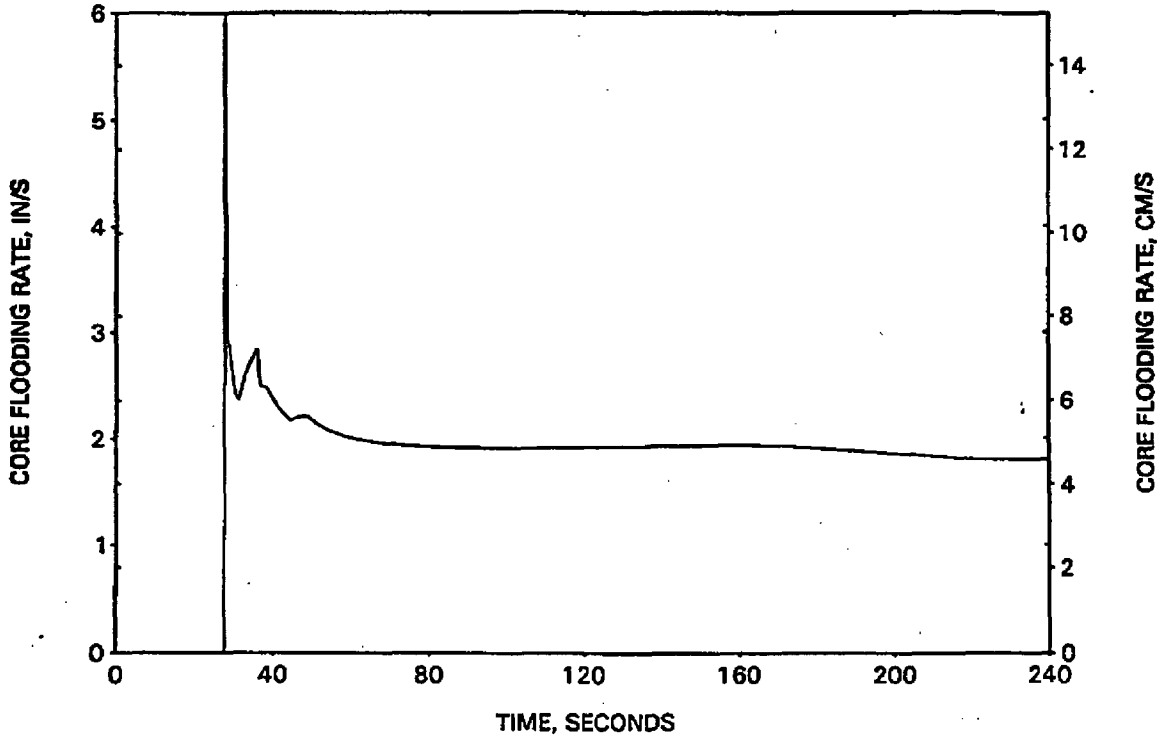

FIGURE A-158. 6.285-FT LOCA LIMIT CASE - HC CLAD TEMP AT RUPTURED AND PEAK UNRUPTURED LOCATIONS.

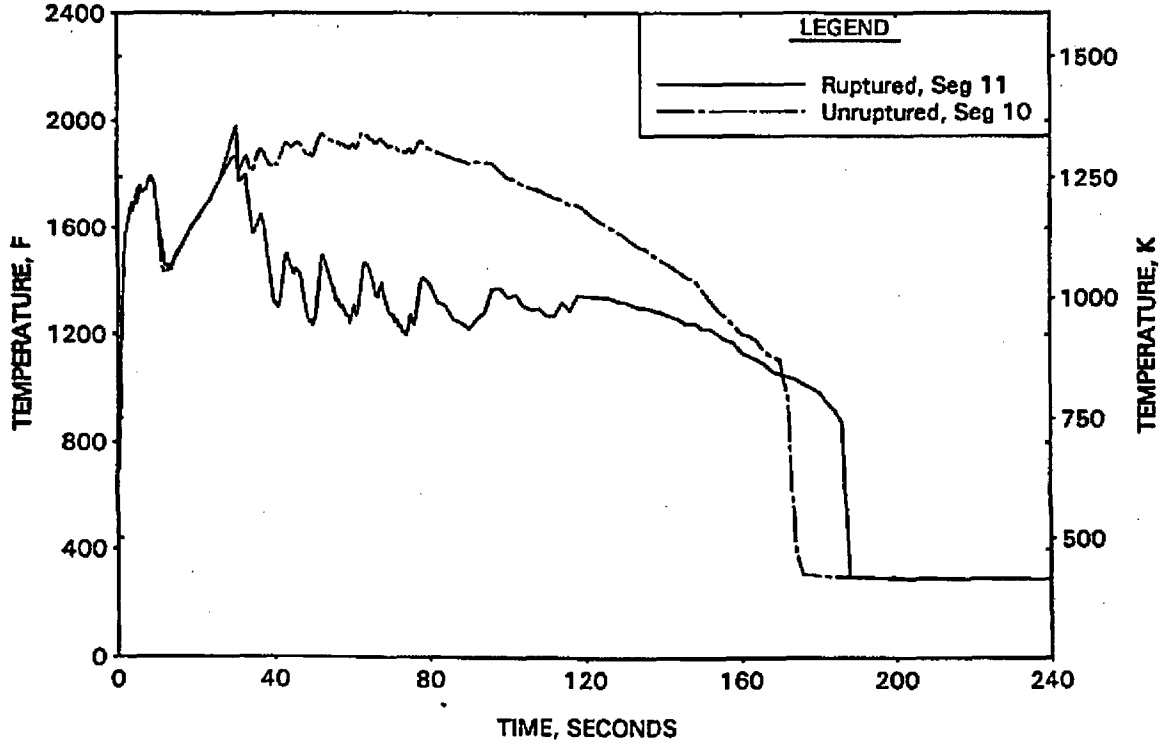

FIGURE A-159. 6.285-FT LOCA LIMIT CASE - FILTERED HC HTC AT RUPTURED AND PEAK UNRUPTURED LOCATIONS.

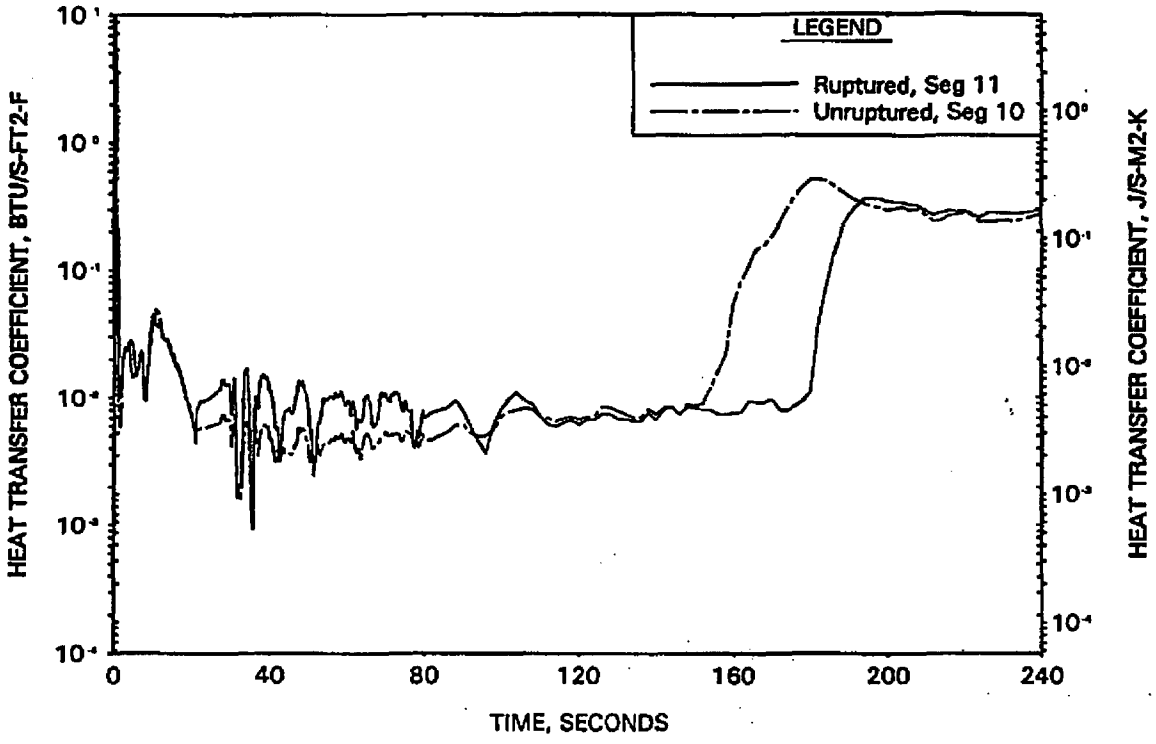

FIGURE A-160. 9.705-FT LOCA LIMIT CASE - REACTOR VESSEL UPPER PLENUM PRESSURE.

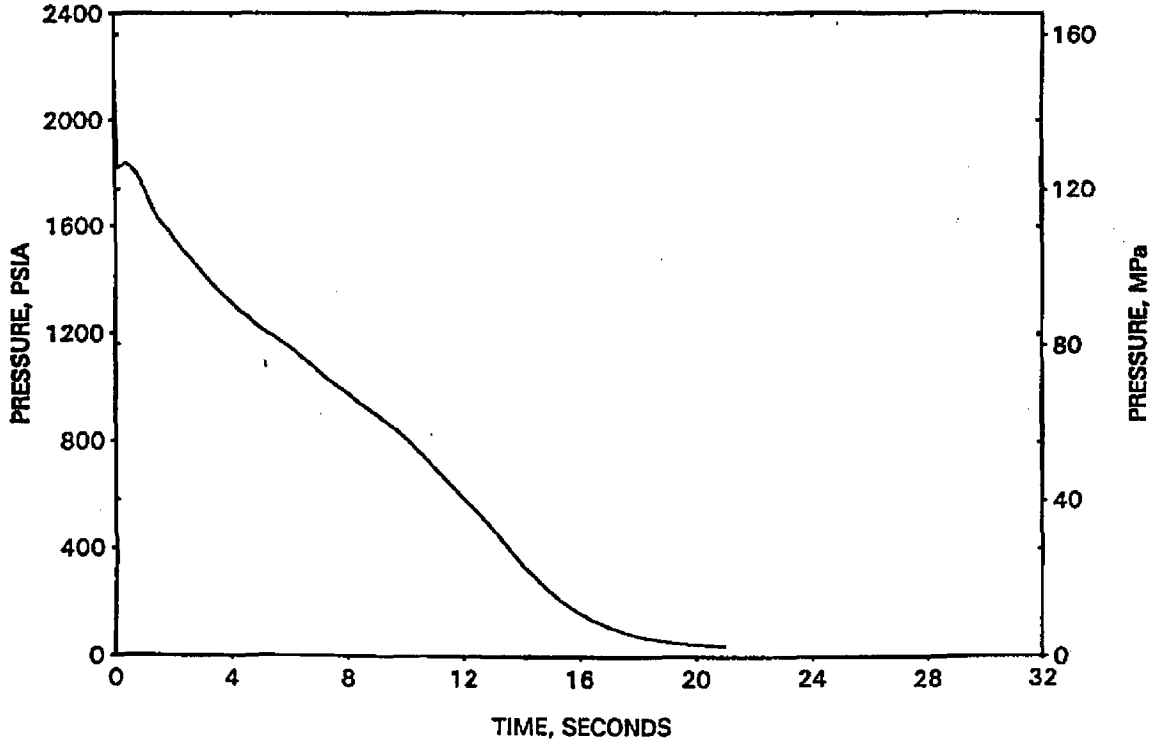

FIGURE A-161. 9.705-FT LOCA LIMIT CASE - BREAK MASS FLOW RATE.

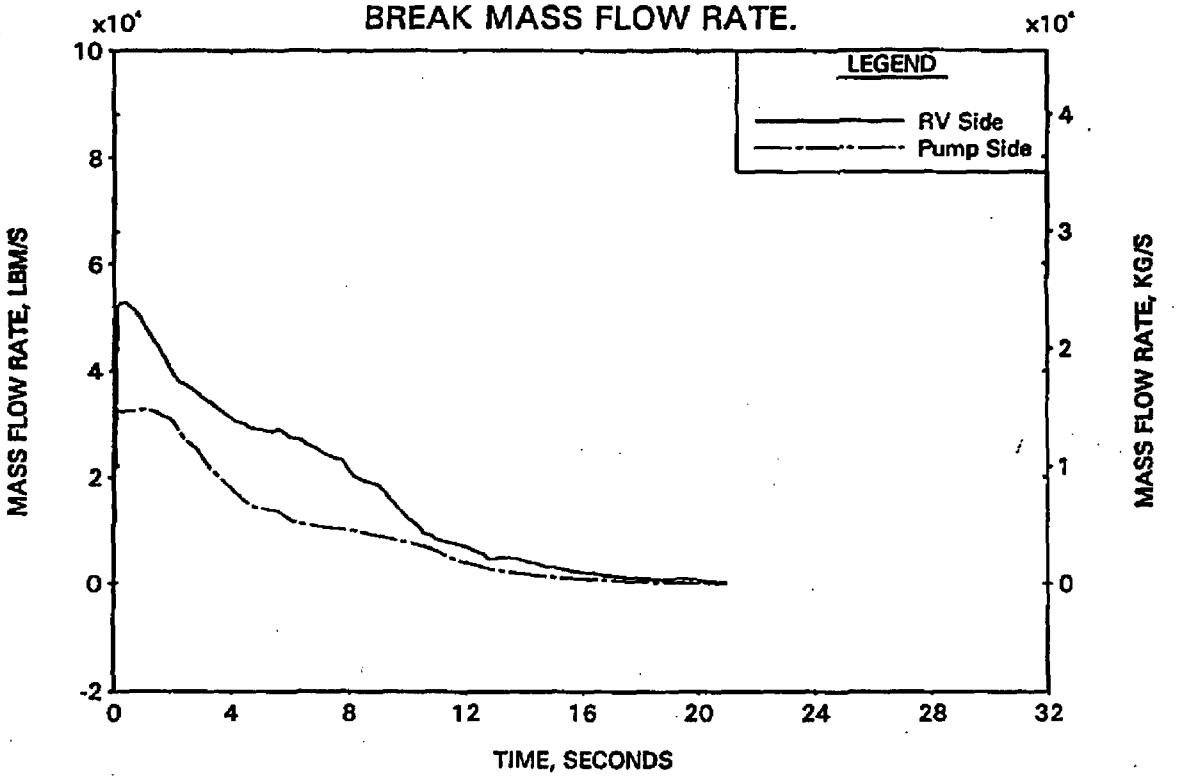

FIGURE A-162. 9.705-FT LOCA LIMIT CASE - HC MASS FLOW RATES AT RUPTURED AND PEAK UNRUPTURED LOCATIONS.

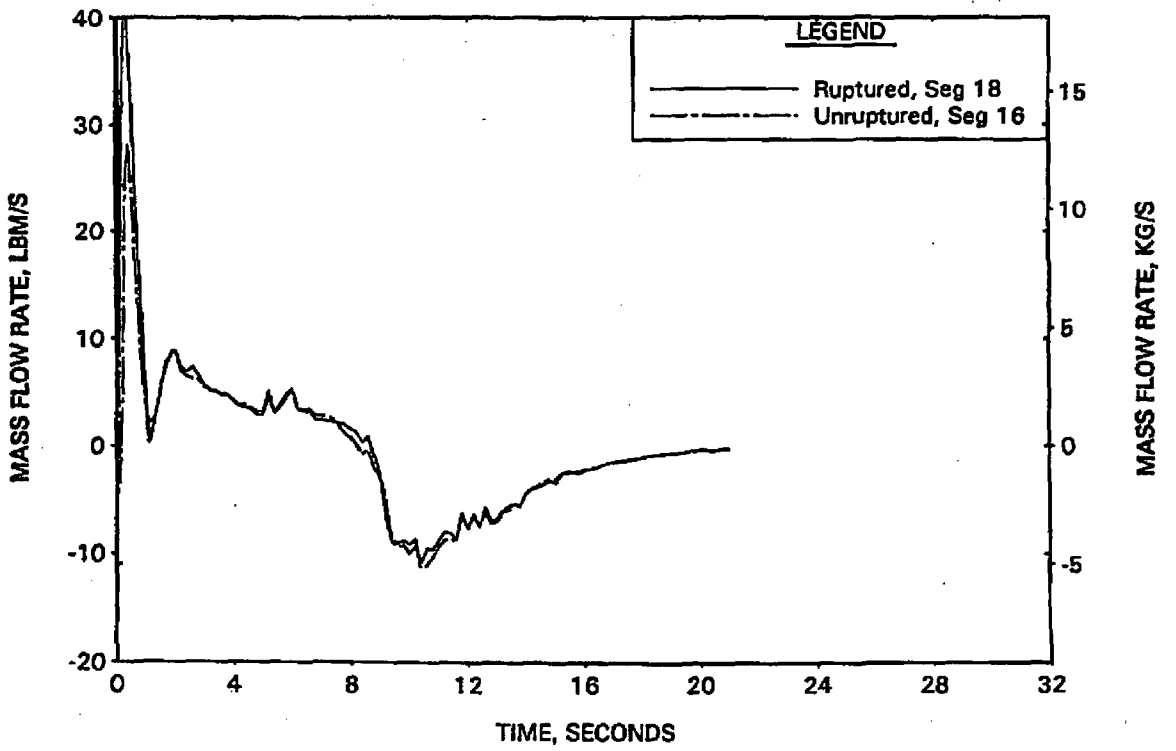

FIGURE A-163. 9.705-FT LOCA LIMIT CASE - CORE FLOODING RATE.

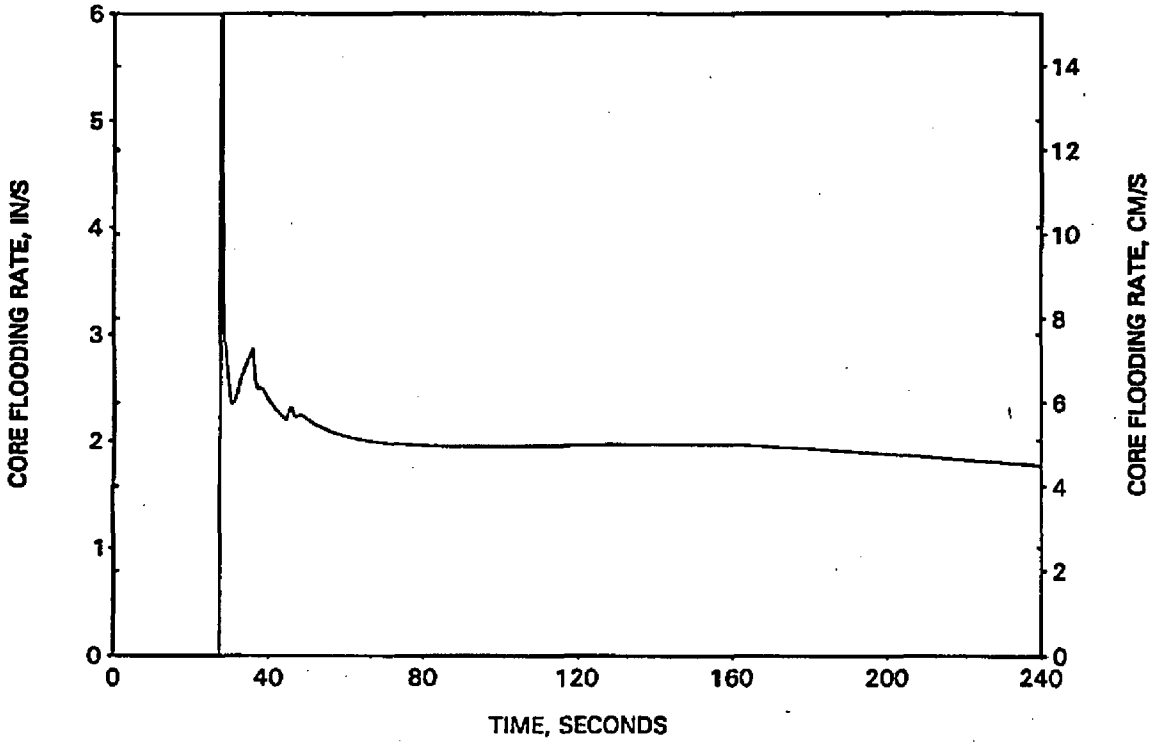

FIGURE A-164. 9.705-FT LOCA LIMIT CASE - HC CLAD TEMP AT RUPTURED AND PEAK UNRUPTURED LOCATIONS.

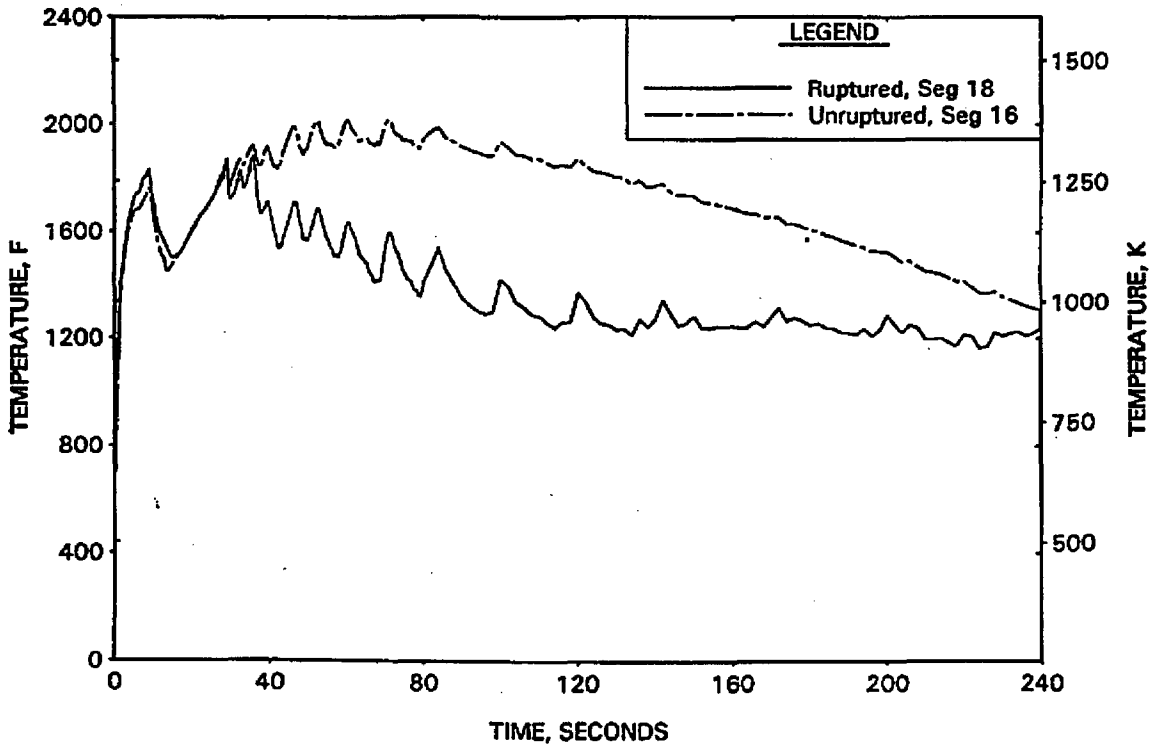

FIGURE A-165. 9.705-FT LOCA LIMIT CASE - FILTERED HC HTC AT RUPTURED AND PEAK UNRUPTURED LOCATIONS.

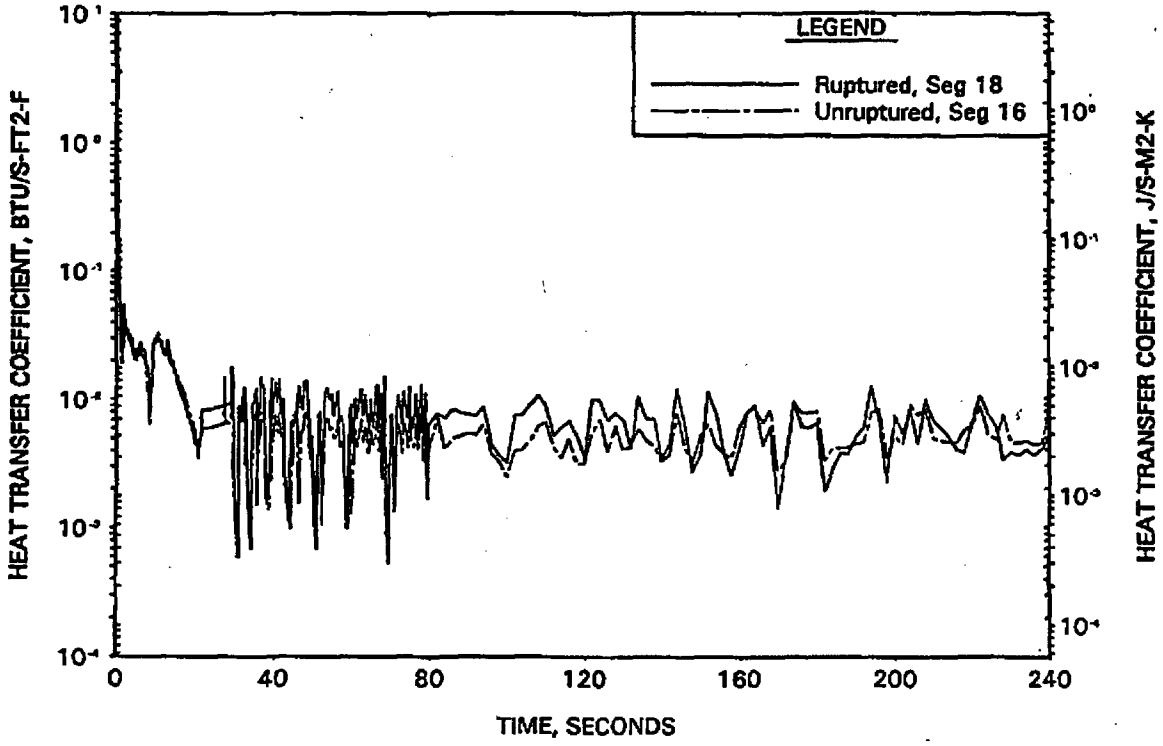

FIGURE A-166. MINIMUM VS MAXIMUM ECCS STUDY - CONTEMPT CONTAINMENT PRESSURE.

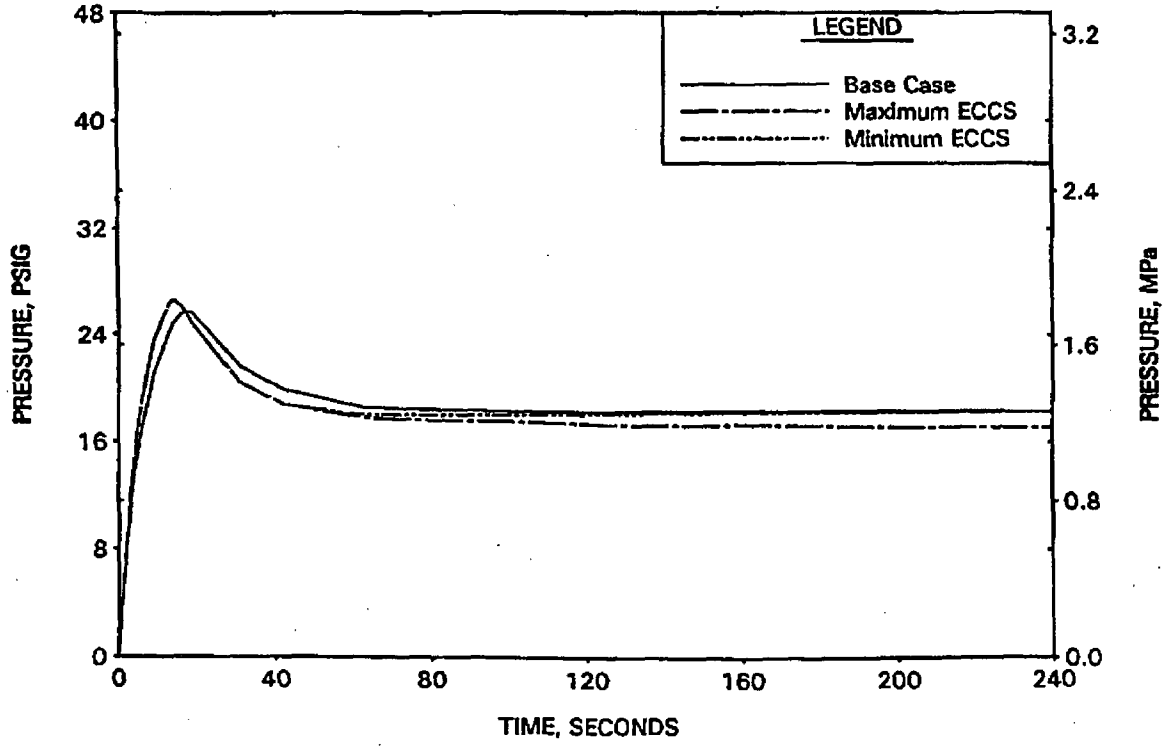

FIGURE A-167. MINIMUM VS MAXIMUM ECCS STUDY - CORE FLOODING RATE.

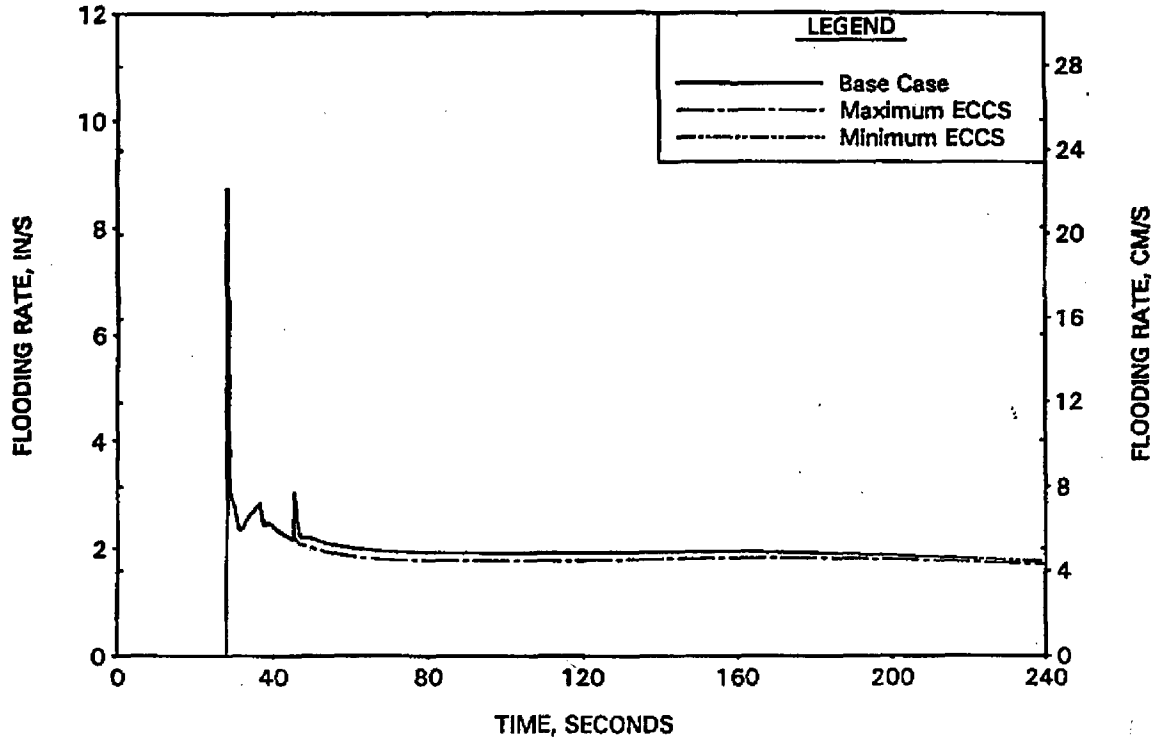

FIGURE A-168. MINIMUM VS MAXIMUM ECCS STUDY - CORE WATER LEVEL.

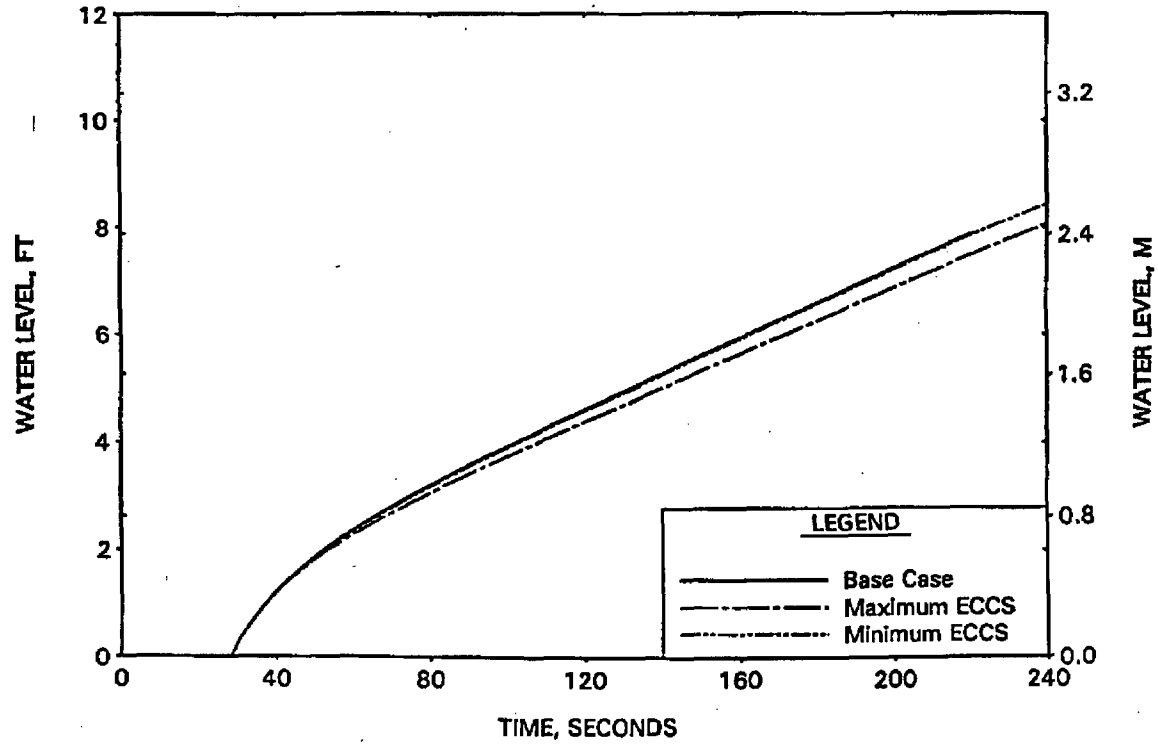

FIGURE A-169. MINIMUM VS MAXIMUM ECCS STUDY - DOWNCOMER WATER LEVEL.

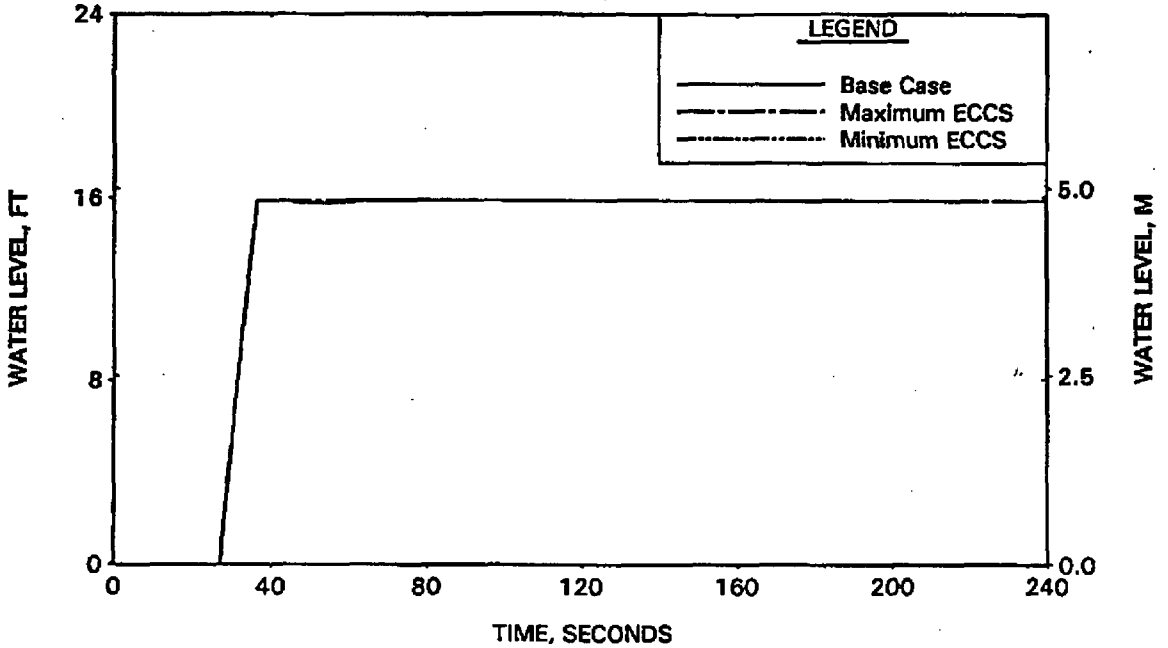

FIGURE A-170. MINIMUM VS MAXIMUM ECCS STUDY - CARRYOUT RATE FRACTION.

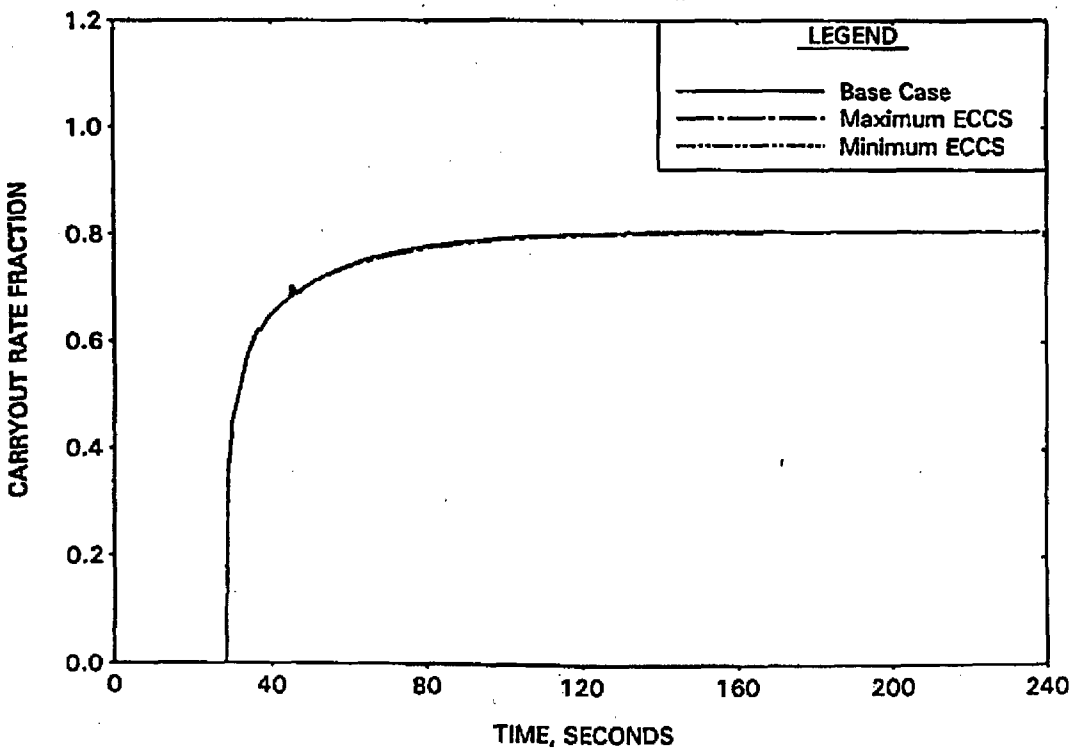

FIGURE A-171. MINIMUM VS MAXIMUM ECCS STUDY - HC CLAD TEMP AT RUPTURED LOCATION.

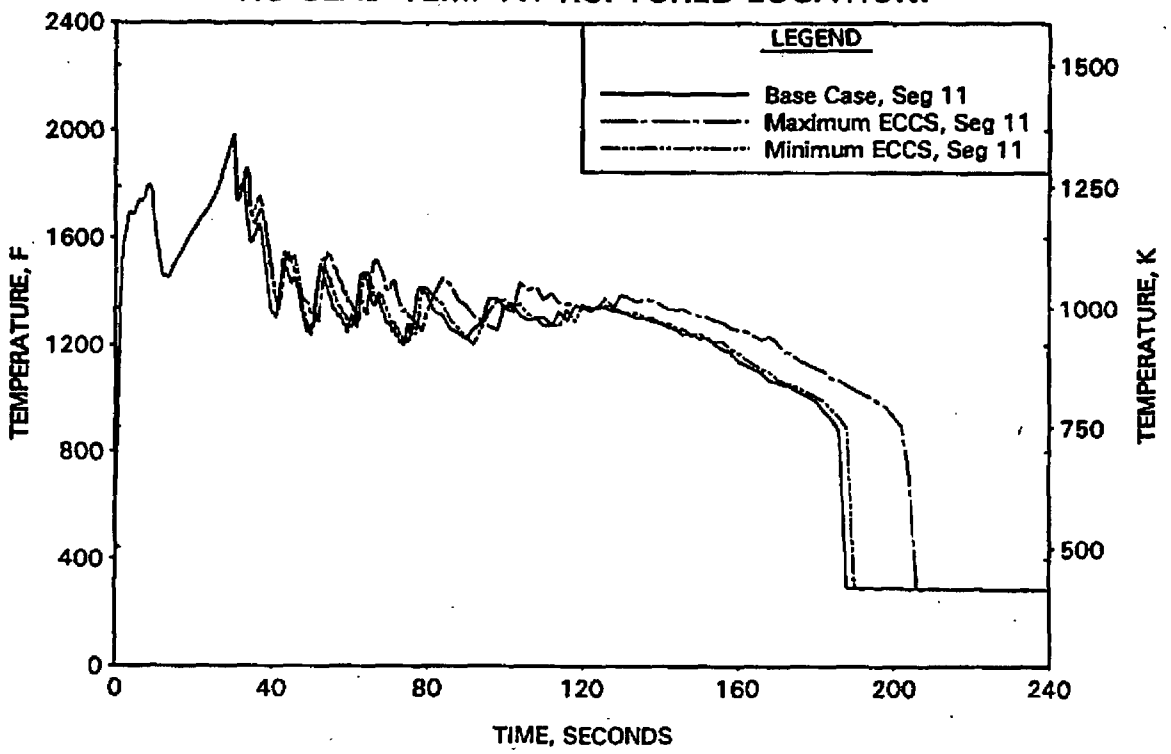

FIGURE A-172. MINIMUM VS MAXIMUM ECCS STUDY - HC CLAD TEMP AT PEAK UNRUPTURED LOCATION.

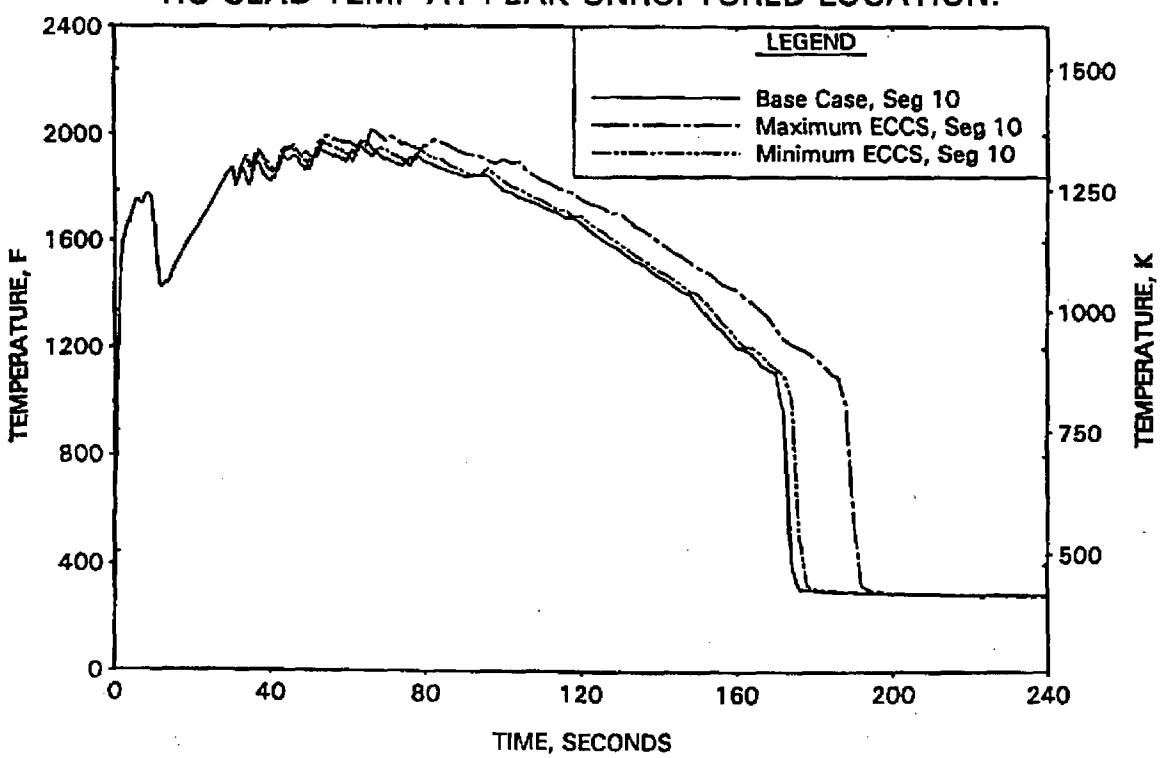

FIGURE A-173. MINIMUM VS MAXIMUM ECCS STUDY - FILTERED HC HTC AT RUPTURED LOCATION.

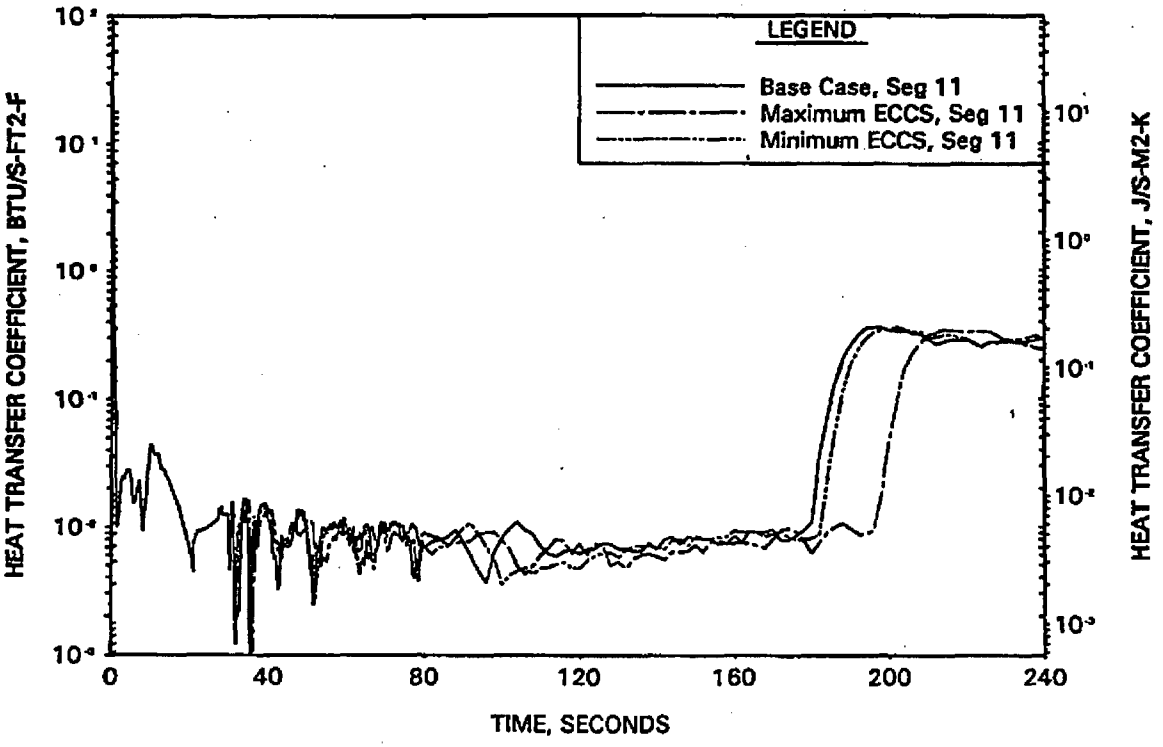

FIGURE A-174. MINIMUM VS MAXIMUM ECCS STUDY - FILTERED HC HTC AT PEAK UNRUPTURED LOCATION.

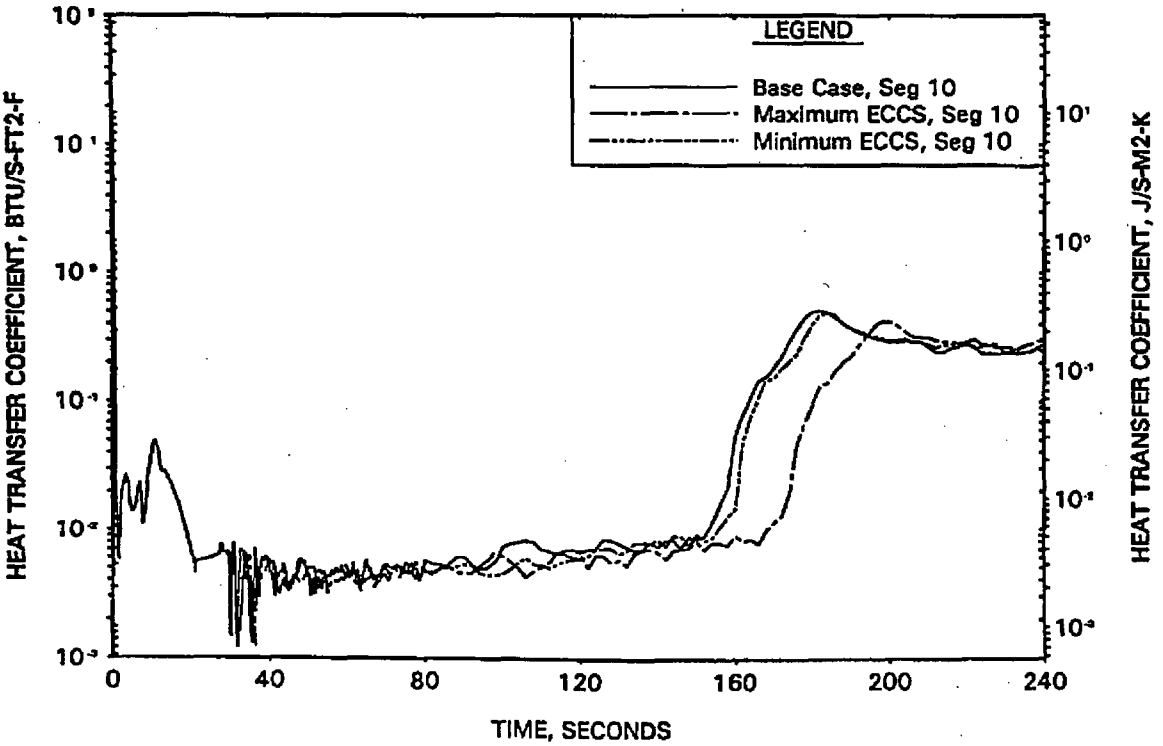

FIGURE A-175. MINIMUM VS MAXIMUM ECCS STUDY - HC QUENCH FRONT ADVANCEMENT.

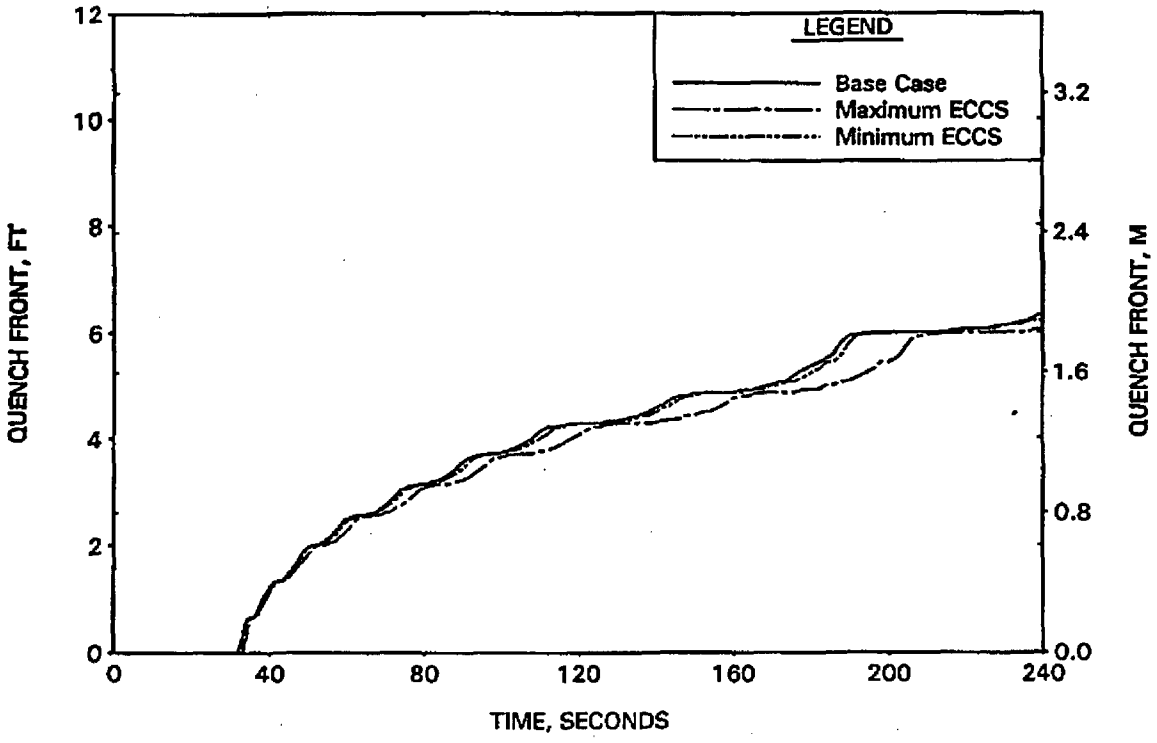

FIGURE A-176. MINIMUM VS MAXIMUM ECCS STUDY - AC QUENCH FRONT ADVANCEMENT.

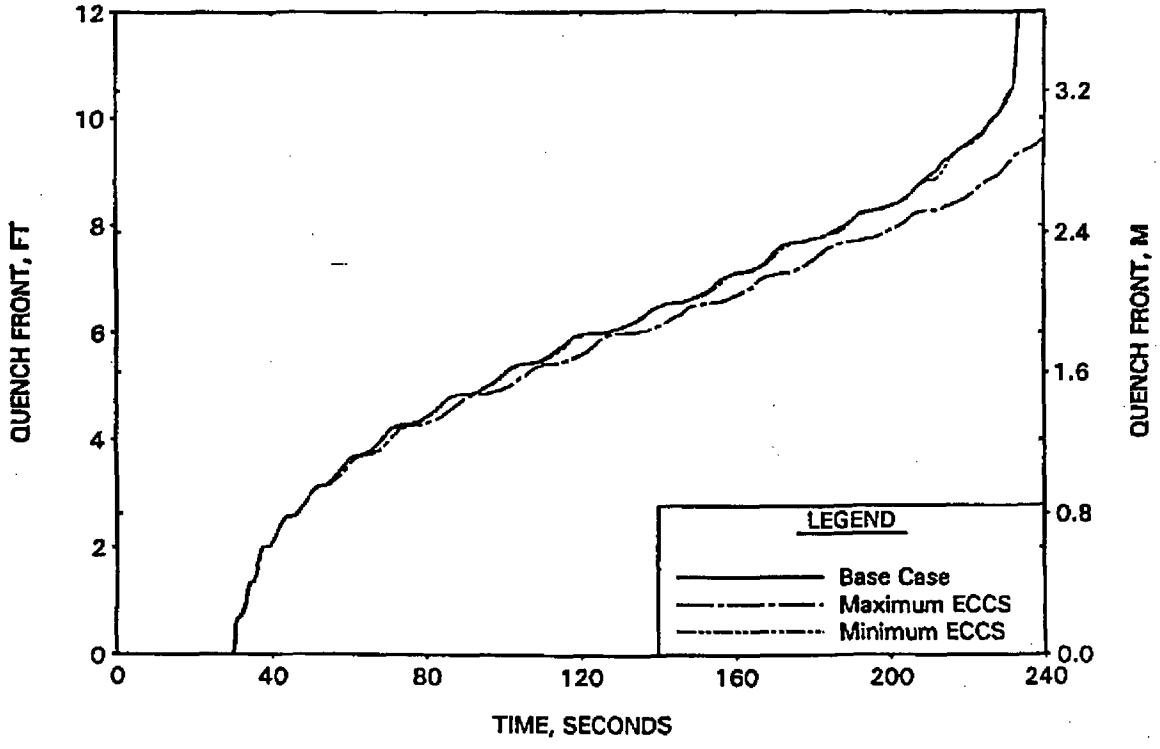

FIGURE A-177. MOST SEVERE BREAK CASE - REACTOR VESSEL UPPER PLENUM PRESSURE.

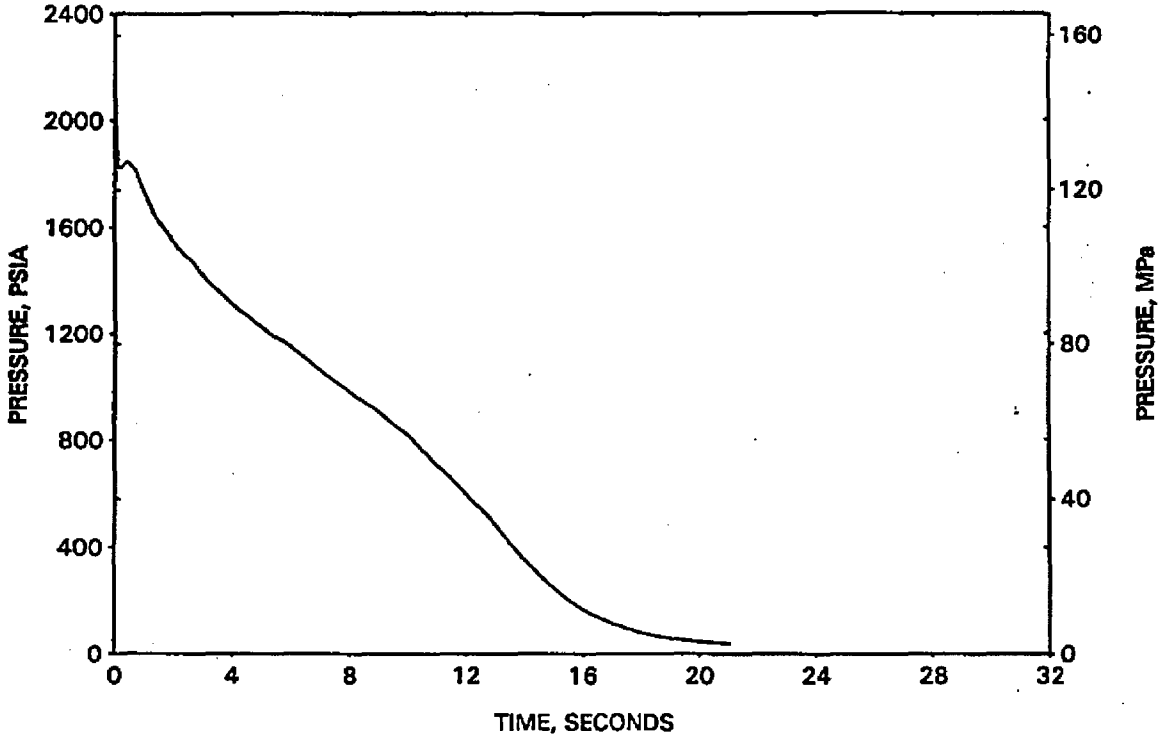

FIGURE A-178. MOST SEVERE BREAK CASE - BREAK MASS FLOW RATE.

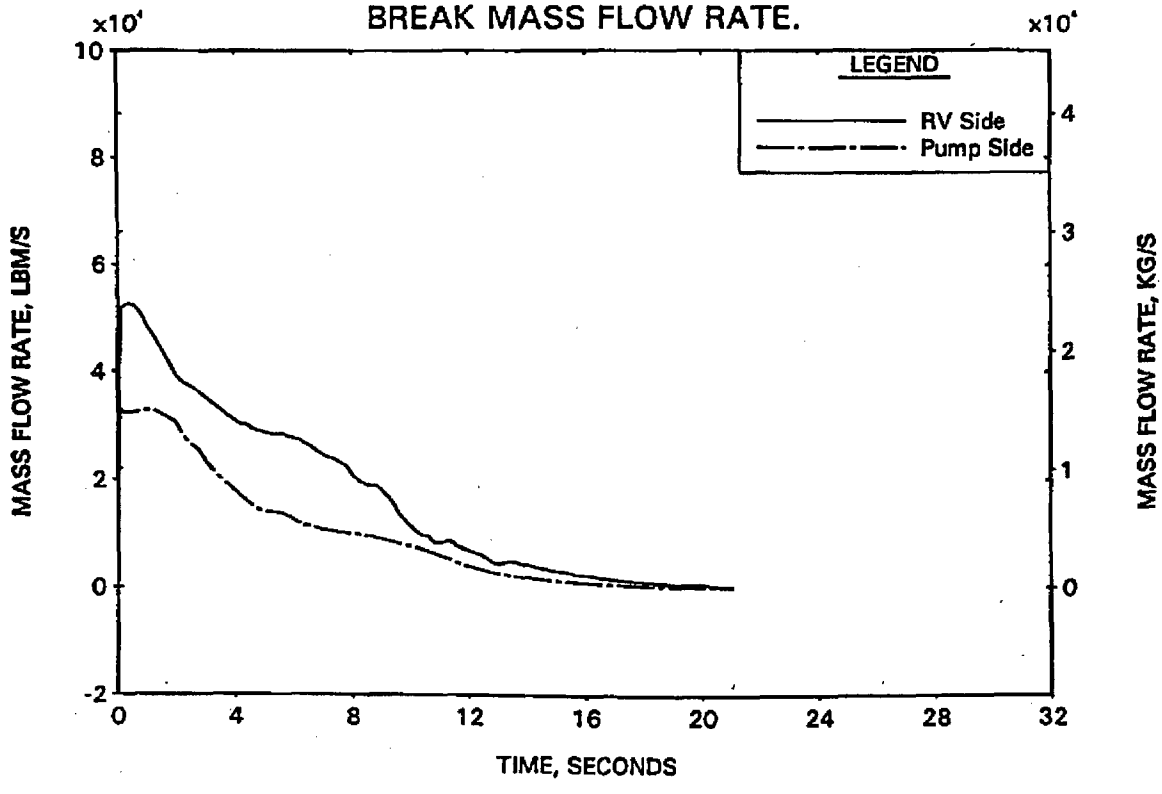

FIGURE A-179. MOST SEVERE BREAK CASE - HC MASS FLOW RATES AT RUPTURED AND PEAK UNRUPTURED LOCATIONS.

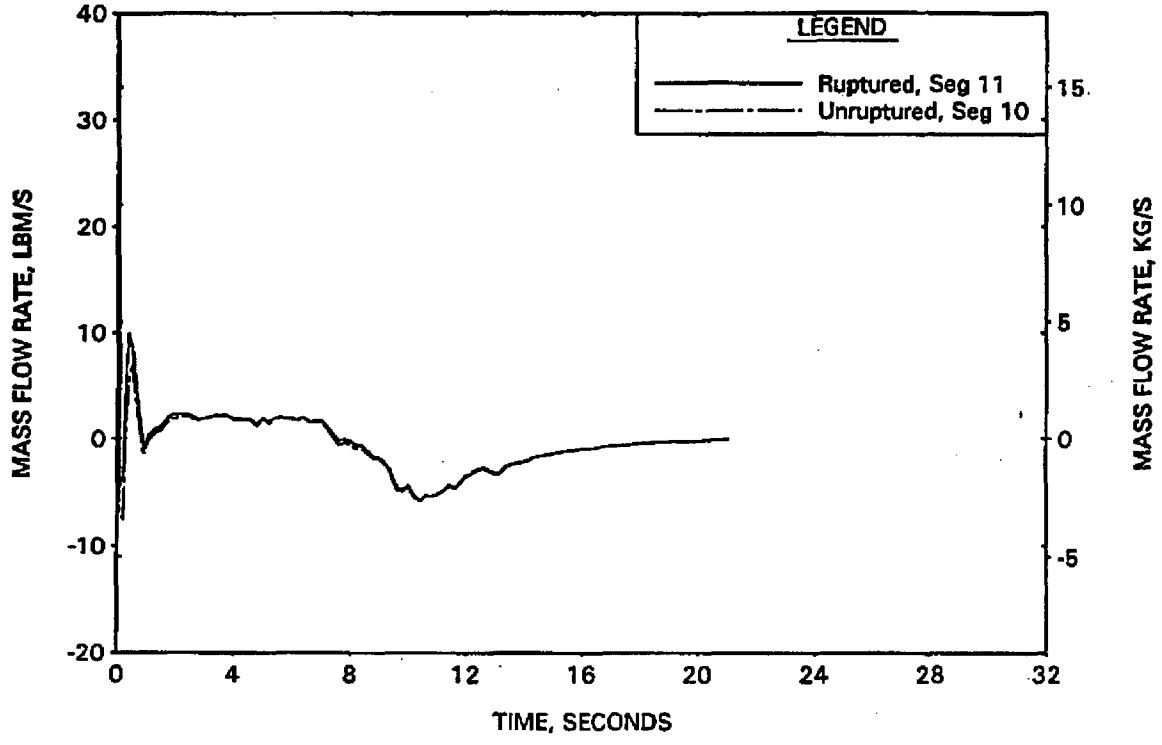

FIGURE A-180. MOST SEVERE BREAK CASE - CORE FLOODING RATE.

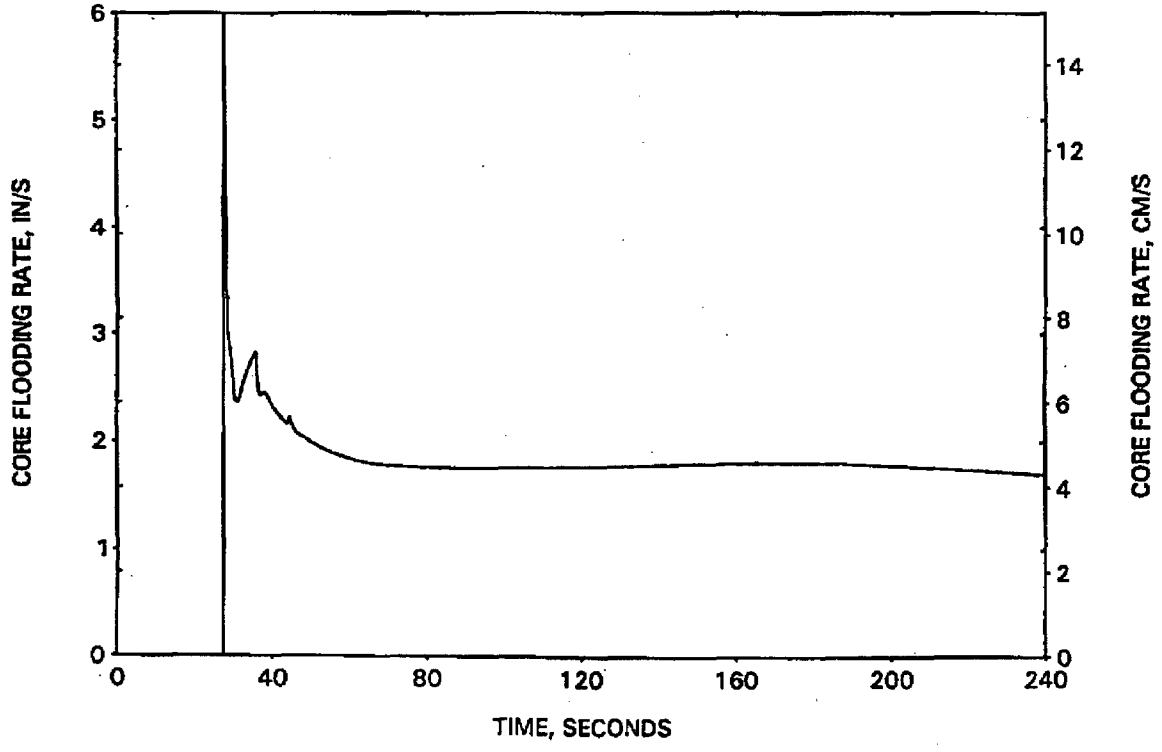

FIGURE A-181. MOST SEVERE BREAK CASE - HC CLAD TEMP AT RUPTURED AND PEAK UNRUPTURED LOCATIONS.

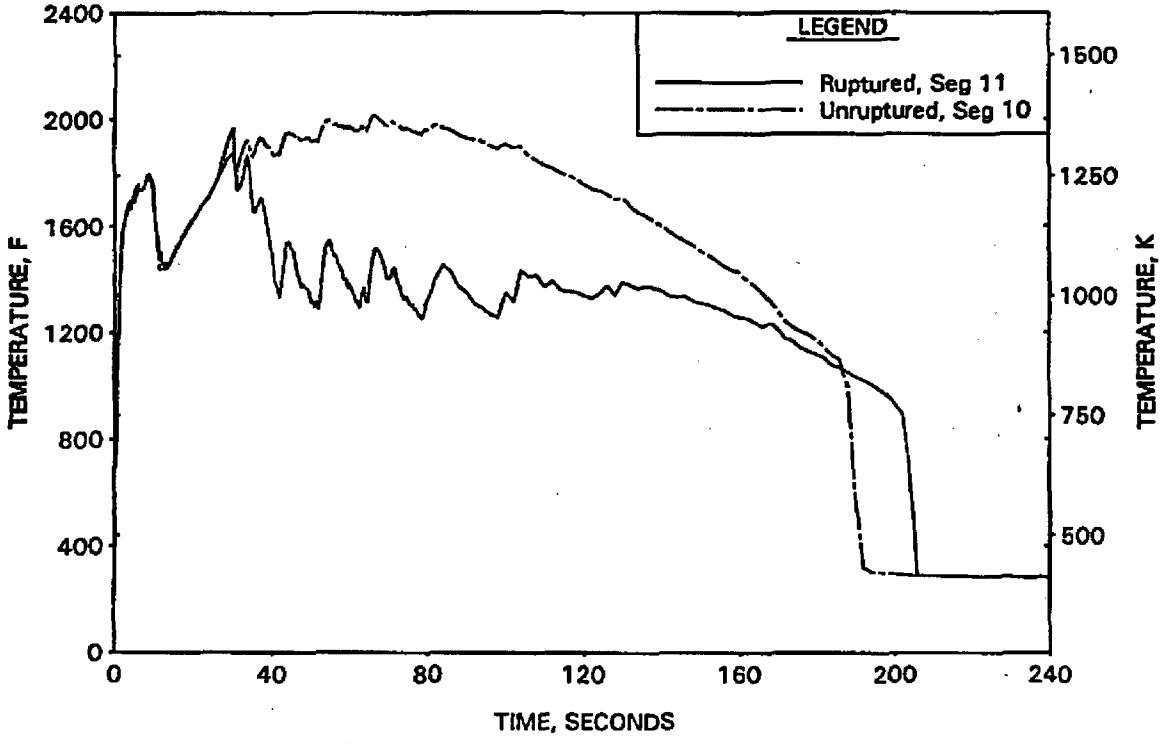

FIGURE A-182. MOST SEVERE BREAK CASE - HC FUEL TEMP AT RUPTURED AND PEAK UNRUPTURED LOCATIONS.

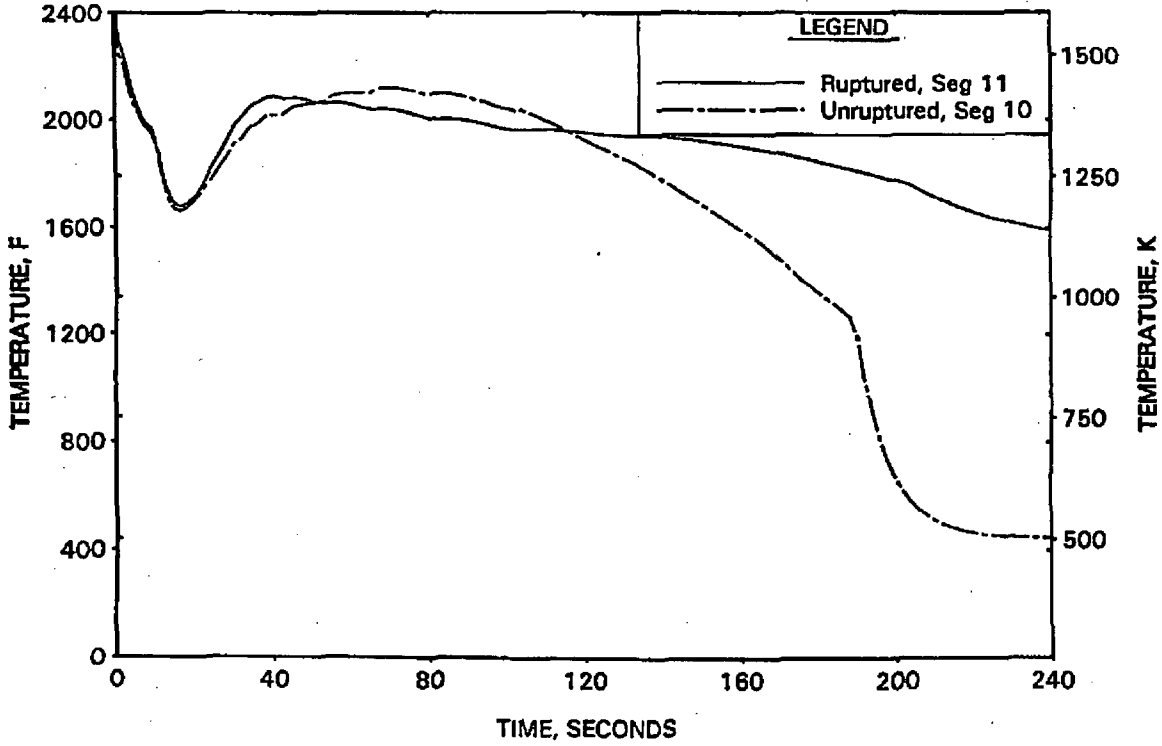

FIGURE A-183. MOST SEVERE BREAK CASE - FILTERED HC HTC AT RUPTURED AND PEAK UNRUPTURED LOCATIONS.

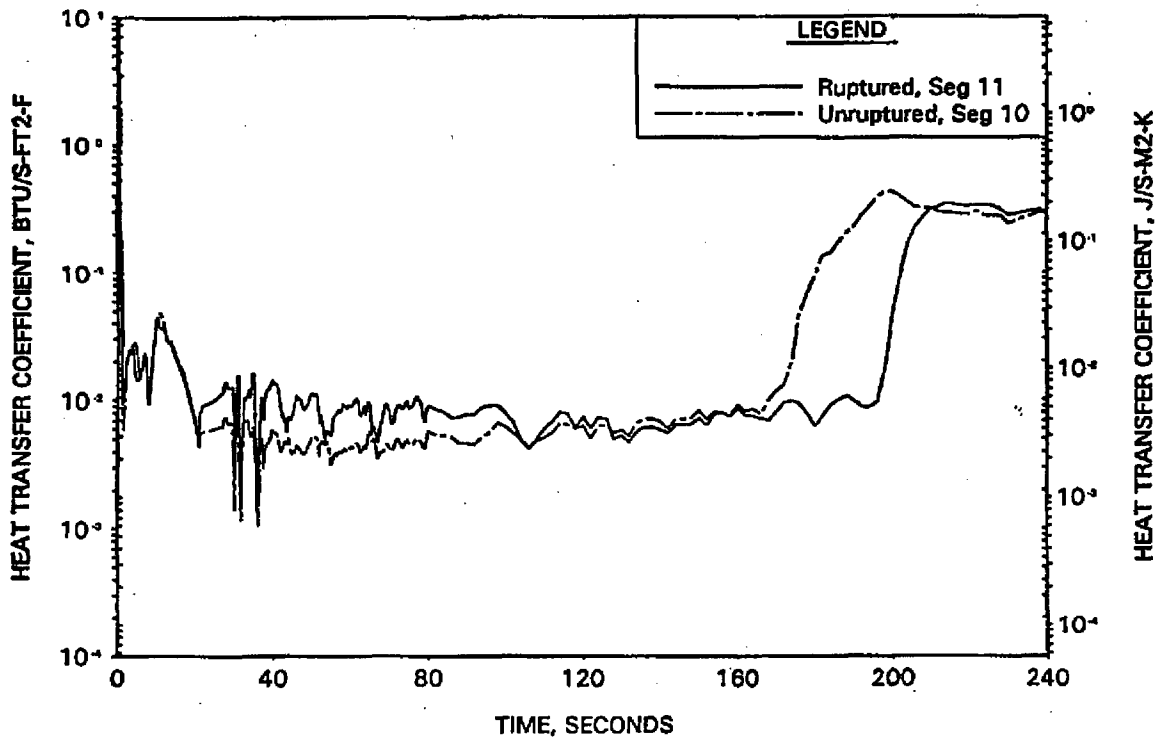

FIGURE A-184. MOST SEVERE BREAK CASE - QUENCH FRONT ADVANCEMENT.

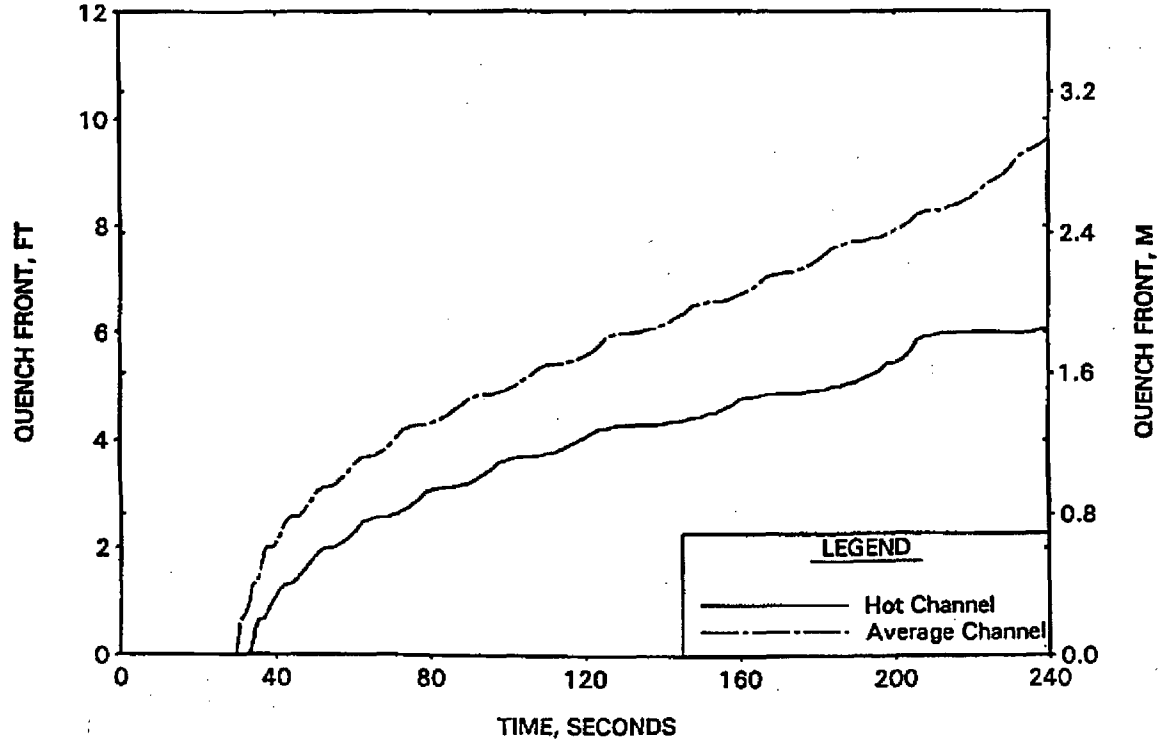

FIGURE A-185. REPRESENTATIVE PCT VERSUS BREAK SIZE.

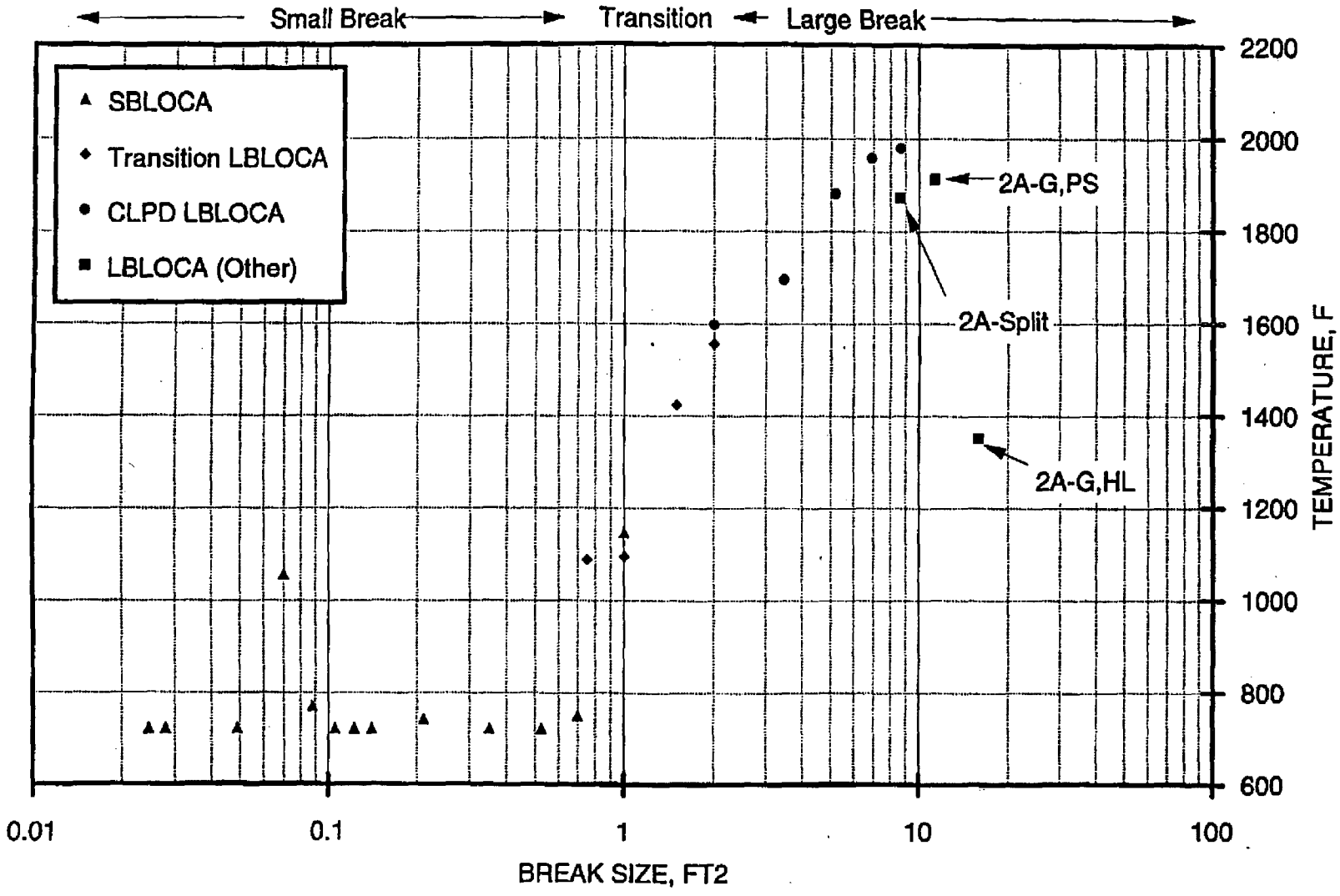

AREVA NP, INC.

BAW-10192NP-02

BAW-10192NP

Topical Report
Revision 2
August 2008

- BWNT LOCA -

BWNT Loss-of-Coolant Accident
Evaluation Model for Once-Through
Steam Generator Plants

Volume II - Small Break

B AREVA NP Inc.
P. O. Box 10935
Lynchburg, Virginia 24506

This page is intentionally left blank.

Copyright © 2008

AREVA NP Inc.
All Rights Reserved

This page is intentionally left blank.

AREVA NP Inc.
Lynchburg, Virginia 24506

Topical Report BAW-10192NP
Revision 2
August 2008

- BWNT LOCA -

BWNT Loss-of-Coolant Accident Evaluation Model for Once-Through Steam Generator Plants

Volume II - Small Break

Key Words: Small Break, LOCA, Transient, Water Reactors, Evaluation Model

ABSTRACT

This document presents the generic large and small break models to be used by AREVA NP Inc. (previously known as Babcock & Wilcox, B&W Nuclear Technologies, or BWNT) for evaluating the performance of the emergency core cooling systems (ECCS) following a loss-of-coolant accident (LOCA) for all classes of B&W-designed pressurized water reactors (PWR). The large break model is discussed in Volume I and the small break model in Volume II. Volume III is the licensing addendum, which provides a historical record of related correspondence including responses to NRC questions, NRC Safety and Technical Evaluation Reports, and NRC approval letters. The models have been developed and compared with the required and acceptable features contained in Appendix K of the Code of Federal Regulations, 10CFR50. The evaluation models are shown to conform to Appendix K requirements.

This page is intentionally left blank.

ACKNOWLEDGMENT

AREVA NP Inc. wishes to acknowledge the effort by J. A. Klingenfus, K. S. Pacheco, and W. T. Sneed in preparation of the material and completion of the analyses contained in this topical report.

This page is intentionally left blank.

Topical Revision Record

Volume II - Small Break

Documentation

Revision	Description
0	Original Issue
1	Revision of LBLOCA model Volume I only. (This revision was withdrawn and therefore was not approved)
2	Update NCR-approved source references (e.g. RELAP5, BEACH, M5) Modify Rev. 0 texts to reflect the methods from new source references approved by the NRC (e.g. hot pin methodology, Gadolinia) Expand the discussions on coolable geometry and long-term cooling (e.g. GSI-191) Add references to the RAIs in the main document Typographical corrections (Changed pages from Rev. 1 are not included in Rev. 2)

This page is intentionally left blank.

VOLUME II CONTENTS

VOLUME II CONTENTS (Cont'd)

List of Tables

List of Figures

List of Figures (Con't)

List of Figures (Con't)

List of Figures (Con't)

List of Figures (Con't)

List of Figures (Con't)

List of Figures (Con't)

List of Figures (Con't)

List of Figures (Con't)

List of Figures (Con't)

List of Figures (Con't)

List of Figures (Con't)

List of Figures (Con't)

This page is intentionally left blank.

1. INTRODUCTION

This report describes the features of the emergency core cooling system (ECCS) evaluation model (EM) used by AREVA NP Inc. (previously known as Babcock & Wilcox, B&W Nuclear Technologies, or BWNT) for application to all classes of B&W-designed pressurized water reactors (PWRs). The plant designs for which the evaluation model is applicable are categorized in Table 1-1. There are system design differences for the nuclear steam system (NSS) and the ECCS within each category. These systems, however, are broken into components which are similar in both geometry and thermal hydraulic behavior. This similarity enables these component design features to be individually modeled and coupled using consistent techniques in a generic EM applicable to all plant types. Specific design information for each plant category is considered input to the evaluation model and is generated using the assumptions and techniques described herein. The evaluation model can be used for analysis of fuel designs with either Zircaloy or M5 alloy cladding. For core designs employing the M5 alloy for fuel pin cladding, the material properties, inputs, methods, and correlations, described in BAW-10227P-A (Reference 11) shall supersede, as appropriate, those described for Zircaloy within this report

The "Acceptance Criteria for Emergency Core Cooling Systems for Light Water Nuclear Power Reactors" (10CFR50.46) was issued by the NRC in January 1974. Appendix K of 10CFR50 defines the required and acceptable features of models to be used to evaluate the performance of the ECC systems. The information presented in this document defines the BWNT evaluation model and shows that the model conforms to Appendix K requirements.

The topical report is presented in three volumes. The first volume presents the large break evaluation model. The second volume presents the small break evaluation model. Volumes I and II contain the following seven sections, which define the respective evaluation models:

1. Definition of model versus input (Section 3).

2. Features of the evaluation model and statements of conformity to Appendix K (Section 4).

3. The calculational technique used to evaluate the maximum local cladding oxidation (Section 5).

4. The calculational technique used to evaluate the maximum hydrogen generation (Section 6).

5. The technique used to evaluate conformance to the coolable geometry criterion (Section 7).

6. The technique used for establishing conformance to the long-term cooling criterion (Section 8).

7. Required documentation necessary to meet 10CFR50.46 (Section 9).

Volume III, the licensing addendum, is included for the purpose of retaining licensing data, responses to NRC questions, position papers, SERs, etc.

Table 1-1. Applicable PWR Plant Categories.

Plant Category	Number FAs	RCS Loop Geometry	Fuel Design	SG Type	ECCS System
1	177	Lowered	15 x 15	OTSG(1)	High Head HPI
2	177	Raised	15 x 15	OTSG(1)	Low Head HPI
3	205	Raised	17 x 17	IEOTSG	High Head HPI

where

OTSG = Once-Through Steam Generator (Recirculating)
IEOTSG = Integral Economizer Once-Through Steam Generator (Non-Recirculating)
HPI = High Pressure Injection

Note (1)- The 177 FA B&W plants have been planning for and replacing the original OTSGs in combination with life extension activities. The replacement steam generator designs use similar straight shell and tube steam generators and are designated as the "Enhanced" OTSG or "Replacement" OTSG designs. These steam generators are functionally equivalent to the original OTSG such that the evaluation model does not need any changes other than what is required in the input geometrical parameters and heat structure properties in the analytical models. When OTSG is described in the text of the evaluation model it refers to the original as well as the replacement designs.

This page is intentionally left blank.

2. COMPLIANCE TO 10CFR50.46

The "Acceptance Criteria for Emergency Core Cooling Systems for Light Water Power Reactors" (10CFR50.46), issued by the Nuclear Regulatory Commission in January 1974, include five criteria that must be met before an emergency core cooling system is acceptable. Conformance to these criteria is established in the following manner:

1. The peak cladding temperature shall not exceed 2200 F.

   The peak cladding temperature is calculated with the evaluation model described herein and shown not to exceed 2200 F.

2. The percentage of local cladding oxidation shall not exceed 17%.

   In the analysis performed to satisfy Criterion 1, the EM calculated total oxide thickness (combining both inside and outside oxide layers) at the location of maximum local oxidation is calculated and shown to be less than 0.17 times the total cladding thickness. A supplemental check of the local oxidation limits with respect to a realistic initial oxidation (or pre-accident oxidation) plus the accident-induced oxidation is also included as described in Section 5.

3. The maximum hydrogen generated during the transient shall not exceed that which would be generated by the oxidation of 1% of the reactor cladding.

   The amount of core wide zirconium oxidation which occurs during a small break LOCA is generally much less than for large break LOCA due to the lower cladding temperatures

and the smaller portion of the core that has a significant temperature excursion. This criterion is satisfied by a conservatively determined approach which interpolates and integrates the hot and average channel local oxidation values over the core power distribution. The final oxidation fractions are reduced by the initial values to calculate the additional oxidation, and therefore the total hydrogen production during the LOCA. This criterion is satisfied by showing that the increase in core-wide metal-water oxidation is less than one percent.

4. Calculated changes in the core geometry shall be such that the core remains amenable to cooling.

   The changes in geometry that were calculated during the analysis for Criterion 1 are examined to ensure that no gross core blockage or deformation occurs when it is combined with external analyses not explicitly controlled by this Evaluation Model as described in Section 7.

5. The mode of long-term cooling shall be established.

   The analysis is continued until the cladding temperatures at all locations in the core have decreased to near the coolant saturation temperature, the core is covered by two-phase coolant mixture, a stable thermal-hydraulic configuration has been established, and no additional challenges to core cooling are foreseen. At this time the path to long-term cooling is established. Cooling for the long-term is established by pumped injection with no interruptions or decreases in coolant flow thereby maintaining the core temperature at an acceptably low value while removing decay heat. Section 8 gives additional details for showing compliance with this criterion.

Appendix K sets forth certain required and acceptable features of the evaluation model that must be used to show compliance to the five acceptance criteria of 10CFR50.46. Compliance of the BWNT evaluation model to Appendix K is shown in Section 4.

This page is intentionally left blank.

3. DEFINITION OF SBLOCA MODEL VERSUS INPUT

The information presented in this document defines the AREVA ECCS evaluation model for application to all B&W-designed plants. In particular, this document describes the techniques and assumptions used in the evaluation of the consequences of a loss-of-coolant accident. These techniques and assumptions constitute the model. The required features of the ECCS evaluation model are set forth in Appendix K to 10CFR50. The evaluation model for small breaks is given in Chapter 4 along with statements of its conformance to Appendix K. The evaluation model will be changed only if the NRC issues rule changes or if improved analytical techniques become available.

Specific category-related information (such as system design, power level, etc.) is considered input to the model. These numbers are developed using the techniques and assumptions described in the model. This report covers the model only. All other information needed to perform the necessary analyses is considered input. Input may change throughout the design life of a nuclear steam system requiring a reapplication of the evaluation model while not affecting the evaluation model per se.

This page is intentionally left blank.

4. SMALL BREAK EVALUATION MODEL

4.1. Model Applicability

The small break evaluation model described in this section is applicable to all the general plant categories presented in Table 1-1. Any item that is applicable only to certain plant categories due to differences in design, such as RCS geometry, containment pressure, ECCS design or fuel design will be specifically identified. There are no significant RCS design differences between the plants within each category.

4.2. Transient and Computer Code Description

A postulated RCS piping break is considered to be a small break when the cladding departure from nucleate boiling (DNB) does not occur within the first few seconds after break opening. SBLOCA analyses are used to determine the maximum cross-sectional break areas up to 0.75 ft^2 that do not show initial clad DNB. The break range, which is established at nominal, full power conditions with all RCPs operating, is generally from 0.5 to 0.75 ft^2 and is dependent on the fuel design and plant boundary conditions (e.g. SGTP, RCS flow, RCS average temperature) used in the analysis. The large and small break studies with this EM have shown that the large break phenomena of ECC bypass and reflood do not apply to breaks of this size or smaller. The brief description of the behavior of small break transients that follows identifies the major phenomena simulated in the evaluation technique.

In general, a small break loss-of-coolant transient begins with a subcooled depressurization of the RCS to the hot leg and reactor vessel upper plenum saturation pressure. This is followed by an extended saturated blowdown. If the reactor coolant (RC) pumps continue to operate, the resultant forced circulation provides effective and continuous core cooling throughout the transient.

The reactor coolant system void fraction will increase (frequently coming quite close to total voiding) until the decay heating rate, the ECCS injection, and the break flow come into equilibrium. Thereafter, the system void fraction will slowly decrease as excess ECCS water is injected, and the decay heating rate continues to decline. Eventually the system will depressurize sufficiently to be put into a long-term cooling configuration. Because of the near-total voiding of the system, the NRC has required that the reactor coolant pumps be manually or automatically tripped early in the transient. Therefore, most SBLOCA analyses are performed with the RC pumps assumed off-line.

If the RC pumps do not continue to operate, the transient evolves in a more complicated fashion. Beginning at RC pump coastdown, the system undergoes a transition from forced flow conditions to natural circulation. During the saturated blowdown phase, steam and water will separate within the RCS leading to the formation of trapped steam pockets in the upper reactor vessel and upper hot leg regions. Core heat transfer is by pool nucleate boiling and is adequate to keep the cladding cool so long as the core is covered by a mixture of steam and water. Loss of RCS liquid inventory continues until the ECCS injection rate matches the total RCS flashing and boiling contributions. If the liquid inventory loss is severe, part of the core may uncover. The portion of the core above the mixture level will be cooled by steam flow. Generally, the steam flow rates are insufficient to maintain the cladding near the saturation temperature and the cladding temperature increases. Continued depressurization of the system eventually allows the ECCS injection to match the declining decay heat boiloff rate. With the decrease in system inventory halted, the vessel and RCS begin to refill. Eventually, the system is depressurized to a condition at which it can be placed in long-term cooling.

The RELAP5/MOD2-B&W (Ref. 1) code is used to predict the reactor coolant system thermal-hydraulic behavior, the average core and

hot channel void distributions, and the hot and average core cladding temperature response. This allows the continuous, integrated determination of all physical parameters affecting the peak cladding temperature, other than the containment pressure. The containment pressure is set conservatively high or provided by CONTEMPT (Ref. 2) analyses for those break sizes for which the break flow could unchoke. Additional information for containment pressure is provided in the RAI response to Question 2 in Volume III page LA-59.

4.3. Features of Model

This section addresses the features of the BWNT small break evaluation model for plants with once-through steam generators. Compliance of the model with 10CFR50, Appendix K, is described in Section 4.4. The evaluation model described sets forth guidelines for the use of various code options and models. The organization parallels that of Appendix K.

4.3.1. Heat Sources

The analysis considers the heat sources listed below. These sources are time-dependent, and calculation of the heat sources within the code is dependent on the phase of the accident.

4.3.1.1. Initial Power

It is assumed that the reactor has been operating continuously at the analyzed power level which is at or above the licensed power plus uncertainties due to power level instrument errors. A value of 2 percent of rated power is used for the uncertainty unless the uncertainty is demonstrated to be smaller.

4.3.1.2. Core Peaking Factors

The core peaking factor is that of an outlet skewed power profile, shown in Figure 4-1, with the hot channel radial peaking factor adjusted to be consistent with or above the technical specification limit for that elevation. The location of the peak corresponds to the LBLOCA axial peak of [ ] which is specified at the mid-point between fuel spacer grids containing the 10-ft elevation. This outlet peak creates a conservative peak cladding temperature (PCT) simulation by reducing the power and the corresponding boiling contributions in the lower core region. Reduction of the pool boiling leads to less mixture level swell and less steam flow available to cool any uncovered portions of the fuel rods. The skewed peak also produces higher heating rates in the uncovered core region.

4.3.1.3. Core Stored Energy

The initial temperature distribution and other related parameters for the core and hot channel will be obtained as for large break LOCA evaluations (Section 4.3.2.3 of Volume I of this report). This section specifies the use of an NRC-approved steady-state fuel pin model (currently TACO3 for UO_2 fuel, or GDTACO for gadolinia fuel, Ref. 3 and Ref. 9) as the source of the initial fuel volume-averaged temperatures and pin parameters for use in the analyses. The average fuel temperatures will be adjusted using a pin gap conductance multiplier to match within 20 F, those predicted by the fuel thermal code.

4.3.1.4. Fission Heat

The fission power of the reactor is calculated using the point kinetics model in the RELAP5/MOD2-B&W computer code (described in

Section 2.3.1 of BAW-10164). Credit is taken for reactor trip and control rod insertion. The response of the RCS following a small break is characterized by slow reductions in RCS pressure and system flow. These reductions result in lower forces (ΔP and flow) opposing control rod insertion than those present during normal operation. Thus, control rod insertion is credited upon initiation of the low RCS pressure reactor trip. Provisions are made to analyze this event conservatively; that is, a minimum tripped rod worth is used with appropriate delay and insertion times. The core is assured to be shut down by the fully inserted control rods and the borated water supplied by all of the ECC systems.

4.3.1.5. Decay of Actinides

The power from the decay of actinides is included. The calculation conservatively accounts for the energy generated from the radioactive decay of actinides, including neptunium, plutonium, and the isotopes of uranium. (There is additional information provided in the RAI response to Question 5 in Volume III page LA-94.)

4.3.1.6. Fission Product Decay Heat

The ANS standard fission product decay heat curve for infinite irradiation published in October 1971 is used with a factor of 1.2 to determine fission product decay heat during the analysis. The coefficients used to produce total fission product decay plus actinide contributions shown in Figure 4-7 of Volume I are specified as inputs to the RELAP5/MOD2-B&W reactor kinetics model.

4.3.1.7. Heat Distribution

The hot channel represents [ ] fuel assemblies that are peaked to a factor consistent with that of the highest power rod. A fraction of the neutrons and gamma particles generated in the hot channel leak into the surrounding bundles. In turn, neutrons and gamma particles from the surrounding bundles are absorbed within the hot channel. Since the hot channel has a higher radial power, the net power deposited within the fuel of the hot channel is less than that generated within the bundle. Therefore, an energy deposition factor is used within the analyses to account for the fraction of hot channel power that originates within the fuel pellet of the hot channel. The fraction of the power lost from the hot channel (sometimes referred to as power flattening)is deposited uniformly in the fluid of the average channel.

SBLOCA analyses with urania-gadolinia fuel are generally not performed. The peaking of the gadolinia fuel is reduced from the UO_2 fuel peaking to account for changes in the thermal-conductivity and volumetric heat capacity associated with the urania-gadolinia fuel. These reductions are important during the LBLOCA transient to ensure that the PCT of the UO_2 fuel pins bounds that of the gadolinia fuel pins. When lower peaking factors are considered for the slower evolving SBLOCA transient, the gadolinia PCT will be less than the UO_2 PCT. If the gadolinia peaking reduction is not applied, then additional justification for the gadolinia PCT is needed.

[

]

[ ]

The power at the peak in the core (PLP) is evaluated by the following formula:

$$PLP = \frac{(1.0 + U) \times kW \times P_f \times F \times P(t)}{\text{total pin feet in core}}, \quad (4\text{-}1)$$

where

PLP = (peak linear power) linear heating rate, kW/ft,
kW = rated power, kW,
P_f = total peaking factor,
F = appropriate power distribution factor, and
P(t) = normalized transient power,
U = Fractional power level increase to account for uncertainties. It is taken as 0.02 unless the plant has installed equipment that can be used to justify reduced instrument uncertainties.

[ ]

4.3.1.8. Metal-Water Reaction

The rate of energy release from metal-water reaction is calculated by the implicit form of the Baker-Just rate equation without steam limiting. Details of the model appear in Section 2.3.2.4 of BAW-10164 (RELAP5/MOD2-B&W).

The initial oxide thicknesses on the outside and inside cladding surfaces are beginning-of-life values (minimum thickness) or consistent with the time in life that maximizes peak cladding

temperature. The initial thicknesses are calculated as described in Section 4.3.2.8 of Volume I of this topical report.

4.3.1.9. Primary Metal Heating

Heat transfer from the reactor vessel walls, piping, and non-fuel internal structures are taken into account. Appropriate metal slabs are simulated in each control volume of the RELAP5/MOD2-B&W model using the system heat transfer model. The general heat structure model for RELAP5/MOD2-B&W is explained in Section 2.2 of BAW-10164. A previous sensitivity study on the effect of increasing the primary heat addition (Section 5.7 of topical report BAW-10091, Ref. 4) showed minimal effect for this heat source in a small break application.

4.3.1.10. Primary-to-Secondary Heat Transfer

Primary-to-secondary heat transfer in the steam generator is modeled to allow the secondary side to act as a heat sink as well as a heat source during an analysis using the models and heat transfer correlations described in Section 2.2 of BAW-10164. Operator actions identified in the Emergency Operating Procedures Technical Bases Document (Ref. 8) may be credited to mitigate the severity of the transient. Specific actions include increasing the secondary side level to error-adjusted minimums and initiating a continuous secondary side cooldown at reasonable rates and times as defined in the guidelines. The operator actions credited in any analyses will be documented and justified in plant-specific SBLOCA EM calculations. Plant-specific levels of steam generator tube plugging (SGTP) will be considered and included in the physical model inputs as appropriate.

4.3.2. Reactor System Hydrodynamics

4.3.2.1. Noding Scheme for RELAP5/MOD2-B&W

The noding description of the RCS used in the RELAP5/MOD2-B&W computer model for small break analysis is shown in Figures 4-2 through 4-5 for the 205-FA plant design. Figures 4-6 and 4-7 show the loop and steam generator noding arrangements to be used for the 177-FA lowered-loop plant analyses. The 177-FA raised-loop

arrangement allows for the computation of hot channel cladding and vapor temperatures independent of the average core and provides resolution of the mixture height to within [ ]. Upper and lower unheated core regions are simulated to better represent the void fraction distribution at the top and bottom of the core.

[

]

The control volumes are selected to preserve key volumes in the system: (1) volume in the RV below the bottom of the active fuel, (2) volume below the top of the active fuel, (3) reactor vessel volume below the bottom of the hot and cold leg nozzles, (4) loop volume below the RC pump spillover point, (5) cold leg volume on either side of the pump spillover point, and (6) hot leg piping volumes split at the top of the U-bend. As in the large break noding scheme, the small break noding is a two-by-four

representation of the RCS with a pressurizer connected to the intact loop.

4.3.2.2. Break Noding and ECCS Injection Simulation

Cold Leg Breaks

[

]

[

]

ECCS flow rates and splits for the pumped injection systems are normally determined by a network analysis outside of the evaluation model. Within the evaluation model calculations, the flows are specified as tables of injection flow rate versus pressure. In determining the injection tables, the ECCS piping and valve arrangements are selected to minimize injection into the intact loops. The discharge pressure for the ECCS will generally be the RCS pressure with the multiple discharge paths all flowing against a downstream control volume pressure. For a rupture within the ECCS system, the effect of the pressure drop across the break and ECCS-RCS mixing is considered. This may, as in the double-ended rupture of the HPI or CFT line, require that one of the multiple discharge paths of an ECC system discharge directly to containment.

[

]

[ ]

Hot Leg Breaks

For a hot leg break, the special ECCS noding arrangements are not required. The break orientation is simulated as described for the cold leg breaks with the top, bottom, or central orientation options when the break is simulated from a horizontal pipe. Vertical pipe break locations simulate the break directly out of the piping control volume. For hot leg breaks, all ECCS injection is available for core cooling. The ECCS backpressure corresponds to that at the injection location.

4.3.2.3. Flow Model for RELAP5/MOD2-B&W

Flow between control volumes is determined by the phasic momentum equations. Included in the formulation of the momentum equations are terms that account for (1) temporal change of momentum, (2) momentum convection, (3) momentum change due to compressibility, (4) momentum flux resulting from area change, (5) pressure loss resulting from wall friction, (6) pressure loss due to area change, and (7) gravitational acceleration. Two-phase friction effects are also taken into account. The derivation of the

governing fluid flow equations used in RELAP5/MOD2-B&W is given in Section 2.1 of topical report BAW-10164.

4.3.2.4. Discharge Model

The discharge of subcooled fluid through the break is determined using the extended Henry-Fauske model. Once the liquid in the break volume saturates, the discharge is based on the Moody model per the Appendix K requirement. To avoid a step change in the flow between the two models, a transition region is used (See equation on Page 2.1-109 of BAW-10164). The transition region uses an under-relaxation technique to smooth the flow whenever the upstream void fraction is between a specified range, α_{lower} and α_{upper}. The Murdock-Bauman model is used for superheated discharge. Appendix C of the RELAP5/MOD2-B&W topical report (Ref. 1) contains tabular functions for each of the discharge correlations.

The RELAP5/MOD2-B&W EM choked flow model allows input of four discharge coefficients as functions of the leak inlet conditions. Separate coefficients can be used for subcooled, transition to two-phase, two-phase, and steam flows. The correlation switching logic for the small break method is based on enthalpy and void fraction criteria. The subcooled coefficient is used for void fractions less than α_{lower}. The transition discharge coefficient is used for void fractions between α_{lower} and α_{upper}. The two-phase discharge coefficient is used when the void fraction is greater than α_{upper}, and the leak enthalpy is less than the break volume saturated steam enthalpy. The superheat discharge coefficient is applied whenever the leak inlet enthalpy is greater than or equal to the break volume saturated steam enthalpy.

Based on the results obtained in the Appendix A analyses, the break discharge model that is best suited for EM analyses uses a

break discharge coefficient of 1.0 for all phases or regimes. All of the demonstration applications in Appendix A produced break void fractions that increased quickly from zero to ninety-five percent. The Moody model produces reasonable flows near these conditions, therefore a discharge coefficient of 1.0 is most appropriate.

The first analyses contained in Appendix A used the break discharge coefficient method from BAW-10168 (Ref. 6). That model was based on comparisons against experimental data (Ref. 6, pp. LA-251 through LA-269). The Moody critical flow model was observed to overpredict two-phase leak flows for void fractions greater than twenty to thirty percent while underpredicting the flow for lower void fractions. Preservation of the relative discharge rates in the subcooled, two-phase, superheated region is important for providing reasonable leak flows in SBLOCA analyses that confirm the adequacy of the ECCS. Overprediction of the two-phase discharge leads to accelerated RCS depressurization, which increases the ECCS injection and may result in nonconservative clad temperature predictions.

The initial discharge coefficient application was selected to best represent the relative discharge relationships. The subcooled discharge coefficient of 1.0 is used because extended Henry-Fauske correlates well against most test data. The two-phase transition region uses the Moody model with a discharge coefficient of 1.0. This region is defined with α_{lower}, set to a one-percent void fraction, and α_{upper}, set to a seventy-percent void fraction. The Moody two-phase discharge coefficient is set to 0.7 for void fractions greater than seventy percent. The superheated regime coefficient is maintained at a conservatively low value of 0.7, to provide continuity of the break flow at the saturation-to-superheat boundary.

These coefficients were used for the initial sensitivity studies and CLPD spectrum contained in Appendix A. Section A.8 contains

two spectrum cases, the 0.1- and 0.3-ft^2 breaks, which were reanalyzed with a Moody two-phase discharge coefficient of 1.0, and with the break area decreased by 0.7 to preserve the saturated break flow rate. These revised cases calculated higher peak cladding temperatures. Investigation of the results revealed that during the critical boiling pot phase of the analyses, the break volume void fraction was approximately 98 to 99 percent. The data in Reference 6 indicated that the Moody discharge rates above 95 percent void fraction are closer to the experimental rates. That is, the discharge coefficient of 0.7 should be increasing back to 1.0. Therefore, the low or high void discharge model is most appropriate for the typical pumps-tripped CLPD EM applications for B&W plants.

Regime	Range of Application	Intermediate Break Voiding Normalized Value	High or Low Break Voiding Normalized Value
Subcooled	$\alpha_g <$ 1%	1.0	1.0
Transition	$\alpha_g \geq$ 1% & $\alpha_g \leq$ 70%	1.0	1.0
Two-phase	$\alpha_g >$ 70% & $H_{mix} < H_{g,sat}$	0.7	1.0
Superheat	$H_{mix} \geq H_{g,sat}$	0.7	1.0

Based on the results obtained in the Appendix A analyses, the model that is best suited for most EM analyses of B&W plants is the high or low void model. This model will be used for the typical cold leg SBLOCA, CFT line break, or HPI line break applications without reactor coolant pumps operating. The intermediate void model is still retained as an option for EM calculations that may have extended periods of intermediate void fractions in the break control volume. This intermediate void model may be used for hot leg breaks or other SBLOCA analyses in which the reactor coolant pumps remain in continuous operation. The break void fraction history will be the primary criterion by which the appropriateness of the discharge model is judged. Some analyses may need to be performed with both discharge coefficient models to ensure that a reasonable representation of the break flow is obtained. Whenever the intermediate void break discharge model is selected for use, its selection will be clearly identified and explained.

The break area is varied as a part of the spectrum approach to identify the worst case. The spectrum considers the worst break location (generally bottom of the pipe) and defines the CLPD location to be the most limiting location due to the loss of HPI liquid directly out of the break before reaching the reactor vessel. In addition, CFT and HPI line breaks will be analyzed as special breaks to determine the most limiting small break LOCA. These breaks are handled separately because of the severe reduction of the ECCS into the RCS. These breaks, in combination with the CLPD spectrum, ensure that the most-limiting SBLOCA is identified, investigated, and shown to comply with all 10CFR50.46 requirements.

4.3.2.5. Core Flow Model

Core flow rates during the transient are calculated by RELAP5/MOD2-B&W. The most challenging SBLOCA phase for the flow model is the last phase of the event, boildown and recovery. The core contains a boiling mixture of steam and water with steam passing upward through the RVVVs and possibly flowing through the cold leg pump suction regions of those legs in which the loop seal, or liquid trap, has been evaporated. If the accident is severe, the mixture level will be somewhere in the upper region

[ ]

Flow diversion out of the hot channel, either normal diversion or that due to rupture, is modeled through crossflow paths connecting

[ ]

[ ]

Adequate prediction of the mixture level in the core assures appropriate cladding heatup when the level is below the top of the heated core elevation. Fluctuations in the mixture level may result in cyclic dryout and rewet of control volumes near the top of the mixture level. During the CFT injection phase, variations in the core mixture levels have been related to cyclic downcomer steam condensation rates that feed back in the form of CFT flow spurts for slower transients. In turn, these flow spurts cycle the condensation rates thus perpetuating the oscillatory behavior.

[ ]

4.3.2.6. Phase Separation and Countercurrent Flow

[ ]

regime maps that are used to determine the phase separation within the RCS system components. Vertical flow, horizontal flow, and high mixing (pumps-on LOCA) maps are included. These models are described in detail in Section 2.1.3 of the RELAP5/MOD2-B&W

[ ]

4.3.2.7. Pump Model

The RC pumps are represented by a two-phase dynamic pump model. Two-phase pump head and torque degradation are also accounted for in the model. The pump models are described in Section 2.1.5.2 of the RELAP5/MOD2-B&W topical report BAW-10164.

Selection of the pump homologous two-phase difference curve and void-dependent multiplier will be based on reference to an applicable sensitivity study that confirms the conservative application of the pump model. As part of the analytical work to justify changes to the operator action time to trip RCPs during a CFT line break, the M3-modified two-phase degradation multiplier was determined to be the most appropriate and also produced the highest overall cladding temperatures. The final SER related to this topic (Reference 12) approved the use of the M3-Modified curve for all B&W plants when predicting time

available for operator action to trip RCPs following loss of subcooling margin.

4.3.2.8. Mixture Height Calculation

[

]

4.3.2.9. Single Failure Condition

The single failure assumed for small breaks is that which results in the minimum ECCS injection reaching the reactor vessel downcomer pool region. In conjunction with the loss of offsite power, any single failure that results in the loss of one train of pumped ECC injection is the most conservative assumption for SBLOCA analyses. Containment backpressure has little effect on small break transients, since the break remains choked throughout the core refill process. A single failure chosen to minimize the containment backpressure, would therefore, have no effect on the transient and would possibly increase ECC injection.

4.3.3. Heat Transfer and Thermal Analysis

4.3.3.1. Flow Controlled Portion of Transient

Heat transfer is flow-controlled while core flow remains greater than approximately one percent of full flow for the pumps-tripped case, and it is continuously flow-controlled for the pumps

operating case. During flow coastdown, for a pumps-off small break LOCA, heat transfer is by forced convection to liquid or by nucleate boiling. The cladding stays within a few degrees of the coolant saturation temperature, and the heat flux does not approach the CHF value. The RELAP5/MOD2-B&W hot channel provides analysis of this phase of SBLOCA using the EM core heat transfer package from the LBLOCA model, except for the critical heat flux correlation and the nucleate and flow film boiling lockouts. The BWC CHF correlation is used for SBLOCA analyses of Mark-B fuel types with non-mixing-vane grid. The BHTP CHF correlation as described in BAW-10164P (Ref. 1) is used for SBLOCA analyses of Mark-B-HTP fuel. The BWUMV CHF correlation, an improvement to the BWCMV correlation, is selected for SBLOCA analyses of mixing vane grid fuel types (currently Mark-B11, Mark-BW, and Mark-CZ). Consistent with previous evaluation models and with the

[ ]

of the RELAP5/MOD2-B&W topical report (Ref. 1). The RELAP5 SBLOCA heat transfer option, which allows a return to nucleate boiling and does not lock in to flow film boiling, is also selected. These lockouts are LBLOCA-oriented and not appropriate for simulation of the SBLOCA transient.

A small break with the reactor coolant pumps operating is characterized by a continuous flow of coolant through the core. The pump-induced core flow evolves from its initial subcooled condition, to one of high quality, and then back to liquid during the course of the transient. The reactor coolant pumps cavitate and degrade in performance during the transient, recovering to full volumetric flow as the system void fraction approaches 100 percent. The cladding temperature excursion is calculated by RELAP5/MOD2-B&W, which contains a complete boiling curve simulation.

4.3.3.2. Quiescent Portion of Transient

For the SBLOCA without RC pumps running, the system is considered to be in a quiescent condition once the core flow has decreased to a few percent of its initial value. Should the core remain covered during the accident, no thermal excursion occurs. Numerous experiments, conducted at power levels two to three times higher than those that occur during the quiescent period of a small break LOCA, have demonstrated that pool heat transfer is sufficient to keep the cladding within a few degrees of the coolant saturation temperature.

Should the core become partially uncovered, heat transfer within the portion of the core covered by a steam-water mixture is provided through pool nucleate boiling. Above the mixture level, heat transfer is determined by forced convection to steam and by radiation. The RELAP5/MOD2-B&W hot channel also provides analysis for this phase of SBLOCA. The EM core heat transfer package from the LBLOCA model is used, except for the critical heat flux correlation and the nucleate and flow film boiling lock-outs. The CHF correlations described in Section 4.3.3.1 are used. The RELAP5/MOD2-B&W SBLOCA heat transfer option, which allows a return to nucleate boiling and does not lock in to flow film boiling, is also selected. These lock-outs are LBLOCA-oriented and not appropriate for the orderly simulation of SBLOCA. The degree of superheat in the steam flow is calculated locally within RELAP5/MOD2-B&W with allowance for radial flow diversion. Upon refill of the core, a return to pool nucleate boiling is allowed for the portion of the core being recovered by the steam-water mixture.

4.3.4. Cladding Swelling and Rupture

The small break evaluation model includes a provision for predicting cladding swelling and rupture. The model is the same as that used for the large break blowdown model (Sections 4.3.3.1, 4.3.3.2, and 4.3.3.3 of Volume I of this topical report) and is based on NUREG-0630 data for zircaloy cladding and M5 data for M5 cladding. Flow diversion is modeled through the use of hot and average channels, cross flow, and a provision to increase the axial resistance at the ruptured location. The crossflow resistance from the hot to average channel is set at an appropriate, but low value, maximizing flow diversion should it occur. The crossflow resistance from the average to hot channel is modified to prevent cold steam from diverting out of the average channel to the hot channel (see Section 4.3.2.5).

Once rupture has been calculated, the heat transfer, heat conduction, and metal-water reaction models are updated for the resultant strain and the availability of interior clad surface for oxidation.

Time-in-life calculations for SBLOCA applications are not required unless the fuel pin heatup is sufficient to cause cladding rupture. End-of-life pin pressures can be high, which increase the cladding hoop stresses, thereby improving the likelihood of rupture for those cases that do experience heatup. To maximize the likelihood of rupture, a high initial internal pin pressure (> 2200 psia), with the beginning-of-life stored energy and oxide thicknesses is used to cover conservatively the entire range of fuel pin burnup. Any case that predicts clad rupture with these conditions is further analyzed by adjusting of the time of rupture to match the time of peak clad temperature. This adjustment is achieved via a modified internal pin pressure to force rupture to occur near the worst time during the temperature excursion. The worst time in life is therefore determined by interpolation on the

LOCA internal pin pressure versus time-in-life condition. A consistent time-in-life calculation option is reserved should the BOL stored energy and oxide thickness be overly conservative.

The pseudo time-in-life method described in the preceding text has been facilitated by using multiple separate pins to determine the most limiting clad rupture time. The separate pins with varying initial pin pressures are used in a single analysis to minimize the number of iterations (e.g. cases) that may need to be performed to confirm the worst time for cladding rupture and its effect on peak cladding temperature. (There is additional information provided in the RAI response to Question 11 from Volume III page LA-64.)

4.4. Compliance

This section shows that the features of the small break evaluation model described in Section 4.3 conform to the required features of the evaluation model set forth in Appendix K. To accomplish this, the organization of this section parallels that of Appendix K, and references are made to the appropriate parts of Section 4.3.

I. Required and Acceptable Features

A. Heat Sources During LOCA

Section 4.3.1 of the model directly incorporates all of the requirements of this section of Appendix K.

B. Swelling, Cladding Rupture, and Fuel Rod Thermal Parameters

The small break model contains provisions for calculating the effects of clad swelling and rupture and changes in fuel rod thermal parameters with time (Section 4.3.4).

C. Blowdown Phenomena

C.1. Break Characteristics and Flow

C.1.a. Spectrum of Breaks

The small break analysis includes a spectrum of break areas up to the size that causes initial cladding DNB (Section 4.3.2.4). CLPD break sizes in the range of approximately 0.5 to 0.75 ft^2 are expected to produce initial DNB depending on the fuel design and plant boundary conditions. Breaks larger than this are evaluated with the large break evaluation model.

C.1.b. Discharge Model

The discharge model described in Section 4.3.2.4 complies with the intent of Appendix K. Literally, Appendix K could be interpreted as requiring a constant discharge coefficient of 1.0 throughout the two-phase (Moody) range. However, BWNT considers that this requirement is dictated by the large break so that the leak flow

at the largest break area will not be underpredicted. The spectrum of break areas below this largest break is continuous, making maximization of the flow for any given spectrum calculation not an issue. With the selection of discharge models used in the SBLOCA evaluation model, use of a discharge coefficient of 1.0 may in some cases be nonconservative during the two-phase period. Therefore, the discharge coefficient logic and map described in Section 4.3.2.4 are used.

To establish the selection map relative to the strict requirement of Appendix K, sensitivity studies have been done and documented in Appendix A. As was demonstrated, the relationship of subcooled and saturated discharge modeling requires that the two-phase flow not be overpredicted to provide assurance that calculational results are sufficiently conservative. The selection of the appropriate map is defined within the evaluation model discharge coefficients discussion contained in Section 4.3.2.4. Therefore, the modeling selected by the evaluation model is acceptable relative to the requirements of Appendix K.

The range of discharge coefficients required by Appendix K is implicit for SBLOCA through the break area spectrum approach. This results because an overall discharge coefficient is only a proportionality constant on the break area.

C.1.c. End of Blowdown

The end of blowdown does not apply to small break LOCA because effectively all event occurrences of significance take place during the depressurization phase, before the RCS and containment pressure reach an equilibrium. Similarly the phenomena of bypass and entrainment of liquid by reverse downcomer flow do not occur. The provisions of this section of Appendix K are thus large break specific and not addressed by the small break evaluation model.

C.1.d. Noding Near Break and ECCS Injection Points

Noding in these areas is conservatively modeled (Section 4.3.2.2).

C.2. Frictional Pressure Drops

Section 4.3.2.3 of the model directly incorporates all of the requirements of this section of Appendix K.

C.3. Momentum Equation

The flow model used is based on the RELAP5/MOD2-B&W phasic momentum equations and includes the effects listed in Appendix K (Section 4.3.2.3).

C.4. Critical Heat Flux

The CHF correlations employed are acceptable per Section 4.3.3.1 and 4.3.3.2. A return to nucleate boiling is not prevented by the SBLOCA evaluation model. This prohibition in Appendix K is large break-oriented and not appropriate for the orderly simulation of SBLOCA.

C.5. Post-CHF Heat Transfer Correlations

The correlations and method of application used for post-CHF heat transfer are acceptable (Section 4.3.3). The lockout of transition boiling is not applied during SBLOCA calculations. This prohibition in Appendix K is large break-oriented and not appropriate for the orderly simulation of SBLOCA.

C.6. Pump Modeling

As required, the reactor coolant system circulation pumps are represented by a two-phase, dynamic pump model (Section 4.3.2.7).

C.7. Core Flow Distribution During Blowdown

Flow through the core is smooth because of the nature of the small break accident (Section 4.2). As a result, filtering of the core flow is not required for surface heat transfer calculations. An additive form loss due to flow blockage from clad rupture is calculated by the code. The impact on the core flow distribution and resultant hot pin temperature calculation are determined as described in Section 4.3.4.

D. Post-Blowdown Phenomena - Heat Removal by ECCS

D.1. Single Failure Criterion

The single failure chosen minimizes ECCS injection into the RCS (Section 4.3.2.9).

D.2. Containment Pressure

In most small breaks, the small discharge area and the slow depressurization result in the leak flow remaining choked until after long-term cooling has been established. In such situations, containment pressure does not influence the transient. However, some of the larger small breaks may unchoke before the core is completely recovered. The containment pressure will affect depressurization somewhat in these cases, but because core refill is slow with small breaks, slight variations in pressure do not significantly influence the rate of recovering. Containment pressure is not a critical factor in these accidents as long as the value used is reasonable.

D.3. Calculation of Reflood Rate

The typical reflooding period as envisioned for large breaks does not occur for small breaks. Those requirements which can be logically extended to small breaks are applied; the other requirements are interpreted as large break-specific and not considered further. Appendix K places a requirement on the reactor coolant pumps during reflood. The effect and function of the requirement applies only to large breaks. For small breaks the reactor coolant pumps are modeled as on or off depending on the assumptions of the case. The carryout rate fraction is a large break reflooding parameter not applicable to small breaks wherein core steam velocities are insufficient to entrain liquid.

The effects of CFT nitrogen cover gas being injected are not considered in the small break model. These effects are inconsequential or beneficial, and it is conservative not to model them. Dissolved gases have been evaluated in a bounding manner and shown to have inconsequential impacts on the course of LOCA transients (Section 4.3.6.3 of Volume I).

The determination of the carryout fraction during reflooding of the core is not necessary in small break analyses because of the slow core recovery, the relatively low cladding temperatures reached while uncovered, and the low power level. This results in a small amount of steam being formed with a correspondingly low separation velocity, which is not capable of significant liquid entrainment.

D.4. Steam Interaction with Accumulator Water

[ ]

mass transfer are, therefore, calculated directly by RELAP5/MOD2-B&W as described in Section 2.1.3.4 of the RELAP5/MOD2-B&W topical report BAW-10164.

D.5. Refill and Reflood Heat Transfer

During core recovery, heat transfer above the core mixture is by steam cooling only. As sections of the core are recovered, they are cooled by film boiling until nucleate boiling can be appropriately established (Section 4.3.3.2). This method conforms to the requirements of Appendix K.

This page is intentionally left blank.

FIGURE 4-1. SMALL BREAK AXIAL POWER DISTRIBUTION
9.705-FT AXIAL POWER SHAPE

FIGURE 4-2. SBLOCA LOOP NODING ARRANGEMENT (205 RL PLANT).

FIGURE 4-3. SBLOCA REACTOR VESSEL NODING ARRANGEMENT (205 RL PLANT).

Figure 4-4. IEOTSG SBLOCA NODING ARRANGEMENTS.

Figure 4-5. CLPD BREAK NODING ARRANGEMENTS.

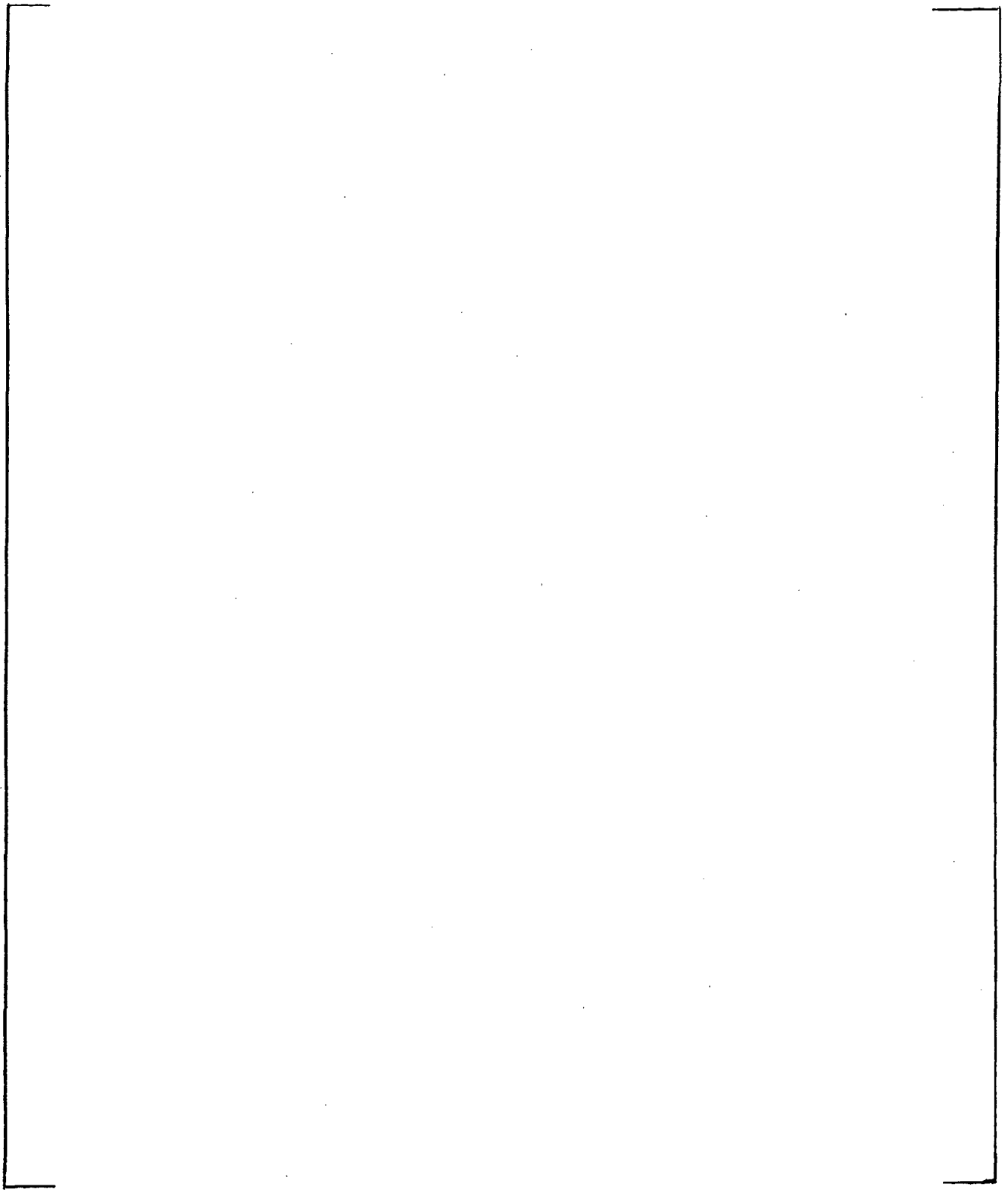

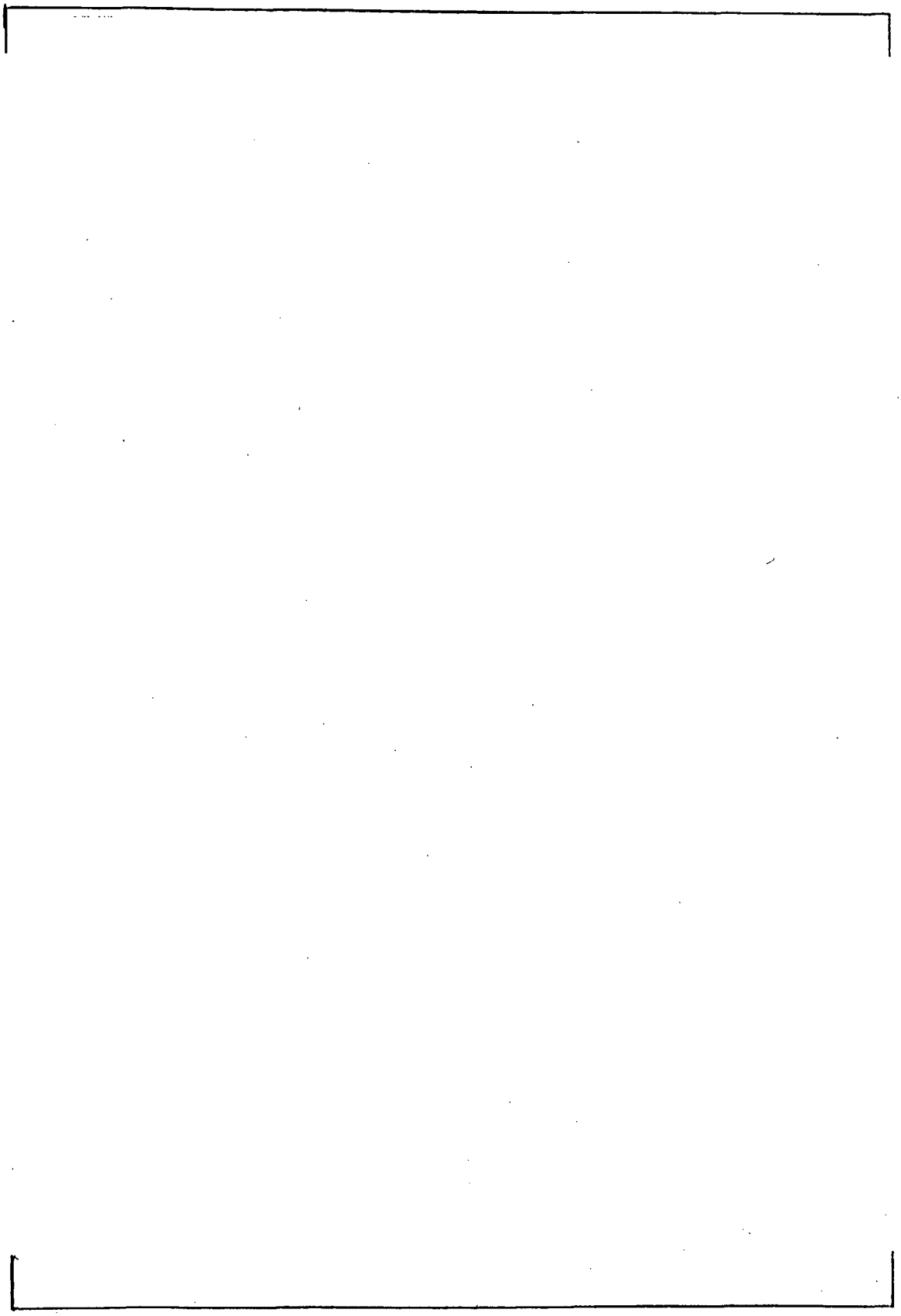

Figure 4-6. SBLOCA LOOP NODING ARRANGEMENT (177 LL PLANT).

Figure 4-7. OTSG SBLOCA NODING ARRANGEMENTS.

This page is intentionally left blank.

5. LOCAL CLADDING OXIDATION

Criterion 2 of 10CFR50.46 requires that the maximum local degree of cladding oxidation not exceed 17 percent. Compliance to this criterion is obtained by evaluating the results of the calculation for peak cladding temperature. In the calculation, local cladding oxidation is computed as long as the cladding temperature remains above 1000 F. The amount of oxide thickness at each location is computed on a mass basis. In addition, a check of the local oxidation limits with respect to a realistic initial oxidation (or pre-accident oxidation) is performed to ensure that the 17 percent criterion would not be exceeded with a realistic initial oxidation. This supplemental check can be performed in one of two ways, using either a composite approach or separate analysis. The composite approach is the simplest form, but it will produce the minimum margin to the oxidation limit. It adds the transient oxidation increase predicted by the peak cladding temperature analyses with the minimum initial oxide layer to the initial realistic oxidation value. If this composite method is too restrictive, a separate oxidation verification case can be performed by using the realistic oxide thickness as input to a new analysis to show that the reduction in the transient oxide increase will keep the total oxidation less than the 17 percent criterion.

This page is intentionally left blank.

6. MAXIMUM HYDROGEN GENERATION

Criterion 3 of 10CFR50.46 states that the maximum amount of hydrogen generated from cladding oxidation during a LOCA shall be limited to one percent of the entire cladding in the heated core region. The demonstration of compliance to this criterion is accomplished by calculating the amount of core-wide hydrogen generation, via oxidation increases, for the limiting SBLOCA analysis.

The determination of whole-core oxidation increase for each analysis is provided by one of two methods. The first method simply compares the hot channel average oxidation increase against the 10CFR50.46 criteria. If the hot channel average oxidation increase is less than or equal to one percent, then the whole-core hydrogen generation increase will be reported as less than one percent, and no additional calculations will be performed. This is generally the case for SBLOCAs since only a small portion of the core undergoes a heatup above 1000 F.

The hot channel average hydrogen generation rate is determined by

$$\overline{O_x}\Big|_{hc} = \sum_{chan}\left(Z_{seg} \cdot O_x(Z)_{hc}\right) \Big/ \sum_{chan}\left(Z_{seg}\right). \qquad (6\text{-}1)$$

Should the hot channel average hydrogen generation exceed one percent, then a detailed calculation will be used. This method uses the hot and average channel oxidation increases with a typical core power map to calculate the whole-core average oxidation increase. This calculation involves a detailed summation of the weighted axial contributions interpolated from the hot and average channel local oxidations at each axial elevation.

The detailed method determines the metal-water reaction at each core axial position as shown graphically in Figure 6-1 of Volume I. The hot and average channel local oxidation increases are used to determine the oxidation increase for assemblies in which the radial power factor lies between them. The assemblies with radial power factors below the average channel value use the average channel oxidation increases. The whole-core oxidation increase at each elevation is multiplied by the normalized axial length for the segment to give a normalized volume weight. The sum of this volume weight results in a conservative whole-core hydrogen generation value for the transient.

The axial oxidation increase for assemblies in which the radial power factor falls between the hot and average bundles is calculated by a linear interpolation on local power level.

$$O_x(x,y,z) = O_x(Z)_{hc} - \left[O_x(Z)_{hc} - O_x(Z)_{ac}\right] \frac{P_l(Z)_{hc} - P_l(x,y,z)}{P_l(Z)_{hc} - P_l(Z)_{ac}} \qquad (6\text{-}2)$$

For radial power factors less than the average bundle, the axial oxidation is set to that of the average channel.

$$O_x(x,y,z) = O_x(Z)_{ac} \qquad (6\text{-}3)$$

The channel average oxidation for any bundle is computed by

$$\overline{O}_x\Big|_{(x,y,z)} = \sum_{chan}\left[Z_{seg} \cdot O_x(x,y,z)\right] \Big/ \sum_{chan}\left(Z_{seg}\right) . \qquad (6\text{-}4)$$

The variables used in the equations in this section are identified by

$O_x(x,y,z)$ = the increase in oxidation at location (x,y,z) in the core,

$O_x(z)_{hc}$ = the increase in oxidation which occurred at elevation z in the hot channel,

$O_x(z)_{ac}$ = the increase in oxidation which occurred at elevation z in the average channel,

$P_l(x,y,z)$ = the local power at location (x,y,z) in the core,

$P_l(z)_{hc}$ = the local power at elevation z in the hot channel, and

$P_l(z)_{ac}$ = the local power at elevation z in the average channel.

An integration of these channels over the entire core results in the core-wide oxidation increase or the amount of hydrogen generation. The core-wide integration requires an assembly power distribution. The distribution, shown in Figure 6-2 of Volume I, has been selected for its conservatism in placing a disproportionately high fraction of the core near the hot channel value.

Conservatism in the calculation comes from three sources: (1) the amount of oxidation in the base run is computed using the Baker-Just correlation, which is recognized to be about fifty percent conservative; (2) the core power distribution is a reasonable and representative distribution that has been pushed to the peak powers allowed by plant technical specifications; and (3) the use of a power ratio to determine the degree of oxidation for lower power zones is conservative. Since the oxidation rate increases exponentially with temperature, a decrease in power can be expected to produce a greater than proportional decrease in oxidation. Use of the average channel oxidation as a minimum adds additional margin of conservatism.

To demonstrate the expected range of results of the technique, it was applied to the most severe small break LOCA transient (Section A.9). The hot channel average oxidation increase was calculated to be 0.004 percent (Table A-25). No average channel oxidation

increase occurred. Therefore, the amount of core-wide metal-water reaction that is predicted for this case is negligible. As with most SBLOCAs, the hydrogen generation rate is far below the one percent criterion of 10CFR50.46. The hot channel average oxidation increase will be used almost exclusively to demonstrate compliance with 10CFR50.46.

7. COOLABLE GEOMETRY

Criterion 4 of 10CFR50.46 states, "Calculated changes in core geometry shall be such that the core remains amenable to cooling." The analysis for predicting the peak cladding temperature, local oxidation, and whole core hydrogen generation involves specific analysis of the hottest fuel pin in the core. Compliance with this criterion involves a variety of considerations and analyses not explicitly controlled by this Evaluation Model but referenced by fuel reload analyses to demonstrate compliance to this 10CFR50.46 criterion. These calculations include consideration of the condition of the fuel rods, the fuel assemblies, and other components in the core just prior to the LOCA transient plus any changes in geometry calculated as a result of the mechanical loads from the limiting structural LOCA event plus an independent seismic event. It also includes consideration of the transient thermal effects on these components from the 10CFR50.46 LOCA break consequences.

The mechanical loads from the seismic plus the limiting structural LOCA are statistically combined and compared to the elastic limits for the fuel bundles used in core at normal full power conditions. When the loading is less than the elastic limit, the nominal fuel bundle flow areas are used in the 10CFR50.46 LOCA analyses. If the loading exceeds the elastic limits, the deformation or distortion of the impacted fuel bundles will be applied to the channel geometry used in the prediction of the first three 50.46 criteria.

Any initial structural deformation predicted, is used to predict any local flow blockage that will be combined with any changes in the core geometry that occur due to the fuel pin swelling and rupture consequences from the analyzed 50.46 LOCA. Compliance with this core cooling criteria is demonstrated when there is no gross core flow blockage that prevents adequate fuel pin heat

removal or disfiguration of the control rod guide tubes that restricts control rod insertion beyond that which is credited in the LOCA analyses. For compliance purposes, gross core blockage is defined as greater than 90 percent blockage for any bundle. If necessary, it is acceptable to apply power limitations to peripheral or low power bundles if they have significant initial mechanical distortions or gross flow blockage greater than 90 percent. In these situations, the reduction in power can be used to compensate for more severe time-dependent reductions in the flow area and transient coolant flow necessary to demonstrate compliance to this criterion.

The analyses include the effect of clad swelling and flow blockage based on NUREG-0630 for Zircaloy-4 cladding or Appendix K of BAW-10227P-A for M5 cladding, and shows that the peak temperatures remain below 2200 F. The combination of core geometry, coolant flow, and local power for all other bundles in the core is also considered. The conclusions drawn for the coolable core geometry of the hot bundle is generally applicable to all other bundles because the transient cladding temperatures remain below that of the fuel pin analyzed in the peak cladding temperature calculation and there is less power to be removed. Therefore, all fuel pins and assemblies also remain in a geometry "amenable to cooling."

8. LONG-TERM COOLING

Criterion 5 of 10CFR50.46 states, "A low core temperature must be maintained following the calculated successful initial operation of the ECCS and that decay heat must be removed for an extended period of time." As with the coolable core geometry criterion, this criterion involves a variety of considerations and analyzes not explicitly controlled by this Evaluation Model but referenced by fuel reload analyses to demonstrate compliance to this 10CFR50.46 criterion. This section describes some of the considerations and assumptions used to meet this condition.

8.1. Establishment of Long-Term Cooling

The analysis of a small break LOCA that establishes the first three criteria of 50.46 is continued until the cladding temperatures at all locations in the core have decreased to approximately the coolant saturation temperature, the core is covered with a two-phase mixture level, and no additional challenges to core cooling are foreseen. At this time the path to long-term cooling is established. The core temperature is maintained within a few degrees of the coolant temperature through a continuous flow of water maintained by the ECCS.

Plant operators follow the emergency operating procedures that have been established to support successful short-term and long-term core cooling. They have been reviewed by the NRC for the smooth transition to long-term cooling during which water is recirculated from the reactor building sump through a heat exchanger to the reactor vessel. Although the procedure for depressurization of the reactor coolant system is more complicated, the safety requirements are the same as those for large breaks, Chapter 8, Volume 1 of this report.

8.2. Boric Acid Concentration

Since all ECC systems inject borated water, salts could build up, precipitate, and block core channels during long-term cooling. To prevent this, operator action is taken to establish a flow of water through the core regardless of the type or location of the break. A concentration calculation that accounts for boiling at the decay heat rate with minimal or no core throughput (water passed through the core) is performed from the initiation of the event to the time of operator action. The concentration calculated must be shown to be below the saturation limit of boric acid for the core conditions. The rate of concentration at the time of operator action is shown to be less than the loss of boric acid caused by the throughput flow. This assures that the concentration will thereafter decrease.

9. REQUIRED DOCUMENTATION

This section verifies compliance with the documentation requirements (Part II) of the Appendix to 10CFR50 and is arranged according to the section division of Part II.

II. Required Documentation

1.a. The computer codes that form the basis for the SBLOCA ECCS evaluation model are described in an approved revision of the following BWNT topical report:

RELAP5/MOD2-B&W	BAW-10164 (Ref. 1)
CONTEMPT	BAW-10195A (Ref. 2)

These topical reports include the derivations of the equations used in the codes, starting with fundamental physical laws and including all approximations. Any assumptions made in the derivation of the solution technique used by the code and the value of all code-specified parameters are disclosed in this report. The report also describes the general application of the code to applicable problems including input parameter selection.

The computer code options used in the SBLOCA evaluation model are summarized in Table 9-1. At several locations throughout the computer code, correlations have been programmed to include user input multipliers. These constants shall all have a value of one unless specifically stated to the contrary. Programmed constants that are part of the correlations or part of BWNT implementation of the correlations will have the value as published in the code topical report.

1.b. Any changes in the ECCS evaluation model that result in a deviation of more than 50 F in the calculated cladding

temperature transient will be documented by appropriate amendments to the evaluation model description.

1.c. BWNT computer codes, including their source coding, are controlled through a systematic process that has been audited and approved by the NRC. Each code is tracked by a unique name, version number, and revision level. Authorization to change an approved version of a code involves a multiple review and approval process. The source listing of the current or past approved versions of ECCS codes can be made available to the NRC, at the BWNT offices in Lynchburg, Virginia, upon their request.

Inputs used during an evaluation can be categorized as follows:

Generic: User supplied values or constants whose values are controlled by the evaluation model. The materials properties are an example of this type of input.

Prescribed: Input for which a determining procedure is specified in the evaluation model without the specification of a value. The use of hot fluid volumes within the RELAP5/MOD2-B&W model is an example of this type of input.

Plant: Input which is taken from documentation for the individual plant or plants to be covered by the evaluation. Plant geometry inputs are examples of this type of input.

Case: Input which will vary depending on the accident being evaluated. Break area is an example of this type of input.

The BWNT evaluation model controls these different types of inputs in differing ways. Generic and Prescribed inputs are controlled in the same fashion as code options, and are documented in context within the evaluation model report. A summary of the generic and prescribed inputs is given in Table 9-2.

Plant input is controlled by BWNT internal calculational procedures and not by the evaluation model. These procedures are written to adhere to ANSI quality assurance standards. For the most part these procedures require that the inputs come from controlled design documentation, that they be referenceable, that use be documented, and that an independent review be conducted to assure that this has been done. The documents attesting to this for any given evaluation are controlled documents, maintained at the BWNT offices in Lynchburg, Virginia, and are available for audit upon request.

Case input is similar to assumptions. It is not controlled by either the evaluation model or BWNT procedures other than that it must be documented along with the plant input in controlled, stored records of the calculation. Case input is also available for audit upon request.

2. Convergence of solution techniques is demonstrated in Appendix A, of this topical report volume. System modeling and noding are described in Section 4.3.2. Time step selection is presented in Appendix A, Volume II of this report.

3. Appropriate sensitivity studies are presented in Appendix A of this volume. Additional sensitivity studies, which must be performed for each specific plant category, will be documented as part of the plant-specific analysis.

4. Predictions and experimental data are being compared continually for the evaluation model. Code topical reports contain current comparisons with applicable experimental data as appropriate.

5. The BWNT topical report, listed in Section 9.II.1.a which, along with this report, describe the ECCS evaluation model, provide the technical basis for the adequacy of the computational methods as well as compliance with 10CFR50. The evaluation model description provides sufficient flexibility that it is applicable to all the plant categories presented in Table 1-1.

Table 9-1. Additional SBLOCA Evaluation Model Guidelines, Code Options Used in SBLOCA Evaluation Model.

OPTION	SELECTION
RELAP5/MOD2-B&W	
[	]
Fine Mesh Rupture Option	Used
Concentric or Nonconcentric Fuel Pellet Simulation	Use Nonconcentric option with TACO3 or GDTACO boundary conditions
Critical Flow Model	Subcooled - Ext. Henry-Fauske Two-phase - Moody Superheat - Murdock-Bauman
[	]
Friction	Calculated by RELAP5/MOD2-B&W
[	]
Heat Transfer Model	Core model is used for the active core heat structures the System model is used elsewhere
High Pressure, High Flow CHF Correlation	Fuel Design Specific CHF: BHTP for Mark-B-HTP fuel BWC for other Mark-B fuel BWUMV for Mark-B11 and Mark-C fuel
[	]
Metal-Water Reaction Model	Baker-Just, 1000 F threshold temperature
Rupture Temperature	A plastic weighted, time averaged ramp rate is used
Rupture Form Loss Resistance	Automatic code calculation for hot and average channels only

Table 9-1. Additional SBLOCA Evaluation Model Guidelines, Code Options Used in SBLOCA Evaluation Model. (Cont'd)

OPTION	SELECTION
RELAP5/MOD2-B&W	
[	]

Table 9-2. Additional SBLOCA Evaluation Model Guidelines, Generic and Prescribed Inputs for the SBLOCA EM.

INPUT	SELECTION
RELAP5/MOD2-B&W	
Fluid Volumes	Hot - from design drawings
Attached Piping Volumes	Only the CFT line and pressurizer surge line volumes are included. The total of other attached piping volumes lies within the accuracy of the system volume calculation and are not included
Initial Reactor Coolant System Flows	The system flows are those used in the at power minimum DNB analyses. The hot and cold leg temperatures are set by nominal control system response to that RCS flow
Two-Phase Pump Degradation	Conservative selection of two-phase difference curve (RELAP5 vs SEMISCALE) and void-dependent multiplier M1 versus M3-Modified).
Initial Inventories for Reactor Coolant System, Secondary System, and ECCS Systems Pressure	Set by nominal operation design levels, except for CFT. The CFT inventory and pressure is set based on sensitivity studies that consider minimum to maximum ranges. The volume of attached piping except for the CFT line and pressurizer surge line are not included in the LOCA model
Primary Metal	Structures are lumped together by material properties, thicknesses, and location. Grouping is user controlled

Table 9-2. Additional SBLOCA Evaluation Model Guidelines, Generic and Prescribed Inputs for the SBLOCA EM.

(Cont'd)

INPUT	SELECTION
RELAP5/MOD2-B&W	
Over Power Factor	Uncertainties (2% unless determined to be otherwise) due to power level instrumentation error applied to core power
[	]
Decay Heat	120% ANS 1971 based on core power plus uncertainty. Actinide power accounts for the energy generated from the radioactive decay of actinides, including neptunium, plutonium, and the isotopes of uranium
Initial Fuel Temperatures	Adjusted to agree within ± 20 F to an NRC approved steady-state fuel performance code (such as TACO3 or GDTACO)
Rupture Data	NUREG-0630 ramp rate-dependant data for Zircaloy-4 cladding. Data from Appendix K of BAW-10227P-A for M5 cladding

Table 9-2. Additional SBLOCA Evaluation Model Guidelines, Generic and Prescribed Inputs for the SBLOCA EM.

(Cont'd)

INPUT	SELECTION
RELAP5/MOD2-B&W	
Time Step Control Option	Option 3, mass error checking, consistent hydrodynamic and heat structure solution time advancement
ECCS Fluid Temperatures	Set at, or conservatively above, the nominal year average temperatures per system
ECCS Time Delays	Includes provision for signal, diesel start-up, pump start-up, and line filling for all evaluations
Containment Pressure	Set from FSAR, bounding analysis, or CONTEMPT analysis
Steam Generator Tube Plugging	SGTP is set at or above the plant tube plugging level

This page is intentionally left blank.

10. REFERENCES

1. J. A. Klingenfus, et al., "RELAP5/MOD2-B&W -- An Advanced Computer Program for Light Water Reactor LOCA and Non-LOCA Transient Analysis," BAW-10164P-A Rev. 6, AREVA NP, Lynchburg, Virginia, June 2007.

2. Y. H. Hsii, "CONTEMPT - Computer Program for Predicting Containment Pressure-Temperature Response to LOCA," - B&W-Revised Version of Phillips Petroleum Co. Program (L. C. Richardson, et. al., June 1967), BAW-10095A Revision 1, AREVA NP, Lynchburg, Virginia, April 1978.

3. D. A. Wesley and K. J. Firth, "TACO3 - Fuel Pin Thermal Analysis Code," BAW-10162P-A, AREVA NP, Lynchburg, Virginia, October 1989.

4. B. M. Dunn, et al., "B&W's Evaluation Model Report with Specific Application to 177 FA Plants with Lowered Loop Arrangement," BAW-10091, AREVA NP, Lynchburg, Virginia, August 1974.

5. P. R. McHugh and R. D. Hentzen, "Natural Circulation Cooling in U.S. Pressurized Water Reactors," NUREG/CR-5769, EGG-2653, January 1992, U.S. Nuclear Regulatory Commission, Washington D.C.

6. BAW-10168P, "RSG LOCA - BWNT Loss-of-Coolant Accident Evaluation Model for Recirculating Steam Generator Plants," Revision 4, AREVA NP, Lynchburg, Virginia, July 2000.

7. BAW-10154P-A, "B&W's Small-Break LOCA Evaluation Model," AREVA NP, Lynchburg, Virginia, July 1985.

8. "Emergency Operating Procedures Technical Bases Document," B&W Owners Group Operator Support Committee, Rev. 10, January 2006.

9. D. A. Wesley, et al, "GDTACO - Urania Gadolinia Fuel Pin Thermal Analysis Code," BAW-10184P-A, Revision 0, B&W Fuel Company, Lynchburg, Virginia, February 1995.

10. BAW-10179P, "Safety Criteria and Methodology for Acceptable Cycle Reload Analyses," Revision 7, AREVA NP, Lynchburg, Virginia, December 2005.

11. D. B. Mitchell and B. M. Dunn, "Evaluation of Advanced Cladding and Structural Material (M5) in PWR Reactor Fuel," BAW-10227P-A, Revision 1, AREVA NP, Lynchburg, Virginia, June 2003.

12. NRC Letter from Herbert M Berkow, NRC to James F Mallay, Framatome ANP dated April 10, 2003, "Evaluation of Framatome ANP Preliminary Safety Concern (PSC) 2-00 Relating to Core Flood Line Break and Operator Action Time (TAC No. MA9973)."